Εθνικό Μετσόβιο Πολυτεχνείο
Σχολή Πολιτικών Μηχανικών
Εργαστήριο Εδαφομηχανικής

National Technical University of Athens
School of Civil Engineering
Soil Mechanics Laboratory

Διπλωματική Εργασία

Γεωργίας Ευθυμίου

Επιβλέπων:
Καθηγητής Γ. Γκαζέτας

Στατική και Δυναμική Ανάλυση Κοίλων Κυλινδρικών Φρεάτων

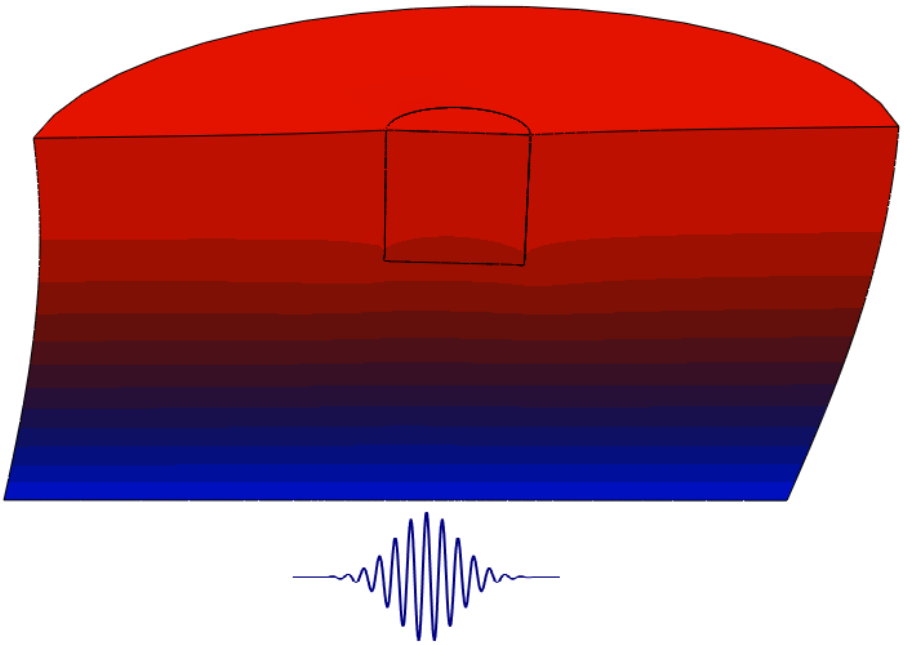

Static and Dynamic Analysis of Circular Skirted Foundations

Diploma Thesis by

Georgia Efthymiou

Supervised by:
Professor G. Gazetas

Αθήνα, Μάρτιος 2017

Athens, March 2017

Ευχαριστίες

Έχοντας φθάσει στο τέλος της διπλωματικής μου εργασίας, θα ήθελα να ευχαριστήσω θερμά τον καθηγητή μου κ. Γ. Γκαζέτα, αρχικά για την ελευθερία που μου έδωσε στην επιλογή του θέματος, ώστε να μελετήσω κάτι που πραγματικά με ενδιαφέρει, καθώς και για το γεγονός ότι η συνεργασία μαζί του με δίδαξε πολλά στην πρώτη μου προσπάθεια στη δημιουργική διαδικασία της έρευνας και αναμφισβήτητα διεύρυνε τον τρόπο σκέψης μου σε θέματα μηχανικού.

Επιπλέον, ιδιαίτερες ευχαριστίες οφείλω στη Δρ. Ευαγγελία Γαρίνη για τη βοήθεια και τις συμβουλές που μου έχει προσφέρει.

Τέλος, θα ήθελα να ευχαριστήσω την οικογένεια και τους φίλους μου για τη διαρκή υποστήριξή τους όλο αυτό το διάστημα.

ΠΕΡΙΛΗΨΗ

Η παρούσα διπλωματική εργασία ερευνά τη στατική και δυναμική απόκριση κοίλων κυλινδρικών φρεάτων, γνωστά ως suction caissons, για τη θεμελίωση παράκτιων ανεμογεννητριών. Ως εναλλακτική στο συμβατικό μονοπάσσαλο, ο οποίος κυριαρχεί στη βιομηχανία, η θεωρητικά οικονομικότερη λύση του suction caisson είναι απαραίτητο να διερευνηθεί λεπτομερώς. Ο κώδικας πεπερασμένων στοιχείων ABAQUS v.6.13 χρησιμοποιείται για τις αναλύσεις. Για όλες τις περιπτώσεις που εξετάζονται εδώ, η απόκριση του suction caisson συγκρίνεται αποτελεσματικά με εκείνη της παράπλευρης επιφάνειάς του (γνωστή ως skirts), με σκοπό να εκτιμηθεί ο ρόλος της τελευταίας στη συνολική απόκριση του συστήματος, να διαφωτισθεί η μηχανική του προβλήματος και ενδεχομένως να χρησιμοποιηθεί ως υβριδικό θεμέλιο. Πιο συγκεκριμένα, οι δύο τύποι θεμελίων μελετώνται σε όρους ελαστικής και μη-γραμμικής δυσκαμψίας. Καμπύλες που παρουσιάζουν την ελαστική δυσκαμψία των skirts ως ποσοστό της δυσκαμψίας του suction caisson, δημιουργήθηκαν για ομοιογενές και Gibson έδαφος. Επιπροσθέτως, μια μεθοδολογία πρακτικής φύσης αναπτύχθηκε, με την οποία υπολογίζεται η δυσκαμψία ενός άκαμπτου suction caisson σε έδαφος Gibson. Η φέρουσα ικανότητα των θεμελίων εκτιμάται επίσης, με τους αντίστοιχους μηχανισμούς αστοχίας να παρουσιάζονται. Ακόμη, η κινηματική αλληλεπίδραση του συστήματος εδάφους-θεμελίωσης εξετάζεται για διέγερση με αρμονικού τύπου τροποποιημένους παλμούς Gabor και σεισμικές καταγραφές. Η επιρροή της συχνότητας διέγερσης υπογραμμίζεται σε συναρτήσεις μεταφοράς και δυναμικές εδαφικές ωθήσεις που ποσοτικοποιούν τα αποτελέσματα της κινηματικής αλληλεπίδρασης. Η αριθμητική μελέτη περιλαμβάνει μεταβολές στη γεωμετρία των θεμελίων, καθώς και παραδοχές για τη διεπιφάνεια εδάφους-θεμελίωσης. Σημαντικότερα, αυτή η μελέτη αποδεικνύει ότι τα skirts μόνο θα μπορούσαν δυνητικά να αντικαταστήσουν το πλήρες θεμέλιο σε συγκεκριμένες συνθήκες, συντελώντας σε εξοικονόμηση κόστους και υλικών. Σε αυτή τη βάση προτείνεται τελικώς η γενική ιδέα ενός υβριδικού θεμελίου που αποτελείται από έναν κοίλο κύλινδρο, ο οποίος συνδέεται μέσω ακτινικών δοκίδων με τον πύργο της θαλάσσιας ανεμογεννήτριας.

ABSTRACT

This diploma thesis investigates the static and dynamic response of skirted circular foundations, known as suction caissons, for offshore wind turbine towers. As an alternative to the conventional monopile, which currently dominates the industry, the theoretically more economical solution of the suction caisson foundation needs to be thoroughly researched. Finite element code ABAQUS v.6.13 is used for the analyses. For all cases examined herein, the suction caisson response is effectively compared to that of its sidewalls (skirts) alone, in order to assess the role of the latter in the overall response of the system, gain deeper insight into the mechanics of the problem, and if possible, even utilize it as a hybrid foundation. More specifically, the two foundation types are studied in terms of elastic and nonlinear stiffness. Curves that present the elastic stiffness of the skirts alone as a proportion of the stiffness of the suction caisson are produced for a homogeneous and a Gibson soil. Additionally, a methodology of practical nature is developed, with which the stiffness of a rigid suction caisson in a Gibson soil is calculated. The bearing capacity of the foundations is also assessed, with respective failure mechanisms being presented. Moreover, the kinematic interaction of the soil-foundation system is examined for excitation with modified Gabor pulses of harmonic type and recorded earthquake motions. The influence of the excitation frequency is highlighted in transfer functions and dynamic earth pressures, which quantify the effects of kinematic interaction. The numerical study involves variations in the geometry of the foundations, as well as the soil-foundation interface assumptions. Most significantly, this study demonstrates that the skirts alone could potentially substitute the full foundation under certain circumstances, leading to cost and material savings. On this basis, a concept of a hybrid foundation is finally proposed, consisting of a hollow cylinder that is connected via radial stiffeners with the offshore wind turbine tower.

Contents

Chapter 1

Literature Review

1 Literature Review

1.1 Introduction

1.1.1 Scope of Study

The turn to renewable energy sources for electricity production has been gaining gradually more ground. Among others, the exploitation of wind energy through wind turbines has resulted in the development of a huge industry. Wind turbines can be divided in two general categories: onshore and offshore. While many countries undertake onshore wind turbine projects, the offshore wind turbine industry is still at an initial stage. The key advantage of offshore wind turbines is the maximum exploitation of wind energy, since in the open sea wind conditions are higher and steadier. Additionally, the choices for the creation of a wind turbine park are obviously more in the sea.

Offshore wind turbines are considerably more expensive than onshore, due to their large initial costs related with installation. In order for the offshore wind energy production industry to become a more feasible option, the reduction of expenses is necessary. Given that the cost of foundation of these turbines may reach up to 35% of the total cost (Byrne & Houlsby, 2003), a lot of research has been carried out in order to make the design of the support structures less expensive and conservative, without giving up safety and design code requirements (Bransby & Randolph, 1998; Byrne & Houlsby, 2002, 2003; Gourvenec & Randolph, 2003; Van der Tempel, 2006; Gourvenec, 2007; Bransby & Yun, 2009).

Until lately, the design of offshore wind turbines was based on the offshore oil industry design codes. However, this has been recognized insufficient, due to the ratio of horizontal to vertical forces on the structures being much greater for wind turbines, reaching values of over 60% and creating large eccentricities. This can be seen in **Figure 1.1**, where a typical 3.5 MW offshore wind turbine is compared to a jack-up platform (Byrne & Houlsby, 2003).

Presently, there are limited choices for the foundation of offshore wind turbines, depending on the site conditions and water depth, as **Figure 1.2** presents. Specifically, in shallow waters, “gravity base” solutions can be applied, resisting moments mainly with their self-weight. In medium water depths, the monopile dominates the industry, with the alternative being the suction caisson, which resembles an upturned bucket. As water depth increases, the single-foundation solution becomes uneconomic, thus multipod structures are used for foundation.

Studies on the development of alternative solutions for the foundation of offshore structures including wind turbines keep on being published. Bienen et al. (2012) studied numerically a hybrid skirted foundation consisting of a skirted mat with an internal suction caisson. Vulpe et al. (2013) investigated numerically the undrained capacity of a skirted spudcan. Winged piles in sand under monotonic and cyclic loading were studied experimentally by Bienen et al. (2012).

Dimmock et al. (2013) investigated a type of hybrid subsea foundation consisting of a shallow mat foundation connected with short piles. Finally, Anastasopoulos & Theofilou (2015) analyzed the performance of a hybrid foundation for offshore wind turbines that combines a monopile with a lightweight steel circular footing; this hybrid foundation is based on the concept of Stone et al. (2007). **Figure 1.3** presents these original ideas.

Consequently, establishing an innovative solution for the foundation of offshore wind turbines could potentially lead to cost and material savings, contributing thus to the progress of the industry. In this study, the static and dynamic response of the suction caisson foundation is investigated numerically. Moreover, the response of the suction caisson is effectively compared to that of its sidewalls (skirts) alone, in order to establish the role of the latter in the total response of the system, gain deeper insight into the mechanics of the problem, and if possible, even utilize it as a hybrid foundation.

1.1.2 The Suction Caisson Foundation

The suction caisson, also referred to as bucket foundation, is a circular skirted foundation, which is an alternative to the monopile that is vastly used for the foundation of offshore wind turbines. For the design of suction caissons, the usual aspect ratio of skirt length (L) to foundation radius (a) is $L/a \leq 2$. Compared to surface footings, the skirts transfer the loading to deeper and typically stronger soil, mobilizing thus higher bearing capacity. Additionally, the ease in the installation procedure of the suction caisson is one of its key advantages. In specific, the installation is achieved by transferring the foundation at the desired location and then pumping out the water between the foundation and the confined soil (also known as soil plug). As can be noticed in **Figure 1.4**, the simple mechanism consisting of the difference between the external and internal pressures leads the foundation steadily to its chosen position. Furthermore, due to the created suction, the lid becomes welded to the soil, thus tensile capacity is achieved. A lot of research has been conducted for the assessment of the capacity of this foundation type, through experimental and numerical methodologies (Bransby & Randolph, 1998; Byrne, 2000; Bransby & Yun, 2009; Houlsby et al., 2005, 2006; Kelly et al., 2006; Gourvenec, 2007).

The limited use of suction caissons is due to the fact that the industry has acquired a lot of experience in the monopile as a solution for foundation, being reluctant to a new and comparatively untested type of foundation. Thus, the suction caisson is continuously being researched in order to shed light to the mechanisms involved in the problem.

Byrne & Houlsby (2003) concluded that there is an approximately linear relationship between moments and vertical loads at low vertical load values and produced a preliminary design chart, which is available in **Figure 1.5**, where the diameter for the caisson lid and the length of the skirts can be chosen, based on the self-weight of the wind turbine.

Houlsby et al. (2005) performed field trials investigating the response of a set of model suction caissons lying on clay to transient lateral loading. The researchers suggested a stiffness-based,

as well as a strength-based approach to estimate an approximate value for the diameter of the suction caisson.

It needs to be stressed out that the tensile capacity achieved through suction is questionable after a number of cycles due to wind and wave loading. For this reason, sliding and detachment may take place between the foundation and the supporting soil, as well as flow towards the internal soil, negating the beneficial influence of suction.

1.2 Defining Interface Nonlinearities in the Design of Skirted Foundations

Most of the publications on the suction caisson foundation on clay, have considered full contact between the supporting soil and the foundation (Bransby & Randolph, 1998; Gourvenec & Randolph, 2003; Gourvenec, 2007; Bransby & Yun, 2009). This choice has been made on the basis of:

a) the nature of the design loads, which is assumed as short-term and
b) the installation procedure of the suction caisson, which allows the development of tensile capacity due to negative excess pore pressures between the lid of the foundation and the soil plug, since the latter tends to swell when the foundation is subjected to uplift.

Clukey & Morrison (1993) showed by centrifuge tests that the tensile capacity of the suction caisson is about 80% of the capacity in compression. Using the same method, Watson et al. (2000) were led to the conclusion that tensile and compression capacities of the suction caisson are equal. Many other experimental studies, although for deep skirted foundations of a skirt length over radius ratio (L/a) of more than 4, have shown reverse end bearing capacity (Fuglsang & Steensen-Bach, 1991; Steensen-Bach, 1992; Puech et al., 1993; Rao et al., 1997; Randolph & House, 2002; Luke et al., 2005).

However, less research has been carried out for smaller embedment ratios ($L/a \leq 2$), which are more appropriate for the foundation of an offshore wind turbine, either as single gravity based foundations or in a group. As embedment ratio decreases, drainage paths tend to become much shorter, which may result in the diminishment of the suction effect much more rapidly than in higher ratios. In addition, smaller embedment ratios mean lower soil stresses at the skirt tip level, which could lead to the pull-out of the whole soil plug. Finally, loading of an offshore wind turbine is more transient and sustained, resulting in long-term loading conditions, which could probably cause additional drainage.

House & Randolph (2001) performed centrifuge tests in order to determine the uplift resistance of a high embedment ratio suction caisson in cohesive soil, concluding to a friction ratio of $\alpha=0.4$ acting inside and outside of the foundation. The researchers found this number in good agreement with similar studies (Colliat et al., 1995; Mello et al., 1998; Andersen &

Jostad, 1999). According to recent research, the assumption of full contact between the suction caisson and the supporting soil may be false, leading to overestimation of the tensile and compression capacity. Gourvenec et al. (2009) showed by an experimental study that for small L/a ratios, a friction ratio of α=0.3 between the skirts and the soil was developed under transient uplift.

Houlsby et al. (2005) proved analytically that the tensile capacity of a suction caisson in sand under rapid loading is influenced mostly by the pullout rate and the ambient water pressure. The researchers used a sand-skirt interface friction coefficient value of $K \tan\delta=\mu=0.7$. Kelly et al. (2006) through an experimental study using a pressure chamber, showed that increase in ambient water pressure had a positive impact on the tensile capacity of the suction caisson, due to its effect on the relative pressure at which cavitation phenomena take place.

Taking into account the aforementioned, not only full contact between the foundation and the supporting soil can be blindly considered, but under transient loading, such as wind (practically constant) and wave ($T\approx10$ s) loading, the tensile capacity of the suction caisson is obviously questioned. As other publications indicate, it is significant to examine interface nonlinearities, apart from full contact conditions. Due to the difficulty in fully defining the actual interface conditions between the suction caisson and the soil, assumptions should not be generalized.

Subsequently, two assumptions are made in this thesis, regarding the conditions between the foundation and the supporting soil:

(a) fully bonded contact (FBC) that implies infinite tensile capacity allowing thus for no detachment, sliding or uplift and

(b) a tensionless sliding interface (TSI) with reduced maximum shear strength $\tau=\alpha S_u$, utilized principally under undrained loading conditions. Undrained shear stress reduction factor α is taken 0.5 for the interface between the sidewalls and the soil, both internally and externally, and 1 for the interface between the lid and the soil plug, accounting thus for the self-weight of the lid.

1.3 Bearing Capacity

1.3.1 Preface

Foundations need to sustain vertical (V), horizontal (H) and moment (M) loading that is transferred from the superstructure. In the case where these loads singularly or combined exceed specific values, the foundation reaches its bearing capacity, which means that it can no longer cope and failure occurs in the foundation-soil system.

Consequently, assessing the bearing capacity of a foundation has been one of the most prominent issues of Geotechnical Engineering. Prandtl (1921) was the first to calculate

analytically the vertical bearing capacity of a strip foundation lying on a homogeneous half-space. In addition, numerous empirical, numerical and even experimental studies have been conducted for vertical loading under undrained conditions, taking into account various assumptions on soil-foundation interface, soil shear strength profile, etc., (Terzaghi, 1943; Skempton, 1951; Meyerhof, 1951, 1953; Brinch Hansen, 1970; Bransby & Randolph, 1998; Houlsby & Martin, 2003; Salgado et al., 2004). On the other hand, bearing capacity under lateral and moment loading, as well as under combined vertical, horizontal and moment loading, has not been investigated as systematically as the vertical case (Martin, 1994; Bransby & Randolph; 1997, 1998; Yun & Bransby, 2007; Bransby & Yun, 2009; Gourvenec, 2007).

Despite the differences between offshore and onshore loading conditions, design codes proceed to the problem in a similar way that derives from the classical bearing capacity equations established by Terzaghi (1943) for a vertically loaded strip foundation on a uniform Tresca soil. In fact, these equation can be modified by proper factors, in order to take into consideration inclination and eccentricity of loading, foundation shape, embedment and soil shear strength profile.

Due to the oversimplified nature of this kind of methodology, new design approaches have been proposed, including the failure envelope method, which accounts for combination of loads.

1.3.2 Traditional Bearing Capacity Approach

The classical bearing capacity theory and even more modern approaches are based on the plasticity theory. In these solutions, perfect plasticity occurs at failure, without any hardening or softening behavior of the soil. Despite their simplicity, the fact that they have been applied in design for over half a century led to the buildup of great experience used for their optimization. The classical bearing capacity solutions are presented below, underlining undrained conditions, which are considered in this study.

Prandtl (1921) was the first to calculate analytically the bearing capacity of a strip foundation resting on a uniform and cohesive soil half-space under central vertical loading. The ultimate stress at failure is expressed as follows:

$$q_u = (\pi + 2)S_u \tag{1.1}$$

where S_u: undrained shear strength

Subsequently, Terzaghi (1943), Meyerhof (1953) and Vesic (1975) provided empirical expressions for the calculation of the bearing capacity of footings, with the deployment of

special factors accounting for the shape of the foundation, as well as the inclination and eccentricity of loading.

An expansion of the original solution by Terzaghi, the vastly used expression currently is given below:

$$q_u = \frac{Q_u}{BL} = cN_c\zeta_c + \frac{1}{2}B\gamma N_\gamma \zeta_\gamma + qN_q\zeta_q \quad (1.2)$$

where q_U: ultimate failure stress

Q_U: ultimate load that the foundation can bear

B, L: the smaller and larger, respectively, dimension of the foundation

c: soil cohesion

q: effective overburden stress at the level of foundation

γ: soil specific weight

N_C, N_γ, N_q: special factors depending on the friction angle ϕ of the soil

ζ_C, ζ_γ, ζ_q: special factors accounting for a variety of parameters, such as the foundation shape, loading inclination and eccentricity, soil surface inclination, embedment, etc.

Under undrained loading conditions, the above expression is properly modified:

$$q_u = (\pi + 2)S_u\zeta_c + q \quad (1.3)$$

Practically, this is Prandtl's solution, modified for the various problem parameters through ζ_C and increased by the overburden stress q at the base level of foundation. In specific, factor ζ_C includes the effect of embedment, which leads to increased bearing capacity. Two effects contribute in this increase: the *trench effect*, which accounts for the inability of the foundation level to deform freely, due to the overlying soil stresses in the case of embedment and the *sidewall effect*, regarding the additional stresses that develop on the sides of the embedded foundation. These effects are depicted in **Figure 1.6**.

Literature suggests a great variety of factors that take into consideration the effect of embedment (Skempton, 1951; Meyerhof, 1953; Brinch Hansen, 1970; Bransby & Randolph, 1999; Salgado et al., 2004; Gourvenec, 2008). However, the inability to compare all of them lies to the different soil-foundation interfaces assumptions. Skempton (1951), Meyerhof (1953) and Brinch Hansen (1970) consider frictionless soil-foundation interface and do not take into account the sidewall effect in their solutions. Bransby & Randolph (1999) and Gourvenec (2008) assume full contact between the foundation and the soil, which leads to full mobilization of the

soil strength at the interface. The latter two solutions for embedment factors are presented in **Table 1.1**:

Authors	Depth factors d_c
Bransby & Randolph [1999]	$1 + D/B$
Gourvenec [2008]	$1 + 0.86D/B - 0.16(D/B)^2$

Table 1.1. Suggestions for depth factor d_C

Of great importance is the lateral displacement and rotation induced to the foundation, in the case of offshore wind turbines, which are subjected to loads stemming from wind, waves and currents. As a matter of fact, due to embedment, there is a coupling between these two degrees of freedom, which is neglected when researchers investigate the embedded foundations as surface ones with the soil shear strength at the foundation base level (Bransby & Randolph, 1998; Gourvenec, 2007). In order to shed light into the effect of coupling between the horizontal and rotational degree of freedom, the differences between a surface and an embedded foundation will be discussed below.

In undrained conditions, when a surface foundation is subjected to horizontal displacement, it develops a maximum shear force of $A\ S_u$, where A is the area of the foundation and S_u the undrained shear strength of the soil. On the other hand, when horizontal displacement is applied to the top or bottom of an embedded foundation, it will unavoidably rotate as well, as a result of lateral soil pressures; consequently, the maximum possible shear strength is not developed. Accordingly, an embedded foundation that is subjected to rotation, not only will rotate, but will also translate.

Finally, in the classical bearing capacity approach, combined loading is examined as superposition of the separate VM and VH solutions, theoretically describing thus the combined load. In the case of offshore wind turbines, the horizontal and moment loads transferred to the foundation due to wind, wave and current forces, cannot be superimposed as proposed by the classical bearing capacity; instead, they need to be investigated separately. In addition, the vertical loading of offshore wind turbines is not of crucial importance, since large safety factors are established against vertical loads. On the contrary, the fact that this type of structure is subjected to disproportionately large horizontal forces and overturning moments, suggests that emphasis should be placed on these loading conditions.

1.3.3 Alternative Bearing Capacity Methods: The Failure Envelope Approach

In order to overcome the limitations of the traditional bearing capacity approach, regarding geometry, type of loading etc., alternative methods on the calculation of the bearing capacity of foundations were established. More specifically, these methods deploy the so-called failure envelopes or interaction diagrams, which illustrate in a simple manner the combination and interaction between different loads. This alternative approach originated from experimental studies on frictional soils, for which interaction diagrams were developed (Nova & Montrasio, 1991; Martin, 1994; Gottardi et al., 1999). Subsequently, a lot of research has been carried out with the implementation of the failure envelope approach for the assessment of the bearing capacity, taking into account a variety of soil profiles, as well as soil-foundation interfaces.

Failure envelopes can also be produced analytically and numerically. Analytical approach utilizes plasticity theory in order to derive upper and lower bound plasticity solutions by invoking certain kinematic collapse mechanisms or stress fields in the soil (Ukritchon et al., 1998; Bransby & Randolph, 1998; Randolph & Puzrin, 2003). Numerically, failure envelopes can be developed with finite element or finite difference methods. Inducing a displacement controlled path to failure, the failure load and the corresponding kinematic mechanism are determined. For the development of a failure envelope, adequate data points are necessary (Bransby & Randolph, 1998; Taiebat & Carter, 2000, 2002; Gourvenec & Randolph, 2003; Gourvenec, 2007, 2008).

It is common to express these failure envelopes in planes of constant vertical (V), horizontal (H) or moment (M) loading and in some cases in 3D space through a failure surface, as can be seen in **Figure 1.7**. Moreover, the sign convention for surface and embedded foundations as found in the majority of publications is depicted in **Figure 1.8**. It is important to stress out the influence of the load reference point position, when the coupling between the horizontal and rotational degree of freedom is considered. Using the sign convention that is common in most publications, as the embedment ratio increases, the HM failure envelopes tend to develop an asymmetry towards the positive side of the plane, whereas the opposite occurs when the load reference point is chosen at the top of the foundation. This difference is highlighted in **Figure 1.9.**

In most cases, failure envelopes are developed for undrained loading conditions and the general expression for the failure envelope is:

$$f\left(\frac{V}{AS_u}, \frac{H}{AS_u}, \frac{M}{ABS_u}\right) = 0 \tag{1.4}$$

where V, H, M are the vertical, horizontal and moment loads respectively, A is the foundation plan area and S_U the undrained shear strength.

A large proportion of past research has examined the response of surface foundations under combined loading, concluding that the shape of the failure envelopes remained the same,

independent of embedment and that the only difference was the increased size (Martin, 1994; Bransby & Randolph, 1999). However, modern studies found this conclusion false, showing that the shape of HM failure envelopes changes intensely as embedment ratio grows, developing an asymmetry, which actually indicates the coupling between the horizontal and rotational degree of freedom (Yun & Bransby, 2007; Bransby & Yun, 2009; Gourvenec, 2008).

1.3.4 Bearing Capacity of Skirted Foundations

Researchers have been modelling until recently skirted foundations as surface footings with underlying soil shear strength equal to that below the skirt tip level (Bransby & Randolph, 1998; Gourvenec, 2007). A sketch of this assumption is available in **Figure 1.10**. It needs to be stressed out that this methodology fails to take into account the vertical tensile capacity due to the suction that develops between the lid and the soil plug, owing to the installation procedure of the suction caisson. Furthermore, confinement of the soil offers increased capacity in compression, leading the failure down to the skirt tip level (Bransby & Randolph, 1998).

Murff (1994) proposed an expression for the determination of a yield surface regarding this type of foundation, which is provided below:

$$f = \left(\frac{V}{V_0}\right)^2 - \left(1 + \frac{V_t}{V_0}\right)\frac{V}{V_0} + \frac{V_t}{V_0} + \left[\left(\frac{H}{H_0}\right)^2 + \left(\frac{M}{M_0}\right)^2\right]^{0.5} = 0 \qquad (1.5)$$

where V_t is the normalized bearing capacity under purely vertical tension and H_0, M_0 the ultimate horizontal load and moment respectively. In **Figure 1.11**, this curve is plotted in the VM plane (H=0) for zero tensile capacity and tensile capacity equal to capacity in compression as proposed by the results of Watson & Randolph (1997a).

Taiebat & Carter (2000) proposed an approximating algebraic expression that was based on 3D finite element analysis of a circular footing resting on clay in undrained conditions:

$$f = \left(\frac{V}{V_{ult}}\right)^2 + \left[\left(\frac{M}{M_{ult}}\right)\left(1 - a\frac{HM}{H_{ult}|M|}\right)^2\right] + \left|\left(\frac{H}{H_{ult}}\right)^3\right| - 1 = 0 \qquad (1.6)$$

where V_{ult}, M_{ult}, H_{ult} are the ultimate capacities under pure vertical, moment and horizontal loading. For uniform soil conditions the researchers suggested α=0.3 as a good fit.

Bransby & Randolph (1998) investigated the response of skirted foundations under combined loading. Having conducted a finite element study on strip footings in undrained conditions, where full contact between the foundation and the soil was established, they recommended the following expression for a failure surface in VHM space:

$$f = \left(\frac{V}{V_{ult}}\right)^{2.5} - \left(1 - \frac{H}{H_{ult}}\right)^{1/3}\left(1 - \frac{M^*}{M_{ult}}\right) + \frac{1}{2}\left(\frac{M^*}{M_{ult}}\right)\left(\frac{H}{H_{ult}}\right)^5 = 0 \qquad (1.7)$$

where

$$\frac{M^*}{ADs_{u0}} = \frac{M}{ADs_u} - \frac{L}{D}\frac{H}{As_u}$$

L is the height above the foundation level of the rotation center of the foundation at failure, when rotation is imposed on the base. It was deduced that the yield locus in HM plane developed an eccentricity, with the maximum moment sustained with a considerable amount of horizontal load. Subsequently, the coupling between the horizontal and rotational degree of freedom was confirmed, showing that previously suggested expressions for yield loci and plastic potentials of shallow foundations are possibly inappropriate for use in the case of skirted foundations.

Byrne & Houlsby (2003), based on a small number of model tests carried out by Byrne (2000) and Byrne et al. (2003), claim that there is an approximately linear relationship between vertical (V) and moment (M) loading at low vertical loads such that:

$$\frac{M}{D} = \left(f_1 + \frac{f_2}{k}\right)^{-1}(V + f_3 W) \qquad (1.8)$$

where $k = M / (DH)$ is the ratio of moment to horizontal load, $W = 0.25\,\pi\,D^2\,L\,\gamma'$ is the weight of the encased soil plug inside the suction caisson and f_1=3.26, f_2=1.073 and f_3=0.71. On the basis of this expression, they developed a chart that shows the variation of the suction caisson diameter with vertical load. This diagram can be found in **Figure 1.5**.

Yun & Bransby (2007) recommended a conservative fit based on moment transformation, in order to reduce the eccentricity observed at HM failure envelopes due to the coupling of the horizontal and rotational degree of freedom:

$$f = \left(\frac{H}{H_{max}}\right)^2 + \left(\frac{M^*}{M_{ult}}\right)^2 - 1 \qquad (1.9)$$

where $M^* = M - LH$. Parameter *L* is the distance of the alternative load reference point from the foundation level and *M* is the moment at the foundation level (**Figure 1.12**).

Figure 1.13 shows the key failure mechanisms of skirted foundations modelled as equivalent surface footings, as presented by Gourvenec (2007). Under governing moment loading, a near-semicircular scoop mechanism is formed, as can be seen in **Fig.1.13a**. With the mobilization of the maximum moment capacity, which occurs when a considerable horizontal load acts, a wedge-scoop-wedge mechanism, as defined by Bransby & Randolph (1998) takes place, where apart from the central scoop, side wedges appear too, as shown in **Fig.1.13b**. As horizontal

loading gradually dominates, the wedges tend to completely replace the scoop mechanism, which in that case turns into a sliding mechanism. **Fig.1.13c** displays a scoop-wedge mechanism, which appears for maximum capacity under moment loading, if vertical loading is existent. In the case where failure is mainly influenced by horizontal loading, an asymmetric wedge is observed, as in **Fig.1.13d**. Finally, following mobilization of the maximum moment capacity failure manifests as an asymmetric Brinch Hansen mechanism (Brinch Hansen, 1970), which is depicted in **Fig.1.13e**. According to Gourvenec (2007), in the case of increasing shear strength with depth, due to the fact that soil displacements take place in smaller depths relatively to a constant shear strength profile, the above mechanisms tend to make their appearance closer to the surface, where soil strength is reduced.

Bransby & Yun (2009) examined the bearing capacity of skirted foundations by modeling a 2D skirted strip foundation and derived five key failure mechanisms, which can be seen in **Figure 1.14**. These mechanisms differ than the respective ones in the case of a surface footing. It needs to be noted that special failure mechanisms are developed, in which the soil plug is involved (**Fig.1.14c**; **e**). Apparently, these two mechanisms do not appear in the failure of a solid embedded foundation. **Figure 1.15** provides normalized failure envelopes produced by the researchers, which underline the decline in strength of skirted comparatively to solid foundations, however, with the failure envelope shape remaining practically the same.

The case of linearly increasing shear strength profiles has been examined over the years regarding the vertical bearing capacity (Davis & Booker, 1973; Houlsby & Wroth, 1993; Martin, 2001). Nevertheless, combined loading has been recently investigated (Bransby & Randolph, 1998; Ukritchon et al., 1998; Randolph & Puzrin, 2003). According to Ukritchon et al. (1998) the use of special factors that account for inclination and eccentricity of loading may lead to unreliable and non-conservative results.

Gourvenec & Randolph (2003) suggested that in the VH plane (M=0) the shape of the failure envelope does not depend on the geometry of the foundation and the heterogeneity coefficient $\kappa=kD/S_{u0}$ (**Figure 1.16a**), as well as that there is good agreement with the closed-form expression by Green (1954), which is:

$$\bar{v} = 0.5 + \frac{\cos^{-1}\bar{h}+\sqrt{1-\bar{h}^2}}{2+\pi} \quad (1.10)$$

$$\bar{h} = 1 \ \text{ for } \ \bar{v} \leq 0.5 \quad (1.11)$$

where $\bar{v} = \frac{V}{V_0}$ and $\bar{h} = \frac{H}{H_0}$

V_0 and H_0 are the ultimate vertical and horizontal loads respectively.

On the contrary, the degree of inhomogeneity was found to have impact on the shape of the failure envelopes in the VM and VH planes, as can be seen in **Figure 1.16b**.

1.4 Elastic and Nonlinear Stiffnesses of Circular Embedded and Skirted Foundations

1.4.1 Preface

The effect of soil-structure interaction (SSI), which constitutes one of the most significant subjects of Geotechnical Engineering, can be taken into consideration through a stiffness matrix, which can be expressed as follows:

$$\{F\}=[K]\{x\} \tag{1.12}$$

where {x} the displacements/rotations imposed on the foundation, {F} the resultant forces due to these displacements/rotations and [K] the stiffness matrix that involves appropriate moduli, which, multiplied with the vector {x}, result in the forces acting on the foundation.

Knowing the response of the foundation-soil system is of great value, since the foundation and the supporting soil can be replaced by elastic springs (Winkler or elastic subgrade reaction hypothesis) and taken thus into account, contributing to minimization of computational efforts and to an effective calculation process of a structure, with the interactions between the soil-foundation system and the superstructure expressed in terms of forces and moments and their conjugated displacements and rotations.

Extended research has been carried out, providing simplified expressions for a variety of foundation shapes and types (Poulos & Davis, 1974; Gazetas, 1983, 1991; Gazetas & Tassoulas, 1987; Roesset, 1980; Doherty & Deeks, 2003, 2005; Doherty et al., 2005).

In the case of a symmetrical foundation in 3D space, expression (1.12) can be formed as:

$$\begin{Bmatrix} H_1 \\ H_2 \\ V \\ M_1 \\ M_2 \\ T \end{Bmatrix} = \begin{bmatrix} K_H & 0 & 0 & 0 & K_C & 0 \\ 0 & K_H & 0 & K_C & 0 & 0 \\ 0 & 0 & K_V & 0 & 0 & 0 \\ 0 & K_C & 0 & K_R & 0 & 0 \\ K_C & 0 & 0 & 0 & K_R & 0 \\ 0 & 0 & 0 & 0 & 0 & K_T \end{bmatrix} \begin{Bmatrix} u_1 \\ u_2 \\ w \\ \theta_1 \\ \theta_2 \\ \omega \end{Bmatrix} \tag{1.13}$$

The vertical stiffness of the soil-foundation system is represented by the term K_V, while the horizontal stiffness is represented by K_H. The term K_R stands for the rotational or rocking stiffness and K_T for the torsional stiffness. All moduli have units of [Force] or [Moment] per [Displacement] or [Rotation] respectively.

As far as the term K_C is concerned, it represents the coupling between the horizontal and the rotational degree of freedom, which appears for embedded foundations. In the case of surface foundations this term is approximately zero and thus, negligible. When an embedded foundation is subjected to rotation, horizontal reactions appear, as a result by lateral soil

pressures. Accordingly, when an embedded foundation is under horizontal loading, moments reactions become present. K_C is measured in [Force] units.

1.4.2 Elastic Stiffnesses of Surface Foundations

For a circular surface foundation resting on an elastic homogeneous half-space, Gazetas (1991) developed the following expressions for its stiffness components:

K_V	K_H	K_R	K_T
$\frac{4GR}{1-\nu}$	$\frac{8GR}{2-\nu}$	$\frac{8GR^3}{3(1-\nu)}$	$\frac{16}{3}GR^3$

Table 1.2. Elastic stiffness components of a circular surface footing (Gazetas, 1991)

where *G*: soil shear modulus

R: radius of footing

ν: Poisson's ratio of soil

If the soil stratum lies on bedrock, the above values increase. In order to take into account the influence of the rocky substratum, appropriate factors have been developed, which, when multiplied with the corresponding stiffness component of **Table 1.2**, result in the final elastic stiffness of the circular surface foundation. These factors are presented in **Table 1.3**:

Static Stiffness	Increase Factor	Range of validity
K_V	$\left(1+1.28\frac{R}{H}\right)$	H/R > 2
K_H	$\left(1+\frac{1}{2}\frac{R}{H}\right)$	H/R > 1
K_R	$\left(1+\frac{1}{6}\frac{R}{H}\right)$	4 ≥ H/R > 1
K_T	-	H/R > 1.25

Table 1.3. Increase factors of elastic stiffness for circular surface foundations

where H: depth of soil stratum

Depending on the excited degree of freedom and the pressure bulbs that are activated under each loading case, the influence of the bedrock differs. The vertical stiffness is mainly affected by the existence of the rocky substratum, whereas its importance for the torsional stiffness is inexistent.

Veletsos and Tang (1987) determined the vertical and the rocking stiffness of a ring surface foundation lying on an elastic, homogeneous half-space. A sketch of this type of foundation is illustrated in **Figure 1.17**. They expressed the vertical stiffness of the ring foundation, by multiplying the vertical stiffness of a circular surface footing with the dimensionless coefficient α, based on the ratio of width to outer radius of the ring $\Delta R/R_0$. In the case of the vertical stiffness, the variation of α with $\Delta R/R_0$ is shown in **Figure 1.18**. In the case of the rocking stiffness, the variation of α with $\Delta R/R_0$ is provided in the form of a table, in **Figure 1.19**. According to the researches, the difference between the vertical/rocking stiffnesses of the ring foundation and the respective circular footing becomes evident for an extremely low range of $\Delta R/R_0$ and in fact, is generally smaller than expected, when taking into account the contact areas involved. Specifically, for $\Delta R/R_0$ exceeding 0.5, the vertical/rocking stiffnesses of the ring and disk foundation are equal for practical purposes, while for $\Delta R/R_0$=0.1, even though the area of the ring foundation is 19% of the corresponding disk area, the vertical/rocking stiffness of the ring is 82%/86% of that of the surface footing.

1.4.3 Elastic Stiffnesses of Embedded Foundations

As has been previously discussed, embedded foundations outperform surface ones in terms of bearing capacity and stiffness. Two factors contribute to this favorable performance: the *trench effect*, which regards the extension of sliding surfaces beneath the foundation beyond is base and the *sidewall effect* that accounts for extra stresses that develop on the sides of an embedded foundations. A sketch of these mechanisms can be found in **Figure 1.6**.

Consequently, the effect of embedment in stiffness can be taken into consideration as:

$$K_{i_{emb}} = K_{i_{surf}} \cdot \frac{K_{i_{trench}}}{K_{i_{surf}}} \cdot \frac{K_{i_{emb}}}{K_{i_{trench}}} \tag{1.14}$$

Since each one of the above ratios is greater than 1, increase in stiffness due to embedment is established. **Figure 1.20** displays the effect of every factor in the case of horizontal and moment loading.

In order to quantify the effect of embedment in the elastic, static stiffness of a circular surface foundation embedded in a soil stratum of limited thickness *H*, Elsabee & Morray (1977) produced the horizontal and rocking modes, while Kausel & Ushijima (1979) the vertical and torsional modes:

Static Stiffness	Embedment Increase Factor	Range of validity
K_V	$\left(1+\frac{1}{2}\frac{D}{R}\right)\left(1+\left(0.85-0.28\frac{D}{R}\right)\frac{\frac{D}{H}}{1-\frac{D}{H}}\right)$	$\frac{D}{R}>2$ $\frac{D}{H}<0.5$
K_H	$\left(1+\frac{2}{3}\frac{D}{R}\right)\left(1+\frac{5}{4}\frac{D}{H}\right)$	
K_R	$\left(1+2\frac{D}{R}\right)\left(1+0.7\frac{D}{H}\right)$	
K_C	$0.40K_HD$	
K_T	$\left(1+2.67\frac{D}{R}\right)$	

Table 1.4. Embedment Increase Factors (Elsabee & Morray, 1977; Kausel & Ushijima, 1979)

where D: depth of foundation embedment

R: radius of foundation

H: depth of soil stratum

When expressions for the stiffness of a foundation are used, attention needs to be drawn to the location of the foundation point where displacements or rotations are imposed and to the contact conditions between the foundation and the supporting soil. All of the aforementioned expressions assume the load-reference point in the middle of the foundation; and if it is embedded, at the foundation level. Additionally, full contact between the foundation and the soil is taken into consideration, permitting no separation or uplift.

An illustration of a foundation embedded in a soil stratum resting on a rocky substratum is available in **Figure 1.21**.

1.4.4 Elastic Stiffnesses of Skirted Foundations

Using the scaled boundary finite element method, Doherty & Deeks (2003) calculated the elastic stiffness coefficients of different rigid circular foundations, including the suction caisson.

An expansion of this research was carried out by Dohery et al. (2005), who suggested a simplified methodology for the expression of the elastic stiffness of flexible skirted foundations embedded both in homogeneous and inhomogeneous elastic half-space, under drained (ν=0.2)

and undrained (ν=0.499) conditions. This was achieved by the determination of a dimensionless parameter (J), producing exclusive values depending on the stiffness of the system:

$$J = \frac{E_S t}{G_R R} \quad (1.15)$$

where E_S: Young modulus of steel

t: thickness of skirts

G_R: Shear modulus of soil

R: radius of foundation

Taking into account this parameter, the variation of the stiffness coefficients is given by the expression below:

$$K(J) = \frac{K_0 + (J/J_m)^p K_\infty}{1 + (J/J_m)^p} \quad (1.16)$$

Where K_0: stiffness as J → 0 (surface footing)

K_∞: stiffness for large values J (rigid caisson)

J_m: J at $K=(K_0+K_\infty)/2$

p: proportional to the gradient of the curve at J_m, with slope there $p(K_\infty-K_0)/2J_m$

Liingaard et al. (2007) produced tables with non-dimensional values of vertical static stiffness of a suction caisson, using a coupled boundary element/ finite element method. Moreover, they examined the dynamic stiffness of suction caissons in vertical and coupled sliding-rocking vibrations.

1.4.5 Nonlinear Stiffnesses of Foundations

Elastic stiffnesses are realistic only in the small strain domain. In larger displacements, soil nonlinearities become dominant in the response of foundations; thus, elastic stiffness overestimates the true stiffness of the soil-foundation system.

According to the prevailing capacity design, even though considerable plastic deformations are allowed to take place in the superstructure, no substantial yielding must occur in the supporting soil. On the other hand, as was observed in earthquakes such as Northridge (1994) and Kobe (1995), near-fault zones experienced very large ground and spectral accelerations, obviously leading to nonlinear behavior in the soil, as well as in the soil-foundation interface.

Gazetas et al. (2013) studied the nonlinear rocking stiffness of a variety of rigid surface foundation shapes under undrained conditions, taking into account soil and soil-interface nonlinearities and expressing the rocking stiffness as:

$$K_R(\theta, FS) = K_R(0, FS) \cdot \chi(\theta) = K_{R,elastic} \cdot \psi(FS) \cdot \chi(\theta) \quad (1.17)$$

where ψ(FS) is a reduction factor to the initial elastic rocking stiffness due to vertical loading and χ(θ) a reduction factor taking into account nonlinearities and plastic deformation due to large rotations. Specifically, ψ(FS) can be calculated as:

$$\psi(FS) \approx 1 - \frac{0.8}{FS} \quad (1.18)$$

Figure 1.22 provides a chart of χ(θ) as a function of normalized angle of rotation θ/θ_S.

Assessing the nonlinear stiffness of a soil-foundation system is of great value, since full modelling could be avoided, if solutions for such complicated problems could be established for the large displacement/rotation domain.

1.5 Kinematic Interaction

1.5.1 Preface

Soil-structure interaction during an earthquake involves kinematic and inertial interaction. Despite the fact that they act simultaneously under dynamic excitation, it is convenient to separate them into two distinct, successive phenomena. This concept is thoroughly presented in Chapter 5.

Kinematic Interaction, which constitutes the subject of this study, in the majority of cases leads to reduction of the amplitude of the foundation motion relatively to that of the free-field, as a result of base slab averaging, embedment and wave scattering (Luco & Mita, 1987; Veletsos & Prasad, 1989; Elsabee & Morray, 1977). The contribution of each one of these effects is discussed below. It has to be noted that when kinematic interaction is investigated, it is assumed that both the superstructure and the foundation are massless.

Base slab averaging is caused by inclined or incoherent incident wave fields. A surface foundation does not follow the motion of the free-field when incident waves impinge on the foundation with an angle α_V to the vertical axis (wave passage effect) or when the wave is incoherent (ground motion incoherence effect). The result is that the translational component of the foundation motion is reduced in relation to the free-field and a rotational component is introduced. Specifically, the rotational motion involves rocking in the case of inclined SV waves, P waves and Rayleigh waves and torsion in presence of SH waves and Love waves. The reduction

of the translational motion of the foundation and the introduction of rocking and torsion tend to become more evident as the frequency increases. At higher frequencies, the effective size of the foundation is increased compared to the wavelength. Furthermore, the ground motion tends to become more incoherent as frequency increases.

The influence of embedment is of great importance in the phenomenon of kinematic interaction. The motion of an embedded, massless, rigid foundation, which is subjected to vertically propagating, coherent shear waves, is consisted of a translational and a rotational component (**Figure 1.23**). The first one is caused by the overall translation of the subgrade, whereas the latter is due to the shear stresses that develop on the sidewall-soil interface. These shear stresses result from the difference in the horizontal displacements of the surface and of the soil in the embedment region producing 'pseudo-rotation' of the soil. Being rigid, the embedded foundation cannot deform that way, thus it rotates, with the strength of the soil being the main resistance to this rotation.

In conclusion, the main consequence of kinematic interaction is that it leads to "foundation input motion" (FIM), which is different from the motion of the free-field soil, containing a rotational component apart from the translational one. Therefore, the introduction of kinematic interaction factors, which are transfer functions that relate the motion of the foundation to that of the free-field and thus quantify the results of kinematic interaction, has been intensively studied (Kausel et al., 1978; Gazetas, 1984; Day, 1978). The practical significance of such transfer functions is obvious: by multiplying a free-field design response spectrum with the appropriate transfer function, one can obtain the design response spectrum which should be used as input at the base of the superstructure or at the base of the foundation.

1.5.2 Analytical Solutions for Embedded Foundations

Elsabee & Morray (1977) and Day (1978) developed analytical transfer functions, which relate the translational and rotational motion of the base slab to free-field translation in the case of vertically propagating, coherent SH waves. Base slab averaging effects do not exist in this wave field, but foundation translation is reduced in comparison to the free-field due to soil motion reduction with depth and wave scattering effects.

Day (1978) used finite element analysis in order to evaluate the base motions of a rigid, cylindrical foundation embedded in a uniform elastic halfspace (ξ=0 %, ν=0.25) that was subjected to vertically incident, coherent SH waves.

Elsabee & Morray (1977) and Kausel et al. (1978) investigated the kinematic response of a cylindrical foundation embedded in a visco-elastic soil stratum (ξ=5%, ν=0.33) lying on a rigid base. Additionally, an approximate expression for the amplitudes of transfer functions in terms of normalized frequency $\alpha_0=\omega r/V_S$, which was developed by Elsabee & Morray (1977) is given below:

$$\text{translation:} \quad |H_u(\omega)| = \begin{cases} \cos\left(\frac{e}{r}a_0\right) & a_0 \le 0.7\cdot\bar{a}_0 \\ 0.453 & a_0 > 0.7\cdot\bar{a}_0 \end{cases} \tag{1.19}$$

$$\text{rocking:} \quad |H_\theta(\omega)| = \begin{cases} \frac{0.257}{r}\left(1-\cos\left(\frac{e}{r}a_0\right)\right) & a_0 \le \bar{a}_0 \\ \frac{0.257}{r} & a_0 > \bar{a}_0 \end{cases} \tag{1.20}$$

where $\bar{a}_0 = \pi/2\cdot r/e$. Normalized frequency $\bar{a}_0$ corresponds to the fundamental frequency of the soil from the surface to depth e ($\bar{a}_0 = 2\pi f_1 r/V_S$ where $f_1 = V_S/4e$).

The aforementioned expression is also known as the approximate solution by Kausel et al. (1978) for the evaluation of transfer function amplitudes, since Kausel et al. (1978) based partly on the graduate theses of J.Morray and F. Elsabee at the Massachusetts Institute of Technology.

Figure 1.24 presents the results of Day (1978) and Elsabee & Morray (1977) on the amplitude of the transfer functions referring to the case of the halfspace and the finite soil layer for a foundation embedment to radius ratio e/r=1. As it can be observed, for α_0>0.5 the reduction in the translational motion of the foundation becomes more considerable, whereas for α_0>1 the rotational component is more evident and cannot be neglected.

It was found by Elsabee & Morray (1977), that these transfer functions are appropriate for nonhomogeneous soil deposits, given that V_S is averaged across the embedment depth. Furthermore, according to Mita & Luco (1989) the solutions for circular foundations can be implemented to square foundations, by calculating the equivalent cylinder radius as the average of the radii that are necessary to match the area and the inertia of the square base.

Gazetas (1984) studied numerically the kinematic response of end-bearing single piles embedded in various idealized soil deposits and subjected to vertically propagating harmonic shear waves. The results of kinematic interaction are provided in the form of dimensionless graphs. **Figure 1.25** illustrates for the case of homogeneous soil deposit the approximate curve for the transfer function I_U (ratio of horizontal displacements of the pile head to free-field) in terms of normalized frequency F_C, which is expressed as follows:

$$F_C = \frac{f}{f_1}\cdot\left(\frac{E_p}{E_s}\right)^{0.30}\cdot\left(\frac{L}{d}\right)^{-0.50} \tag{1.21}$$

where f_1: fundamental shear frequency of the soil stratum

E_P: Young Modulus of the pile

E_S: Young Modulus of the soil

L: Length of the pile

d: Diameter of the pile

1.5.3 Empirical Studies

Reductions in the ground motion with depth have been reported by Seed and Lysmer (1980) and Chang et al. (1985) with the use of downhole free-field arrays and comparisons between basement and free-field motions.

Ishii et al. (1984) developed empirical transfer functions regarding the translational motion, using earthquake records for 18 partially buried tanks in Japan. Nevertheless, this solution is of limited value since embedment depth to radius ratio e/r, which is of great significance in the phenomenon of kinematic interaction, was not involved in the regression analyses.

However, it needs to be noted that the majority of structures are not adequately equipped with instruments at the level of the foundation in order to measure base rocking, so there is lack of data. Even for structures that are instrumented to record base rocking, separation of the kinematic and inertial rocking effects would be impossible without proceeding to assumptions about the foundation impedance and wave field. As a result, exclusively empirical transfer functions for base rocking due to kinematic interaction are difficult to formulate and have not so far been developed.

Chapter 1: Figures

Literature Review

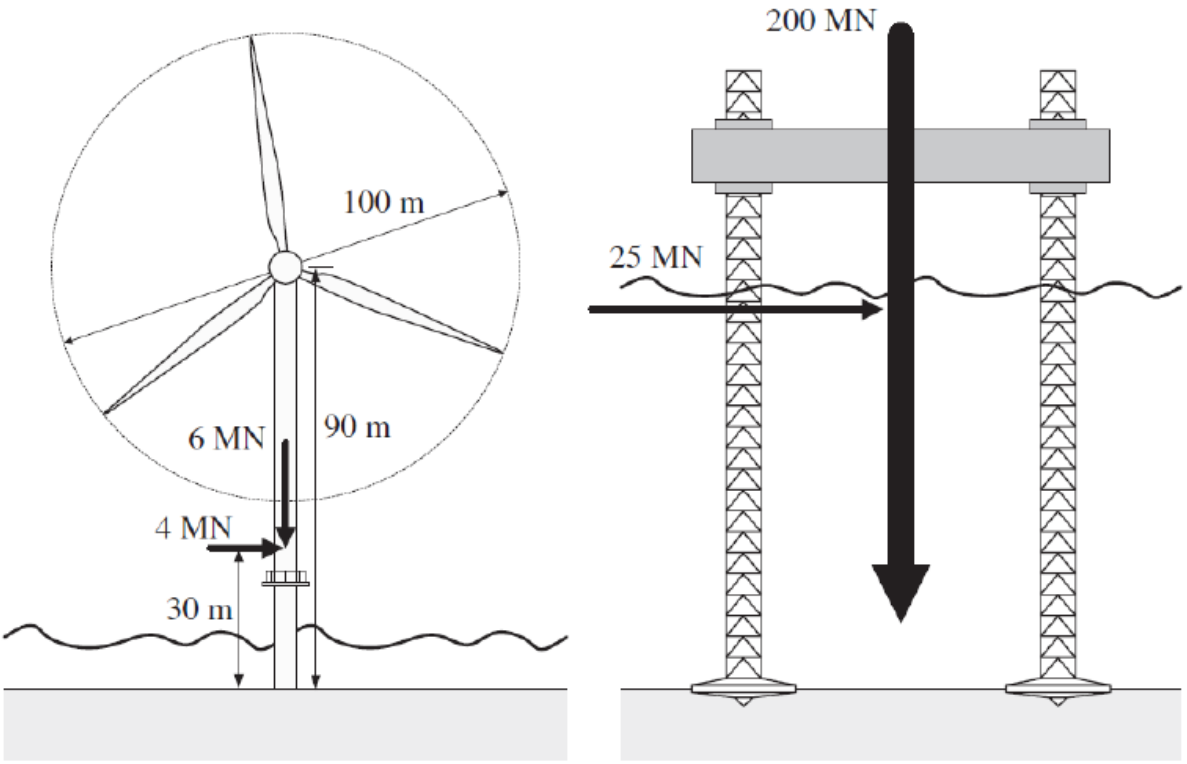

Fig.1.1. Comparison between a 3.5 MW wind turbine and a jack-up platform (Byrne & Houlsby, 2003)

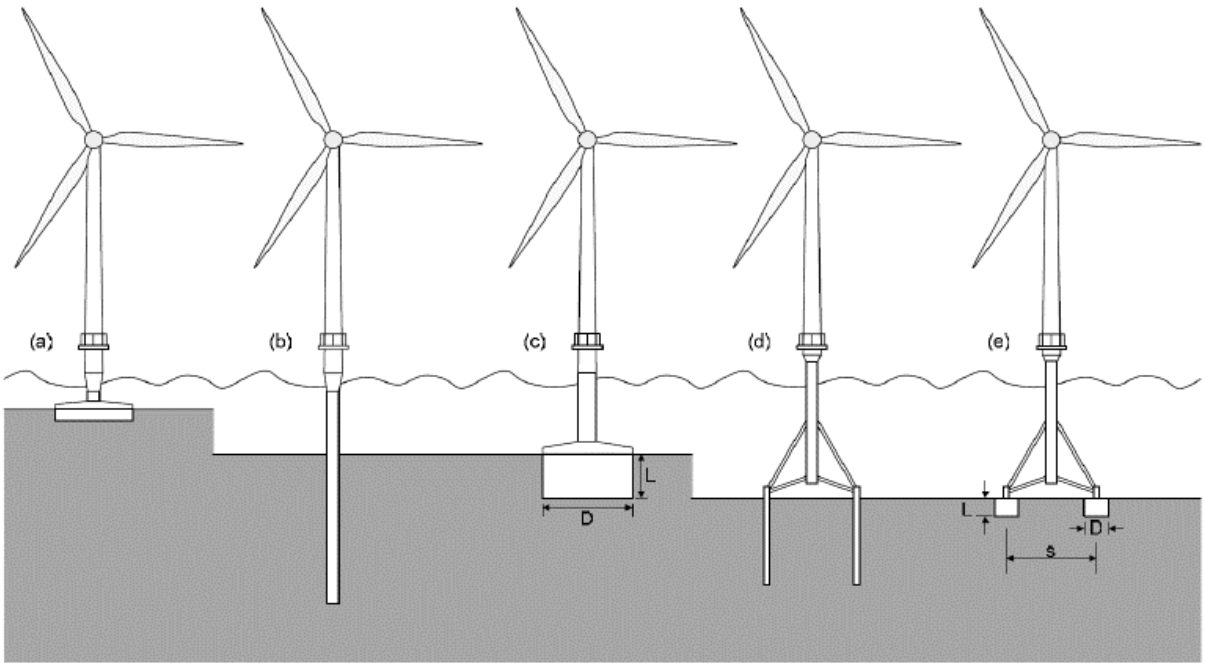

Fig.1.2. Offshore wind turbine foundation options [Byrne & Houlsby, 2006]: (a) "Gravity base"; (b) monopile; (c) suction caisson; (d) multipod structure with 3-4 piles; (e) multipod structure with 3-4 solid or suction caissons

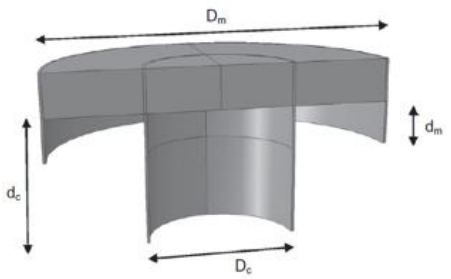

(a)

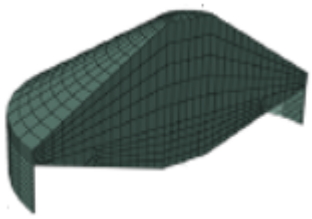

(b)

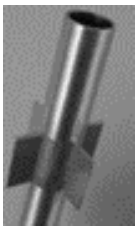

(c)

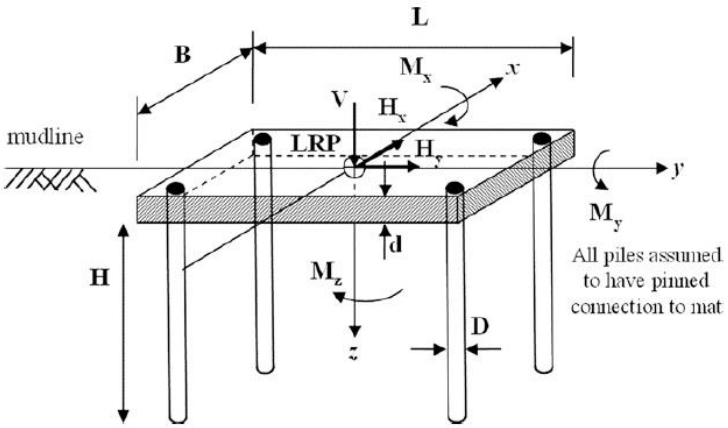

(d)

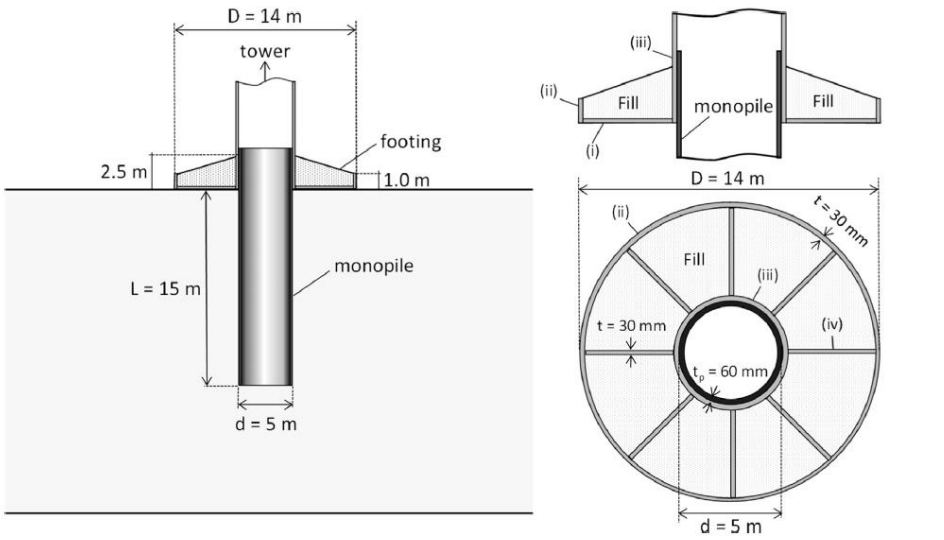

(e)

Fig.1.3. Hybrid foundations for offshore structures: (a) hybrid skirted foundation (Bienen et al., 2012); (b) skirted spudcan (Vulpe et al., 2013); (c) winged pile (Bienen et al., 2012); mat with piles (Dimmock et al., 2013); (d) Monopile-footing foundation (Anastasopoulos & Theofilou, 2015)

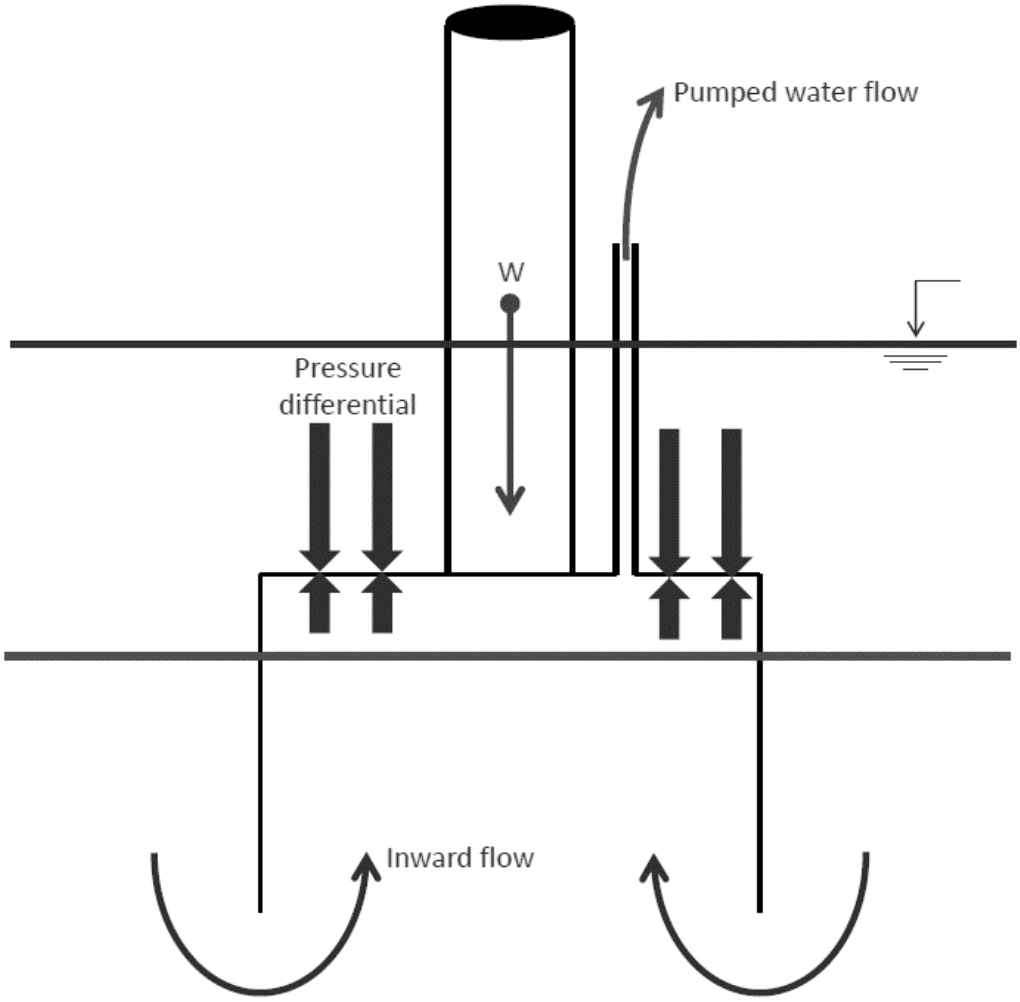

Fig.1.4. Suction caisson installation mechanism

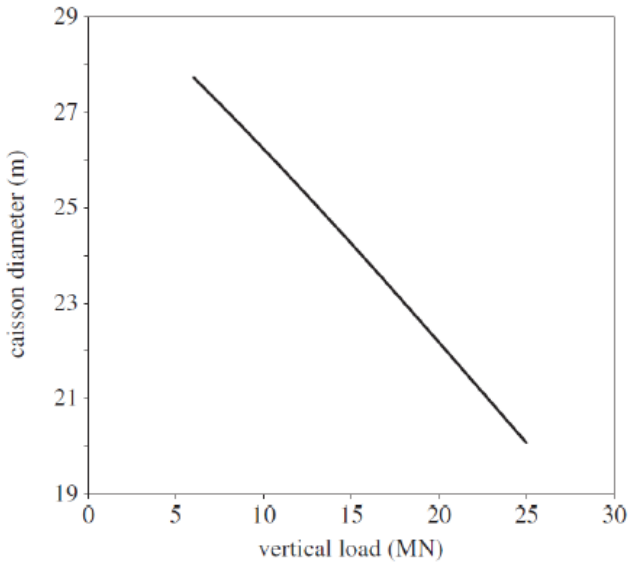

Fig.1.5. Preliminary design chart for a suction caisson foundation based on wind turbine self-weight [Byrne & Houlsby, 2003]

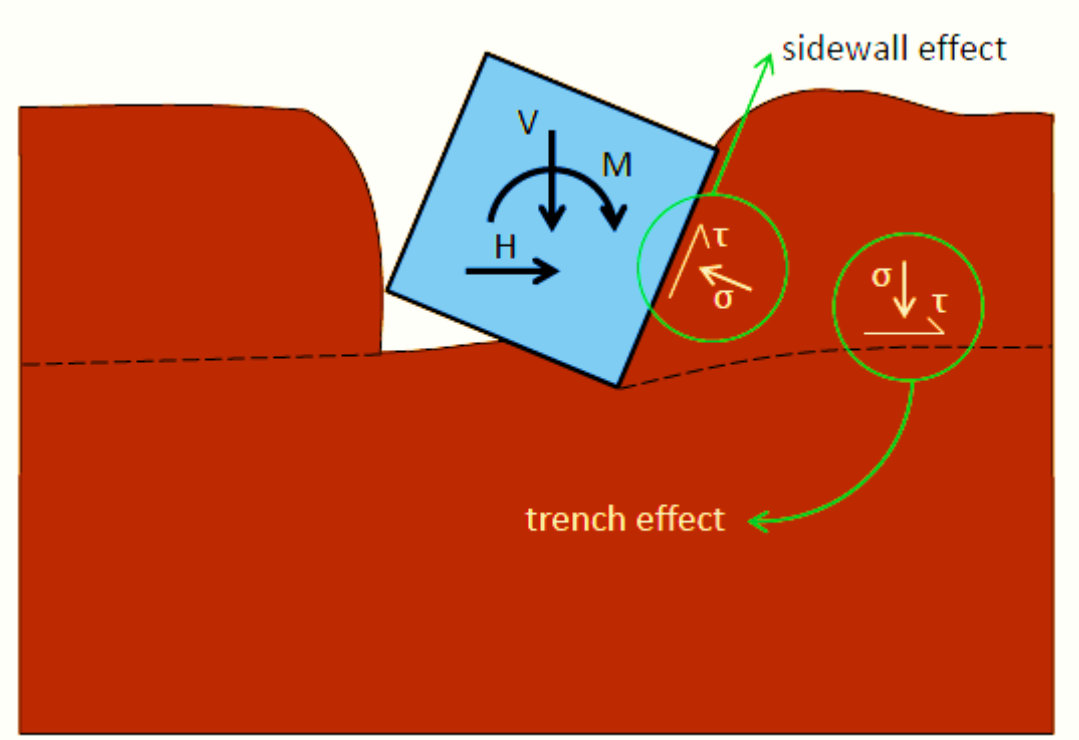

Fig.1.6. Trench and sidewall effect in the case of embedded foundations

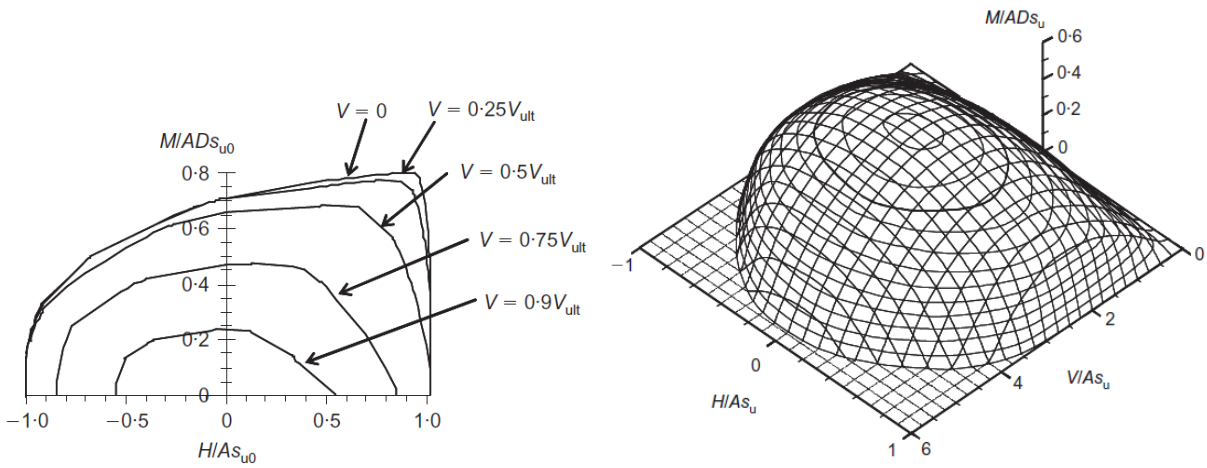

Fig.1.7. Examples of failure envelopes. *Left*: Failure envelopes in 2D space for circular skirted foundations in homogeneous soil under various vertical loads (Gourvenec, 2007). *Right*: 3D failure envelope for general loading of a circular surface foundation with a zero-tension soil-foundation interface in the case of uniform soil (Taiebat & Carter, 2002a)

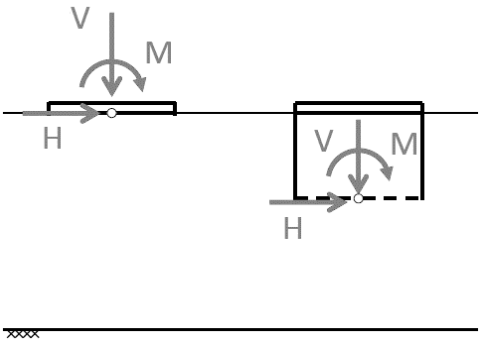

Fig.1.8. Sign convention (positive loads shown) and load reference points in most publications

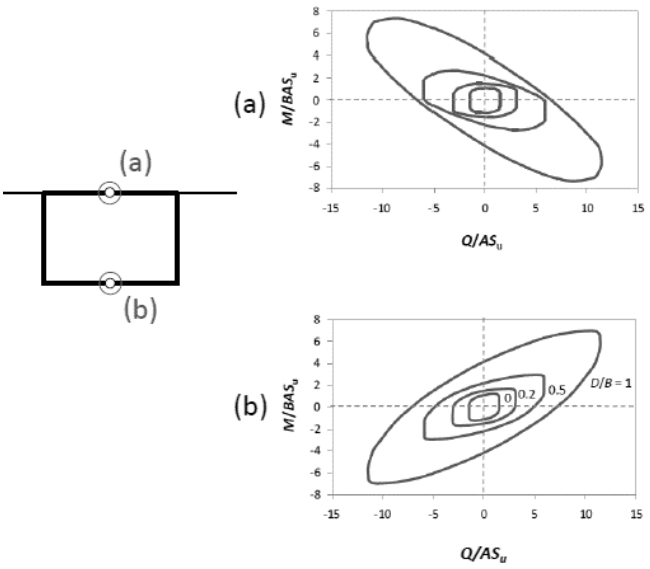

Fig.1.9. Influence of the load reference point position (Ntritsos, 2011)

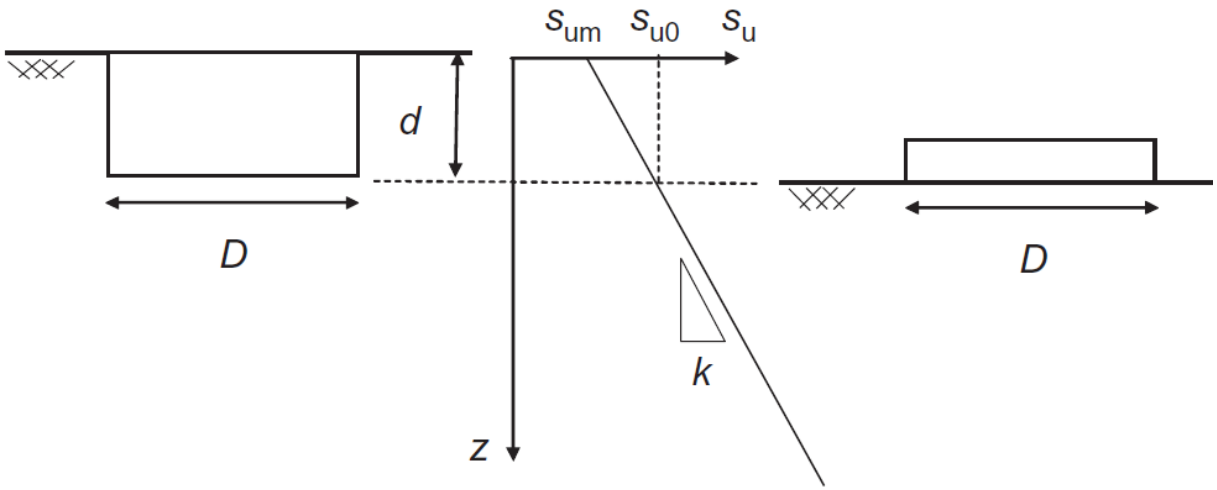

s_{um} = undrained shear strength at mudline

s_{u0} = undrained shear strength at foundation level = $s_{um} + kd$

Heterogeneity coefficient $\kappa = kD/s_{u0}$

Fig.1.10. Modelling of a skirted foundation as a surface footing with soil shear strength equal to that below the skirt tip level (Gourvenec, 2007)

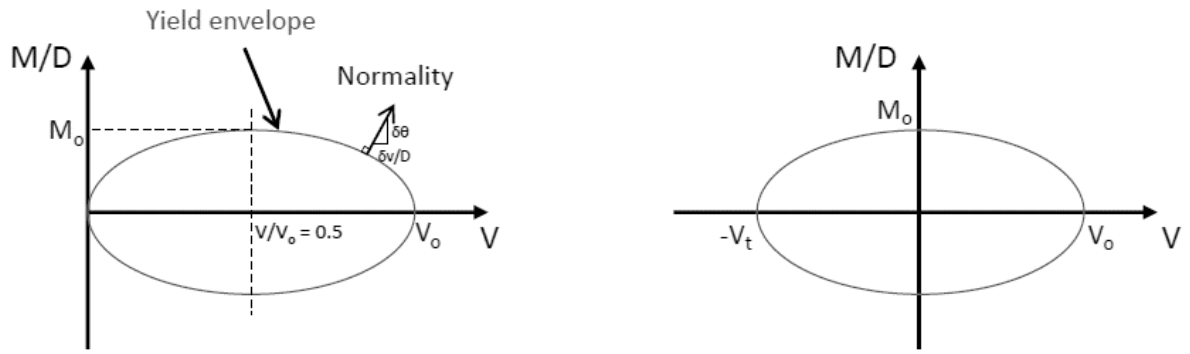

Fig.1.11. Yield envelope approach to combined loading of footings. Elliptical solution by Murff (1994). *Left*: zero tensile capacity; *Right*: tensile capacity equal to that in compression

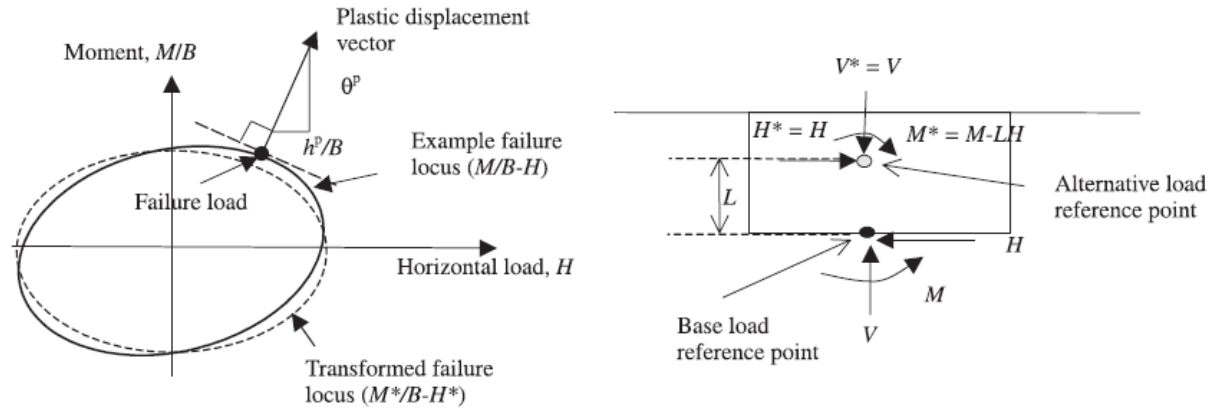

Fig.1.12. *Left*: Failure envelope with and without moment transformation. *Right*: Load equivalence for transformed load reference point (Yun & Bransby, 2007)

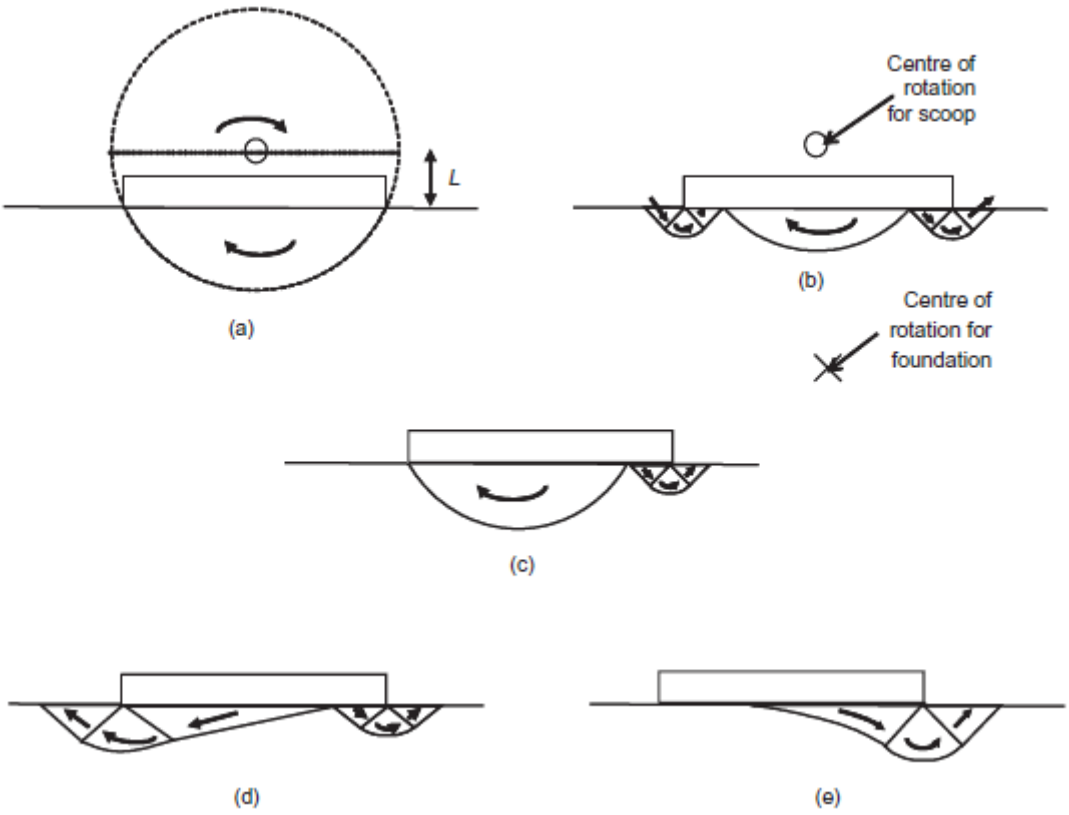

Fig.1.13. Failure mechanisms under general loading (Gourvenec, 2007): (a) scoop; (b) wedge-scoop-wedge; (c) scoop-wedge; (d) asymmetric wedge; (e) Brinch Hansen

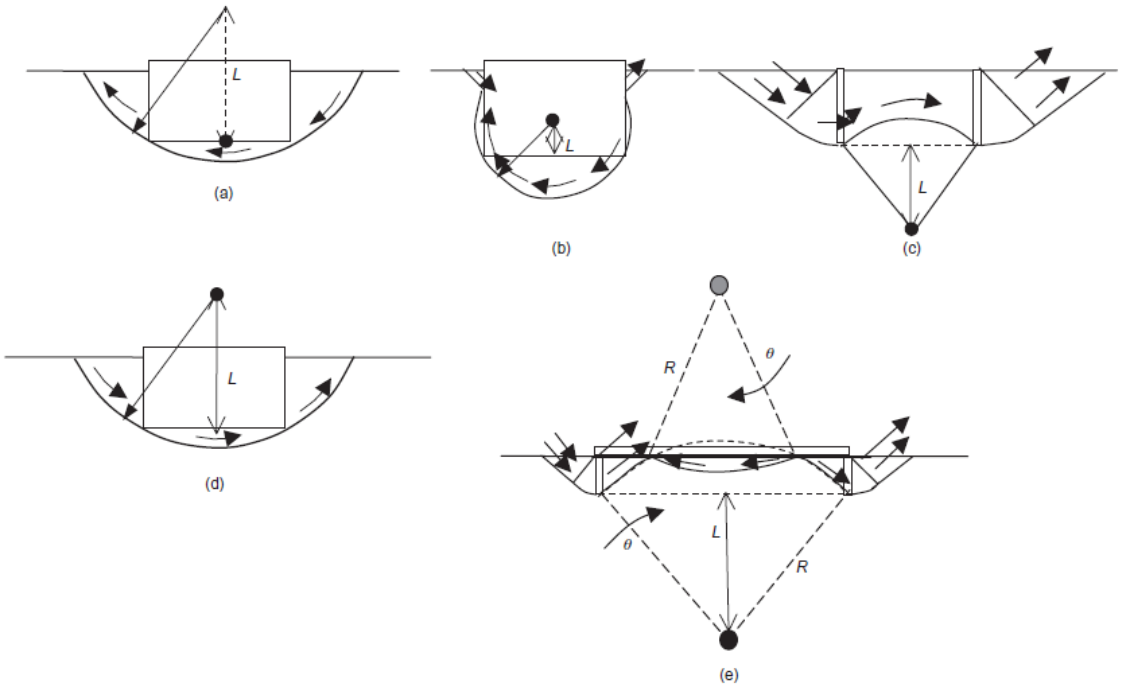

Fig.1.14. Failure mechanisms of skirted strip foundations under combined loading (Bransby & Yun, 2009): (a) forward scoop; (b) scoop-slide; (c) internal Hansen; (d) reverse scoop; (e) internal double scoop

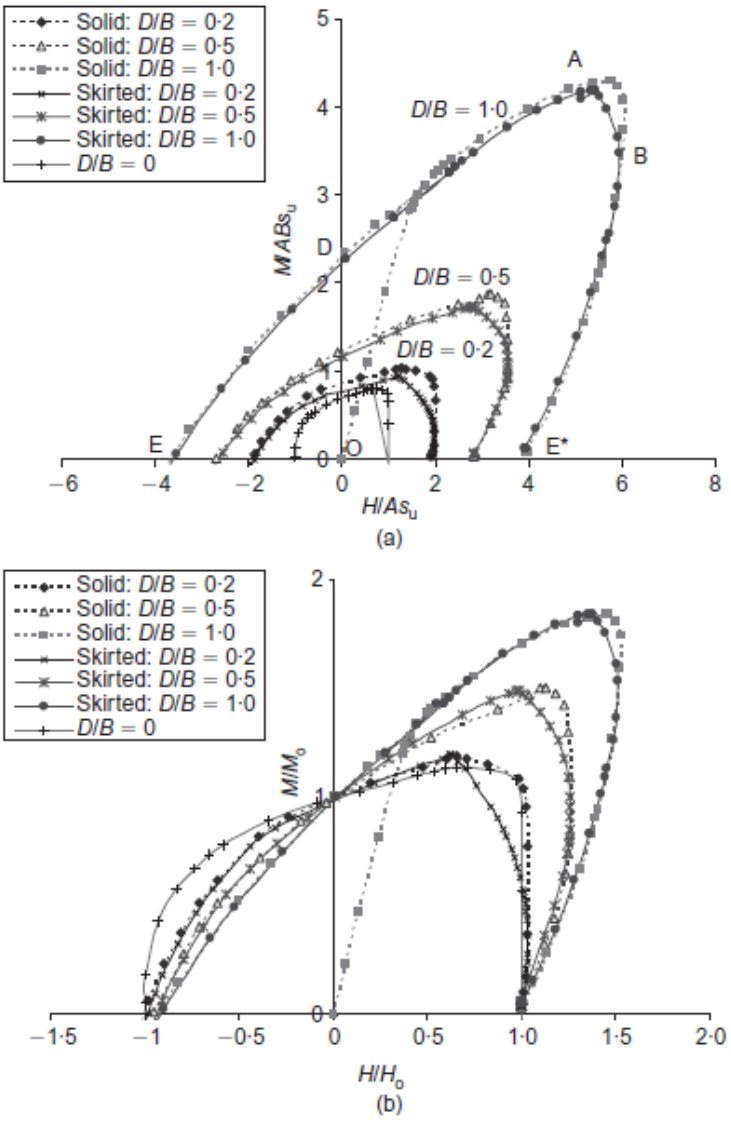

Fig.1.15. (a) Non-dimensional and (b) normalized failure envelopes in the HM space (V=0) for skirted and solid strip foundations (Bransby & Yun, 2009)

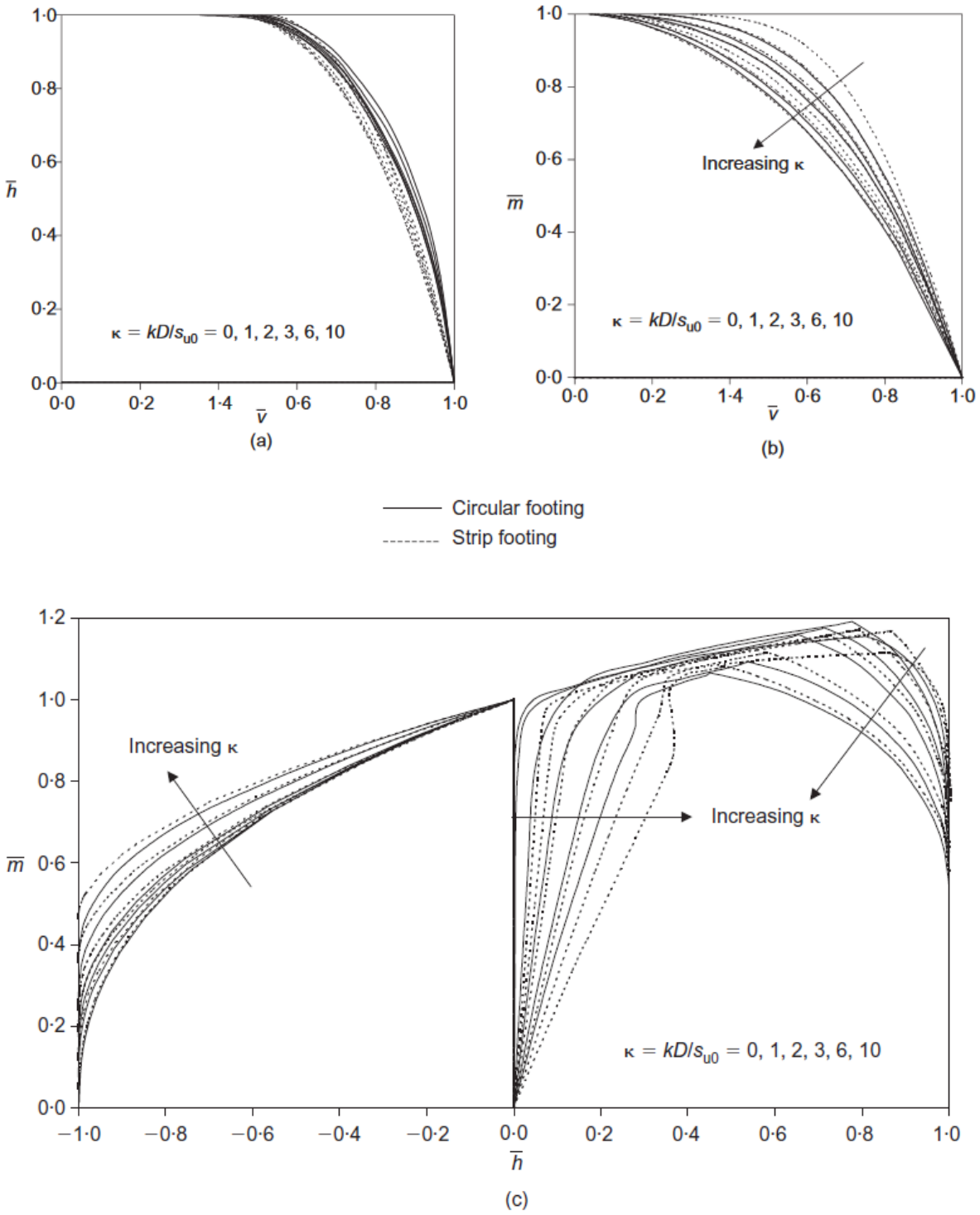

Fig.1.16. Failure envelopes for a variety of inhomogeneity rates kD/S_{u0} in normalized: (a) VH (M=0) plane; (b) VM (H=0) plane and (c) HM (V=0) plane (Gourvenec & Randolph, 2003)

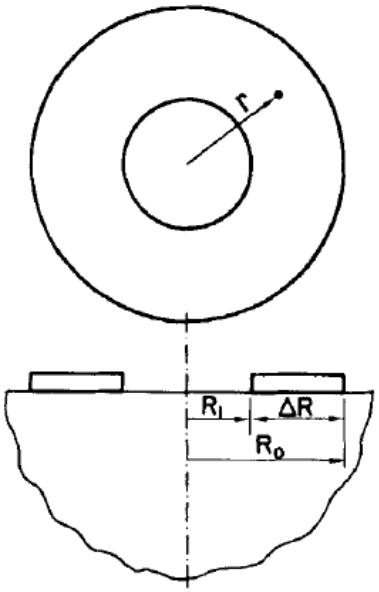

Fig.1.17. Ring foundation resting on homogeneous half-space (Veletsos & Tang, 1987)

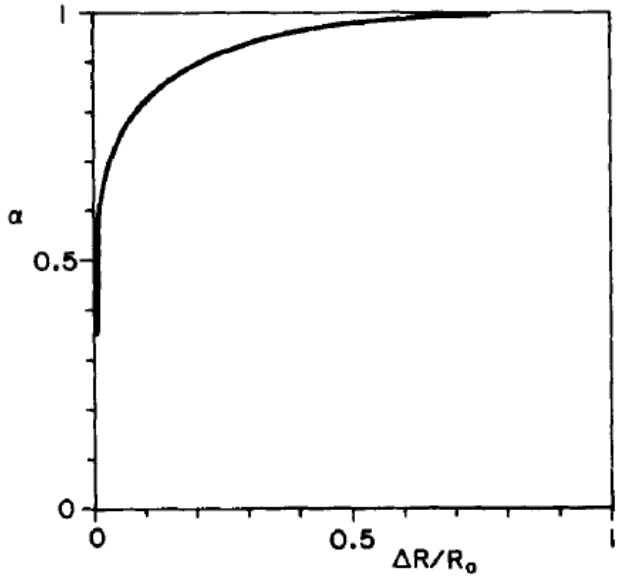

Fig.1.18. Vertical stiffness coefficient α as a function of $\Delta R/R_0$ (Veletsos & Tang, 1987)

$\Delta R/R_o$ (1)	α (2)	$\Delta R/R_o$ (3)	α (4)
0.01	0.5994	0.15	0.9035
0.015	0.6370	0.2	0.9394
0.02	0.6671	0.3	0.9710
0.03	0.7100	0.5	0.9945
0.05	0.7742	0.7	0.9970
0.10	0.8606	1.0	1.0

Fig.1.19. Variation of rocking stiffness coefficient α with $\Delta R/R_0$ (Veletsos & Tang, 1987)

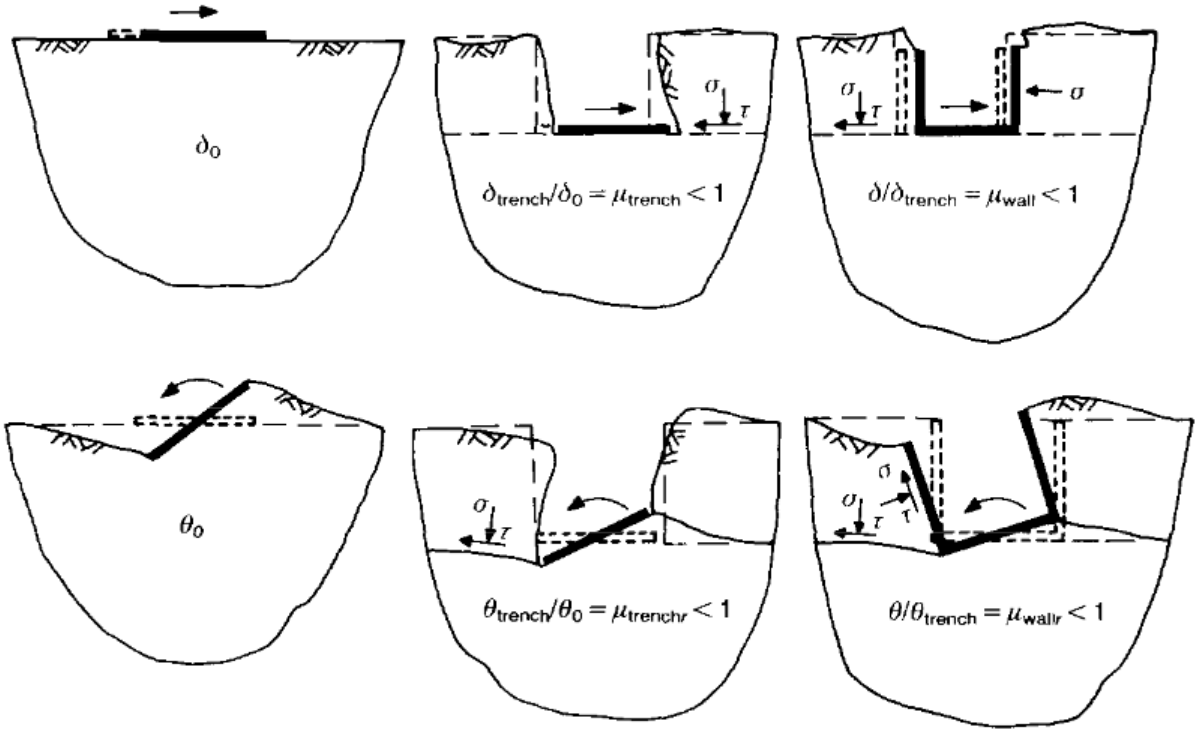

Fig.1.20. Trench and sidewall effects for horizontal and moment loading (Gazetas & Hatziconstantinou, 1988)

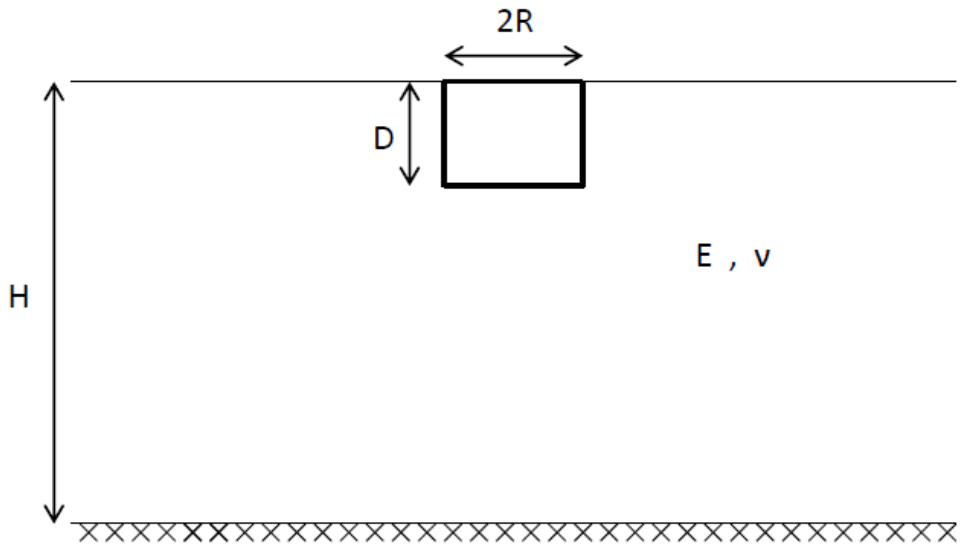

Fig.1.21. Embedded foundation in a soil stratum resting on bedrock

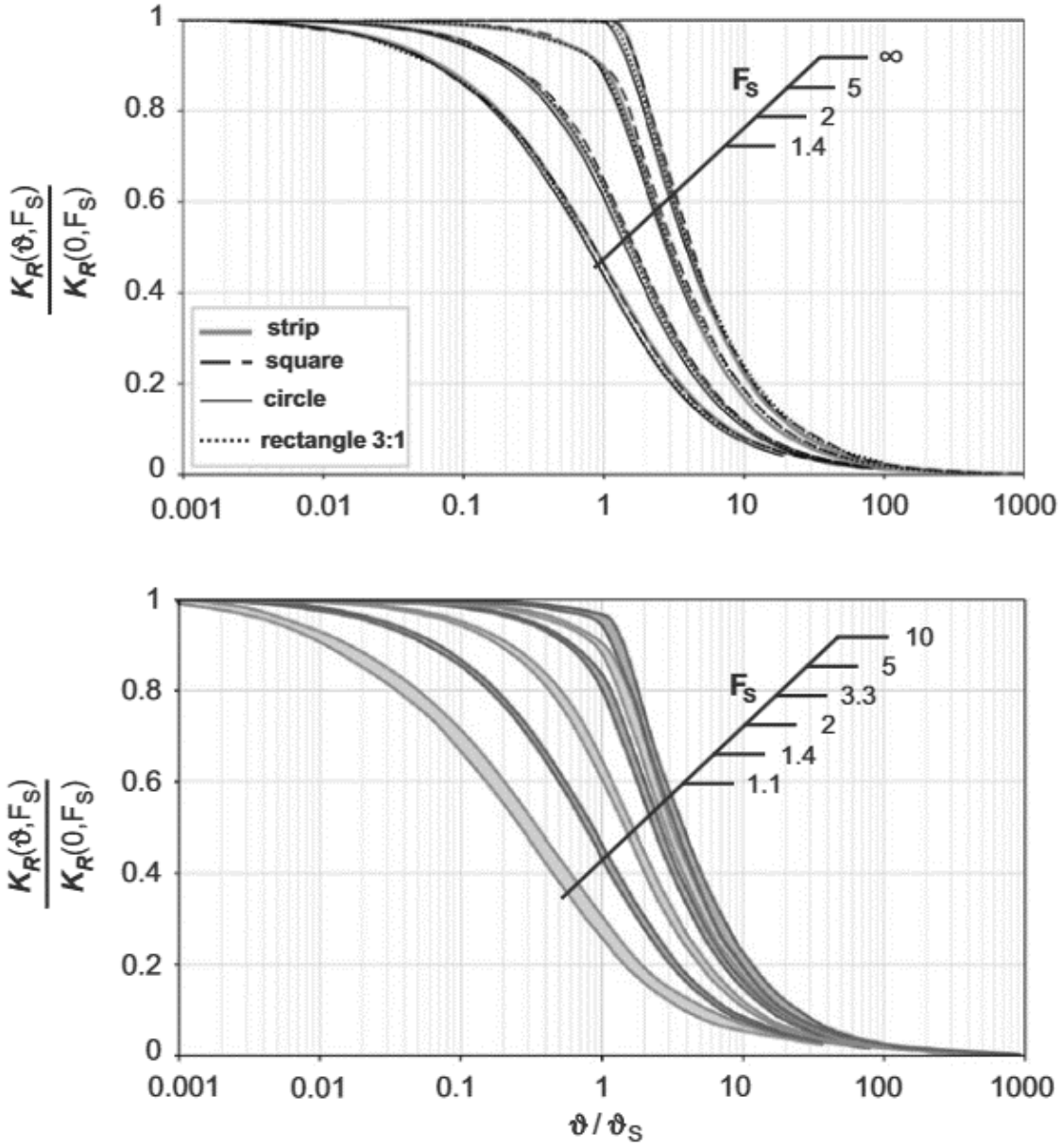

Fig.1.22. Normalized rocking stiffness as a function of angle of rotation normalized by characteristic angle θ_S for various safety factors *FS*. Top: Results for the various footing geometries. *Bottom*: Summarized results for various safety factors. (Gazetas et al. 2013)

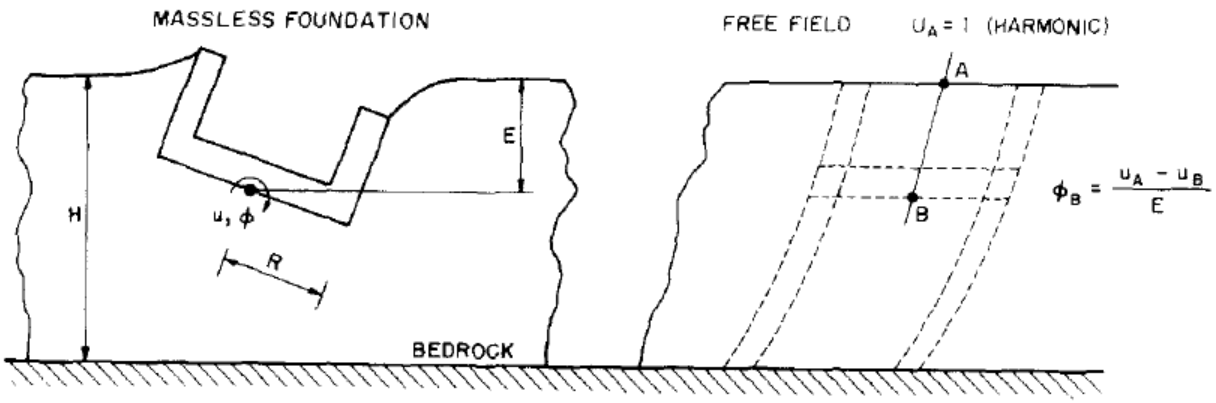

Fig.1.23. Kinematic Interaction problem in the case of an embedded foundation (Kausel et al. 1978)

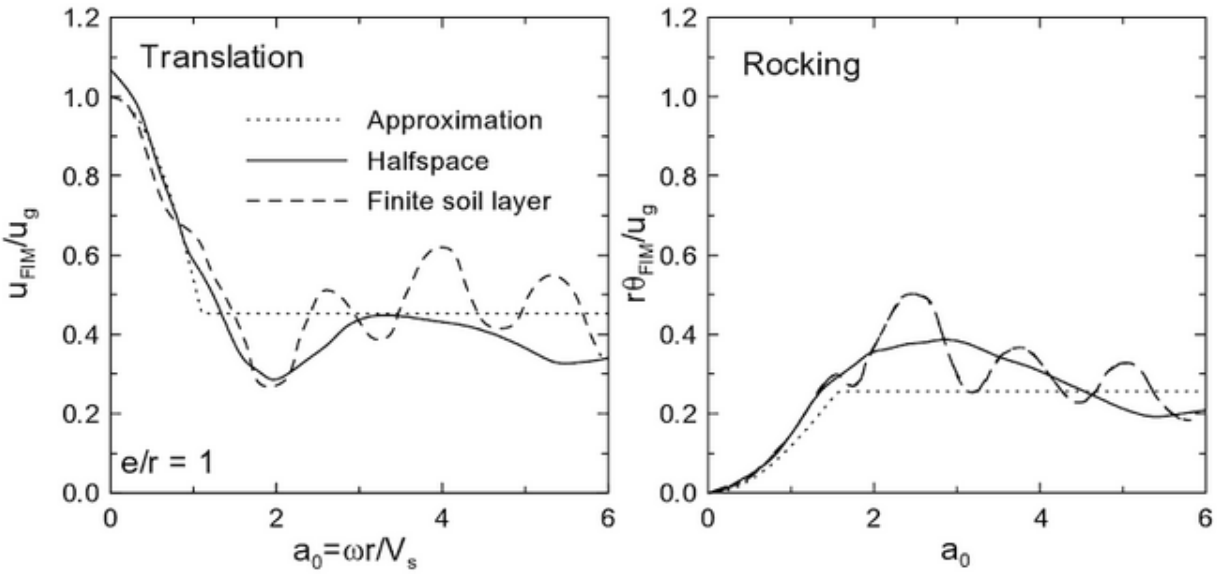

Fig.1.24. Transfer functions for an embedded cylindrical foundation of e/r=1 (Day, 1978; Elsabee and Morray, 1977)

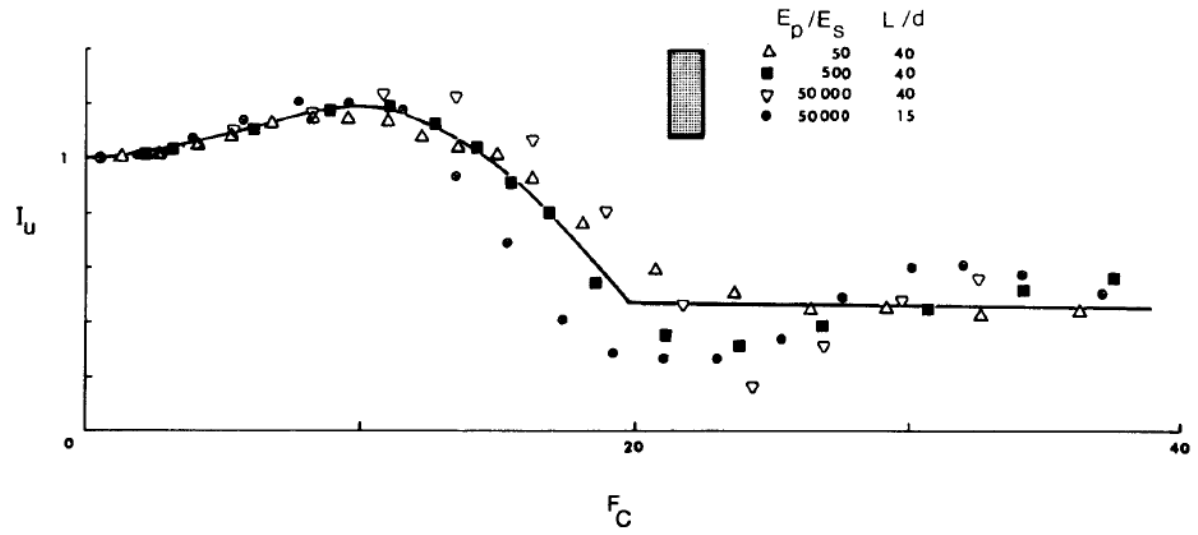

Fig.1.25. Kinematic interaction factor I_U in terms of dimensionless frequency parameter F_C for end-bearing piles in homogeneous soil deposit (Gazetas, 1984)

Chapter 2

Problem Definition & Model

2.1 Problem Definition

2.2 Model and Method of Analysis

2 Problem Definition & Model

2.1 Problem Definition

As has previously been underlined, the suction caisson is an alternative to the monopile, which is the up-to-date choice for the foundation of most shallow to medium depth offshore wind turbines.

In the past, the majority of publications on the response of skirted foundations considered full contact between the soil and the foundation, as well as the ability of the suction caisson to develop tensile capacity (Bransby & Randolph, 1998; Gourvenec & Randolph, 2003; Bransby & Yun, 2009). Moreover, in some studies, the skirted foundation has been modelled as a surface footing resting on a soil of shear strength equal to that below the skirt tip level, with the assumption that all loads are transferred to the base of the confined soil (Gourvenec & Randolph, 2003; Gourvenec, 2007). These hypotheses can be deemed reasonable, if the effect of suction created with installation is maintained during the lifetime of the wind turbine.

In reality, an offshore wind turbine is subjected to thousands of cycles in its lifetime due to wave loading. In an analytical study, Houlsby et al. (2005) proved that the development of tensile capacity is influenced to a large extent by the loading rate and the ambient water pressure. Thus, it seems understandable, that the effect of suction that originally developed during the installation of the suction caisson might have gradually dissipated.

For this purpose, it is of great significance to examine sliding and detachment of the skirted foundations from the soil under extreme loading conditions, such as storm surges and earthquakes, which activate the bearing capacity of the soil-foundation system. It needs to be stressed out, that the mobilization of such mechanisms in the soil does not necessarily lead to failure, due to the cyclic nature of these loading types and the kinematic nature of seismic loads. On the contrary, a new design philosophy allowing for uplift or detachment of the foundation from the soil (geometric nonlinearity) and mobilization of the bearing capacity of the soil (material nonlinearity) has been suggested as an alternative to the conventional design philosophy (FEMA 356, 2000). A lot of research has been conducted on the nonlinear-inelastic response of the soil-foundation system, showing that not only it is unavoidable, but it can also be favorable for the total protection of the structure (Pecker, 1998, 2003; Martin & Lam, 2000; Makris & Roussos, 2000; Faccioli et al., 2001; Kutter et al., 2003; Gazetas et al., 2003, 2007; Gajan et al., 2005; Paolucci et al., 2008; Kawashima et al., 2007; Gajan & Kutter, 2008; Anastasopoulos et al., 2010; Gelagoti, 2012).

Despite the fact that a lot of research has been carried out on the nonlinear response of surface foundations (Taylor et al., 1981; Butterfield & Gottardi, 1994; Faccioli et al., 2001; Gajan et al., 2005; Allotey & Naggar, 2003, 2008; Pender, 2007; Gajan & Kutter, 2008), skirted foundations

have only recently started receiving important attention and in most studies they are assumed to be welded to the ground, without second order effects taken into account.

The scope of this study is to investigate the viability of skirted foundations for offshore wind turbines. For all the cases examined herein, the response of the suction caisson is effectively compared to that of its sidewalls (skirts) alone, in order to assess the role of the latter in the overall response of the system, gain deeper insight into the mechanics of the problem, and if possible, even utilize it as a hybrid foundation. Chapter 3 is based on the first series of analyses for the determination of the bearing capacity of the circular skirted foundation for embedment depth to radius ratios: L/a=0.5, 1 and 2 in undrained conditions. The foundation rests on a soil stratum of clay with uniform shear strength, as can be seen in **Figure 2.1**, which also depicts the geometry of the problem. The second part of the study, found in Chapter 4, is separated in two parts. The first one involves the assessment of the elastic, static stiffness of the suction caisson and the skirts alone in a homogeneous soil, as well as in a Gibson type soil, where the Young Modulus of soil increases linearly with depth *z* from the surface, with a gradient *k*, in a manner of E=*k*z. For the first part specifically, analyses were performed for a range of 0.02÷2 embedment ratios L/a. The second part regards the nonlinear stiffness of the soil-foundation system, which is useful for design purposes (Gazetas et al., 2013). Finally, in Chapter 5 is presented the kinematic response of the L/a=2 suction caisson and skirts alone to modified Gabor pulses, as well as to recorded earthquake motions. In order to quantify the effects of kinematic interaction, appropriate transfer functions that relate the motion of the foundation to that of the free-field, as well as dynamic earth pressures on the sidewalls of the foundation are calculated.

2.2 Model and Method of Analysis

2.2.1 Finite Element Model

The analyses for the investigation of the problem were performed in three-dimensional space with the finite element code ABAQUS, v. 6.13 (2013). Only half of the soil and foundation was modelled since the problem is symmetrical. **Figure 2.2** illustrates the mesh created for the analysis.

The soil body is simulated using 8-node hexahedral continuum elements (C3D8), with a constitutive model that is described in section 2.2.3. The soil submerged specific weight is selected as γ'=10 kN/m^3. For the analyses in Chapter 3, the undrained shear strength of the soil is taken equal to S_u=80 kPa, uniform with depth (**Figure 2.3**) and the Young Modulus of soil over undrained shear strength ratio is selected as E/S_u=2000. The dynamic analyses were performed in undrained conditions for E=240 MPa, hysteretic damping ratio ξ=5% and shear wave velocity V_S=200 m/s. Details can be also found in the respective chapters.

For the modelling of the skirted foundation, linear elastic shell elements (S4) are used. As far as the parameters for the steel are concerned, density is taken at ρ_S=7.85 t/m^3, whereas two values of Young Modulus are examined: 210 GPa and 21000 GPa. The former is the common value for steel, whereas the latter is used to model the whole foundation as rigid. The thickness of the sidewalls is chosen as t_S=0.02 m, which is considered reasonable (Bransby & Yun, 2009), whereas the thickness of the lid is equal to t_L=0.5 m; a value that is sufficient to make it behave as practically rigid, given the high value of Young Modulus for steel. **Figure 2.4** illustrates the models of the two foundation types addressed in this thesis: the suction caisson and the skirts alone.

The semi-cylindrical mesh is divided into 20 sectors. The number of elements in the interface between the soil and the skirts is totally 20 x 20 for L/a=2 and is modified for the smaller ratios accordingly. The number of elements for the lid, as well as for the top area of the model, is kept constant for all embedment ratios in all simulations. Right next to the foundation, moving outwards, a finer mesh consisting of 4 finite element (FE) layers is created in order to reduce numerical inaccuracies and overestimated strength of the soil FE due to element size and the response of the soil as a continuum. Without compromising the accuracy of results, farther from the foundation, the mesh becomes coarser for purposes of computational convenience.

Due to the semi-cylindrical geometry of the model, in polar coordinates its radius and height are equal to 3*D*, where *D* is the foundation diameter. The boundary conditions imposed at the edges of the model are constraint of horizontal displacement towards any direction for the nodes at the periphery faces of the model and constraint of out-of-plane movement for the nodes on the face of symmetry. Additionally, the nodes at the bottom of the model are restricted for any displacement.

For the investigation of the dynamic response of the system, it was necessary to remove the boundary conditions on the periphery. The peripheral nodes at every height were tied together so that the motion of the model is close to that of a shear beam, which is a situation similar to that in a laminar box. In that way, the free-field is modelled properly and the excitation is well imposed at the base of the soil stratum.

Apart from the consideration of Fully Bonded Contact (FBC) between the foundation and the supporting soil, a Tensionless Sliding Interface (TSI) is assumed in the analyses for the determination of the bearing capacity and the nonlinear stiffness of the system. With respect to a more realistic simulation of the contact conditions between the foundation and the soil, a tensionless contact algorithm is applied to interface elements. In specific, these elements connect the nodes of the foundation to the respective nodes of the soil with the same coordinates, with which they are initially in contact. Progressively, depending on the loading conditions, the foundation may slide or even detach from the soil. In order to achieve a reasonably stable time increment and at the same time retain the accuracy of the results, an appropriate exponential pressure-overclosure relationship was implemented in ABAQUS, which defines the response of the interface in the normal direction. Regarding the behavior of the interface in the tangential direction, the maximum shear stress that can be developed is defined as $\tau=\alpha S_u$, where reduction factor α is taken as 1 for the lid-internal soil interface, accounting for

the self-weight of the lid and as 0.5 for the sidewalls-soil interface, both internally and externally.

2.2.2. Sign Convention

The sign convention followed in this study is depicted in **Figure 2.1**. Moreover, the location of the load-reference point can be seen, which is on the centerline at the top of the foundation.

2.2.3 Soil Constitutive Model

The Von Mises failure criterion is assumed with a nonlinear kinematic yield law and associated flow rule. It is a constitutive model that is considered capable to model the plastic behavior of clay in undrained conditions, which is considered independent of the mean effective stress.

According to the Von Mises yield criterion, the evolution of stresses is described as follows:

$$\sigma = \sigma_0 + \alpha \tag{2.1}$$

where σ_0 is the constant value of stress at zero plastic strain and α the kinematic hardening component that defines the evolution of the yield surface in the stress space.

The following function F defines the stress-independent yield surface:

$$F = f(\sigma - \alpha) - \sigma_0 \tag{2.2}$$

With an assumed associated plastic flow, the plastic flow rate is given by:

$$\dot{\varepsilon}^{pl} = \dot{\bar{\varepsilon}}^{pl} \frac{\partial F}{\partial \sigma} \tag{2.3}$$

where $\dot{\varepsilon}^{pl}$ is the equivalent rate of plastic strain.

The stress evolution law involves two components:

a) An isotropic hardening law, which describes the change of the equivalent stress, defining the size of the yield surface as a function of plastic strain:

$$\sigma_o = \sigma_0 + Q_\infty \left(1 - e^{-b\bar{\varepsilon}^{pl}}\right) \tag{2.4}$$

where Q_∞ the maximum change of the size of the yield surface and b the rate of this change with the equivalent rate of plastic strain. For Q_∞=0, the size of the yield surface remains the same and the constitutive model is reduced to a nonlinear kinematic hardening model.

b) A nonlinear hardening law that describes the evolution of the yield surface in the stress field (defined by the parameter α). The kinematic hardening law is defined as a superposition of an exclusively kinematic term (Ziegler linear hardening law) and a softening term, which introduces the nonlinear behavior. The evolution of the kinematic component of the yield stress is expressed as:

$$\dot{a} = C\frac{1}{\sigma_o}(\sigma - \alpha)\dot{\bar{\varepsilon}}^{pl} - \gamma\alpha\dot{\bar{\varepsilon}}^{pl} \quad (2.5)$$

where C the initial kinematic hardening modulus ($C=\sigma_y/\varepsilon_y=E$) and γ the rate of decrease in kinematic hardening with the increase of plastic strain.

The evolution of the kinematic and isotropic hardening components is depicted in **Figure 2.5** for uniaxial and combined loading. The stress evolution law for the kinematic hardening component infers that the parameter α is included in a cylinder with radius:

$$\sqrt{\frac{2}{3}a^s} = \sqrt{\frac{2}{3}}\frac{C}{\gamma} \quad (2.6)$$

where α^S the value of α at saturation. Due to the fact that the yield surface remains bounded, it can be deduced that any stress point must be within a cylinder of radius √⅔ σ_y, where σ_y the yield stress. Accordingly, for large plastic strains, any stress point must be within a cylinder of radius √⅔ ($\sigma^S+\alpha^S$), where σ^S the equivalent stress defining the size of the yield surface for large plastic strains.

The maximum yield stress for a saturated soil is:

$$\sigma_y = \frac{C}{\gamma} + \sigma_o \quad (2.7)$$

Moreover, according to the Von Mises yield criterion, the maximum stress is equal to:

$$\sigma_y = \sqrt{3}\,S_u \quad (2.8)$$

Thus, from (2.7) and (2.8):

$$\gamma = \frac{C}{\sqrt{3}\,S_u - \sigma_o} \quad (2.9)$$

2.2.4 Model Validation

The Von Mises constitutive model has been validated against physical model tests (centrifuge, 1g and large-scale) for: (a) surface and embedded foundations under cyclic loading and seismic shaking (Anastasopoulos et al., 2011, 2012); (b) piles under cyclic loading (Giannakos et al., 2012); (c) bar-mat retaining walls under seismic excitation (Anastasopoulos et al., 2010).

Chapter 2: Figures

Problem Definition & Model

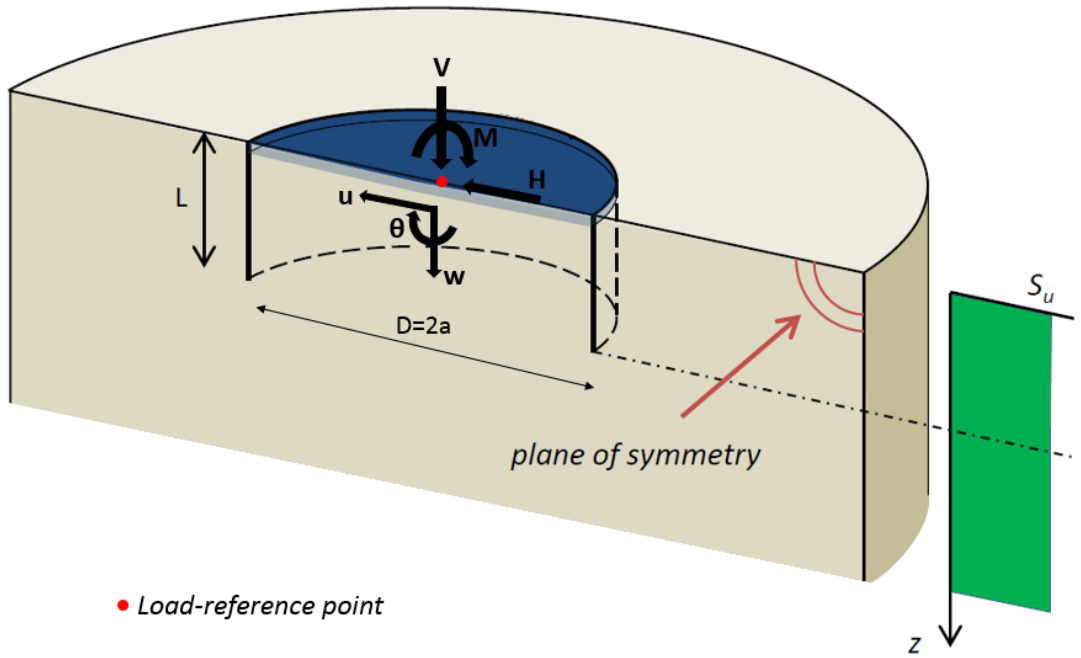

Fig.2.1. Geometry of the problem and sign convention

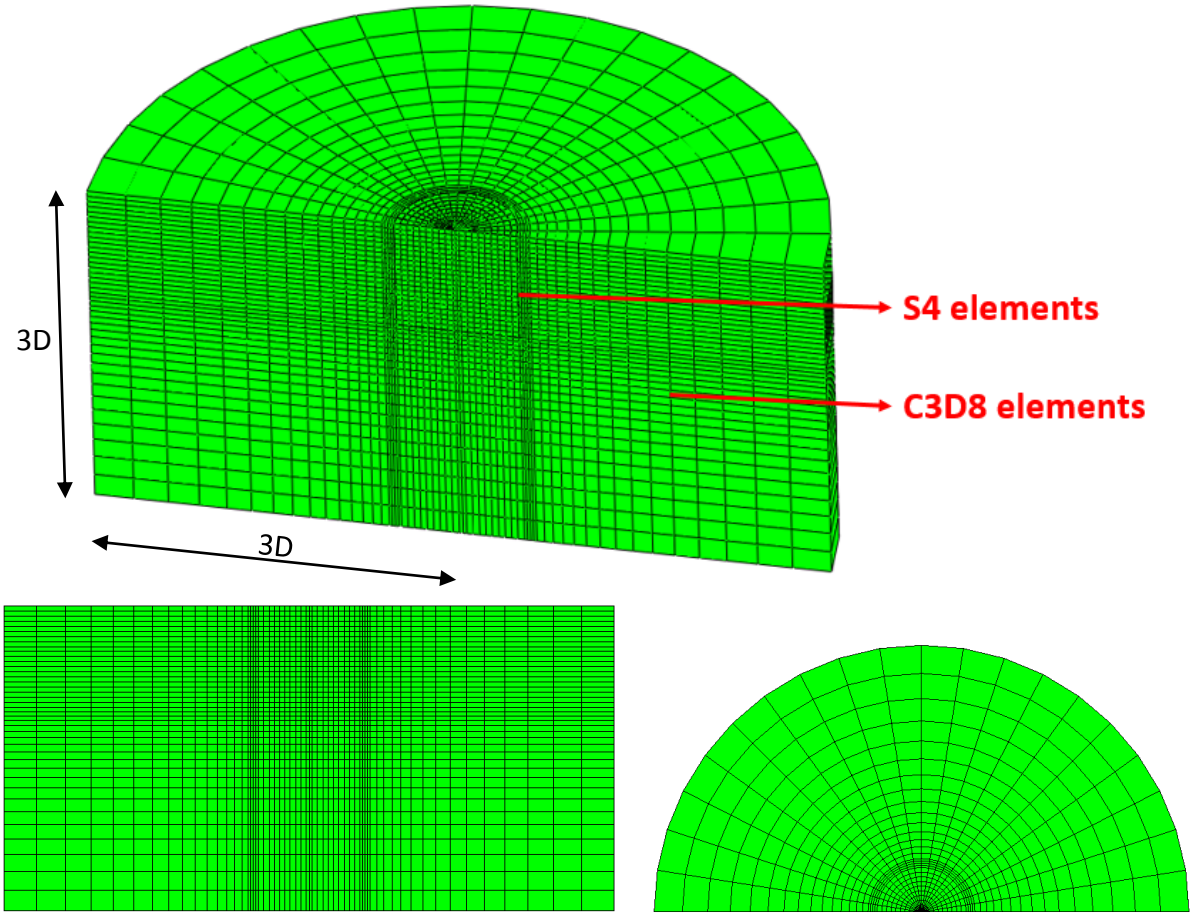

Fig.2.2. 3-D finite element mesh (ABAQUS) of the problem for embedment ratio L/a=2: *Top*: Perspective; *Bottom*: Model face at plane of symmetry (*left*) and top view (*right*)

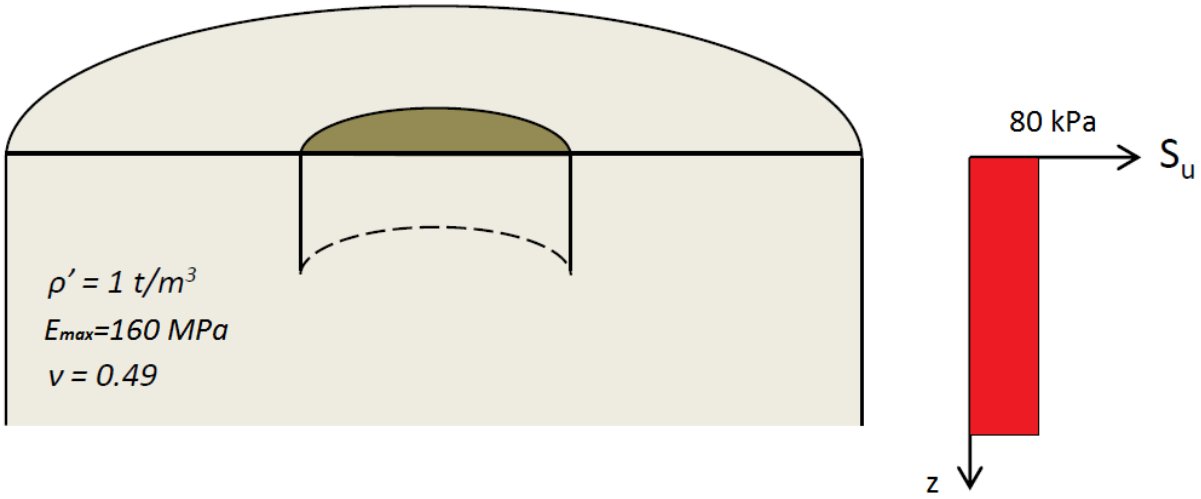

Fig.2.3. Soil characteristics and shear strength profile for the analyses in Chapter 3

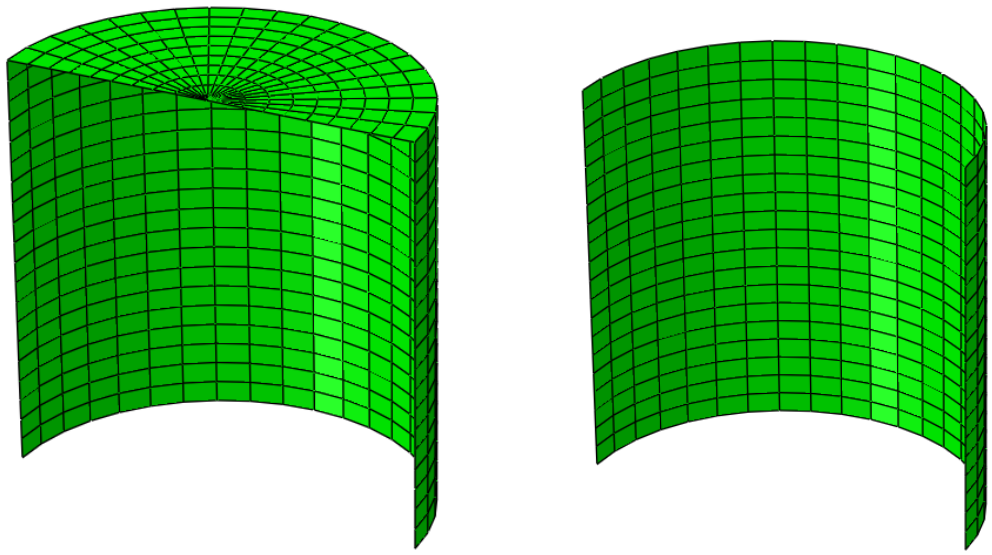

Fig.2.4. Modelling with S4 elements of the suction caisson (*left*) and the skirts alone (*right*)

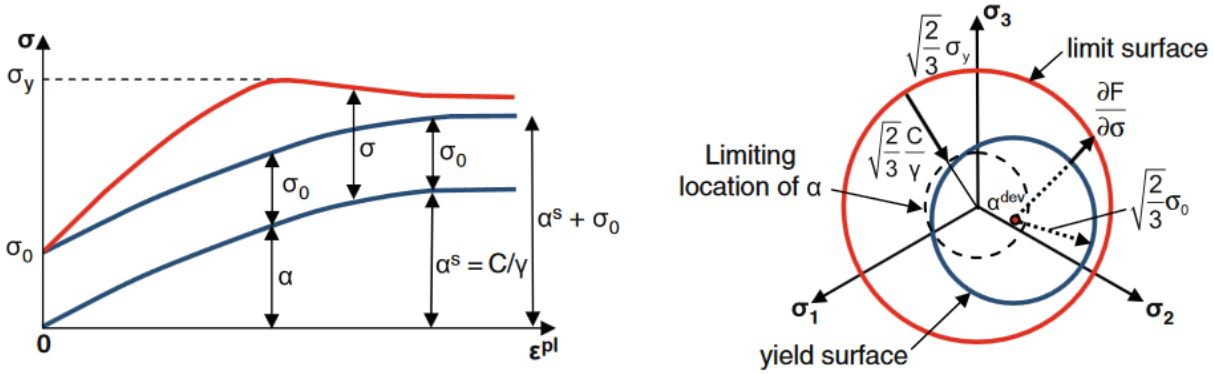

Fig.2.5. Von Mises constitutive model: evolution of the kinematic and isotropic hardening components: (a) Simplified 1-D presentation and (b) 3-D presentation (Anastasopoulos et al., 2010)

Chapter 3

Bearing Capacity

3.1 Preface

3.2 Assumption of Fully Bonded Contact (FBC)

3.3 Assumption of Tensionless Sliding Interface (TSI)

3.4 Conclusions

3 Bearing Capacity

3.1 Preface

Being one of the most important subjects of Geotechnical Engineering, the bearing capacity of the soil-foundation system indicates the safety with which, loads acting on the superstructure are transferred to the foundation and subsequently to the underlying soil. Excess of the bearing capacity has different results under static and dynamic loading. Apparently, for static conditions, the whole system will be led to failure with consequences such as undesirable settlement and/or rotation, detachment, overturn, etc. On the contrary, reaching the bearing capacity under dynamic loading, such as seismic loading, does not necessarily imply failure of the system thanks to the cyclic and kinematic nature of the excitation.

Depending on the type of the superstructure, and of course on the source and nature of loading, loads that are transferred to the foundation differ. Vertical loading is the most critical for typical structures. However, in the case of offshore wind turbines, which are subjected to disproportional horizontal and moment loading, these effects need to be properly considered in the design of the foundation.

The bearing capacity of various foundation types and soil conditions has been thoroughly researched in the past. As far as the suction caisson is concerned, it was until recently modeled as a surface foundation [Bransby & Randolph, 1998; Gourvenec, 2007] or along with the skirts in plane strain conditions [Bransby & Yun, 2009]. In the majority of cases, full contact is established between the foundation and the surrounding soil, permitting no detachment or uplift.

In this study, a 3D half-geometry of the suction caisson and the skirts alone is used in order to assess their bearing capacity and compare it with already published solutions. Two types of interface between the foundation and the surrounding soil were investigated: (*a*) Fully Bonded Contact (FBC) that implies infinite tensile capacity allowing thus for no detachment, sliding or uplift and (*b*) a Tensionless Sliding Interface (TSI) with reduced maximum shear strength $\tau=\alpha S_u$, where factor α is taken 1 (accounting for the influence of the self-weight of the lid) for the interface between the lid and the soil plug and 0.5 between the sidewalls and the soil, both internally and externally (**Figure 3.1**).

Due to the process of the suction caisson's installation, suction is supposed to be maintained in the interior of the skirted foundation, at least for a period of time. Consequently, the assumption of exclusively exterior interfaces, while considering full contact between the soil plug, the lid and the skirts, would be reasonable. However, TSI is introduced in this study internally too, not only for conservative purposes, but also to effectively compare the response of the suction caisson to the skirts alone, since for the latter the effect of suction cannot be speculated. Defining nonlinearities at the interfaces is significant in the static and dynamic

response of embedded foundations [Gerolymos & Gazetas, 2006], since their appearance is inevitable during strong seismic motions.

Two factors contribute to the increased bearing capacity and stiffness of embedded against surface foundations: (*a*) the **trench effect** and (*b*) the **sidewall effect**. The trench effect can be described as follows: in the case of an embedded foundation, the overlying soil due to its weight imposes normal and shear stresses on the level of the embedment, restricting thus the deformation of the soil on that level (it can be assumed that it lies on the level of the skirt tips in the case of a skirted foundation). On the contrary, a free surface, which a foundation lies on, can be freely deformed in absence of external stresses. The sidewall effect regards the transmission of the imposed load with normal and shear stresses, which are developed on the sidewalls of an embedded foundation, mobilizing thus the strength of a larger area of the supporting soil. The aforementioned mechanisms of the trench and the sidewall effect are presented in **Figure 3.2**.

In order to calculate the bearing capacity of embedded foundations, displacements and rotations are conventionally applied at the base of the foundation. However, for the suction caisson, loads deriving from waves, wind and currents are transferred from the tower to the top of the foundation. In case the latter separates from the soil, there may be an alternation in the amount of loading transmitted to the base. Subsequently, the displacement reference point is chosen at the center of the top circular surface of the foundation instead of the skirt tip level.

The Von Mises constitutive model with a ratio of E_{max}/S_u=2000 was used for the analyses. A homogeneous soil profile of constant undrained shear strength S_u=80 kPa was examined. Both the suction caisson and the skirts alone were investigated for embedment depth to radius ratios (L/a) 0.5, 1 and 2. The thickness of the sidewalls is taken as t=0.02 m. The two foundation types were examined for Es=210 GPa and Es=21000 GPa. Therefore, the former will be referred to as "Es,t" foundation, due to the conventional parameters used for its modelling, while the latter as rigid. Emphasis is placed on the rigid foundation, on the one hand due to the convenience in comprehension of its response, without the flexibility of the skirts interfering, and on the other, to assess the influence of the increase in the Young Modulus of steel. All the cases are presented in **Table 3.1**.

Undrained Shear Strength Profile	**S_{um} (kPa)**	**E_{max}/S_u**	**Interface Conditions**	**L/a**	**E_S (GPa)**
Uniform	80	2000	FBC, TSI	0.5,1,2	210,21000

Table 3.1. Parameters in the analyses for the determination of the bearing capacity

3.2 Assumption of Fully Bonded Contact (FBC)

3.2.1 Capacity in Vertical Loading

Being representative of the governing loading condition of the structure due to its self-weight, the bearing capacity in vertical loading has been vastly investigated. The calculation of the vertical bearing capacity of the foundation is achieved by imposition of vertical displacement *w* at the load reference point until failure.

Dimensionless load-displacement curves are provided for the three embedment ratios L/a=0.5, 1, 2 for the suction caisson and the skirts alone. **Figure 3.3** presents the results in the case of the rigid foundation. The vertical bearing capacity is normalized by the area of the lid A and the undrained shear strength S_u.

As can be seen, the bearing capacity and the stiffness of the foundation increases with embedment ratio. Furthermore, for deeper embedment, larger displacements need to be imposed in order to fully mobilize the bearing capacity. Certainly, these observations apply to the suction caisson and the skirts alone. For the same embedment ratio, it is apparent that in the case of the skirts alone, smaller displacements relatively to the suction caisson need to be imposed in order for the system to reach the bearing capacity. The difference between the vertical bearing capacity of the suction caisson and of the skirts alone is approximately 25% for the L/a=2, reaching about 60% for the L/a=0.5. The mechanisms that contribute to these differences will be analyzed further.

Figure 3.4 illustrates the vertical bearing capacity of the foundation with the actual Es, t. From the comparison with the rigid one, there are no differences to be seen. Under vertical loading, the increase from 210 to 21000 GPa in the Young Modulus of steel does not affect the response of the foundation-soil system.

Figure 3.5 presents the failure mechanisms and the contours of the plastic strains for the rigid foundation. First of all, in the case of the suction caisson, failure mechanisms differ from the typical ones suggested by Prandtl (1921) and Terzaghi (1943), forming a central wedge. However, the latter refer to plane strain conditions. Heaving of the surrounding soil for the L/a=0.5 foundation is limited, whereas for the L/a=2 does not exist, due to the influence of embedment and the weight of the overlying soil. Additionally, full shear strength is mobilized along the sidewalls, with their contribution quantified at πLDS_u. Nevertheless, the suction caisson resists to vertical displacements not only by deployment of shear stresses along the external side of its sidewalls, but also by mobilization of normal stresses due to the existence of its lid. However, these normal stresses do not develop directly below the lid, but at the skirt tip level. Finally, the soil plug does not yield, so it can be deduced that the response of the suction caisson is approximately the same to that of a solid embedded foundation. As far as the skirts alone are concerned, their resistance mechanism to imposed vertical loading consists mainly of shear stresses that develop along the sidewalls, both externally and internally. Subsequently,

the resultant resistance force is approximately $2\pi LDS_u$. In the case of the skirts under vertical loading, despite the fact that the plastic deformations of the soil plug are inevitable, they are concentrated in the area of the sidewalls.

Failure mechanisms along with displacement vectors are provided for the L/a=2 and 0.5 rigid suction caisson in **Figure 3.6**. The formation of the central wedge below the skirt tip level is more intense for the small embedment ratio. Furthermore, for the L/a=0.5 suction caisson wedges are seen more clearly at the skirt tips. The most important conclusion is that the soil plug behaves elastically, thus the hypothesis that the vertical load is transmitted to the skirt tip level is confirmed once again, at least for FBC conditions.

In **Figure 3.7** a comparison is presented between the numerical results of the vertical bearing capacity and the classic solutions (conventional approach or CA). Details about these solutions can be found in Chapter 1.

As far as the suction caisson is concerned, the dimensionless vertical bearing capacity factor is taken for a circular surface footing 6.05 [Martin, 2001]. Embedment is taken into account with the use of depth factor d_C, as proposed by Bransby & Randolph [1999]. There is satisfying agreement between the numerical results of this study and the theoretical solution, especially at small embedment ratios. The maximum difference reaches only 6.7%, with the numerical results generally exceeding the CA estimates.

Finally, the vertical bearing capacity of the skirts alone is compared with the theoretical solution, which takes into consideration the mobilization of the undrained shear strength along the sidewalls, both on the internal and the external side, with the resultant force being approximately equal to $2\pi LDS_u$, as stated previously. The results differ by 15% and 36%, for the L/a=2 and 0.5 skirts respectively. This difference is reasonable, since the normal stresses that develop under the skirt tip surface are not taken into account in the theoretical calculation. Increasing the embedment ratio leads the skirts to resist to the imposed vertical loading by developing mainly shear stresses along the sidewalls. If the skirt length is reduced, since there is not adequate area for the shear stress mechanism to fully resist the vertical loading, normal stresses develop under the surface of the skirt tip, as well as under the soil plug. In addition, the results of the skirts alone are compared to the corresponding of the suction caisson, with differences ranging from 25% to 60%, as embedment ratio declines.

3.2.2 Capacity in Horizontal Loading

In the case of offshore wind turbines, where lateral loading is critical, as well as in the seismic response of structures, the determination of the horizontal bearing capacity of the foundation-soil system is of great significance.

Under lateral (and moment) loading, there is an appearance of coupling between the horizontal and rotational degree of freedom, as embedment increases. This coupling is a result of active and passive stresses acting on the sidewalls, which in combination with the lateral force on the foundation, cause it to not only to translate, but to rotate too. However, if the rotational degree of freedom is not restricted, the imposed lateral loading does not lead to the maximum horizontal force that the foundation can develop. In order to fully mobilize the maximum horizontal bearing capacity of the embedded foundation, the rotation needs to be restricted, consequently leading to the development of a non-zero moment acting on the foundation. An investigation of the maximum horizontal force H_{max} that the foundation can develop, given that the rotation is restricted, is presented in this section. For the calculation of H_{max}, horizontal displacement *u* is imposed on the load-reference point of the foundation until failure.

Figure 3.8 provides the dimensionless load-displacement curves for the three embedment ratios examined herein, both for the rigid suction caisson and the skirts alone. Once again it is obvious that bearing capacity and stiffness increase with embedment and that larger horizontal displacements need to be imposed in order to activate the bearing capacity as the embedment ratio increases. Additionally, the results of the foundation with the actual parameters (Es,t) are illustrated in **Figure 3.9**, generally agreeing with the conclusions on the rigid foundation.

The most striking point in all the aforementioned cases, is that between the results of the suction caisson and the skirts alone, there are no substantial differences to be highlighted. As a matter of fact, the differences are negligible for small embedment ratios, turning out to disappear as embedment increases.

The influence of the Young Modulus of steel is evident in **Figure 3.10**, which presents the results of the suction caisson, for E_S=210 GPa (Es,t) and E_S=21000 GPa (rigid). Apparently, there is a rise in the initial stiffness of the rigid foundation against the conventional one, which is indeed considerable for greater embedment ratios. However, the suction caisson reaches the same bearing capacity, whether it is rigid or not.

Figure 3.11 presents the failure mechanisms of the rigid suction caisson and skirts. First of all, it is obvious that the mechanisms are the same for the skirts and the suction caisson. The soil inside the sidewalls does not yield, either for the suction caisson or the skirts alone. Specifically, both of them resist to imposed lateral loading by developing shear stresses at the skirt tip level. In addition, for all embedment rations, especially for the L/a=0.5, two distinctive active and passive pressure wedges with an inclination of 45° appear at the sidewalls. Thus, it can be deduced that the response of the suction caisson and the skirts alone is identical under lateral loading, without the lid of the former participating in any way to the resistance of the lateral loading.

The influence of the embedment ratio in the dimensionless horizontal bearing capacity of the rigid suction caisson is presented in **Figure 3.12**. These results apply to the skirts alone too, with maximum difference at 1.4% for the L/a=0.5 foundation. As it was proven above, the bearing capacity under lateral loading is practically the same for the suction caisson and the skirts alone.

Additionally, it is identical whether the Young Modulus of steel is 210 GPa (Es,t) or 21000 GPa (rigid). Subsequently, **Figure 3.12** is representative of all these cases.

3.2.3 Capacity in Moment Loading

For offshore wind turbines, moment loading is equally prominent as horizontal loading – if not more. In the case of such tall, slender structures, whose height can exceed 100 m, wind loads acting on the top can create significant eccentricities, which in conjunction with the disproportionate low weight can potentially lead to overturn. Conclusively, the bearing capacity of the foundation in moment loading needs to be investigated in order to establish safety in the design.

The coupling between the horizontal and the rotational degree of freedom for embedded foundations, results in the development of translation as rotation is imposed. The subject of study in this section is the determination of the maximum moment M_{max} that the foundation is in position to bear, which develops when the horizontal degree of freedom is constrained.

In **Figure 3.13** and in **Figure 3.14** the dimensionless moment as a function of rotation is presented for the typical (Es,t) and the rigid foundation, respectively. The following general observations apply to both of them. Bearing capacity and stiffness increase with embedment ratio, as expected. In addition, larger rotations are needed for the deployment of the bearing capacity as embedment grows. Interestingly, the response of the skirts alone under moment loading is identical to that of the suction caisson, whereas the difference for the L/a=0.5 ratio is only 10% and can therefore be neglected.

In **Figure 3.15** can be observed the influence of the increase in the Young Modulus of steel from 210 GPa for the conventional (Es,t) foundation to 21000 GPa for the rigid one. As the embedment ratio increases, the initial stiffness is benefited from the rise in E_S, while bearing capacity is not affected. For the L/a=0.5 ratio, which is already rigid due to its small skirt length, there is no actual increase in the stiffness.

Figure 3.16 displays the failure mechanisms that are developed for the rigid suction caisson and skirts alone. The similarities between the former and the latter are indispensable for the embedment ratios L/a=1 and 2. Specifically, the general failure mechanism to be noticed is a shear zone of semicircle form developing below the skirt tips, known as *scoop mechanism.* This is observed for the suction caisson of the small embedment ratio too. In all the above cases, namely for the suction caisson of all embedment ratios and the L/a=1, 2 skirts alone, no plastic strains develop in the soil plug. For the L/a=0.5 skirts on the other hand, the development of internal shear zones along the sidewalls is observed, along with a less distinct and slightly shallower scoop mechanism in comparison with the suction caisson.

From the results in the values of the moment bearing capacity and in the failure mechanisms, the comparison between the skirts alone and the suction caisson shows that their response is

identical for embedment ratios L/a>0.5. Both of them develop the scoop mechanism and at the same time the internal soil does not yield and in conclusion, the lid of the suction caisson does not play any role in the response of the foundation under moment loading.

Finally, **Figure 3.17** highlights the effect of embedment in the dimensionless bearing capacity of the rigid suction caisson under moment loading. The exponential increase of the bearing capacity reveals the significance of the sidewalls in the response of the foundation-soil system to moment loading.

3.3 Assumption of Tensionless Sliding Interface (TSI)

Fully bonded contact (FBC) between the foundation and the soil constitutes in fact more a simplification, than reality. Even in the case of undrained conditions, where full contact could potentially be achieved, the gradual dissipation of initial passive suctions would definitely result in less tensile capacity and perhaps even in sliding and detachment under extreme loading conditions.

It is impossible to determine the actual interface conditions, therefore the assumption of reduced maximum shear strength along the sidewalls, which characterizes the tensionless sliding interface (TSI), is quite reasonable. For a uniform soil, this shear strength does not vary with depth, but remains constant. Specifically, the maximum shear strength is defined as $\tau=\alpha S_u$, which is utilized for undrained loading conditions. Reduction factor α is taken 1 for the interface between the lid and the soil plug, taking thus into account the influence of the lid self-weight, while it is taken 0.5 for the interface between the sidewalls and the soil, both internally and externally.

3.3.1 Capacity in Vertical Loading

Figure 3.18 provides the results for the dimensionless load-displacement curves of the rigid suction caisson and skirts alone. The reduced shear strength along the sidewalls leads the skirts to reach the bearing capacity for significantly smaller displacements relatively to the suction caisson. Specifically, the L/a=2 rigid skirts reach the bearing capacity for w/D=0.002, while the corresponding value for the L/a=0.5 skirts is 0.001. Another apparent inference is that the dimensionless load-displacement curves of the skirts alone, instead of reaching plateau, after the mobilization of the bearing capacity, they show a declining trend. Certainly, the bearing capacity appears just before the separation of the sidewalls and the surrounding soil, after which the skirts simply penetrate the soil as settlement is still imposed.

The case of the typical foundation (Es,t) embedded in homogeneous soil, is presented in **Figure 3.19**, where the above general observations apply too.

The effect of the increase in the steel Young Modulus is shown in the load-displacement curves under vertical loading of the suction caisson and the skirts alone, which are displayed in **Figures 3.20** and **3.21**, respectively. As a matter of fact, in the case of the skirts, the bearing capacity is the same, while for the suction caisson the differences are small.

The failure mechanisms of the rigid suction caisson and skirts are depicted in **Figure 3.22**. As far as the first is concerned, after the exhaustion of the available shear strength that is developed under vertical loading, external sliding along the sidewalls occurs. Since the suction caisson moves vertically as a rigid body along with the soil plug, the mechanism that is activated for resistance involves normal stresses developing below the level of embedment. Subsequently, this mechanism does not differ significantly from the one in the FBC case examined, with the exception that limited plastic strains are observed in the soil plug, close to the skirt tips, since the soil has separated locally there. Regarding the skirts alone, for all embedment ratios, plastic strains due to shear stresses develop along the sidewalls, both externally and internally, as well as below the skirt tips as a result of normal stresses. For the two larger embedment ratios, the latter mechanism is not limited just below the skirt tips, but appears to be extended below the base of the foundation. **Figure 3.23** presents the skirts exclusively and with their position highlighted in the bottom row, to show that they reach the vertical bearing capacity just before sliding.

The dimensionless charts showing vertical bearing capacity as a function of embedment ratio can be found in **Figures 3.24** and **3.25** for the rigid suction caisson and the skirts alone respectively. FBC corresponding results are also provided for comparison. Since the capacity of the suction caisson under vertical loading matches that of an entrenched foundation without sidewalls, for the conventional approach (CA) the following expression that refers to a surface circular footing is used:

$$q_{ult} = 6.05\, S_u + (q + \gamma D) \tag{3.1}$$

where q : overburden stress

γ : specific weight of soil

D : entrenchment depth

Indeed, this expression fits the numerical results for TSI with maximum difference at 3%. As a conclusion, regarding the suction caisson, the sidewalls do not play a substantial role in the bearing capacity, since the load is transferred at the level of embedment.

According to the CA for the case of the skirts alone, the resistance force to the imposed vertical loading is $2\,\pi\,D\,L\,(\alpha\,S_u)$. The maximum difference between the CA estimations and the numerical TSI results is only 2.5%.

Certainly, for both the suction caisson and the skirts alone, the FBC outperform the TSI results.

Figure 3.26 presents the dimensionless vertical bearing capacity of the rigid suction caisson along with that of the skirts alone for comparison, with the former outperforming the latter.

3.3.2 Capacity in Horizontal Loading

Figure 3.27 shows the dimensionless load-displacement curves of the rigid foundation for all embedment ratios. The deviations are maximized between the L/a=0.5 suction caisson and skirts, but they decline as the depth of embedment increases and disappear for the large foundation, as a matter of fact. Furthermore, the appearance of a declining trend in the curves of L/a=1 and 0.5 is due to the detachment and sliding that takes place. The results for the foundation with the conventional parameters are available in **Figure 3.28**, with no further comments to be discussed.

The effect of the Young Modulus of steel is examined both for the suction caisson and the skirts alone, in **Figures 3.29** and **3.30** respectively. The most obvious conclusion is that the response of the rigid foundation is characterized by greater initial stiffness in comparison with the conventional one; effect, which is more prominent as the embedment ratio increases. Additionally, the rigid foundation tends to reach slightly higher bearing capacity.

The failure mechanisms of the rigid foundation under horizontal loading are presented in **Figures 3.31** and **3.32,** along with deformed finite elements and displacement vectors, respectively. Firstly, the form of failure in the case of the suction caisson resembles a slide-wedge mechanism, where the wedge at the opposite side of loading does not appear due to detachment of the foundation from the soil, which remains undeformed. For the large embedment ratio, the soil plug does not yield; however, this not the case of the two smaller ratios, where the internal soil is slightly activated at the skirt tip level. The failure mechanism of the skirts alone for ratios L/a=2 and 1 does not practically differ from that of the corresponding suction caisson ratios. The case is quite different for the L/a=0.5 skirts, where the shear zone at the skirt tip level does not form; instead, two passive wedges appear: the one is seen externally and the other inside the soil plug. The absence of the active wedges is due to detachment of the foundation from the soil.

In order to gain further insight into the subject of lateral loading in the case of TSI as established herein, the development of plastic strains in three different displacement steps is presented for each embedment ratio, in **Figure 3.33** for the skirts alone and in **Figure 3.34** for the suction caisson.

Initially, by examining the evolution of the plastic deformations in the case of the skirts alone (**Figure 3.33**), the following conclusions are made:

- L/a=0.5: In the beginning of the lateral loading, some plastic strains appear along the periphery of the skirts on the external side in the transverse direction of the loading. This is explained by the fact that firstly the shear resistance is mobilized and then the

resistance of the edge, similarly to the case of piles under vertical loading. As imposed displacement increases, the "resistance of the edge" is activated, with the formation of passive wedges.

- L/a=1 and 2: The response at the beginning of the loading is as explained previously. However, even if there are the initial signs of wedges, the system finally chooses to resist by the development of one single wedge and a shear zone at the skirt tip level.

As can be seen in **Figure 3.34**, the response of the suction caisson alone is similar for the three embedment ratios. For small horizontal displacements, the initial response under horizontal loading is the same as the one of the skirts alone; namely shear stresses develop on the periphery of the sidewalls, while signs of wedges start to be evident. However, the system turns out to resist under lateral loading by forming a shear zone at the skirt tip level and a passive wedge in the direction of the loading. Some plastic strains appear finally in the soil plug for L/a=0.5 and 1, whereas for the large suction caisson no signs of yielding are obvious in the confined soil.

In **Figure 3.35** the above cases are presented separately for each embedment ratio in order to highlight the differences and similarities between the suction caisson and the skirts alone.

Finally, **Figure 3.36** presents the dimensionless horizontal bearing capacity of the rigid suction caisson as a function of embedment ratio. Corresponding FBC results are also shown, obviously outperforming the TSI ones. The bearing capacity of the suction caisson and the skirts alone is practically the same under lateral loading, thus the results of the skirts alone are not depicted; in specific, the maximum difference from the results of the suction caisson was 10% in the case of the L/a=0.5 embedment ratio.

3.3.3 Capacity in Moment Loading

The dimensionless moment-rotation curves of the rigid foundation are depicted in **Figure 3.37**. Even though for the large embedment ratio differences between the suction caisson and the skirts are practically inexistent, this is not the case for the smaller embedment ratios. Additionally, **Figure 3.38** shows the respective curves for the foundation with typical values of Es,t. Interestingly, a change appears in the initial stiffness, before reaching the bearing capacity, which is much more obvious for the L/a=2 foundation.

A direct comparison between the rigid and the conventional foundation is available in **Figure 3.39** and **3.40**, for the suction caisson and the skirts alone respectively. It can be deduced that the rigid foundation dominates over the conventional one in terms of initial stiffness – especially as embedment ratio grows. Secondarily, a slight increase of the order of 7% is observed in the bearing capacity of the large foundation.

The failure mechanisms of the rigid suction caisson and skirts alone are illustrated in **Figures 3.41** and **3.42**; the former displays the deformed finite elements too, whereas the latter, the

displacement vectors. First of all, the failure mechanisms of the L/a=1 and 2 suction caisson resemble those of the FBC conditions, with the exception that due to the TSI assumption herein, separation takes place. More specifically, the suction caisson responds to imposed rotation by forming a semi-circular shear zone below the skirt tip level. For the large embedment ratio, no signs of plastic strains are obvious, while for the L/a=1 some limited yielding is noticed in the soil plug, just above the skirt tip level. For the small suction caisson, it seems that it reaches its bearing capacity shortly after the detachment of the lid from the soil plug and before having formed the aforementioned shear zone; instead, some plastic strains are found in the internal soil close to the skirt tips. Regarding the skirts alone, only the greatest embedment ratio matches the failure mechanism of the corresponding suction caisson; as far as the other are concerned, they resist under moment loading mainly by yielding internally of the sidewalls.

To shed light into the mechanisms of the rigid foundation under moment loading, the evolution of the plastic strains for three levels of rotation is presented in **Figure 3.43** for the skirts alone and in **Figure 3.44** for the suction caisson.

Firstly, examining the development of plastic deformations in the case of the rigid skirts alone, with *clockwise* imposed rotation, the following comments can be made:

- L/a=0.5: For small imposed rotation (θ=0.0001 rad), limited plastic strains are observed at the skirt tip level on the external side mostly. As rotation increases, yielding spreads inside the soil plug; it can be deduced that passive resistance wedges start to form – in fact, they are more obvious at the final stage of loading, where separation has occurred (detachment between: skirts-soil plug from the left side & skirts-external soil from the right side).
- L/a=1.0: From the beginning of loading, signs of both active and passive wedges appear at the right skirt tip mainly. As rotation increases, yielding can be noticed on the surface of the soil plug, at the left side, where the separation of the sidewalls from the surrounding soil is about to take place. Additionally, a shear zone starts to form at the skirt tip level and a passive wedge on the left side appears externally. Detachment is also seen at the right side, between the sidewalls and the external soil.
- L/a=2.0: Instead of resisting to imposed rotation with the initial mechanism involving both internal wedges, the large foundation finally detaches from the external soil and a semi-circular shear zone appears below the skirt tip level.

On the other hand, regarding the rigid suction caisson, the observations on the development of plastic strains are the following:

- L/a=0.5: For small imposed rotation, plastic strains are mainly concentrated on the right side of the sidewalls, not only externally, but internally too. The increasing rotation leads to detachment of the sidewalls on the right from the surrounding soil and of the lid from the soil plug, which yields. A passive wedge is observed at the external surrounding soil,

on the left side. Separation can also be seen on the right, between the sidewalls and the external soil.

- L/a=1 and 2: The foundation-soil system resists by the development of a semi-circular shear zone below the skirt tip level, instead of the initial internal wedges for small rotation. Separation is seen between the sidewalls and the external soil, mainly on the right, but also on the left, especially close to the surface.

In **Figure 3.45** a direct comparison between the suction caisson and the skirts alone is available for each embedment ratio.

The dimensionless bearing capacity in moment loading is presented as a function of embedment ratio for the rigid suction caisson and skirts in **Figure 3.46**. At the same time, the respective FBC results are provided, apparently outperforming the TSI ones. Moreover, the TSI results for the suction caisson and the skirts are plotted together in **Figure 3.47**, which shows satisfying agreement as the depth of embedment grows.

3.4 Conclusions

In this chapter, the bearing capacity of the suction caisson and the skirts alone in a soil stratum of constant shear strength was thoroughly investigated for three embedment ratios L/a=0.5, 1 and 2. Emphasis is placed on their comparison; it needs to be noted that when differences in the bearing capacity occur, the suction caisson outperforms the skirts, although in some cases the results showed perfect agreement. More specifically, the following deductions have been made:

Assumption of Fully Bonded Contact (FBC):

- Under vertical loading, the differences between the bearing capacity of the suction caisson and the skirts alone range from 25% (L/a=2) to 60% (L/a=0.5).
- The response of both foundation types is the same under horizontal loading.
- Moment loading leads to perfect agreement in the bearing capacity of the suction caisson and the skirts alone for embedment ratios 1 and 2, while there is a small difference of 10% in the case of the small embedment ratio of L/a=0.5.

Assumption of Tensionless Sliding Interface (TSI):

- Vertical loading results in tremendous differences between the suction caisson and the skirts alone, when the case of a TSI is taken into account. Specifically, the differences in the bearing capacity of the two foundations range from 57% (L/a=2) to 85% (L/a=0.5).
- Under horizontal loading, the bearing capacity of the suction caisson is overall the same to that of the skirts alone, with a difference of 10% noticed for L/a=0.5.
- As embedment ratio increases, the bearing capacity in moment loading of the two foundation types becomes equal. However, for the small embedment ratio, a difference of 35% is observed.

Conclusively, in terms of bearing capacity, the skirts alone can replace the suction caisson, given that their capacity under vertical loading is satisfying. Significantly, under horizontal and moment loading, especially as embedment ratio increases, the loads are transferred to the base and the foundation along with the constrained soil plug move as a rigid body. The existence of the lid in this case does not play any role; thus, the bearing capacity of the skirts alone is practically equal to that of the suction caisson for these loading types. On the other hand, vertical loading is resisted by different mechanisms for the suction caisson and the skirts alone. In specific, for the first, the main contribution to the resistance under vertical loading lies to the mobilization of the soil below the skirt tip level, while for the latter, the major mechanism involves development of shear stresses along the sidewalls, both internally and externally. This leads the suction caisson to outperform the skirts in terms of bearing capacity, especially under TSI assumption, where significant sliding occurs.

Chapter 3: Figures

Bearing Capacity

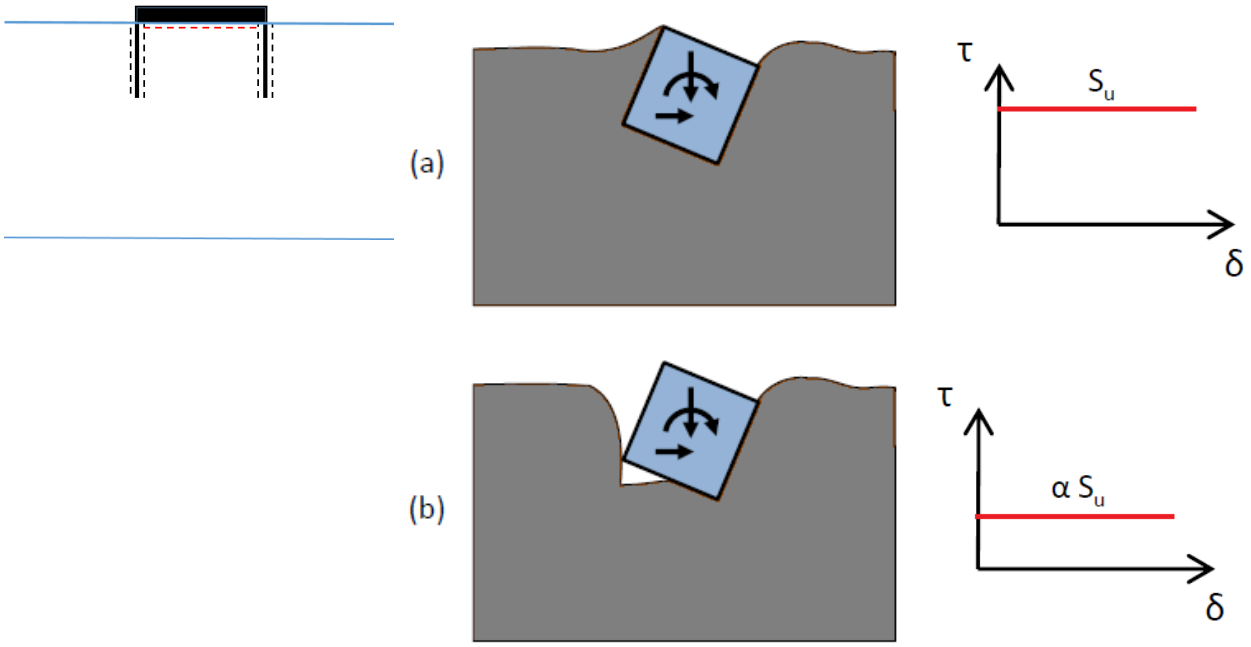

Fig.3.1. *Left:* Foundation-soil interfaces. *Right:* Foundation-soil contact conditions (a) Fully bonded contact [FBC]: infinite tensile capacity and $\tau=S_u$ and (b) Tensionless sliding interface [TSI]: zero tensile capacity and $\tau=\alpha S_u$ permitting separation ($\alpha=0.5$ for TSI between sidewalls and soil, $\alpha=1$ for TSI between lid and soil plug)

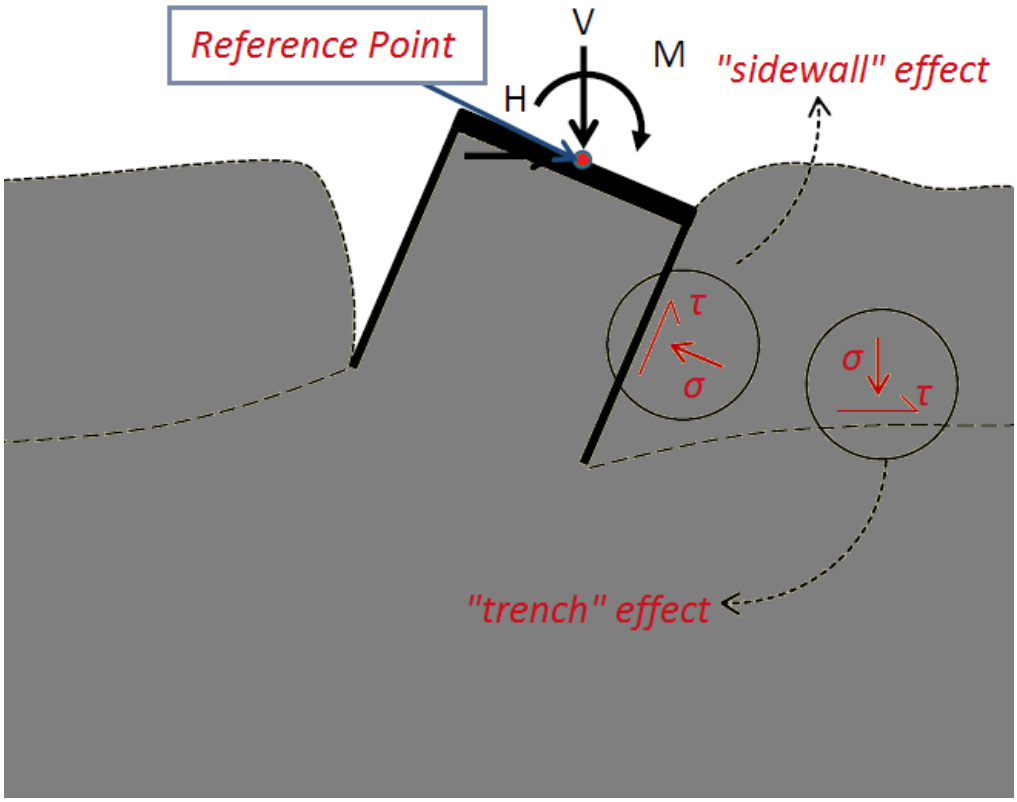

Fig.3.2. The influence of embedment in the case of skirted foundations: the "trench" and "sidewall" effects

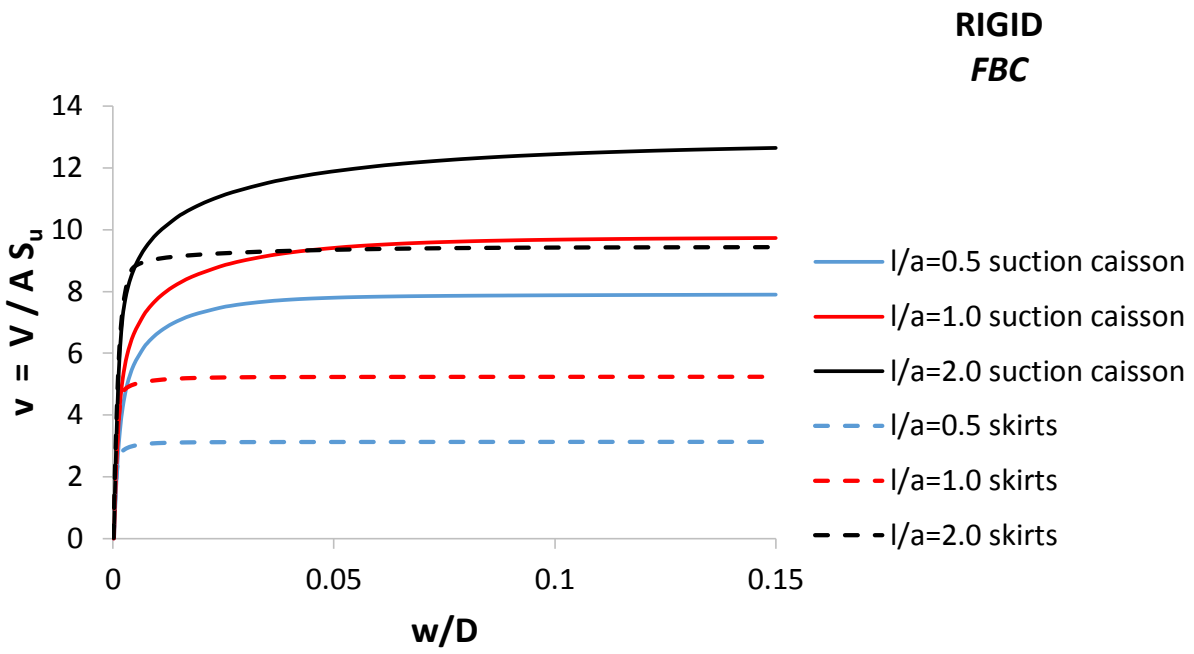

Fig.3.3. Dimensionless vertical load-displacement curves of the rigid foundation under FBC assumption

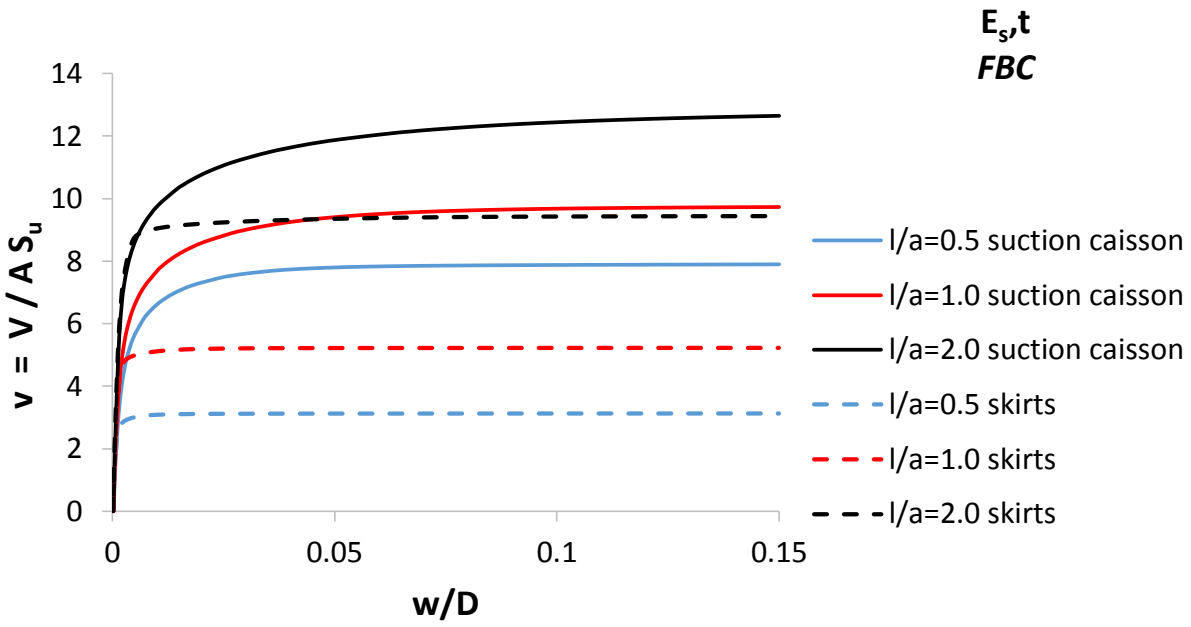

Fig.3.4. Dimensionless vertical load-displacement curves of the (*Es,t*) foundation under FBC assumption

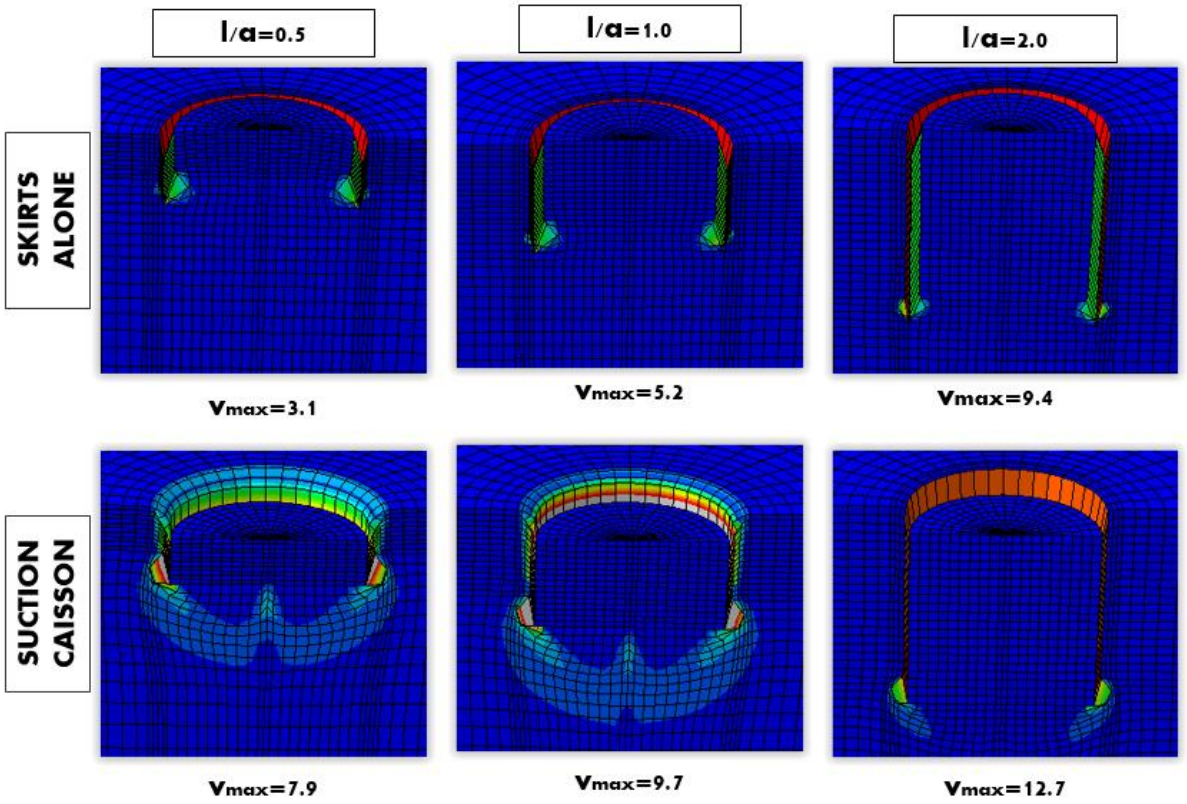

Fig.3.5. Failure mechanisms of the rigid foundation under vertical loading

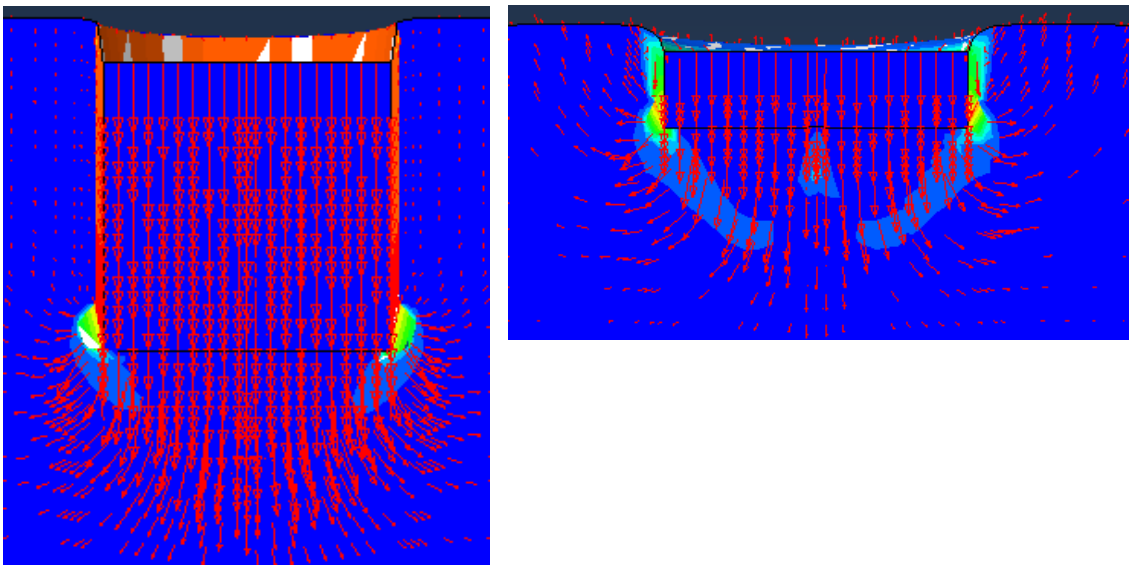

Fig.3.6. Failure mechanisms and displacement vectors of the rigid suction caisson under vertical loading. *Left*: L/a=2. *Right*: L/a=0.5

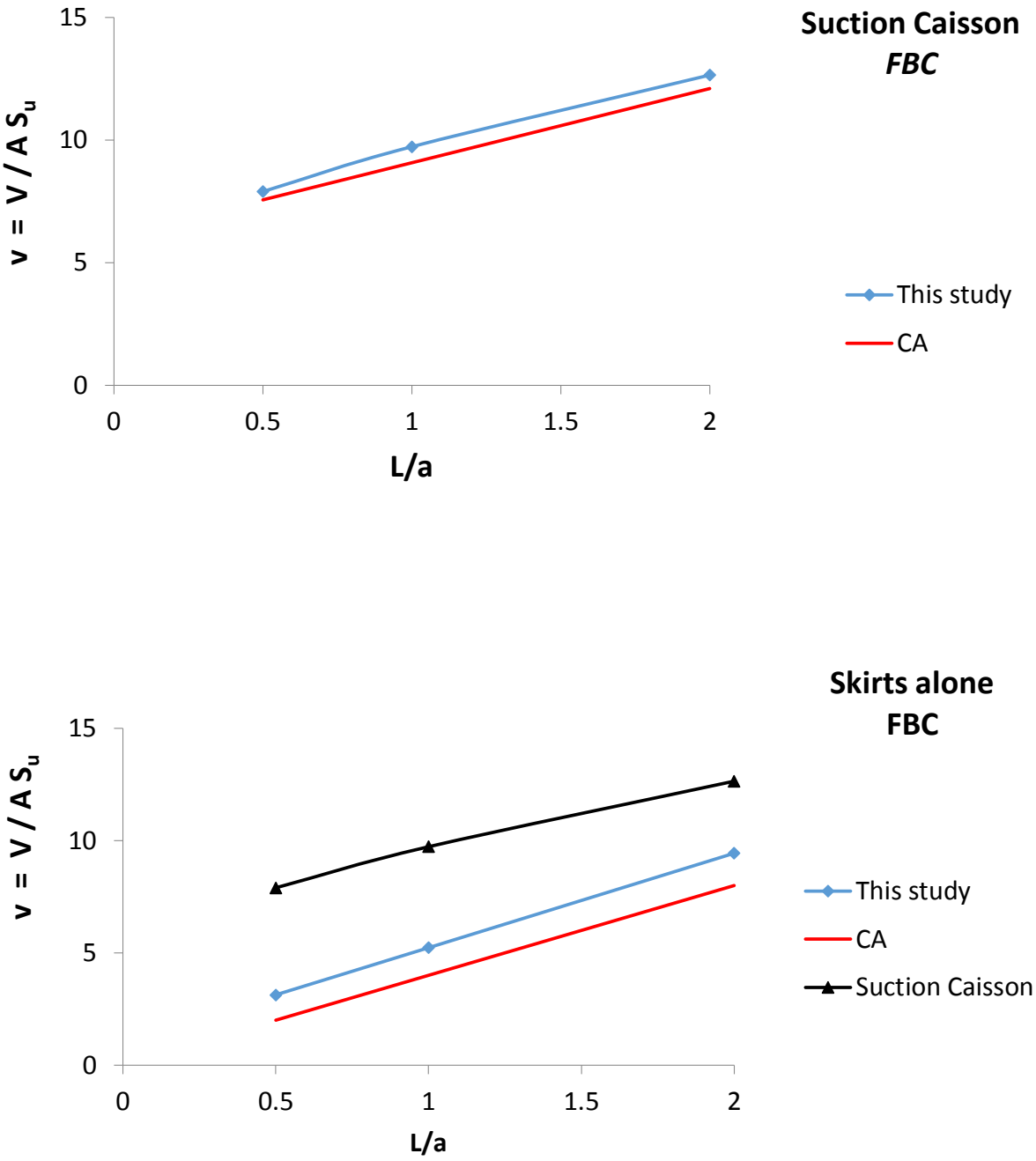

Fig.3.7. Dimensionless vertical bearing capacity as a function of embedment ratio and comparison to Conventional Approach (CA) - *[Rigid foundation, Homogeneous soil profile]*. *Top*: Suction caisson. *Bottom*: Skirts alone

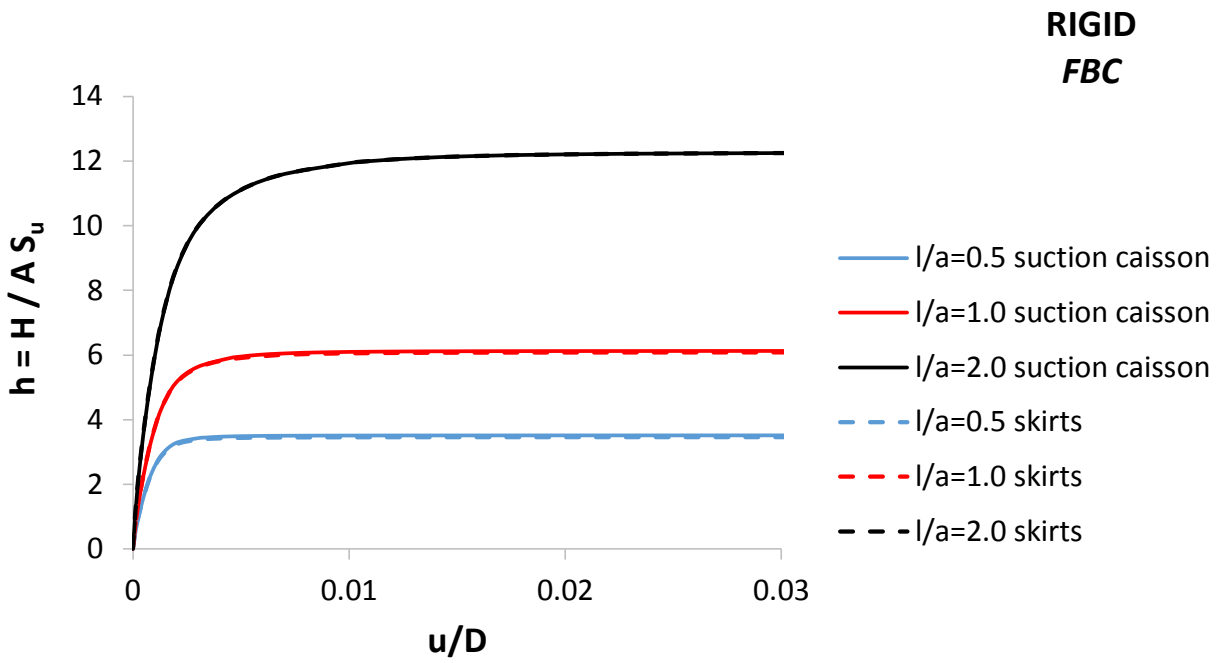

Fig.3.8. Dimensionless horizontal load-displacement curves of the rigid foundation under FBC assumption

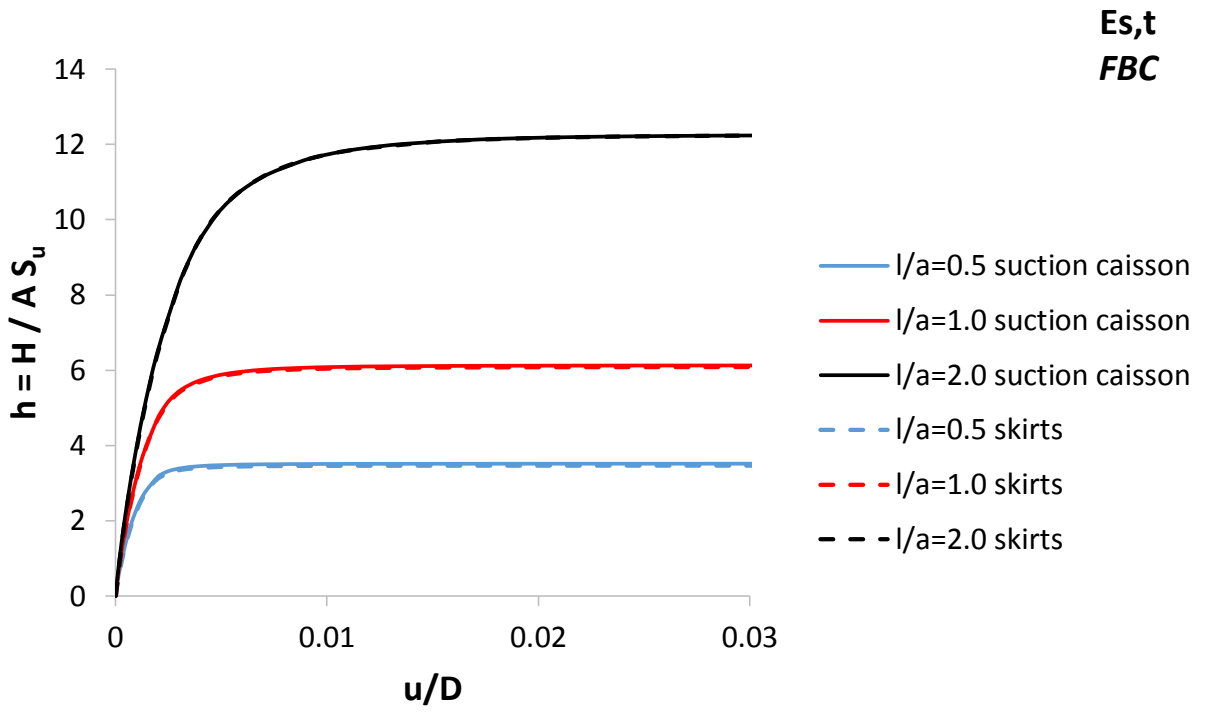

Fig.3.9. Dimensionless horizontal load-displacement curves of the (*Es,t*) foundation under FBC assumption

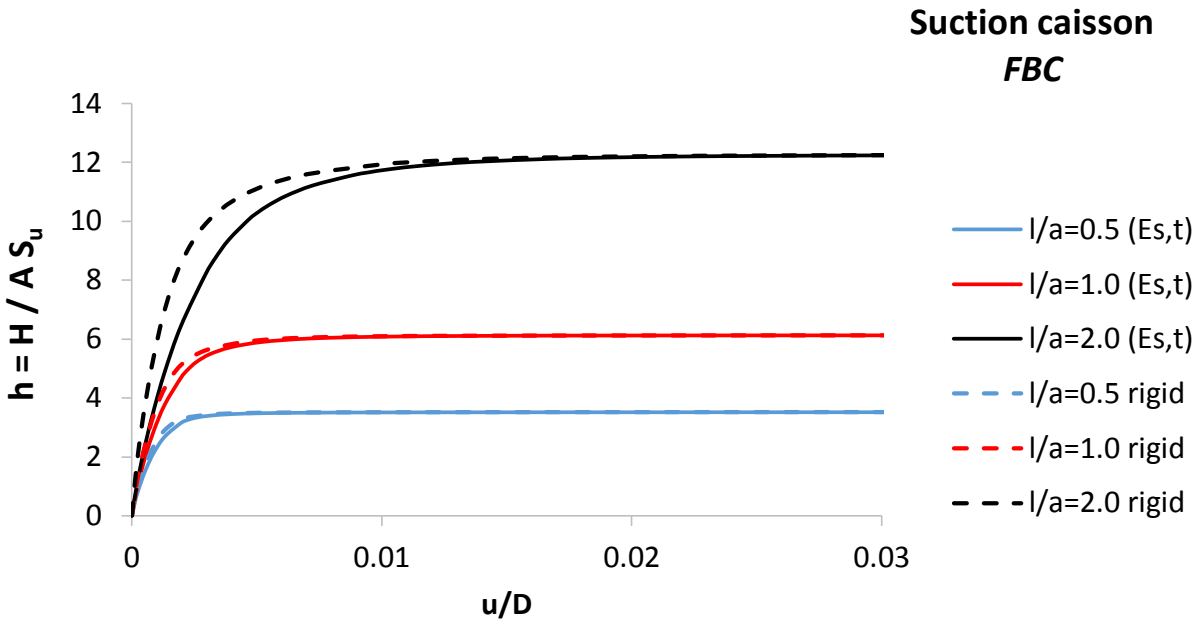

Fig.3.10. Dimensionless horizontal load-displacement curves of the suction caisson (rigid & Es,t) under FBC assumption

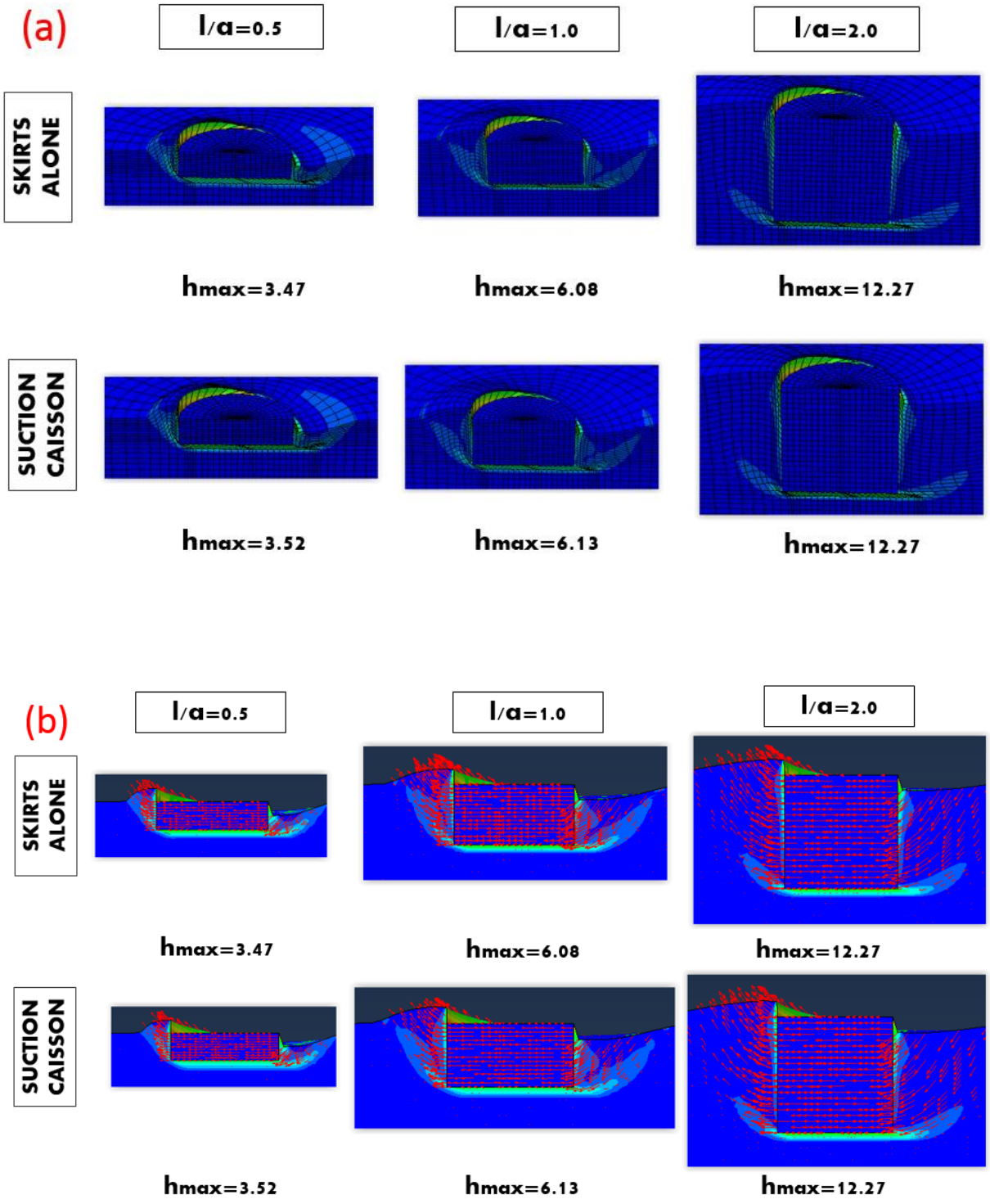

Fig.3.11. Failure mechanisms along with (a) deformed FE and (b) displacement vectors. Rigid foundation under horizontal loading

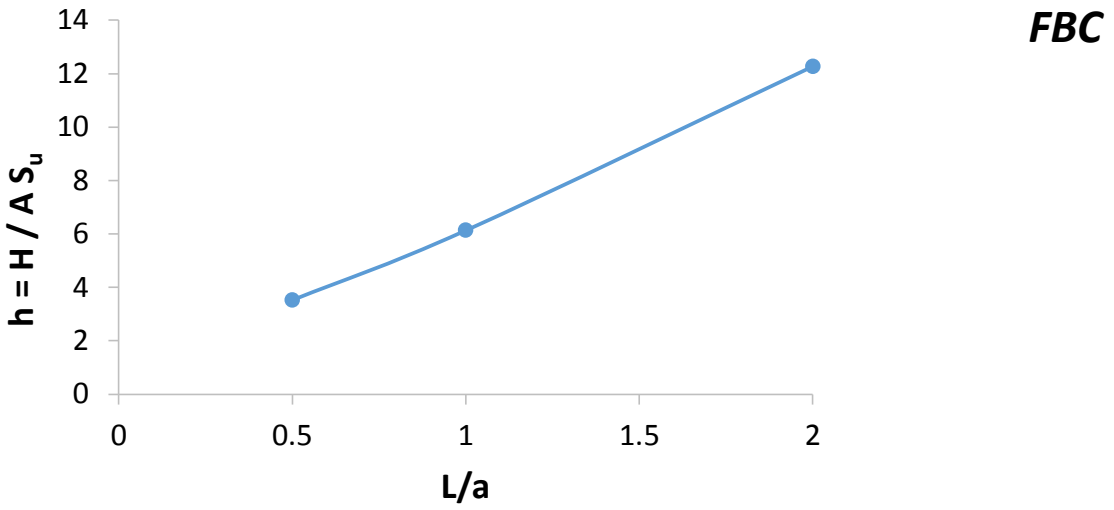

Fig.3.12. Influence of embedment ratio in the dimensionless horizontal bearing capacity of the rigid suction caisson under FBC assumption

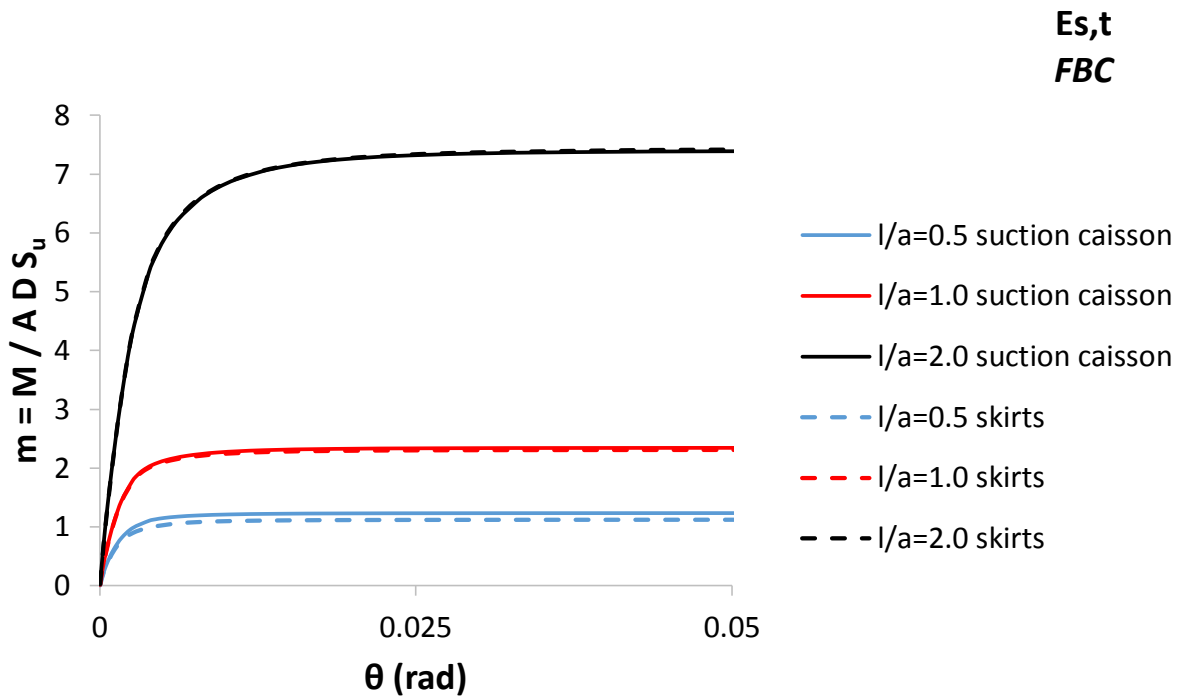

Fig.3.13. Dimensionless moment-rotation curves of the (Es,t) foundation under FBC assumption

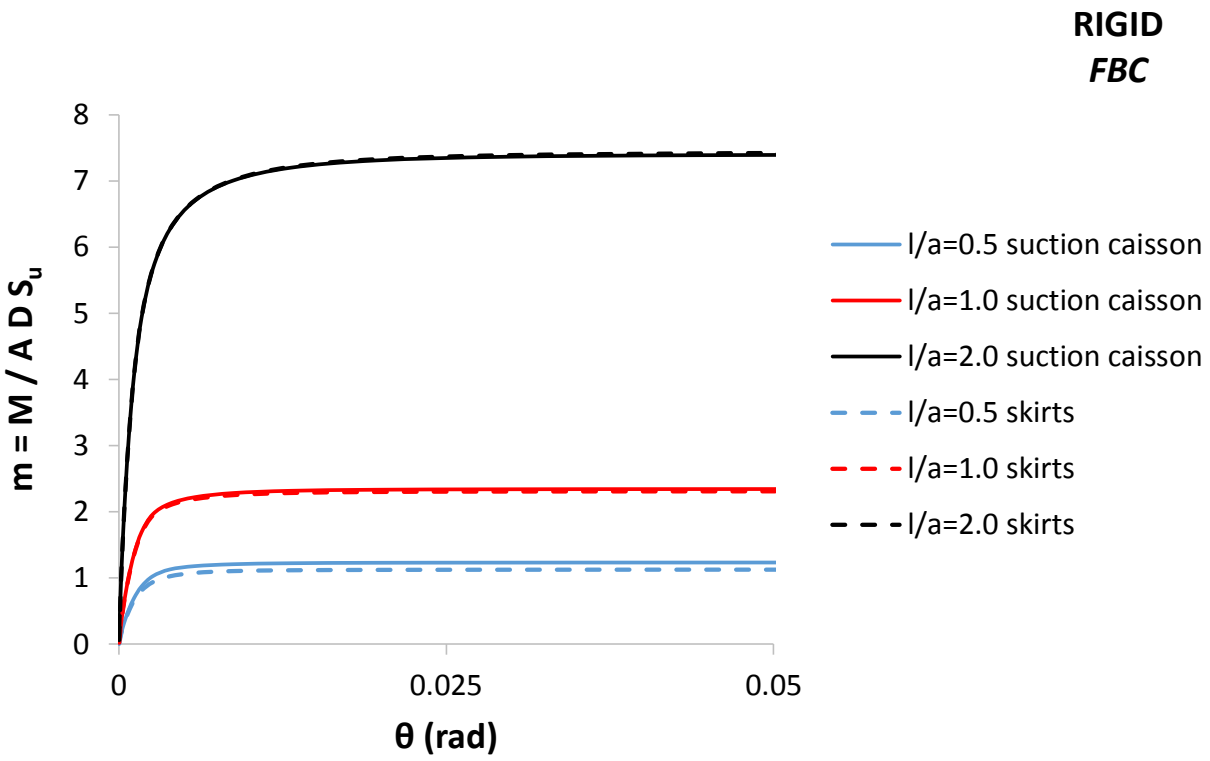

Fig.3.14. Dimensionless moment-rotation curves of the rigid foundation under FBC assumption

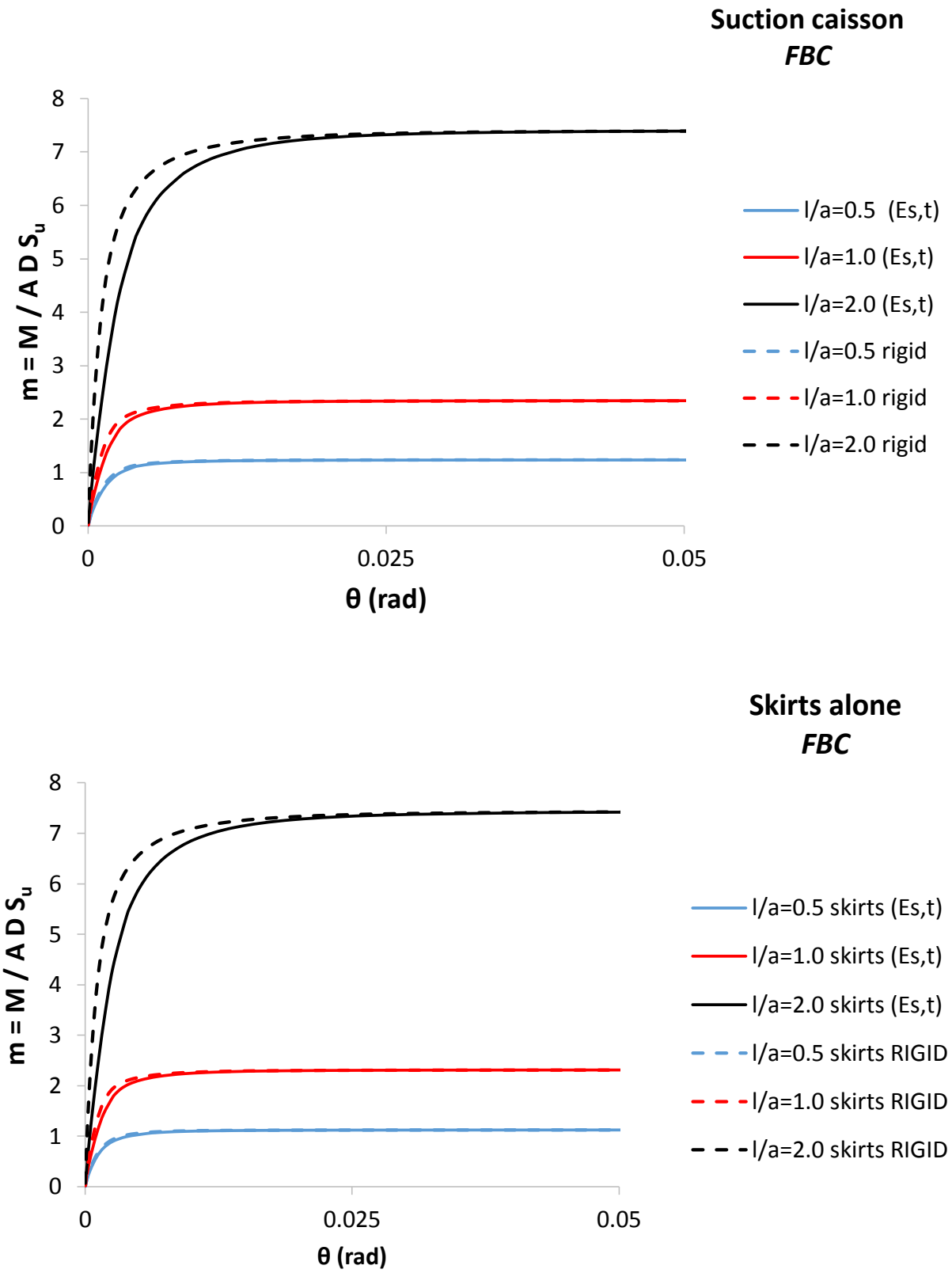

Fig.3.15. Dimensionless moment-rotation curves. *Top:* Suction caisson (Es,t & rigid). *Bottom:* Skirts alone (Es,t & rigid)

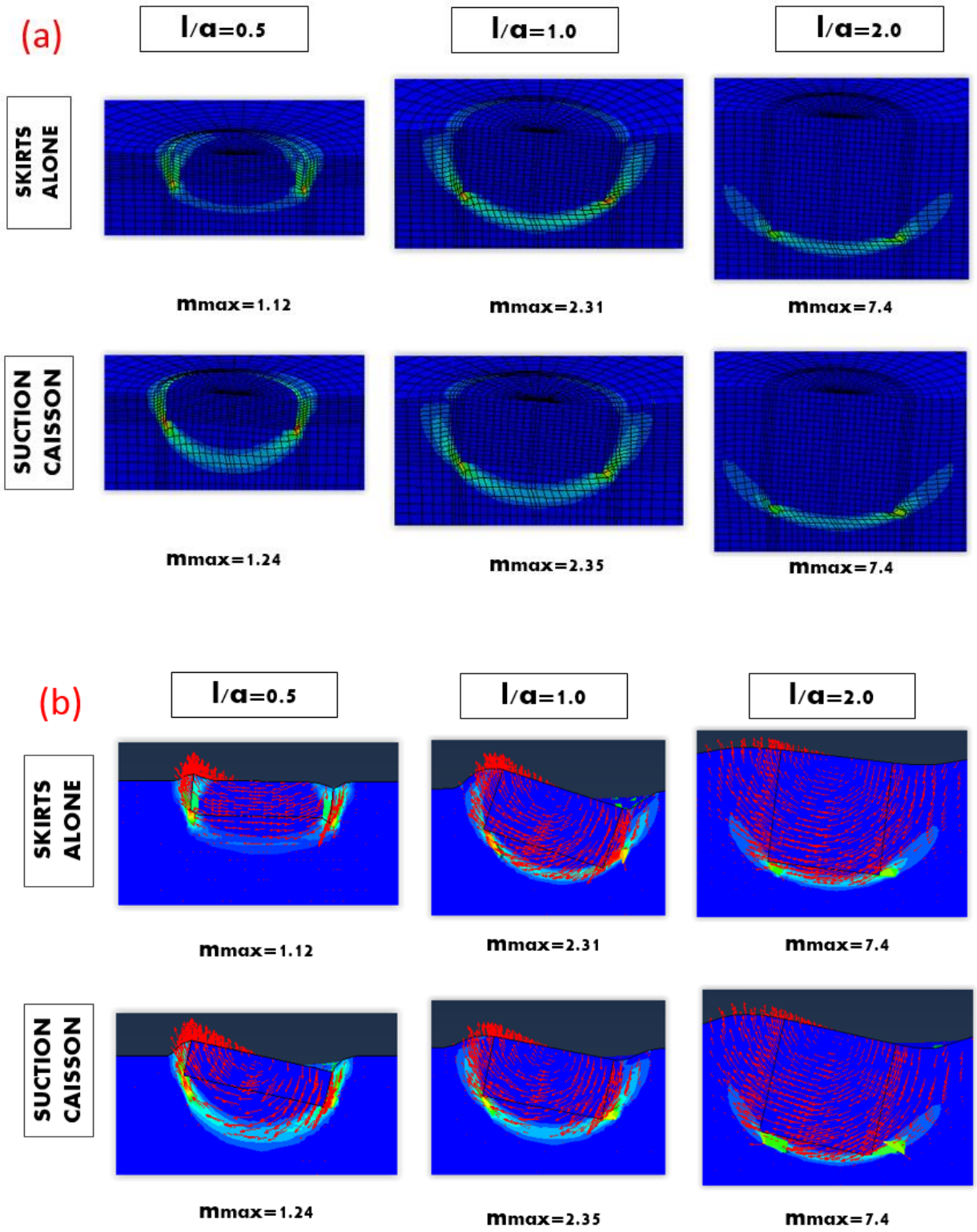

Fig.3.16. Failure mechanisms along with (a) deformed FE and (b) displacement vectors. Rigid foundation under moment loading

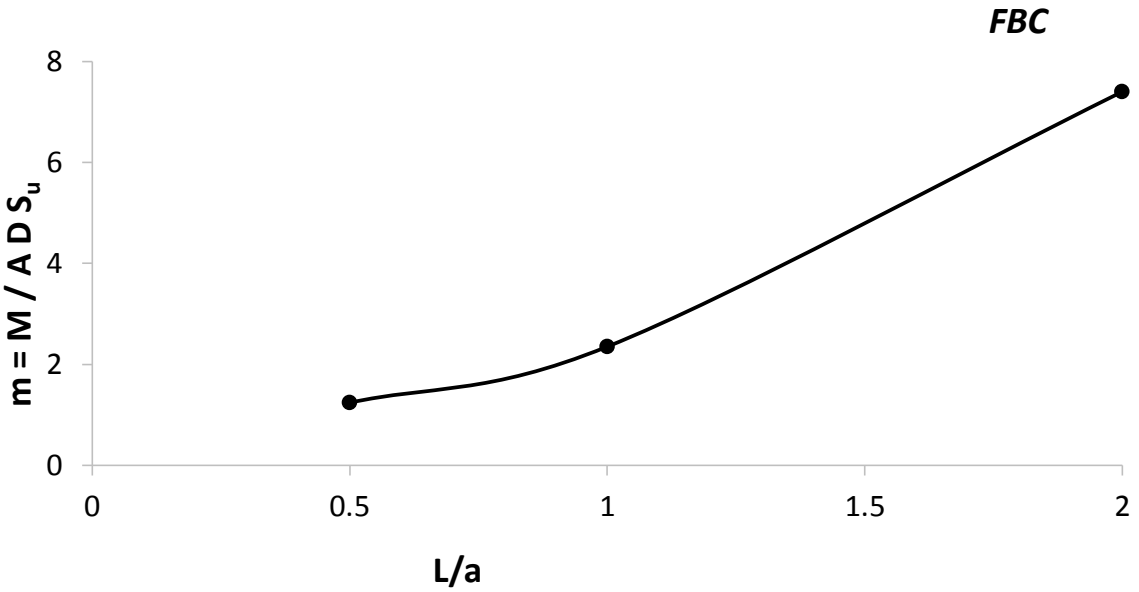

Fig.3.17. Influence of embedment ratio in the dimensionless bearing capacity under moment loading of the rigid suction caisson

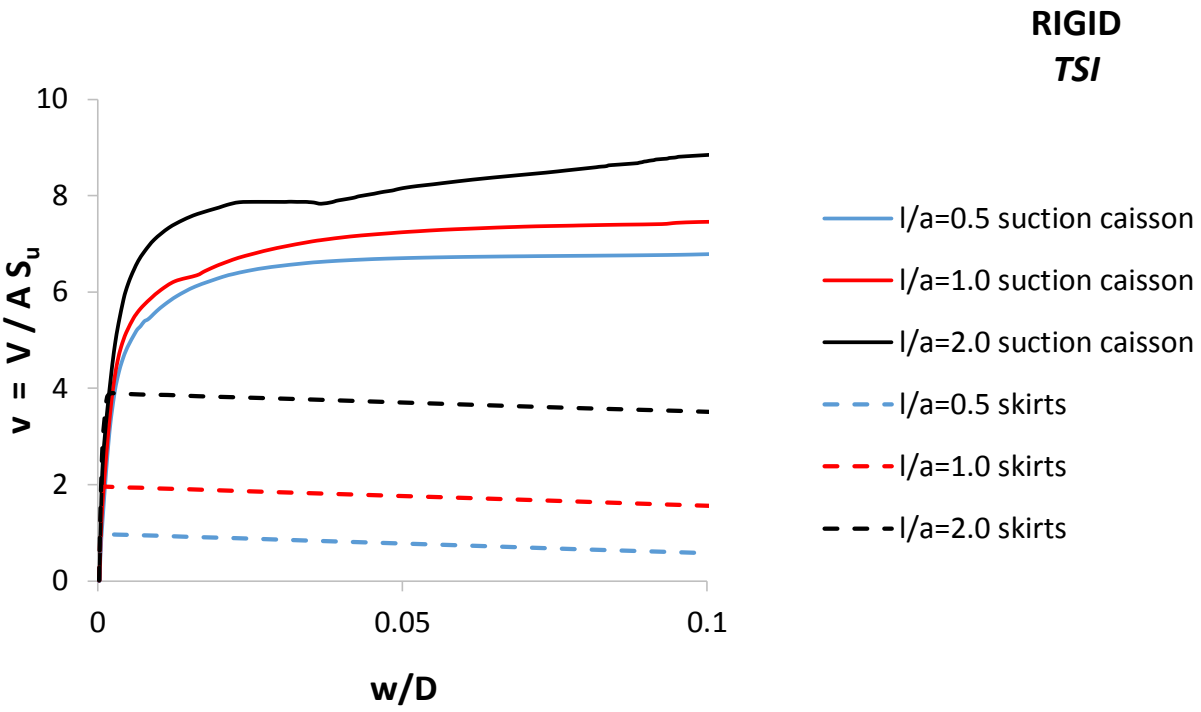

Fig.3.18. Dimensionless vertical load-displacement curves in the case of the rigid foundation under TSI assumption

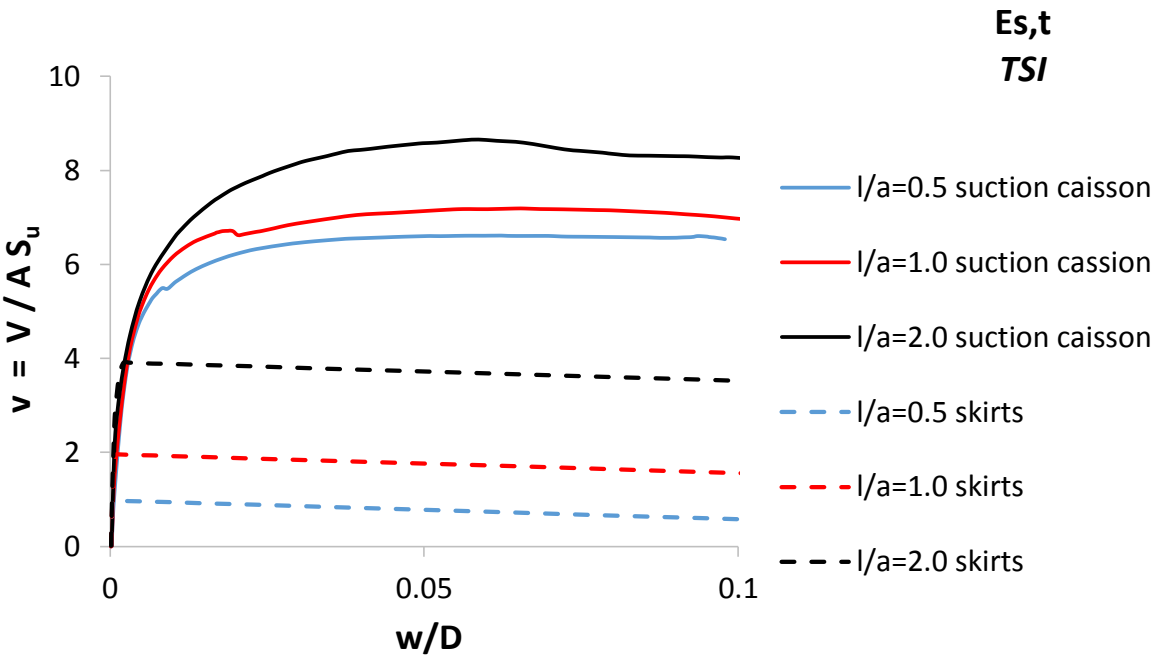

Fig.3.19. Dimensionless vertical load-displacement curves of the (*Es,t*) foundation under TSI assumption

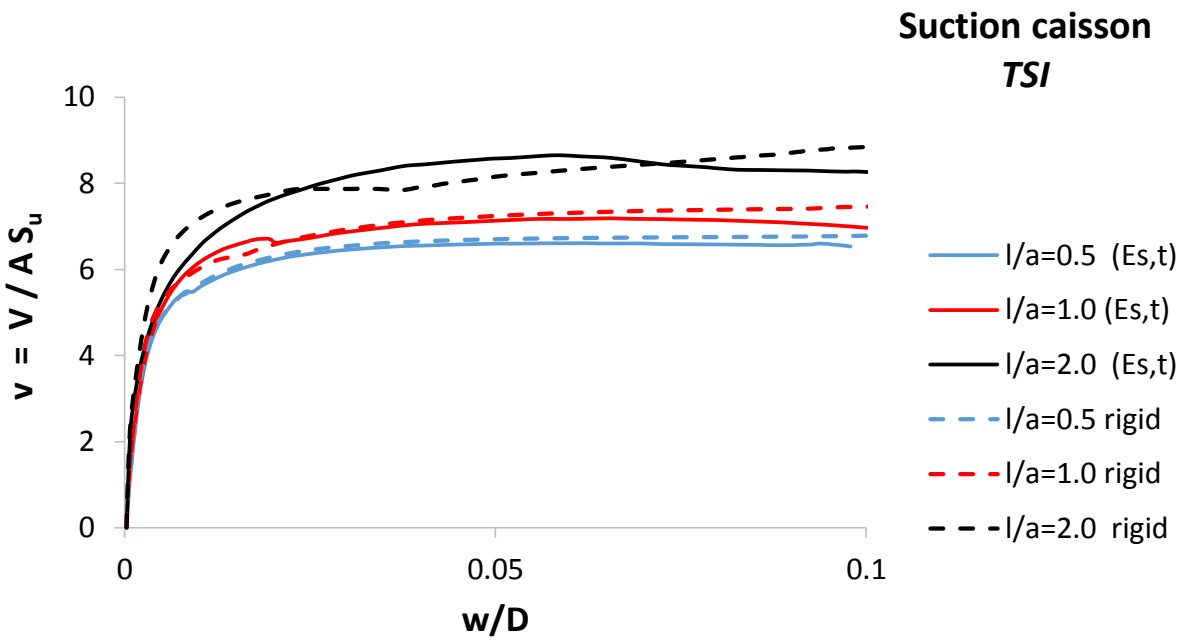

Fig.3.20. Dimensionless vertical load-displacement curves in the case of the suction caisson under TSI assumption

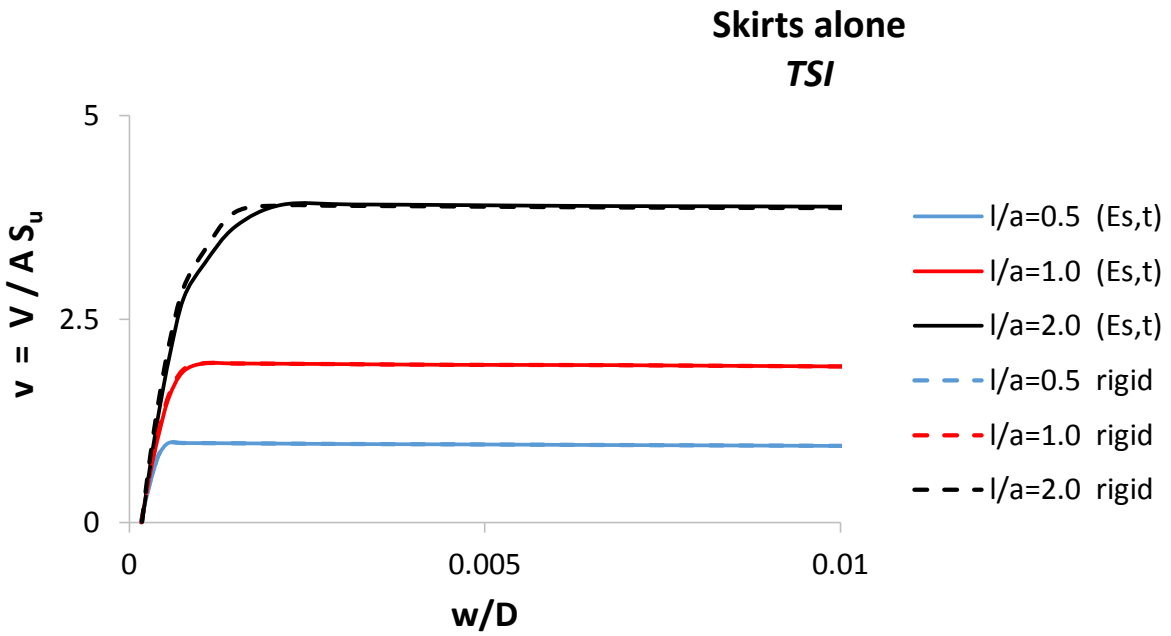

Fig.3.21. Dimensionless vertical load-displacement curves of the skirts alone under TSI assumption

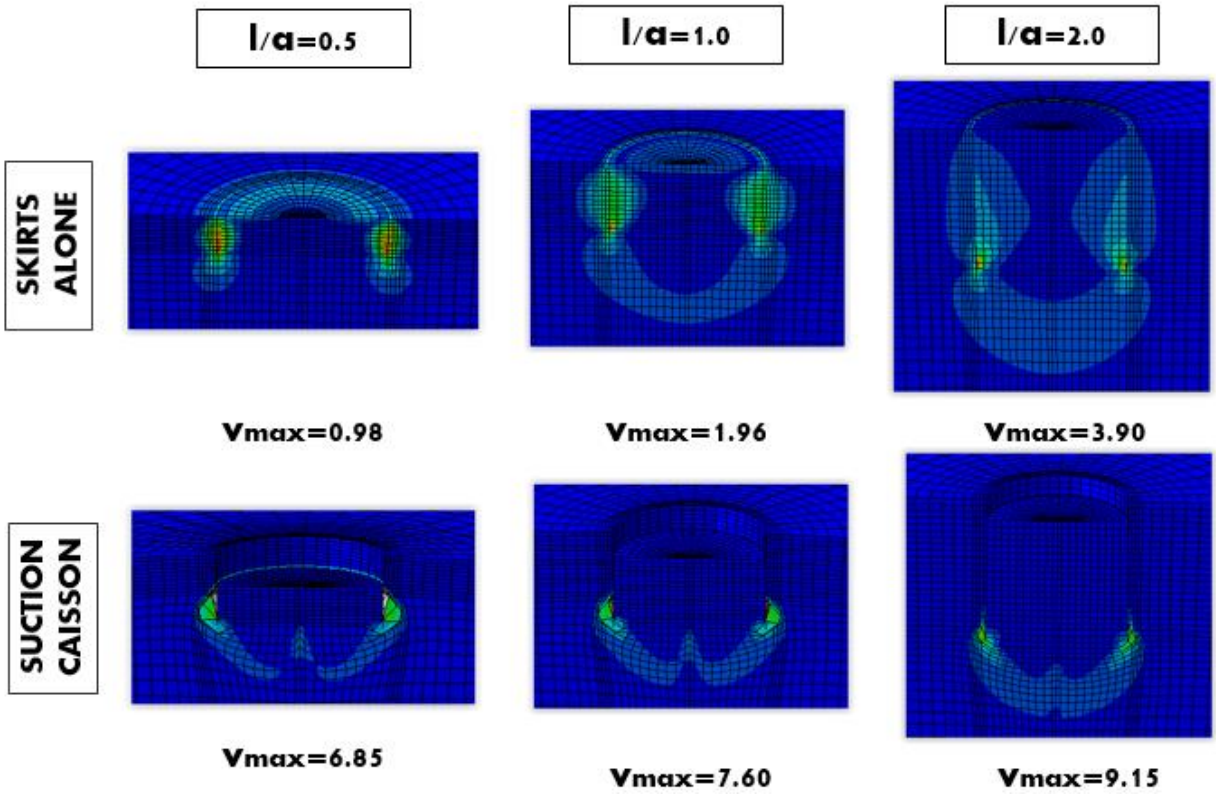

Fig.3.22. Failure mechanisms of the rigid foundation under vertical loading [TSI assumption]

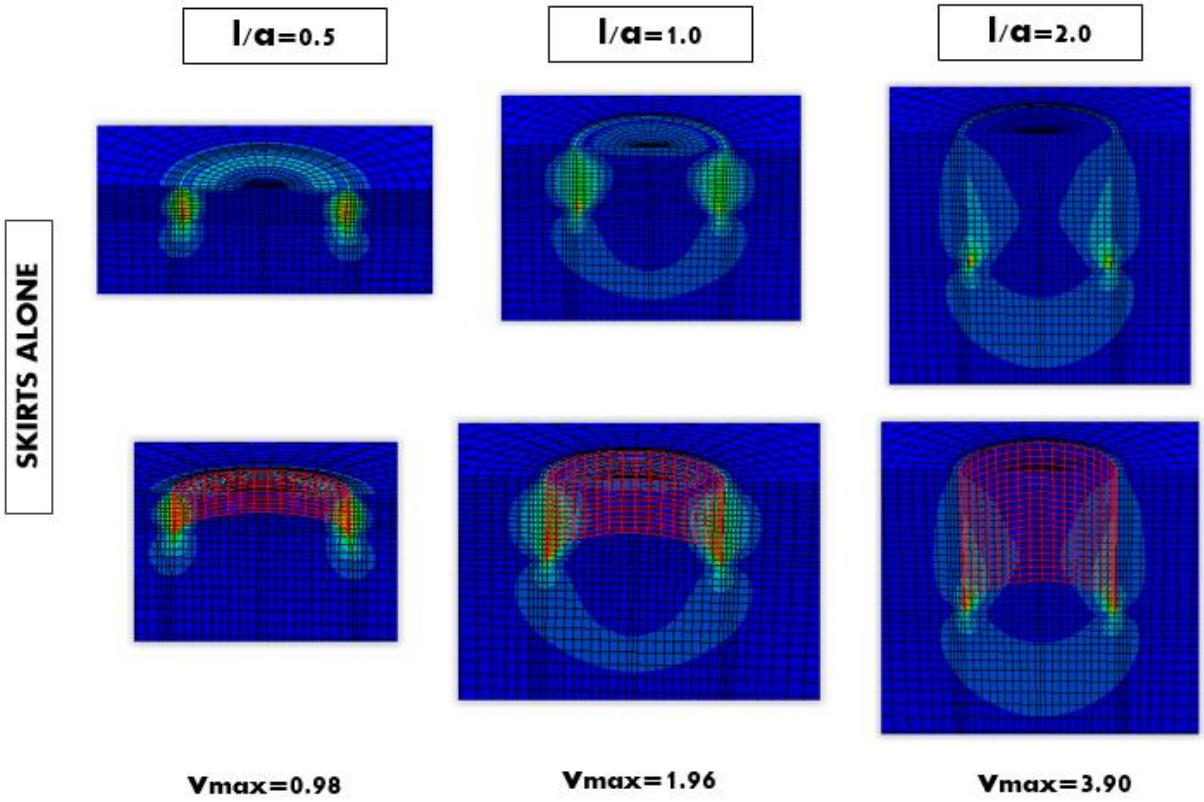

Fig.3.23. Failure mechanisms of the rigid skirts alone (highlighted in the bottom row) under vertical loading

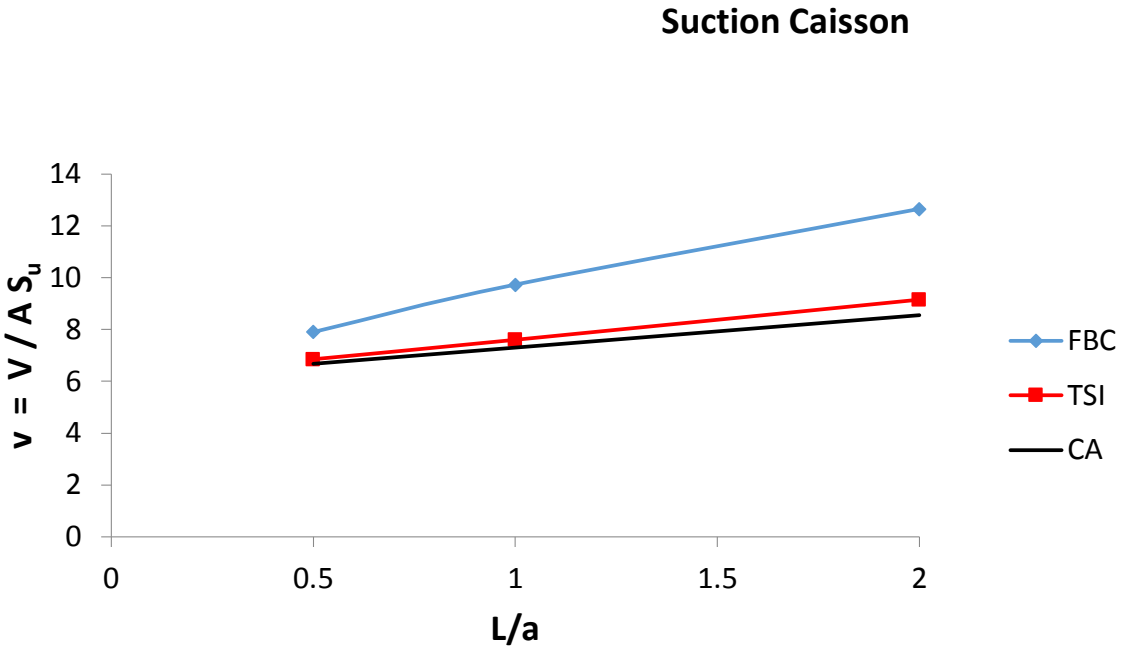

Fig.3.24. Dimensionless vertical bearing capacity of the rigid suction caisson as a function of embedment ratio and comparison to Conventional Approach (CA)

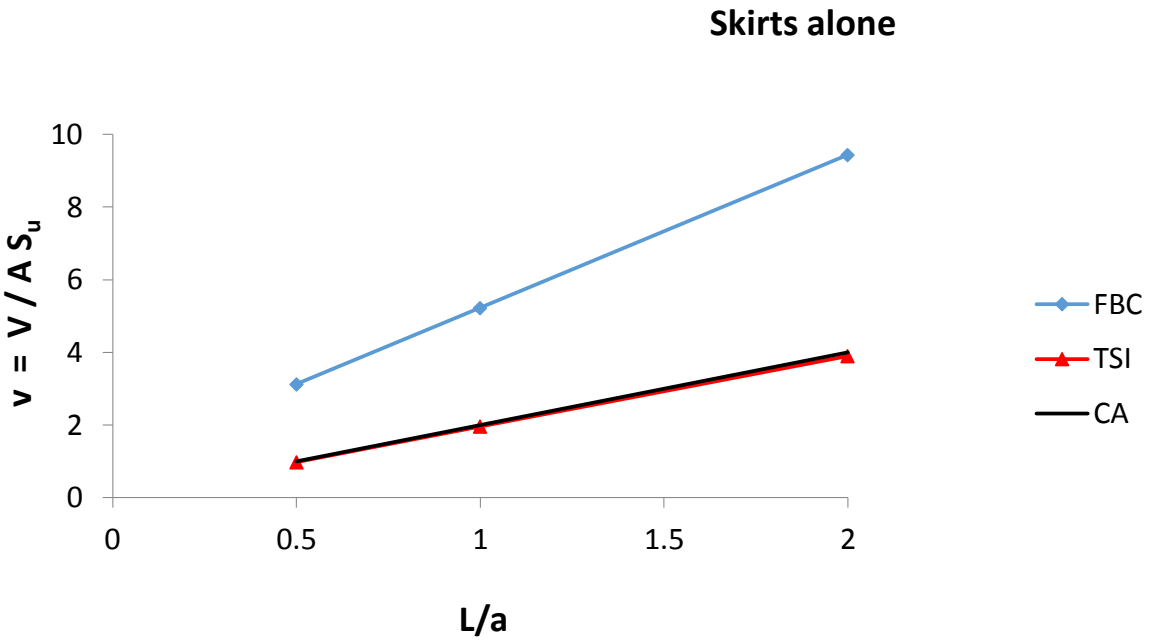

Fig.3.25. Dimensionless vertical bearing capacity of the rigid skirts alone as a function of embedment ratio and comparison to Conventional Approach (CA)

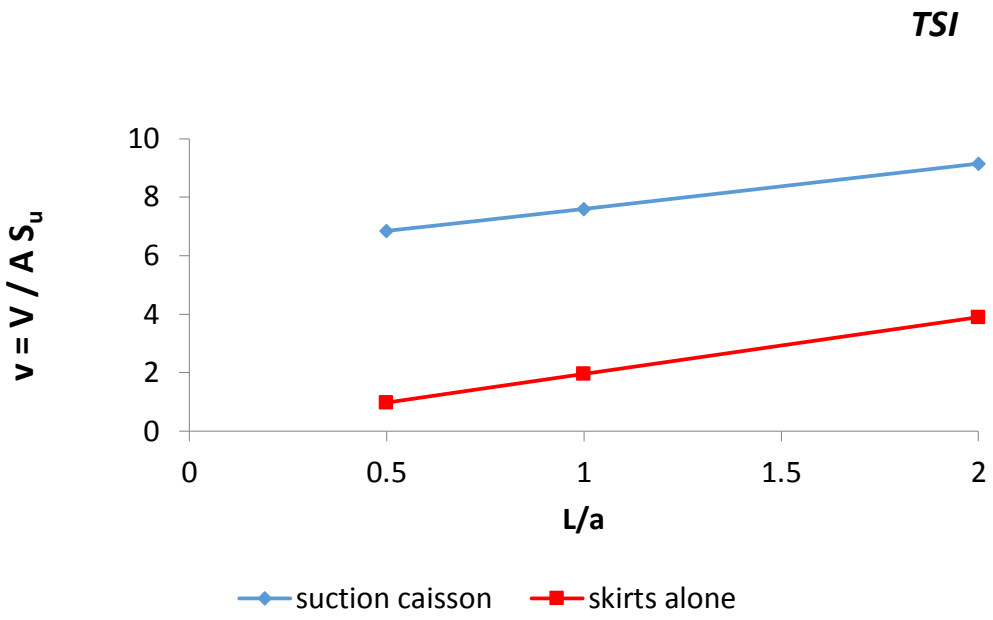

Fig.3.26. Dimensionless vertical bearing capacity of the rigid foundation as a function of embedment ratio

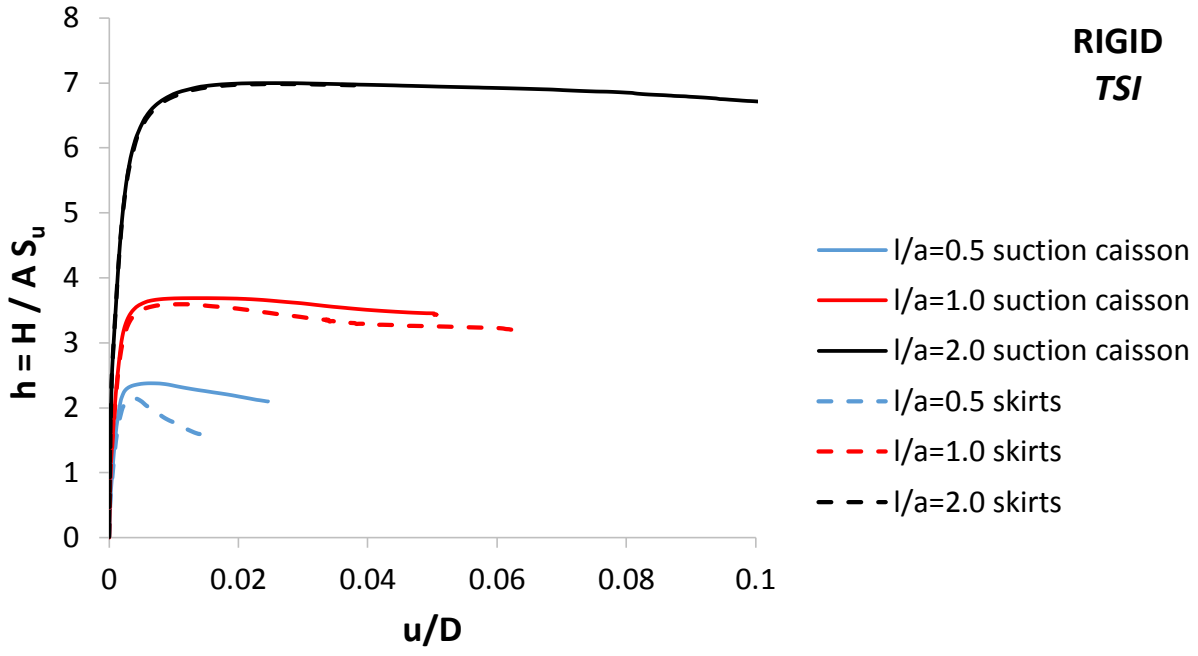

Fig.3.27. Dimensionless horizontal load-displacement curves in the case of the rigid foundation under TSI assumption

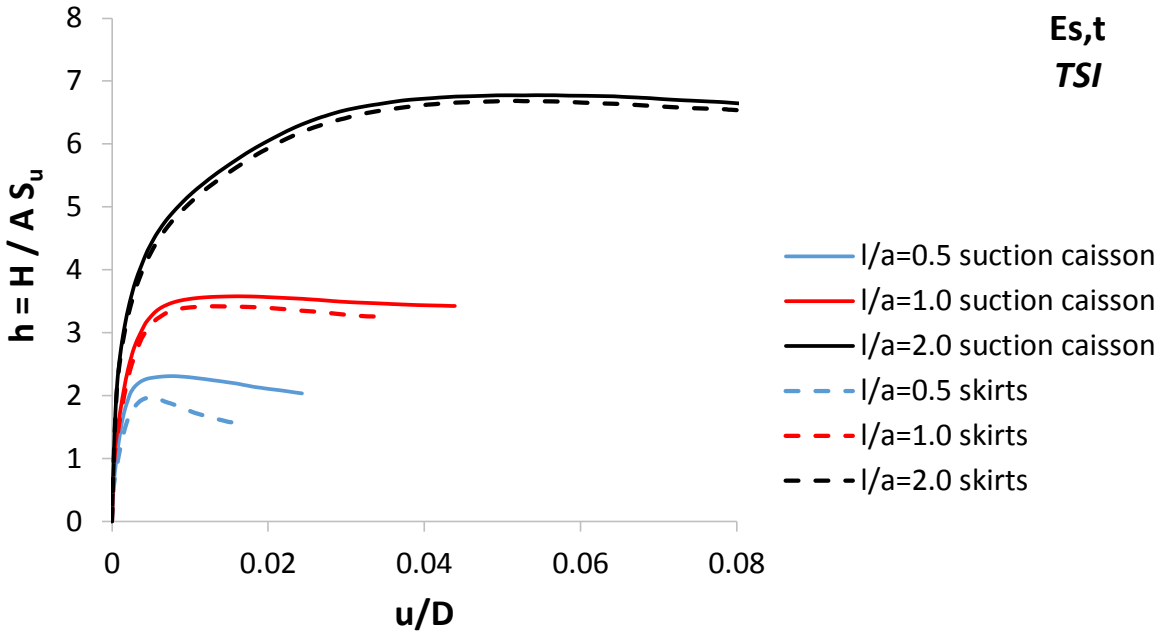

Fig.3.28. Dimensionless horizontal load-displacement curves of the (Es,t) foundation under TSI assumption

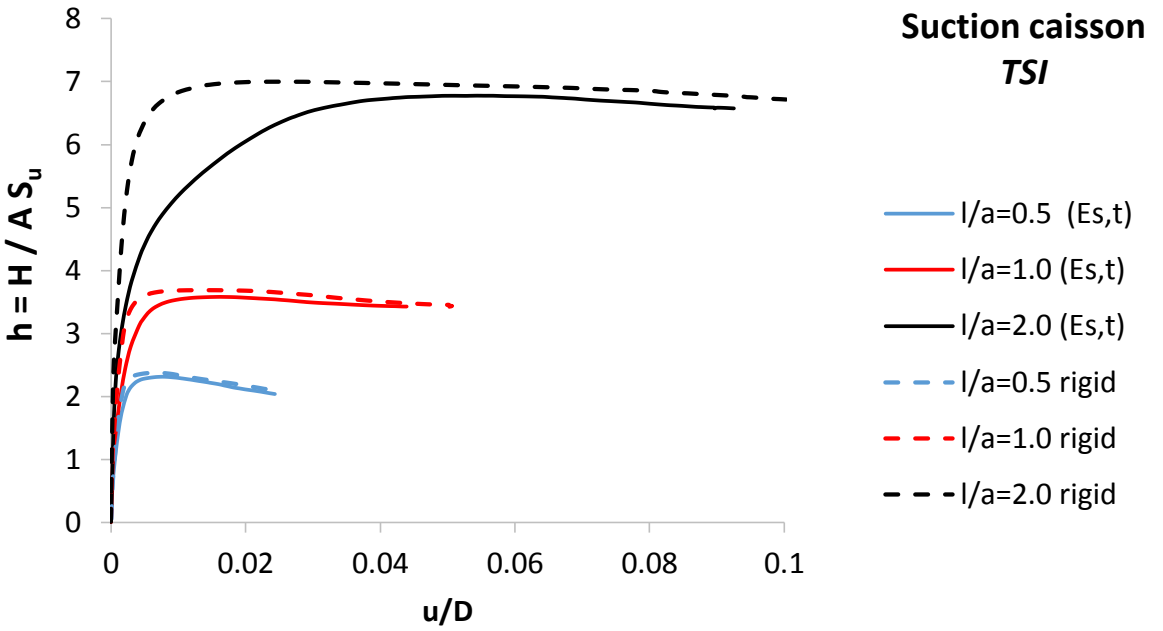

Fig.3.29. Dimensionless horizontal load-displacement of the suction caisson under TSI assumption

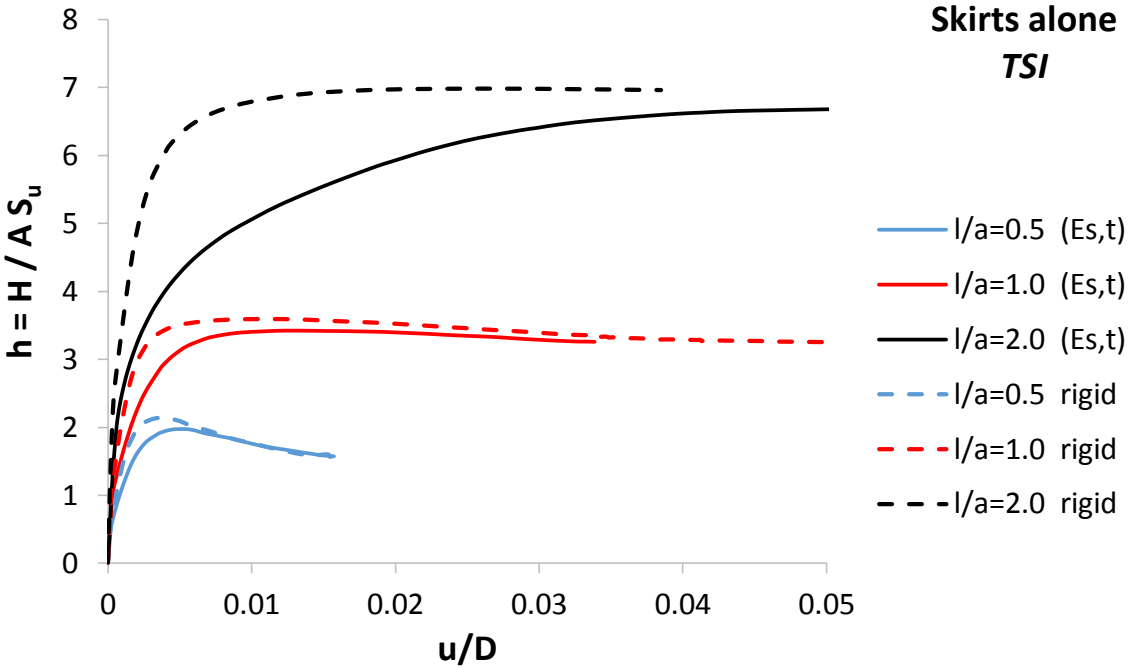

Fig.3.30. Dimensionless horizontal load-displacement of the skirts alone under TSI assumption

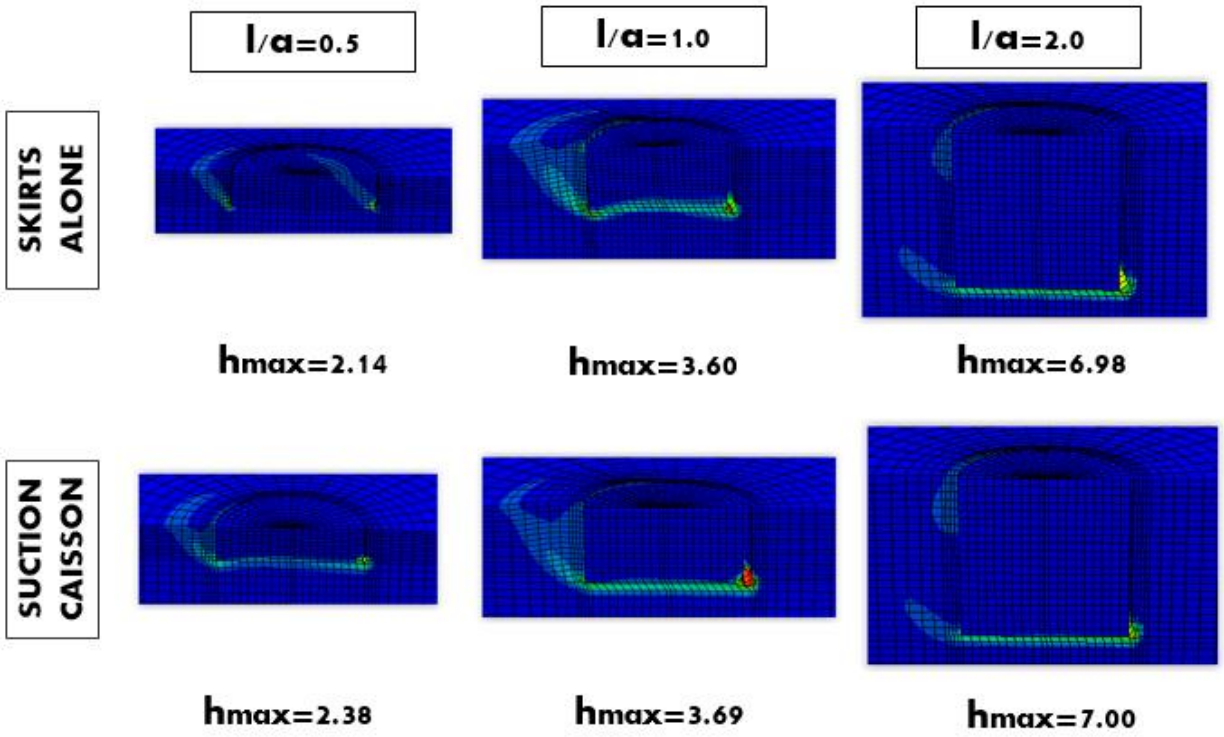

Fig.3.31. Failure mechanisms along with deformed FE - Rigid foundation under horizontal loading [TSI assumption]

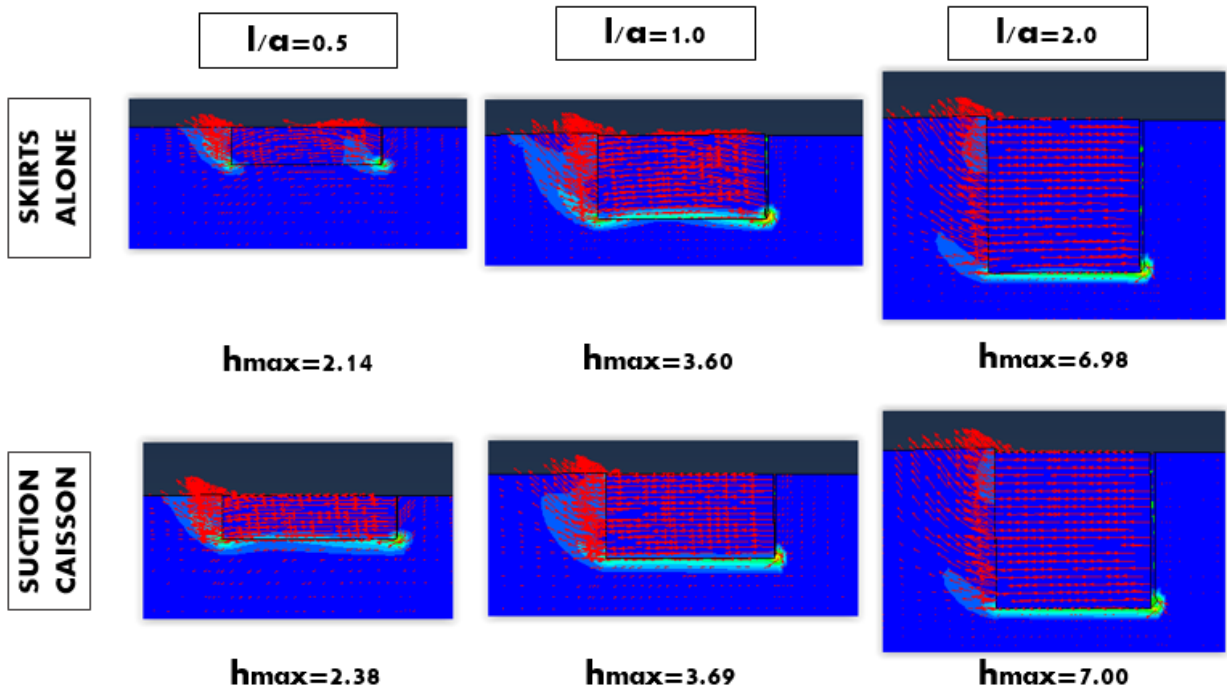

Fig.3.32. Failure mechanisms along with displacement vectors - Rigid foundation under horizontal loading [TSI assumption]

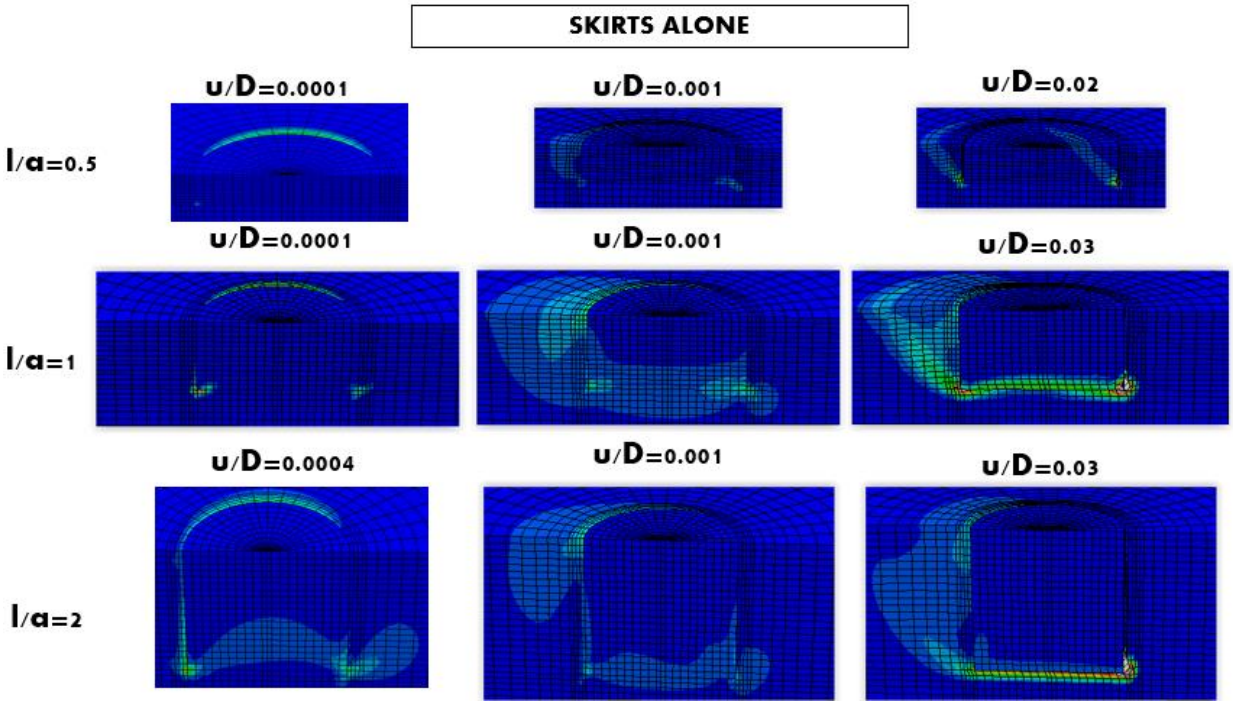

Fig.3.33. Evolution of plastic strains in the case of the rigid skirts alone under horizontal loading

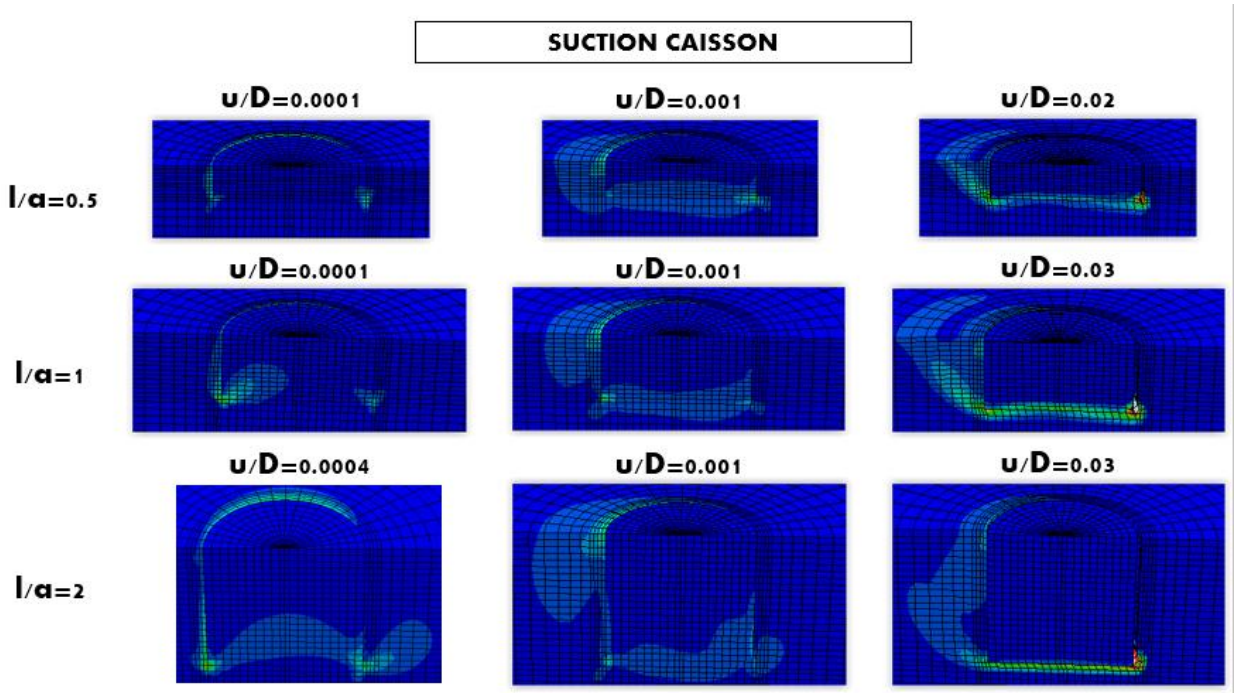

Fig.3.34. Evolution of plastic strains in the case of the rigid suction caisson under horizontal loading

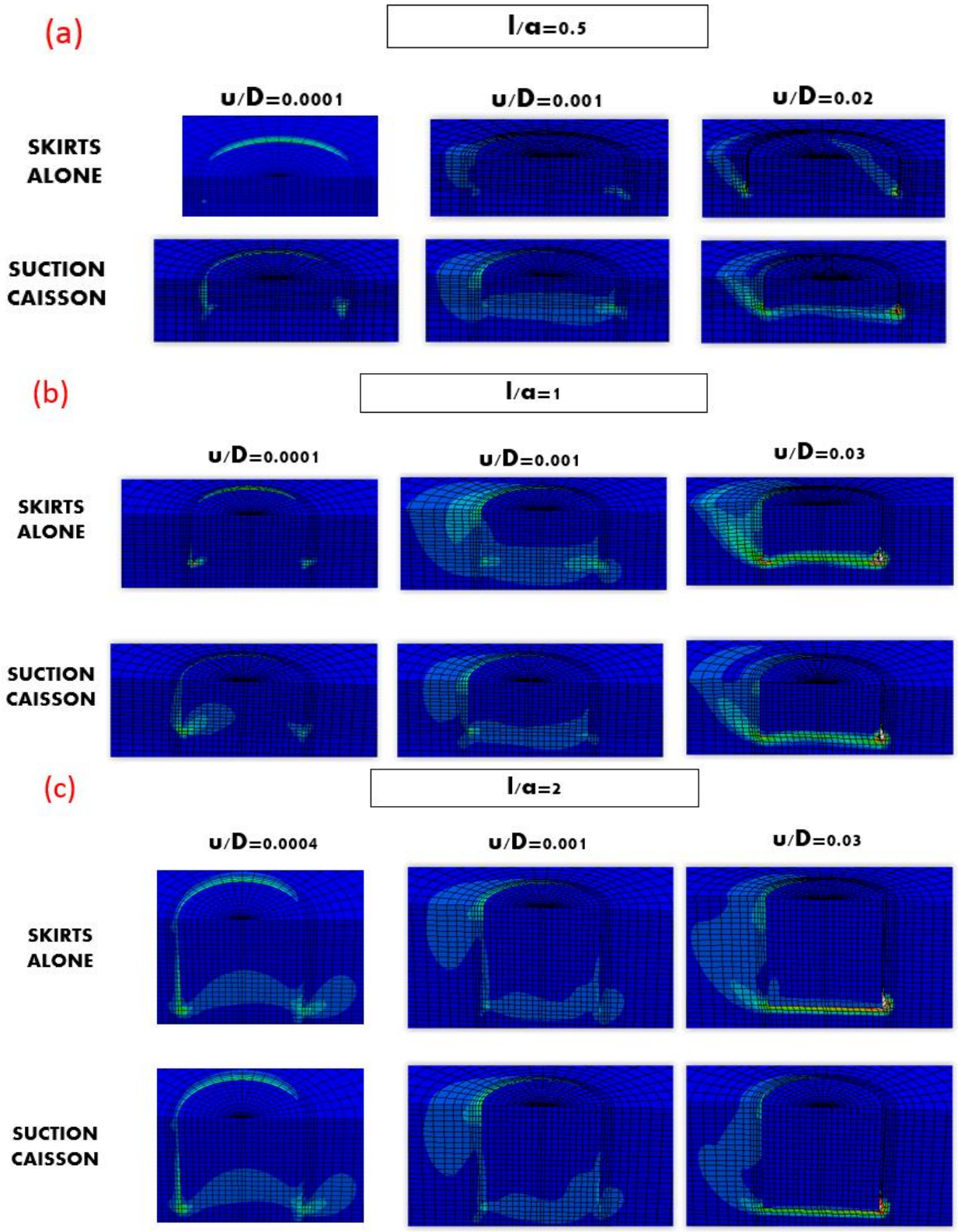

Fig.3.35. Comparison of the plastic strain development between the rigid suction caisson and the skirts alone under horizontal loading. (a): L/a=0.5, (b): L/a=1 and (c): L/a=2

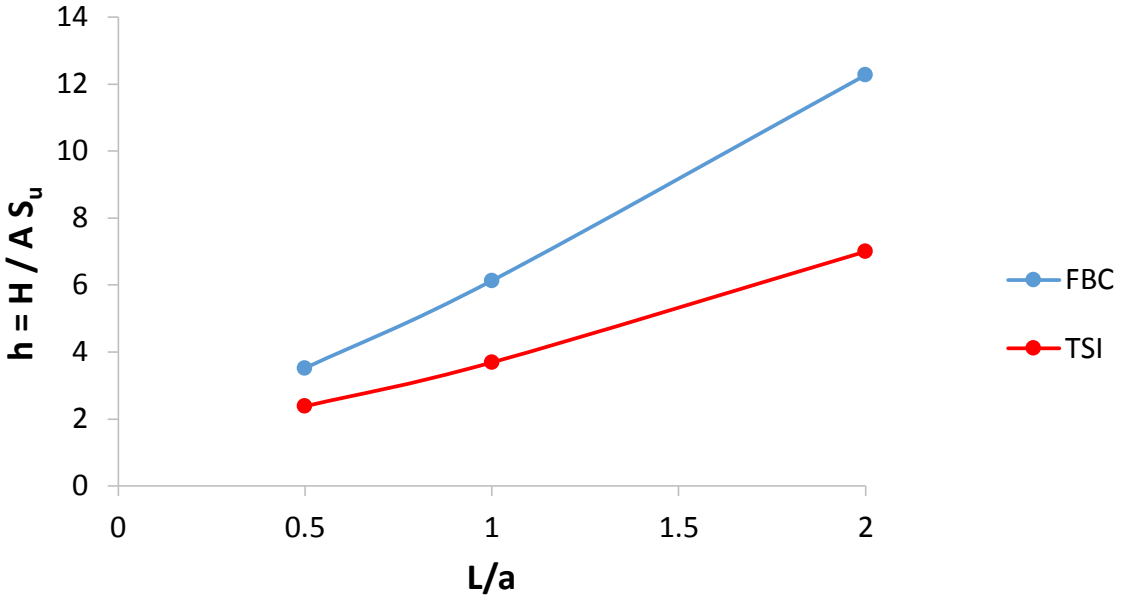

Fig.3.36. Dimensionless horizontal bearing capacity of the rigid suction caisson as a function of embedment ratio under TSI assumption

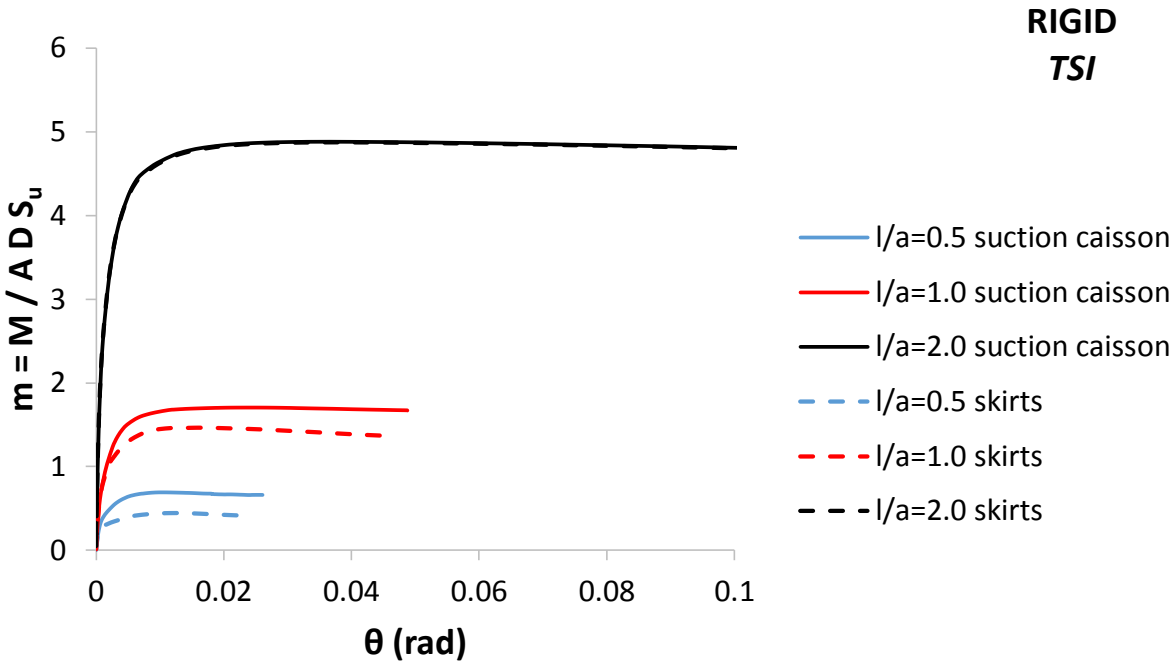

Fig.3.37. Dimensionless moment-rotation curves of the rigid foundation under TSI assumption

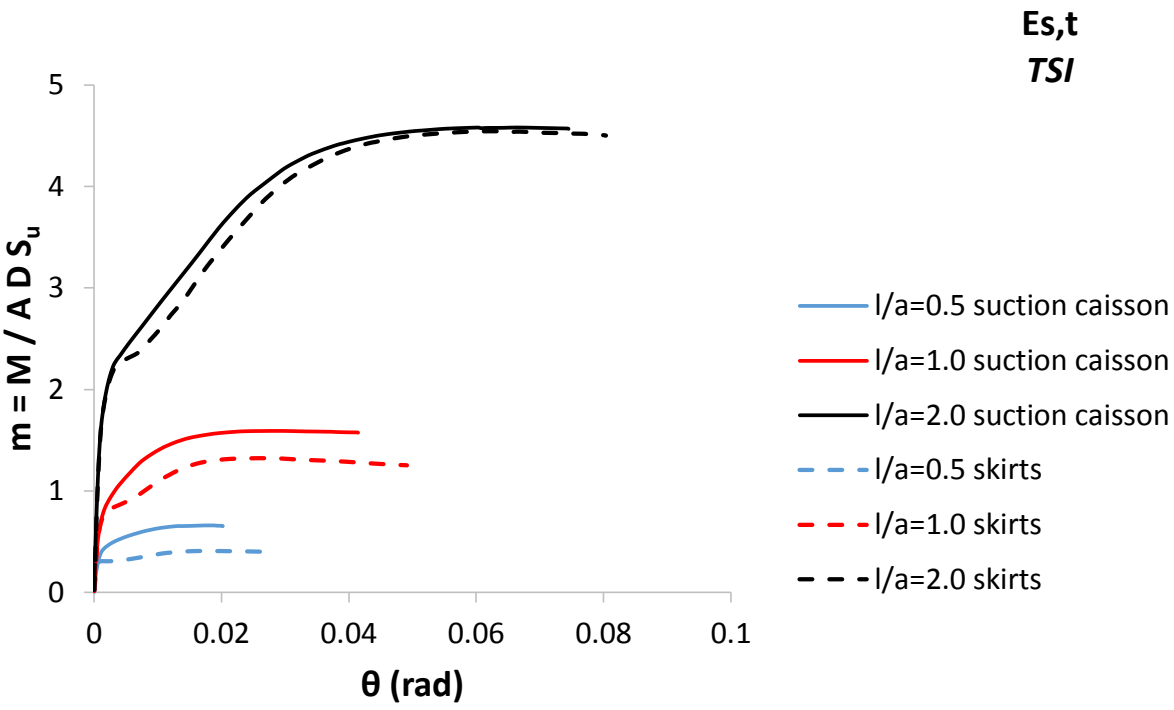

Fig.3.38. Dimensionless moment-rotation curves of the (Es,t) foundation under TSI assumption

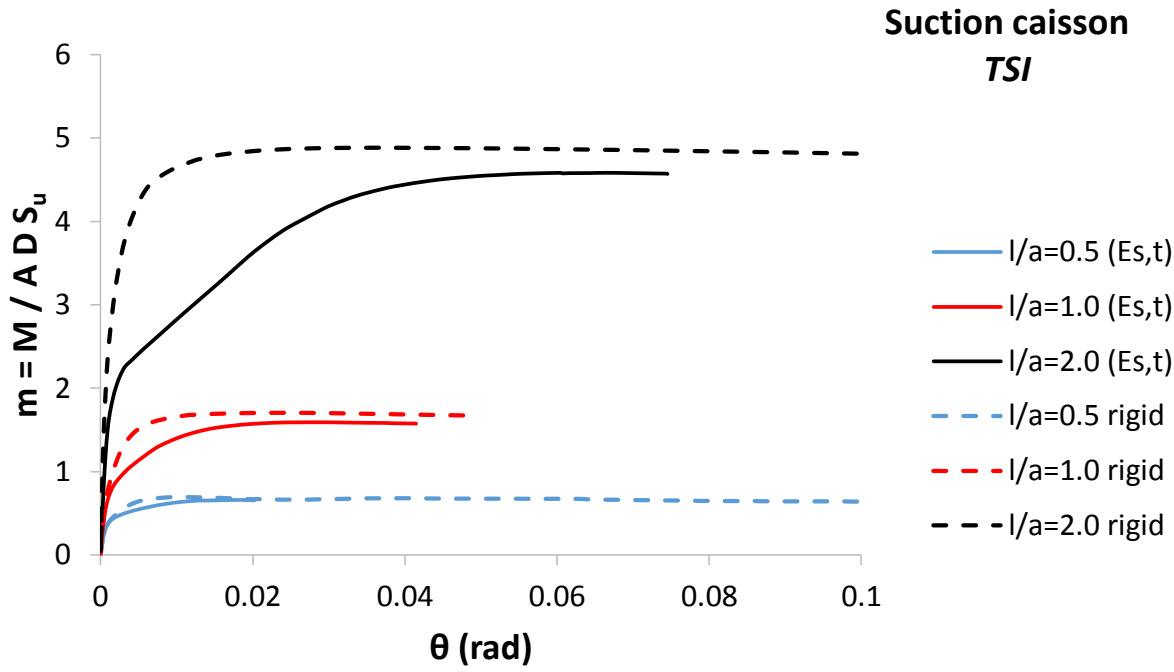

Fig.3.39. Dimensionless moment-rotation curves of the suction caisson under TSI assumption

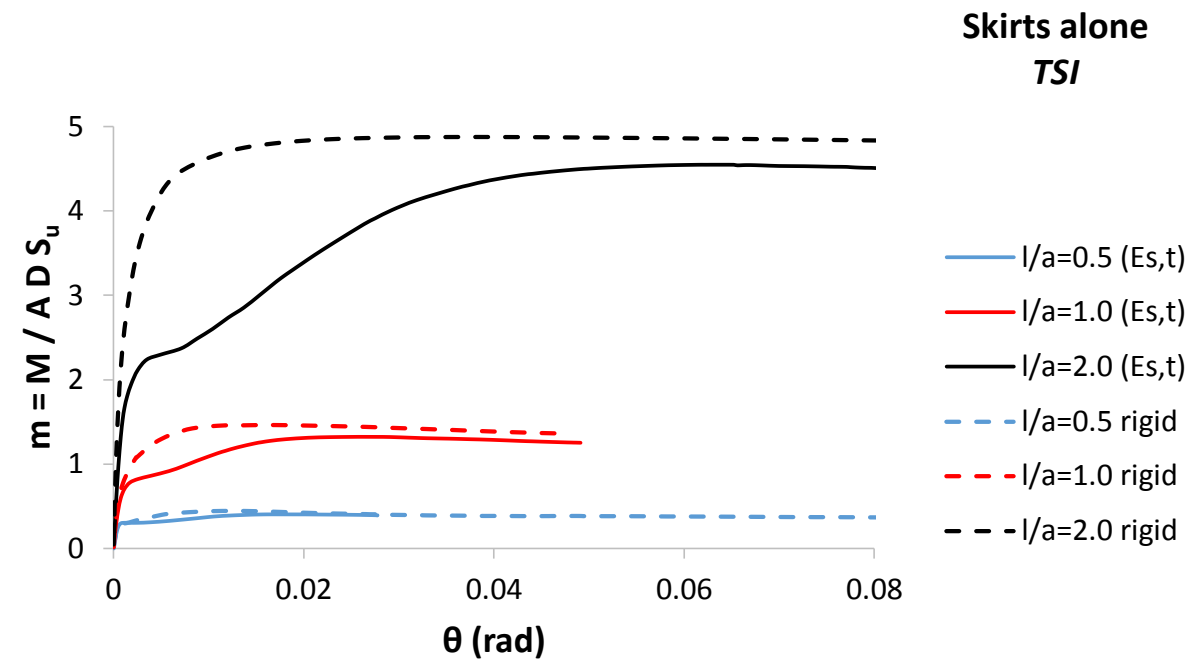

Fig.3.40. Dimensionless moment-rotation curves of the skirts alone under TSI assumption

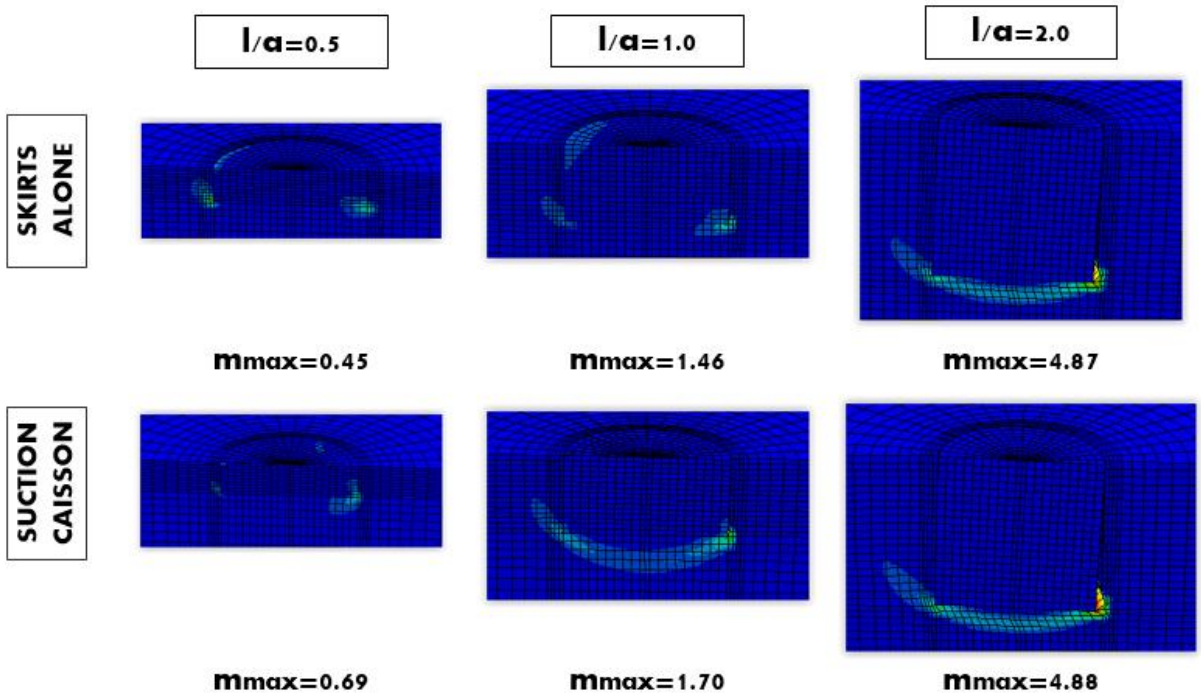

Fig.3.41. Failure mechanisms along with deformed FE. Rigid foundation under moment loading [TSI assumption]

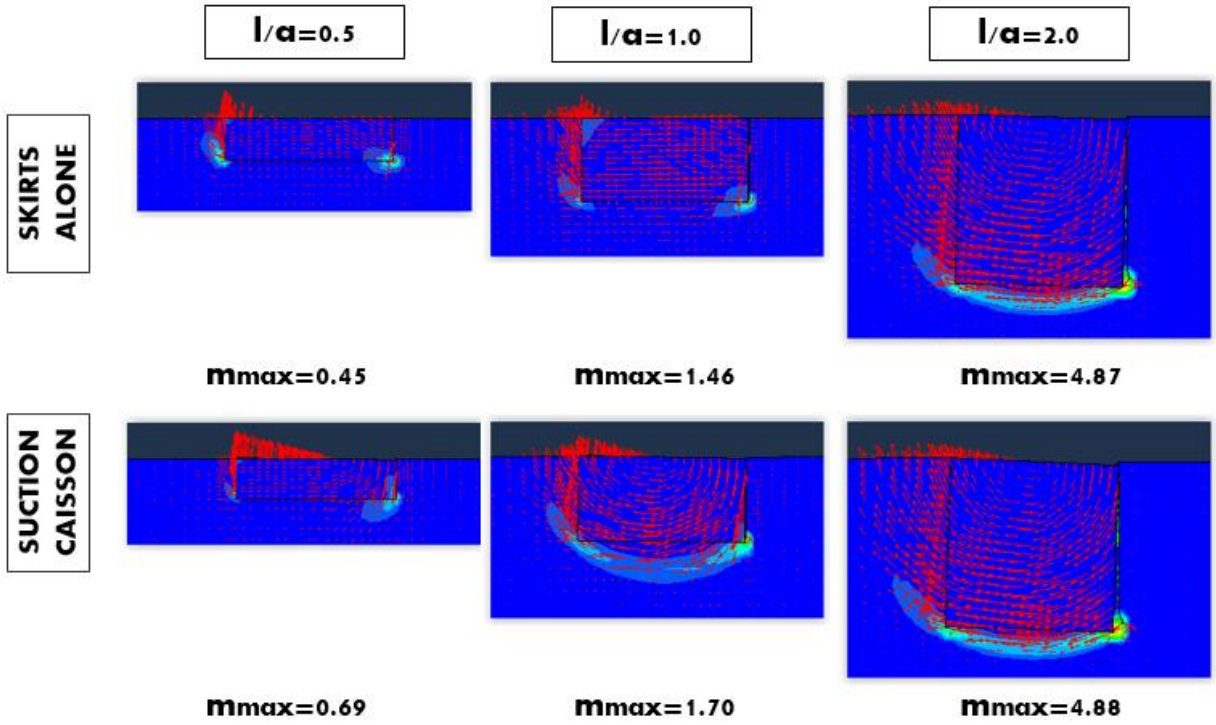

Fig.3.42. Failure mechanisms along with displacement vectors. Rigid foundation under moment loading [TSI assumption]

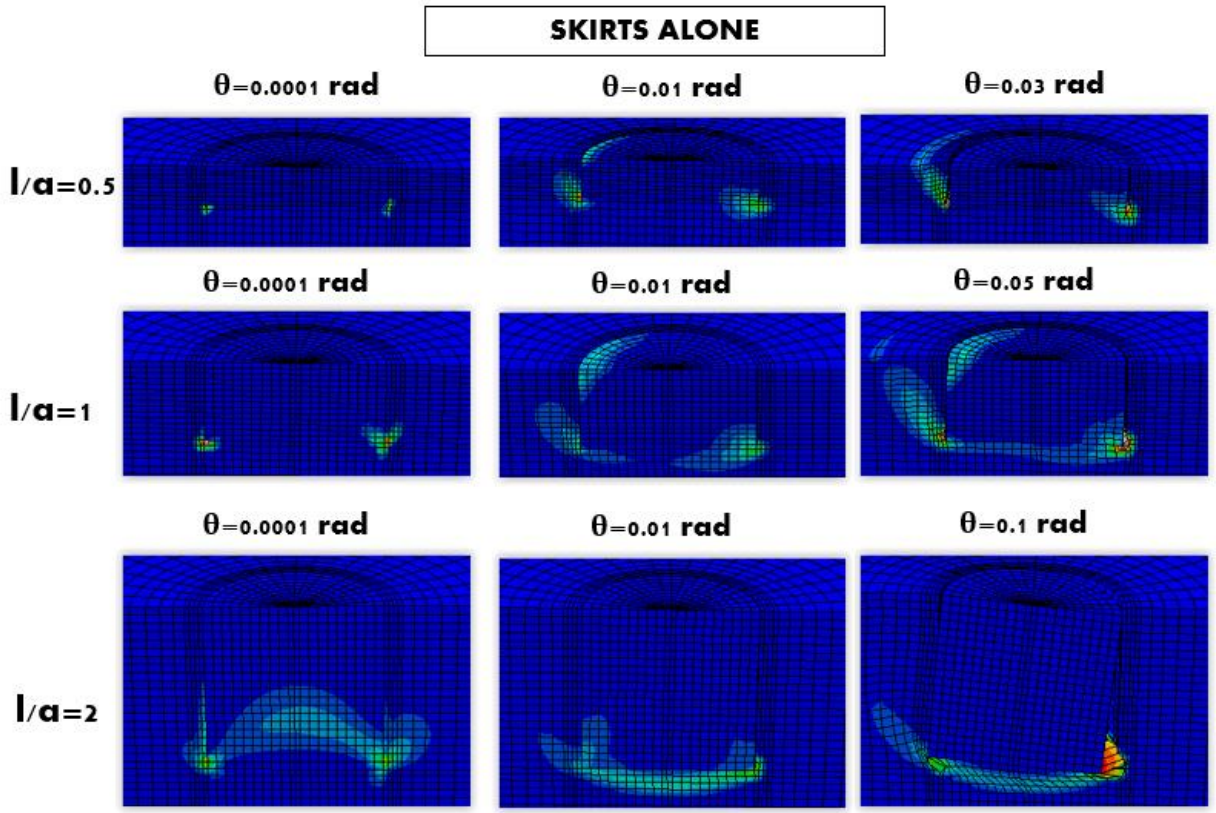

Fig.3.43. Evolution of plastic strains in the case of the rigid skirts alone under moment loading

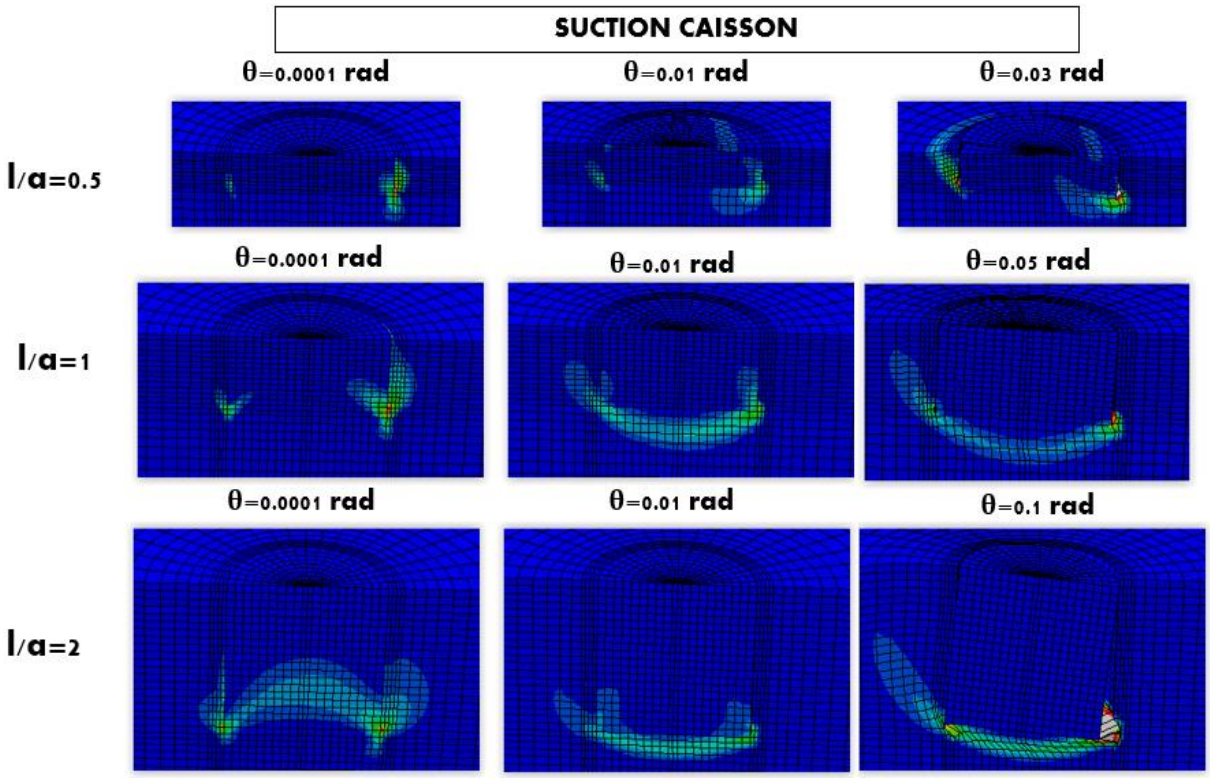

Fig.3.44. Evolution of plastic strains in the case of the rigid suction caisson under moment loading

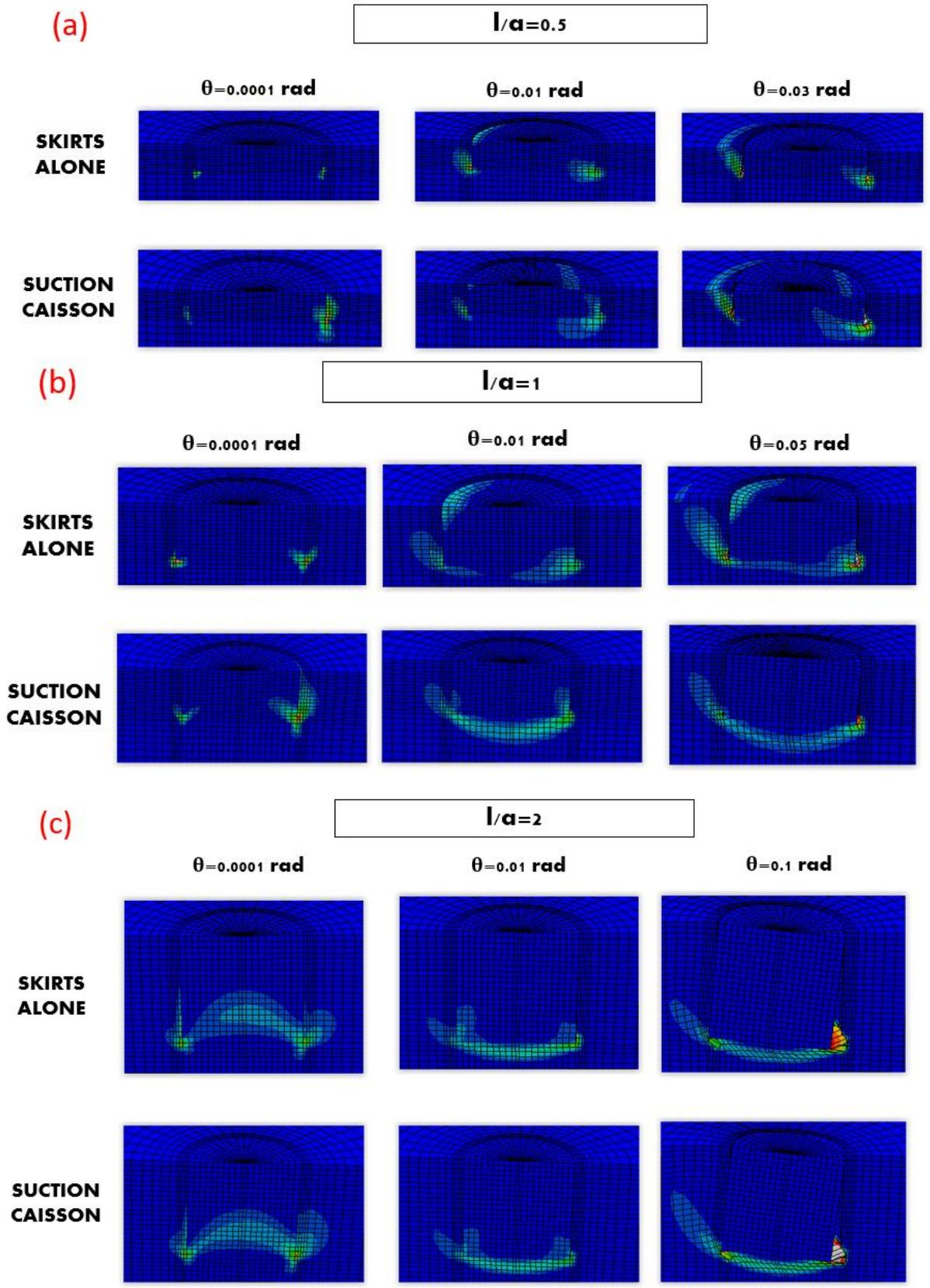

Fig.3.45. Comparison of the plastic strain development between the rigid suction caisson and the skirts alone under TSI assumption. (a): L/a=0.5, (b): L/a=1 and (c): L/a=2

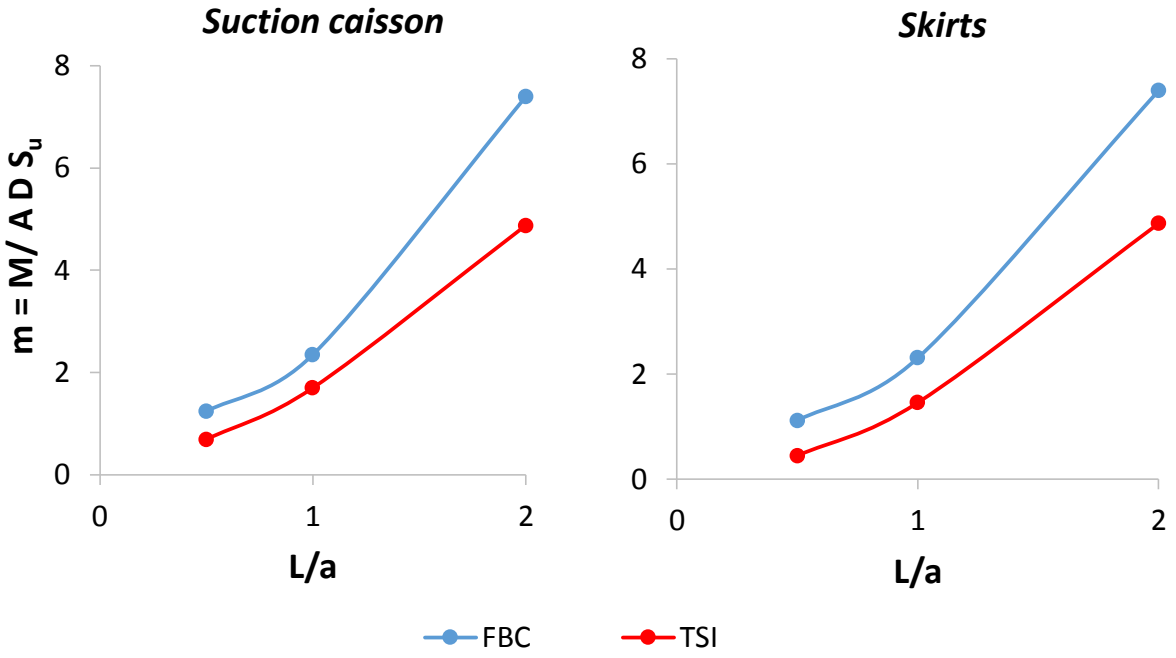

Fig.3.46. Dimensionless bearing capacity of the rigid foundation as a function of embedment ratio, under FBC and TSI assumption. *Left:* Suction caisson; *Right:* Skirts alone

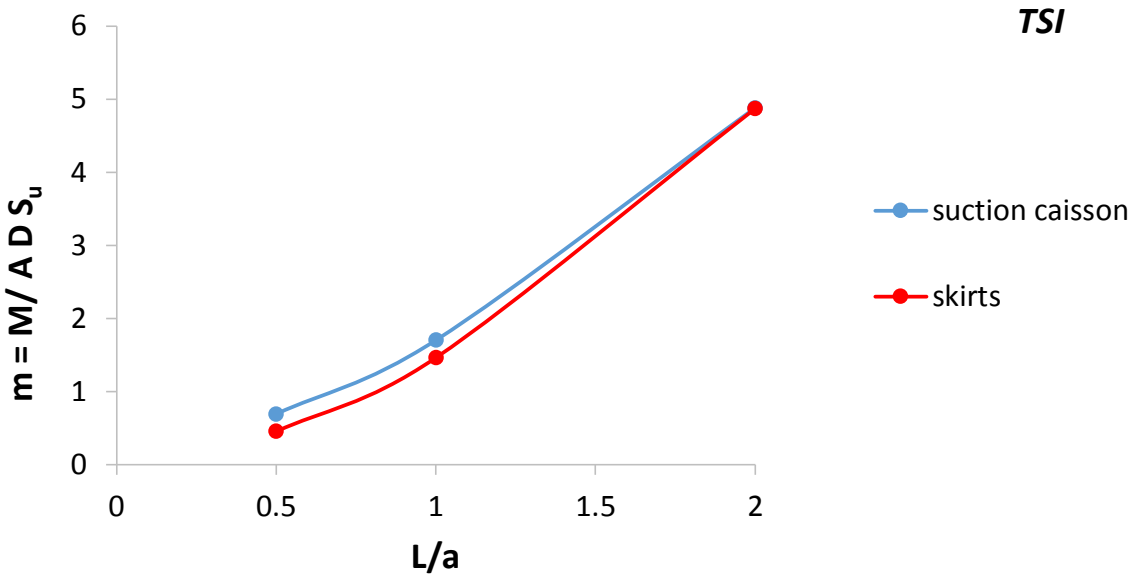

Fig.3.47. Dimensionless bearing capacity of the rigid foundation under moment loading as a function of embedment under TSI assumption

Chapter 4

Stiffness of Skirted Foundations

4 Stiffness of Skirted Foundations

4.1 Preface

Due to Soil-Structure Interaction (SSI), stiffness depends on the characteristics of both the soil and the foundation. The elastic stiffness of the soil-foundation system constitutes a useful means that estimates the behavior of the system in the small-strain domain, where the soil is assumed to develop exclusively elastic deformations. Moreover, calculating the stiffness of the whole system is necessary for the assessment of its natural period, which is a significant parameter in cycling and seismic loading.

In order to describe the total stiffness of the soil-foundation system, a stiffness matrix can be used, similarly to equation (1.13). Under individual types of loading the response of the system may involve only displacements or rotations (in the case of vertical or torsional loading) or combined displacements and rotations, under horizontal or moment loading, owing to the coupling between the degrees of freedom activated, as has been previously discussed.

A lot of research has been carried out for the determination of elastic static and dynamic stiffnesses for a variety of foundation types and shapes (Poulos & Davis, 1974; Gazetas, 1983, 1987, 1991; Roesset, 1980; Doherty & Deeks, 2003, 2005; Doherty et al., 2005). **Figure 4.1** presents the elastic stiffnesses for a circular surface footing, as well as increase factors accounting for embedment and the influence of a bedrock, as suggested by Gazetas (1991).

Gazetas et al. (2013) introduced a methodology taking into account geometry and material nonlinearities in the case of a surface footing in undrained conditions, where the effective, nonlinear rocking stiffness of the soil-foundation system is assessed.

Regarding skirted foundations, limited studies on the elastic or nonlinear stiffness of the soil-foundation system have been performed. Doherty et al. (2005) provided tables of coefficients accounting for a variety of embedment cases, Poisson's ratio and skirt flexibility, which, in combination with expression (1.16) are able to determine in a simplified manner the elastic stiffness. The researchers introduced *J*, which is a dimensionless parameter that gives unique values for various system stiffnesses. Interestingly, for large values of *J*, the elastic response of the soil-foundation system is almost equal to that of a rigid caisson.

4.2 Elastic Stiffnesses of Skirted Foundations

4.2.1 Modified Elastic Stiffnesses of Circular Solid Embedded Foundations

Expressions for the stiffness of embedded foundations found in previous publications, consider the location of the reference point on the centerline at the base of the foundation. However, in order to effectively proceed to comparisons between skirted and embedded foundations, this assumption would be problematic due to the flexibility of the skirts, which, depending on its degree, would be responsible for the change of the reference point's relative position; with the exception of the completely rigid skirts of course. Consequently, it is necessary to translate the load reference point to the top of the foundation, which is rigid anyway.

Figure 4.2 illustrates the absolute displacement of the reference point at the top of the solid foundation and the transformed moment for small rotations. Below, using the definitions of the forces/moments and displacements/rotations shown in **Figure 4.2**, in combination with stiffness matrix expressions, appropriate expressions accounting for the translation of the load-reference point to the top of the foundation will be produced. Subscripts *b* and *t* denote that the variable refers to the bottom or top of the foundation, respectively. Apparently, no process for the vertical stiffness will be shown below, since it remains the same, whether the reference point is chosen at the top or at the bottom of the foundation.

$$M_b = K_{R_b}\theta + K_{C_b}u \tag{4.1}$$

$$H_b = K_{C_b}\theta + K_{H_b}u \tag{4.2}$$

$$M_t = K_{R_t}\theta - K_{C_t}(u + D\theta) \tag{4.3}$$

$$H_t = -K_{C_t}\theta + K_{H_t}(u + D\theta) \tag{4.4}$$

The selection of the signs before the cross-coupling stiffness terms has been made to produce positive values of those terms. In specific, when a horizontal force acts at the top of the foundation, it tends to rotate, and a moment of opposite direction needs to be implemented for resistance; subsequently, the coupling term will have a negative sign. Accordingly, the positive sign was used before the cross-coupling term at the bottom of the foundation.

For the definition of the horizontal and rocking stiffness, as well as the coupling term at the top of the foundation, three additional equations are needed. For this transformation, the equation relating the moment at the top to the moment and horizontal force at the bottom of the foundation is the following:

$$M_t \approx M_b - H_b D \tag{4.5}$$

The second equation that involves the equality of the horizontal forces is given below:

$$H_t = H_b \tag{4.6}$$

Finally, for the determination of the system only one last equation remains, which can be given by either cases depicted in **Figure 4.3**, where either the horizontal or the rotational degree of freedom is constricted (u=0 or ϑ=0 respectively). The solution of the system is:

$$\begin{Bmatrix} K_{H_t} \\ K_{R_t} \\ K_{C_t} \end{Bmatrix} = \begin{Bmatrix} K_{H_b} \\ K_{R_b} + \left(K_{H_b} D - 2K_{C_b}\right) D \\ K_{H_b} D - K_{C_b} \end{Bmatrix} \tag{4.7}$$

Thus, with the above equations, the translation of the load-reference point is achieved from the bottom to the top of the foundation.

According to Gazetas (1991), the modified expressions for the stiffnesses of a solid embedded cylindrical caisson, when the reference point is taken at the top, are presented below:

$$K_V = \frac{4GR}{1-\nu}\left(1 + 1.3\frac{R}{H}\right)\left(1 + 0.55\frac{D}{R}\right)\left[1 + \left(0.85 - 0.28\frac{D}{R}\right)\frac{D}{H-D}\right] \tag{4.8}$$

$$K_H = \frac{8GR}{2-\nu}\left(1 + 0.5\frac{R}{H}\right)\left(1 + \frac{D}{R}\right)\left(1 + 1.25\frac{D}{H}\right) \tag{4.9}$$

$$K_R = \frac{8GR^3}{3(1-\nu)}\left(1 + 0.17\frac{R}{H}\right)\left(1 + 2\frac{D}{R}\right)\left(1 + 0.65\frac{D}{H}\right) + \frac{1}{3}K_H D^2 \tag{4.10}$$

$$K_C = \frac{2}{3}K_H D \tag{4.11}$$

Lekkakis (2012) based on the modification of (4.8)-(4.11), proposed similar expressions for the elastic stiffnesses of a solid embedded cylindrical caisson with the load-reference point at the top:

$$K_V = \frac{4GR}{1-\nu}\left(1 + 1.6\frac{R}{H}\right)\left(1 + 0.4\frac{D}{R}\right)\left[1 + \left(0.9 - 0.25\frac{D}{R}\right)\frac{D}{H-D}\right] \tag{4.12}$$

$$K_H = \frac{8GR}{2-\nu}\left(1 + 0.7\frac{R}{H}\right)\left(1 + 1.1\left(\frac{D}{R}\right)^{0.65}\right)\left(1 + 1.15\frac{D}{H}\right) \tag{4.13}$$

$$K_R = \frac{8GR^3}{3(1-\nu)}\left(1 + 0.15\frac{R}{H}\right)\left(1 + 0.95\frac{D}{R}\left(1 + \frac{D}{R}\right)^{1.4}\right)\left(1 + 0.7\frac{D}{H}\right) \tag{4.14}$$

$$K_C = 0.6K_H D \tag{4.15}$$

4.2.2 Elastic Stiffnesses of Flexible Skirted Foundations

Doherty et al. (2005) found that the stiffness of a suction caisson depends on the flexibility of its skirts. The researchers introduced the dimensionless parameter *J*, which takes into account the thickness of the skirts, the radius of the foundation, as well as the foundation and soil Young and shear moduli, producing thus unique values of stiffness. Interestingly, as *J* approaches very large values, the stiffness of the suction caisson tends to become equal to that of a solid, embedded foundation. Accordingly, for small values of *J*, the response of the suction caisson in terms of stiffness matches that of the surface footing.

According to the definition, the stiffness of a foundation equals the resistance force or moment, for imposed displacement or rotation of unit value. However, after Doherty et al. (2005), in order to assess the actual stiffness of the skirted foundation, where the effect of the skirts' flexibility is properly considered, displacements and rotations are not imposed equally on the whole foundation, but on the lid only. In the case of the skirts alone, which is also addressed in this thesis, the displacements and rotations are prescribed on the top periphery of the foundation, on the surface.

In all the analyses conducted herein, the parameters that remain common are: the depth of the soil stratum H=30 m, the foundation radius a=5 m and the skirt thickness t=0.02 m. In addition, it needs to be underlined that the stiffness of a rigid foundation can be assessed by multiplying the stiffness of a solid foundation with the appropriate coefficient from **Table 4.2:**

	Vertical	Horizontal	Rocking	Coupled swaying-rocking
$\frac{K_{rigid}}{K_{solid}}$	$\left(1-0.04\frac{D}{B}\right)$	$\left(1-0.03\frac{D}{B}\right)$	$\left(1-0.035\frac{D}{B}\right)$	$\left(1-0.04\frac{D}{B}\right)$

Table 4.2. Reduction coefficients for K_{rigid}

where D is the embedment depth and B the foundation diameter. However, for the embedment ratios of interest (L/a≤2 or D/B≤1), it can be considered that $K_{rigid} \approx K_{solid}$.

Figure 4.4 presents the percentile differences of the transformed expressions by Gazetas (1991) and Lekkakis (2012) in comparison with the finite element analysis (FEA) results on the rigid suction caisson derived from this study for each stiffness component in the case of soil Young Modulus E=60 MPa, Poisson's ratio ν=0.49 and steel Young Modulus E_S=21000 GPa. The embedment depth to radius ratios (L/a) that were examined, range from 0.02 to 2. Additionally, in **Table 4.1** are available the maximum deviations of the FEA results from the above expressions. Overall, the FEA results herein show better agreement with the expressions by Lekkakis (2012); it needs to be noted that the difference of 25% is observed for the L/a=0.02 embedment ratio. Generally, for embedment ratios equal or larger than 0.5, which constitutes the area of interest in this study, the maximum difference between the FEA results and the expressions by Lekkakis (2012) is at 3% only, whereas the maximum difference from Gazetas

(1991) is at 19%. Therefore, it can be deduced, that the increased Young Modulus of steel used for these FEA analyses, led the suction caisson to respond similarly to a solid embedded foundation in terms of stiffness. This also proves that the imposition of displacements/rotations on the top of the foundation is a reasonable choice for skirted foundations.

	Gazetas (1991) Transformed	**Lekkakis (2012)**
$\mathbf{K_V}$	8%	4%
$\mathbf{K_H}$	17%	3%
$\mathbf{K_R}$	15%	2%
$\mathbf{K_C}$	26%	25%

Table 4.1. Maximum percentile difference from FEA results

A comparison between the elastic stiffnesses of the suction caisson from this study and the results by Doherty et al. (2005) is available in **Figures 4.5** and **4.6**, for Young Modulus of steel 210 GPa and 21000 GPa respectively, in the case of soil Young Modulus E=60 MPa and Poisson's ratio ν=0.49. The normalized values proposed by Doherty et al. (2005) were multiplied with the increase factors accounting for the influence of the rocky substratum from the expressions by Lekkakis (2012), in order to properly compare them with the FEA results of this study. Differences appear mainly as embedment ratio grows, with the maximum reaching 19% in the cross-coupling stiffness for Es=210 GPa. Apart from this, it can be observed that the agreement is quite satisfying.

The FEA results of this study regarding the elastic stiffness of the suction caisson embedded in the homogeneous soil stratum, are presented dimensionless after appropriate normalization in **Figure 4.7** and **Figure 4.8**, for ν=0.49 and ν=0.1 respectively. Attention must be drawn to the fact that, for all the cases, the dimensionless stiffness components involve the effect of the rocky substratum. As embedment ratio decreases, the dimensionless values approach the results for surface footings.

As it can be seen, the increased Young Modulus of steel is evident in the stiffness results for embedment ratios L/a greater than 1. This is understandable, since the foundation becomes more rigid naturally, as the skirt length decreases.

Furthermore, the elastic stiffness of the suction caisson was examined for an inhomogeneous soil deposit too, for ν=0.49. It was assumed that the Young Modulus of soil increases linearly with depth with a gradient k [MN/m^3], in a manner of E=kz. The analyses were performed for two values of k: 0.5 and 1. This type of soil is representative of normally consolidated clays and is called "Gibson soil". It needs to be noted that normalization of the results is performed with the shear modulus at the skirt tip level, G_0. The dimensionless stiffness components are shown in **Figure 4.9**. The distinction between the results for Es=210 GPa and Es=21000 GPa is barely inexistent, due to the poor soil strength close the surface, leading the foundation to respond as rigid in both cases.

All of the aforementioned cases were examined for the skirts alone too. The results are shown as a proportion of the suction caisson's corresponding stiffness. The case of the homogeneous soil stratum is depicted in **Figures 4.10** and **4.11**, for ν=0.49 and ν=0.10 respectively. Accordingly, the case of the inhomogeneous soil deposit with linearly increasing strength is provided in **Figure 4.12**, for ν=0.49. It needs to be highlighted, that for the embedment ratio L/a=2, the response of the suction caisson and the skirts in terms of elastic stiffness is practically the same, for all of the cases investigated. For the L/a=1 foundation, the same observation applies for the homogeneous soil, whereas for the Gibson type soil, even though all the other stiffness components show almost perfect agreement, the vertical stiffness of the skirts is 13% smaller than that of the suction caisson. Regarding the small embedment ratio of L/a=0.5 under undrained conditions, in the homogeneous soil profile, the vertical stiffness component of the skirts is about 10% smaller than the one of the suction caisson, with the difference reaching 32% for the inhomogeneous soil. As expected, the difference between the elastic stiffness of the suction caisson and the skirts alone grows as the embedment ratio decreases, which appears to be more intense for the non-uniform soil profile, due to the reduced strength close to the surface.

Therefore, it is recommended that the determination of the skirts' elastic stiffness can be achieved by multiplying the respective elastic stiffness of the suction caisson with the appropriate value depending on the embedment ratio, found in the curves of **Figures 4.10**, **4.11** and **4.12**.

The comparison between the skirts alone and the suction caisson in terms of deformations for vertical, horizontal and moment loading are presented in **Figures 4.13**, **4.14** and **4.15** respectively, for the case of the L/a=1 foundation in the homogeneous soil profile for ν=0.49. The most obvious difference is under vertical loading, where heaving of the constrained soil in the skirts alone occurs due to the absence of the lid. Under horizontal loading of the skirts, heaving is observed from the one side of the internal soil and settlement from the other. This is also noticed for the moment loading. The soil plug in the suction caisson does not seem to deform on top, due to its confinement by the lid. Nevertheless, it needs to be taken into account, that these differences are apparent because the deformation scale factor is 6 under vertical and horizontal loading. In the elastic domain, where small strains are considered, the absence of the suction caisson's lid does not play a significant role as embedment ratios increase ($L/a \geq 1$) and the elastic stiffnesses of the two foundation types tend to be practically equal.

Finally, in order to assess the elastic stiffness of a suction caisson embedded in a Gibson soil for ν=0.49, a method of practical nature based on the numerical results herein was developed, which involves the use of the expressions (4.12-4.15) for the elastic stiffness of a solid embedded foundation by Lekkakis (2012), but with an equivalent shear Modulus G*=G(Z), found in a depth Z from the surface, in the case of the inhomogeneous soil. As it was previously discussed, a rigid suction caisson responds approximately as a solid embedded foundation in terms of elastic stiffness. Additionally, it was shown that in the Gibson soil, the suction caisson with conventional steel Young Modulus Es=210 GPa showed practically the same results with the rigid suction caisson with Es=21000 GPa, especially for L/a<2, due to the poor soil strength

close to the surface. Thus, it can be deduced that the proposed practical methodology for the suction caisson embedded in the Gibson soil, could be extended for solid embedded foundations too.

The steps of the proposed methodology in order to assess the elastic stiffness of a suction caisson embedded in Gibson soil for ν=0.49, are presented below:

1. Estimation of normalized depth Z/L as a function of embedment ratio L/a, for each elastic stiffness component:

$[K_V]$ $Z/L = 1.5439(L/a)^{-0.528}$ (4.16)

$[K_H]$ $Z/L = 0.9593(L/a)^{-0.321}$ (4.17)

$[K_R]$ $Z/L = 1.06(L/a)^{-0.244}$ (4.18)

$[K_C]$ $Z/L = 1.2056(L/a)^{-0.346}$ (4.19)

2. Calculation of G*=G(Z) in the Gibson soil, for each stiffness component

3. Use of each G* in the respective stiffness component expression (4.12-4.15) for the solid embedded foundation

Figure 4.16 presents the graphs of the expressions for the normalized depth Z/L of the equivalent shear Modulus G* as a function of embedment ratio, for each stiffness component.

4.3 Nonlinear Stiffnesses of Skirted Foundations

4.3.1 Preface

The role of elastic stiffnesses is indispensable for preliminary calculations; however, they can only be considered accurate in the small-strain domain. When displacements and rotations increase, geometry and material nonlinearities prevail, affecting thus the behavior of the system. Therefore, the expressions from the previous sections can no longer be implemented, since they would lead to overestimation of the actual stiffness of the soil-foundation system.

Consequently, the response of the system needs to be thoroughly examined, as it enters the plastic domain, where soil yielding, detachment, sliding and uplift can be observed. Gazetas et al. (2013) studied the degradation of the rocking stiffness of surface foundations depending on

the level of rotation imposed to the foundation and provided appropriate charts and fitting expressions.

In the case of the suction caisson, which involves soil yielding and interfaces both externally and internally of the sidewalls, the problem is a function of a variety of parameters, constituting it nonlinear by nature. The assumptions of: (a) Fully Bonded Contact [FBC] and (b) Tensionless Sliding Interface [TSI] between the foundation and the supporting soil for the homogeneous soil stratum of undrained shear strength S_U=80 kPa, which were presented in Chapter 3, are examined in this section too. The suction caisson and the skirts alone are investigated as rigid (E_S=21000 GPa) for the three embedment ratios L/a=0.5, 1, 2.

Since large safety factors are established for offshore wind turbines under vertical loading, namely $FS_V \geq 20$, and due to the fact that lateral and moment loading deriving from wind, waves, and earthquakes are of crucial importance for this type of tall, slender structures, the vertical stiffness degradation will not be presented herein. Instead, available are the results concerning the degradation of horizontal, rocking and cross-coupling stiffness.

4.3.2 Nonlinear Stiffnesses for Infinite FS_V

The stiffness degradation is studied for a safety factor that approaches infinite under vertical loading. Gazetas et al. (2013) presented the stiffness degradation axis in terms of K(θ, FS)/K(0,FS), since the level of vertical loading affects significantly the initial stiffness before the imposition of horizontal displacement or rotation. Following the same manner and since the only examined FS_V herein is the infinite one, the results are shown in terms of K/K_0, where K is the stiffness varying with horizontal displacement or rotation and K_0 the initial stiffness, that is to say, for approximately zero horizontal displacement or rotation.

Figures 4.17 and **4.18** display the reduction in horizontal and coupled swaying-rocking stiffness, with the rotational degree of freedom being restricted, under FBC assumption. The appearance of the bumps in these curves reveals the development of new failure zones below, around and within the skirts, as they relieve those already formed due to excess displacements. The agreement between the response of the suction caisson and the skirts alone in terms of stiffness degradation is totally satisfying.

The results under TSI assumption, regarding the horizontal and cross-coupling stiffness are shown in **Figures 4.19** and **4.20**. As far as the former is concerned, the response of the suction caisson is approximately equal to that of the skirts alone, whereas in the case of the latter, the differences between the two foundation types, with the dimensionless coupled stiffness of the skirts exceeding in places that of the suction caisson for the smaller embedment ratios, are attributed to the normalization by the initial stiffness that corresponds to each foundation type and embedment ratio. Attention must be drawn to the fact that the initial horizontal stiffness for the TSI assumption is smaller than the one for FBC. Each normalization has been carried out

with the corresponding initial stiffness. Naturally, the initial stiffness under the FBC assumption equals the respective elastic stiffness.

Figures 4.21 and **4.22** illustrate the degradation of the horizontal and cross-coupling stiffness respectively, for the L/a=2 and 0.5 suction caisson. It needs to be noted that the corresponding stiffnesses under the FBC assumption are used for normalization. In the case of the L/a=0.5 foundation, for small displacements, the initial stiffness under TSI assumption is approximately 74-78% of the one for FBC. The reason is the detachment that takes place from very small imposed horizontal displacements when TSI is considered, since the interface has zero tensile capacity. As the imposed displacement grows, the differences tend to extinguish, since for FBC more soil is mobilized and material nonlinearities prevail. Additionally, when the soil behind the foundation is fully mobilized, it does not contribute more to the resistance of the system, thus to its stiffness. A similar behavior is observed for the L/a=2 foundation, with the TSI initial stiffness being 78-82% of the FBC respective one. Once again, for larger displacements the difference is minimized.

Following the same procedure as above, **Figures 4.23** and **4.24** illustrate the results for the rocking stiffness and the cross-coupling stiffness for imposed rotation with the horizontal degree of freedom being constrained, under FBC assumption. The response of the skirts alone matches that of the suction caisson overall, with a small difference noticed for the small embedment ratio. The corresponding results under TSI assumption are shown in **Figures 4.25** and **4.26**. For the rocking stiffness, even though for the L/a=2 aspect ratio the response between the two foundation types cannot be distinguished, some deviations begin to appear as embedment depth decreases. Regarding the cross-coupling stiffness when the horizontal degree of freedom is restricted, there is satisfying agreement between the suction caisson and the skirts alone, for all embedment ratios.

In order to compare the degradation of the rocking and cross-coupling stiffness in the case of TSI and FBC, normalization of each stiffness under TSI assumption by the respective FBC stiffness was carried out. The results for the smallest and largest embedment ratio are shown in **Figures 4.27** and **4.28**. For the L/a=0.5 embedment ratio, the initial stiffnesses for the TSI consideration are 70-73% of the stiffnesses where FBC is taken into account. Accordingly, for the aspect ratio L/a=2, the gap is bridged with the proportions being 73-78%.

4.4 Conclusions

The elastic static stiffness components are calculated for a homogeneous and a Gibson type soil, by imposing displacements and rotations on the lid of the suction caisson and on the top periphery of the skirts alone, in order to properly take into account the flexibility of the sidewalls, following Doherty et al. (2005). Comparisons with results from the literature are provided. The inferences from this study on the elastic stiffness of skirted foundations are presented below:

- The determination of the elastic stiffness of the skirts alone can be achieved through curves developed in this study that provide it as a proportion of the respective suction caisson stiffness, for embedment ratios L/a ranging from 0.02 to 0.2.
- Interestingly, the differences between the two foundation types in terms of elastic stiffness are inexistent for L/a=2 for all the cases investigated, while they start to become evident as embedment ratio decreases.
- A methodology of practical nature is proposed for the estimation of the elastic stiffness of a rigid suction caisson, and as an extension of a solid cylindrical foundation, embedded in Gibson soil of ν=0.49.

In the second part of this chapter, the degradation of the soil-foundation stiffness for an infinite FS_V is presented in the large-strain domain, assuming fully bonded contact (FBC) and a tensionless sliding interface (TSI). The suction caisson and the skirts alone are examined in a soil stratum of uniform S_u for three embedment ratios L/a=0.5, 1 and 2. Charts were developed that show the degradation in the stiffness components as imposed displacements and rotations increase.

- Stiffness degradation is the same for the L/a=2 suction caisson and skirts alone, while differences tend to manifest themselves as embedment ratio decreases.

Chapter 4: Figures

Stiffness of Skirted Foundations

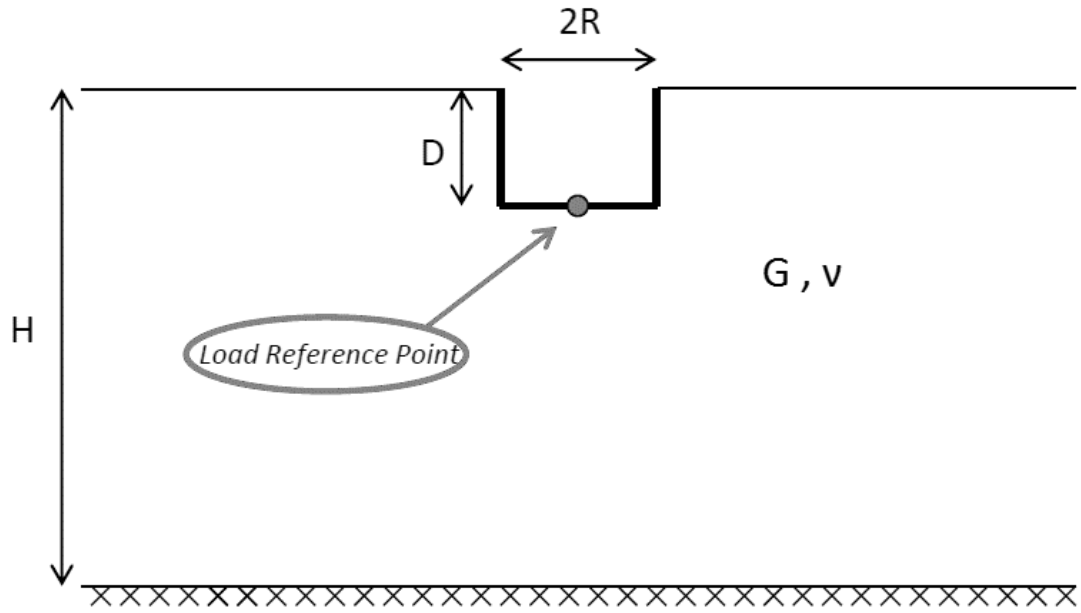

Stiffness	Surface	Rocky Substratum	Embedment
K_V	$\frac{4GR}{1-\nu}$	$\left(1+1.3\frac{R}{H}\right)$	$\left(1+0.55\frac{D}{R}\right)\left(1+\left(0.85-0.28\frac{D}{R}\right)\frac{\frac{D}{H}}{1-\frac{D}{H}}\right)$
K_H	$\frac{8GR}{2-\nu}$	$\left(1+0.5\frac{R}{H}\right)$	$\left(1+\frac{D}{R}\right)\left(1+\frac{5}{4}\frac{D}{H}\right)$
K_R	$\frac{8GR^3}{3(1-\nu)}$	$\left(1+0.17\frac{R}{H}\right)$	$\left(1+2\frac{D}{R}\right)\left(1+0.65\frac{D}{H}\right)$
K_C	—	—	$^1/_3 K_H D$

Fig.4.1. Elastic stiffnesses for a circular footing resting on a homogeneous soil stratum and increase factors accounting for a rocky substratum and/or embedment (Gazetas, 1991)

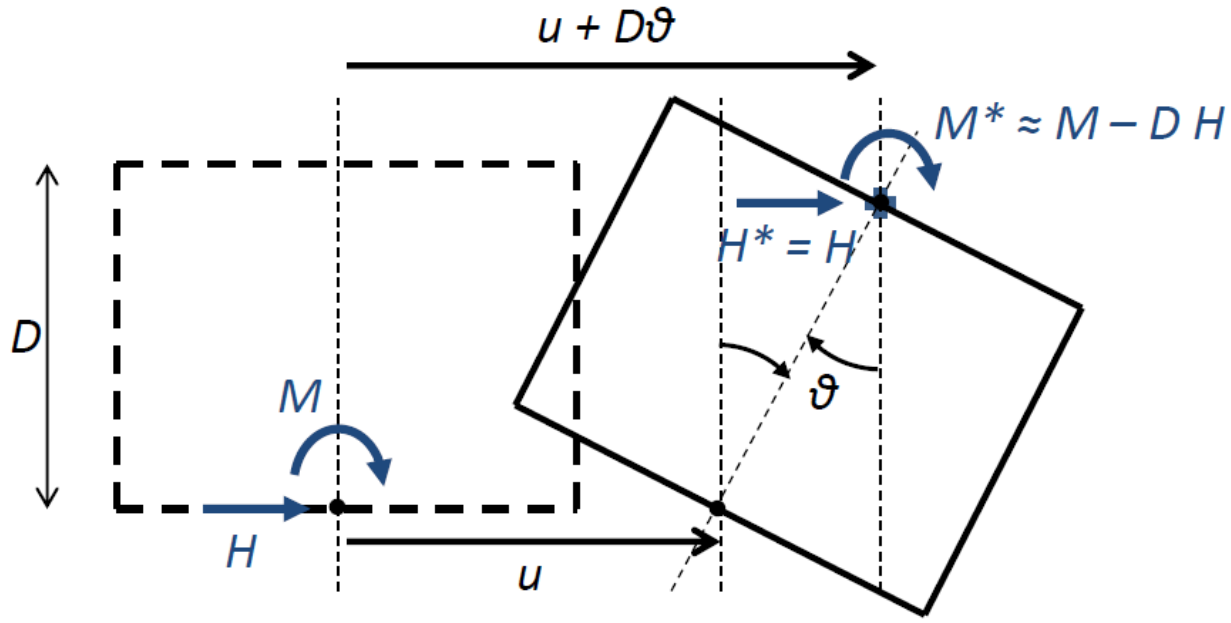

Fig.4.2. Transformed absolute displacement and moment for the translation of the load-reference point at the top of the foundation

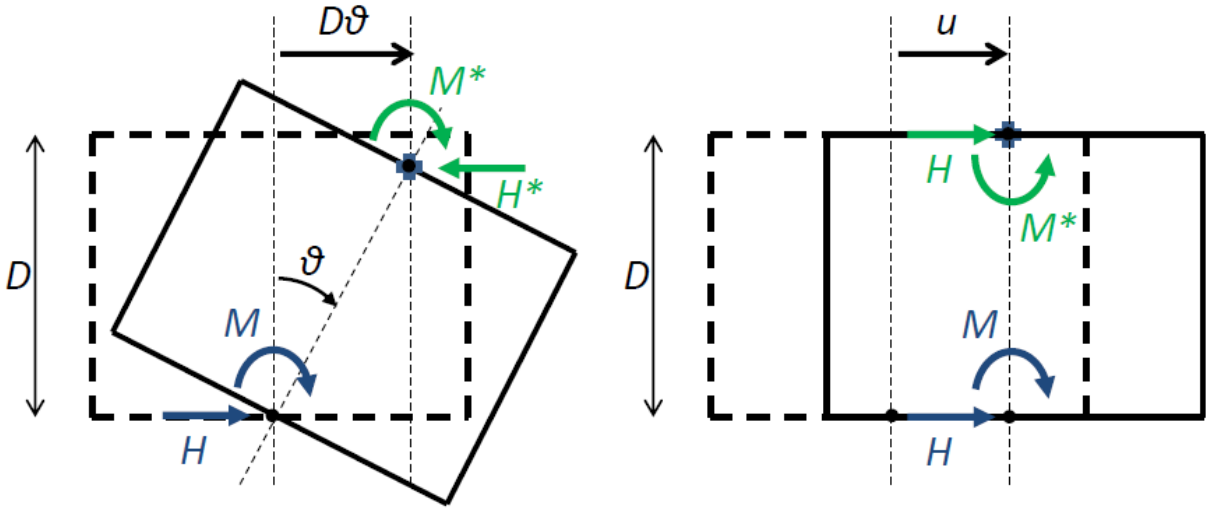

Fig.4.3. *Left*: Imposed rotation at the base with the horizontal degree of freedom restricted; *Right*: Imposed horizontal displacement with the rotational degree of freedom restricted

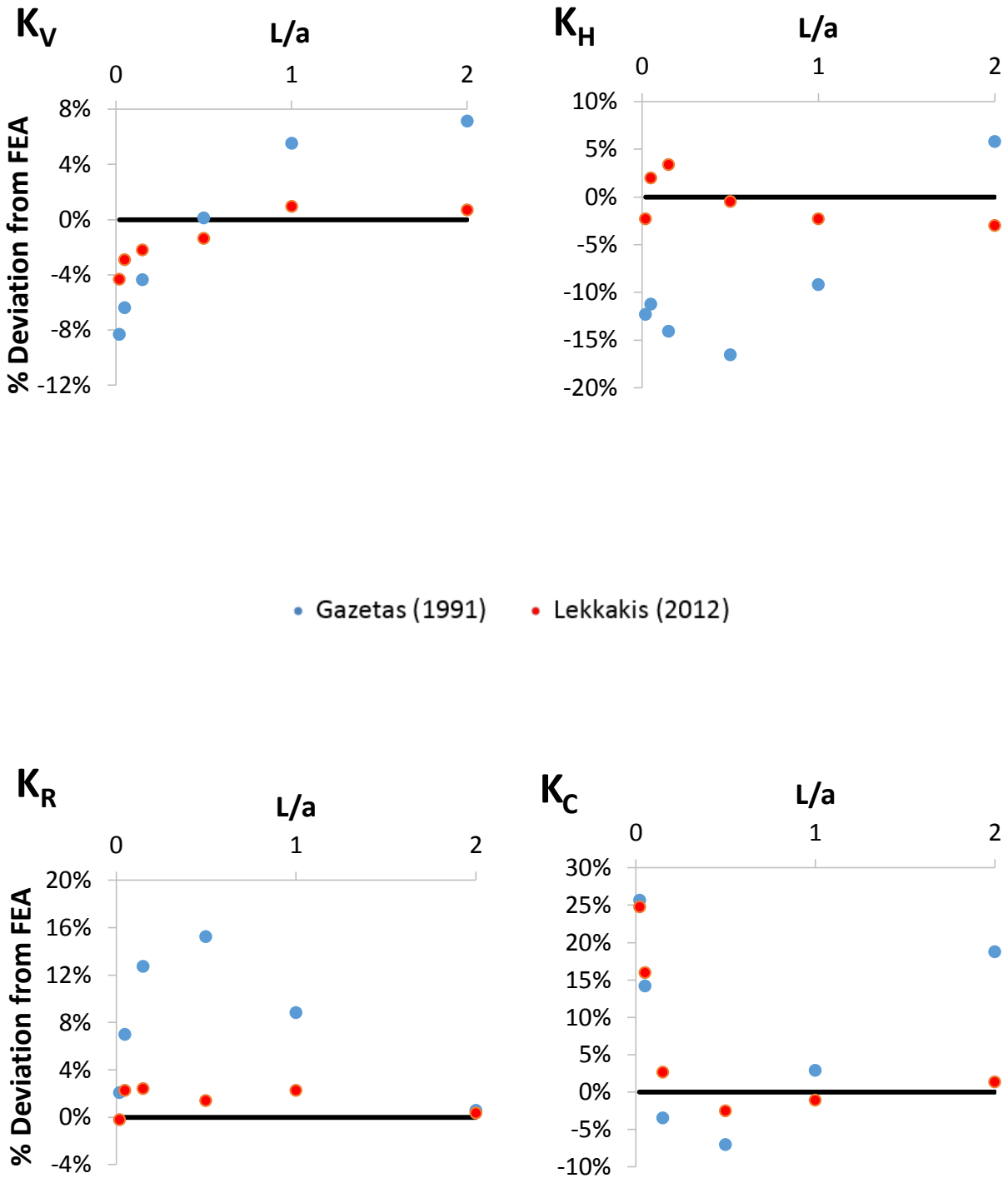

Fig.4.4. Deviation of the expressions by Gazetas (1991) and Lekkakis (2012) from the FEA results of this study for each stiffness component, for the case of soil Young Modulus E=60 MPa, Poisson's ratio v=0.49, soil stratum depth H=30 m, suction caisson radius a(=*R*)=5 m, skirt thickness t=0.02 m, steel Young Modulus E_S=21000 GPa

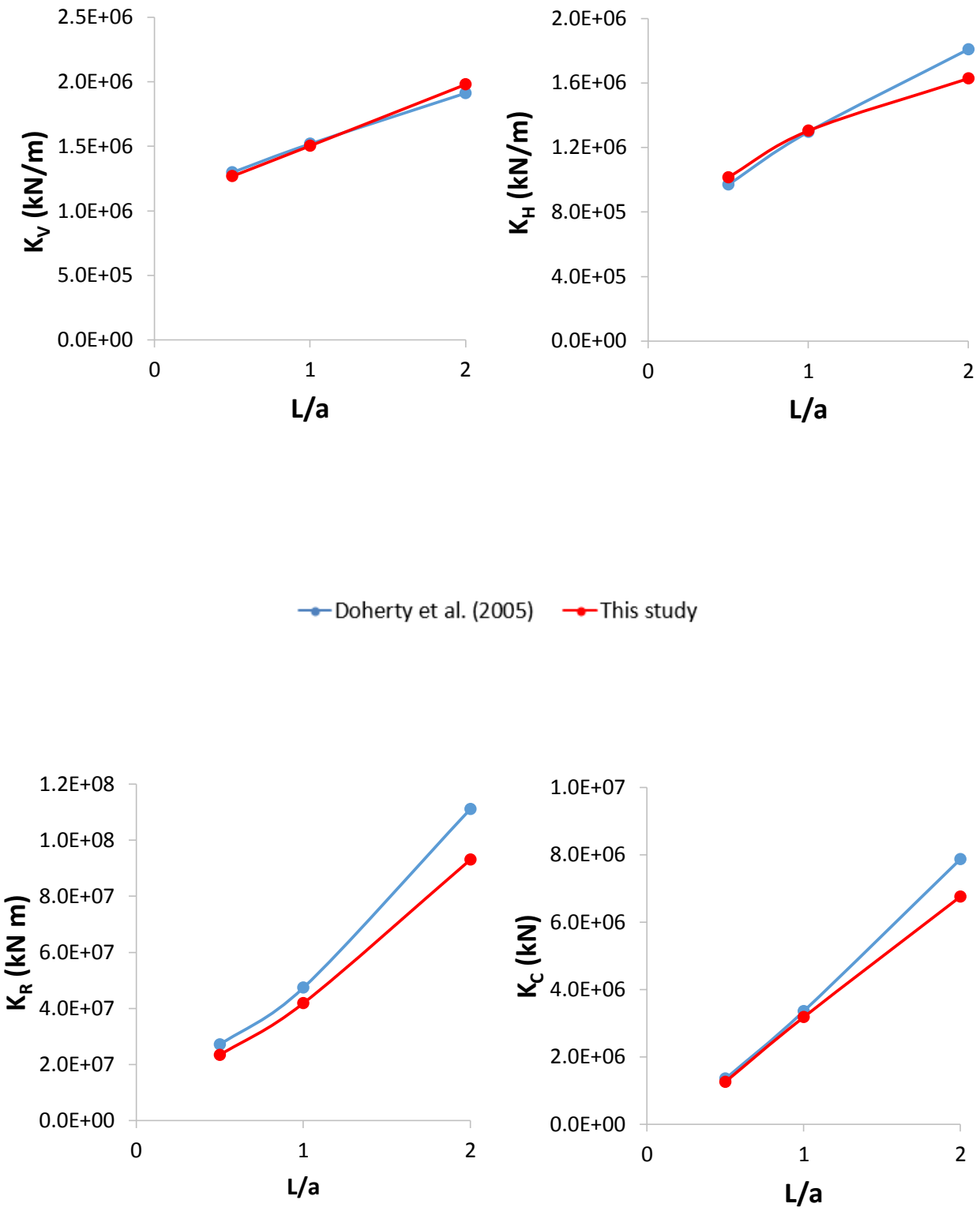

Fig.4.5. Comparison between Doherty et al. (2005) and the FEA results of this study for the suction caisson stiffnesses, for soil Young Modulus E=60 MPa, Poisson's ratio v=0.49, soil stratum depth H=30 m, skirt thickness t=0.02 m, steel Young Modulus E_S=210 GPa

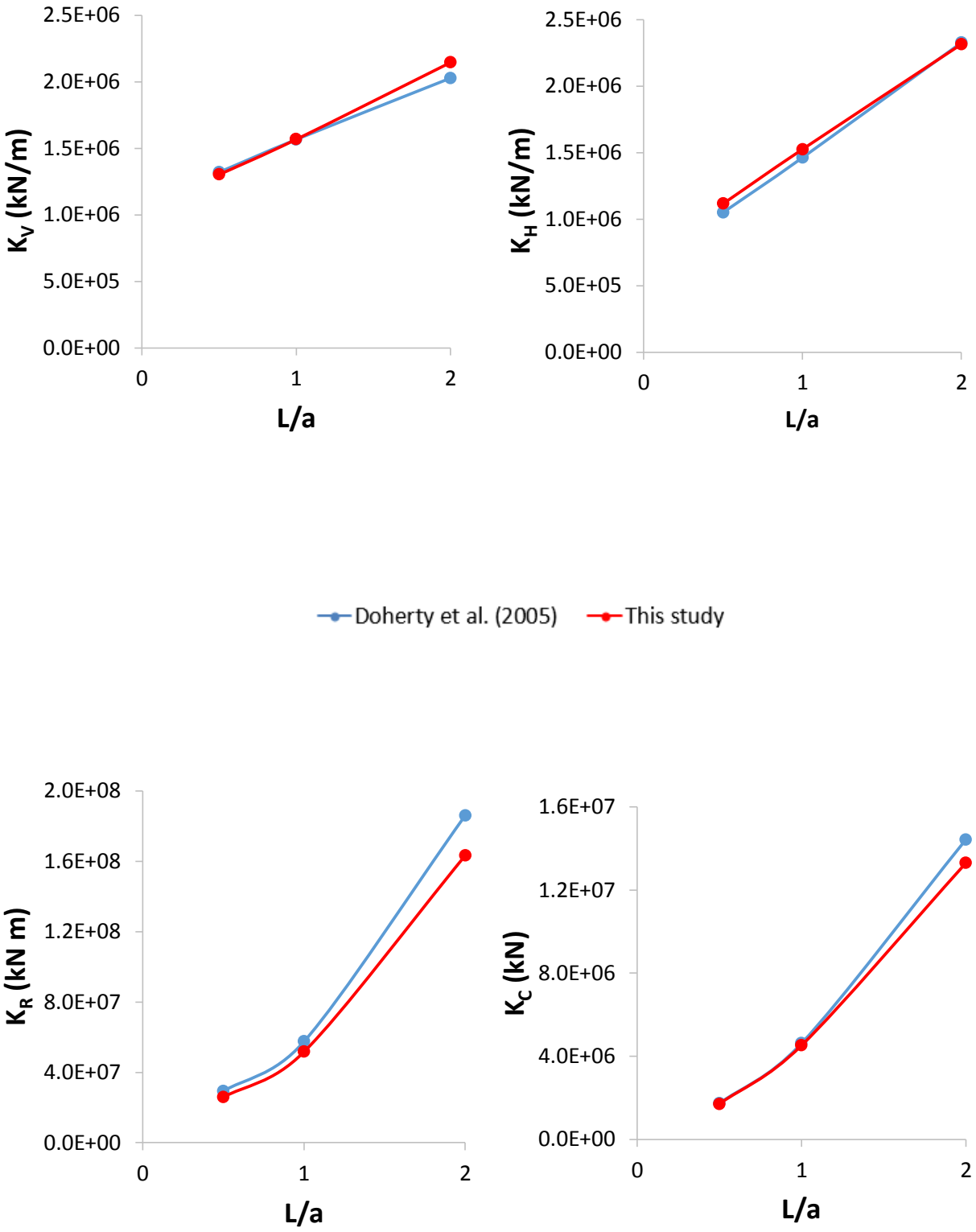

Fig.4.6. Comparison between Doherty et al. (2005) and the FEA results of this study for the suction caisson stiffnesses, for soil Young Modulus E=60 MPa, Poisson's ratio v=0.49, soil stratum depth H=30 m, skirt thickness t=0.02 m, steel Young Modulus E_S=21000 GPa

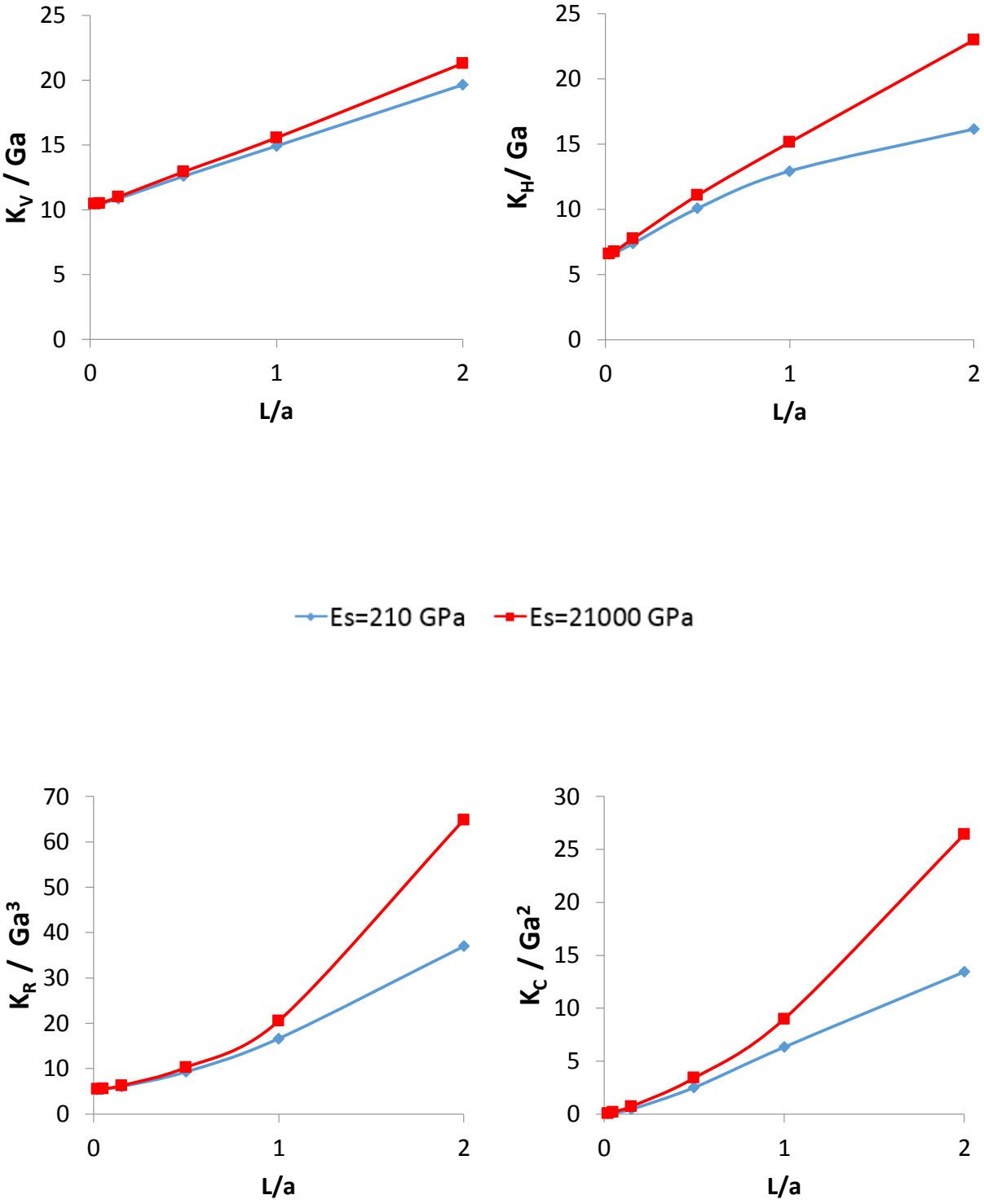

Fig.4.7. Dimensionless elastic stiffnesses of the suction caisson of radius a=5m embedded in the homogeneous soil stratum of H=30 m for Poisson's ratio v=0.49 and skirt thickness t=0.02 m

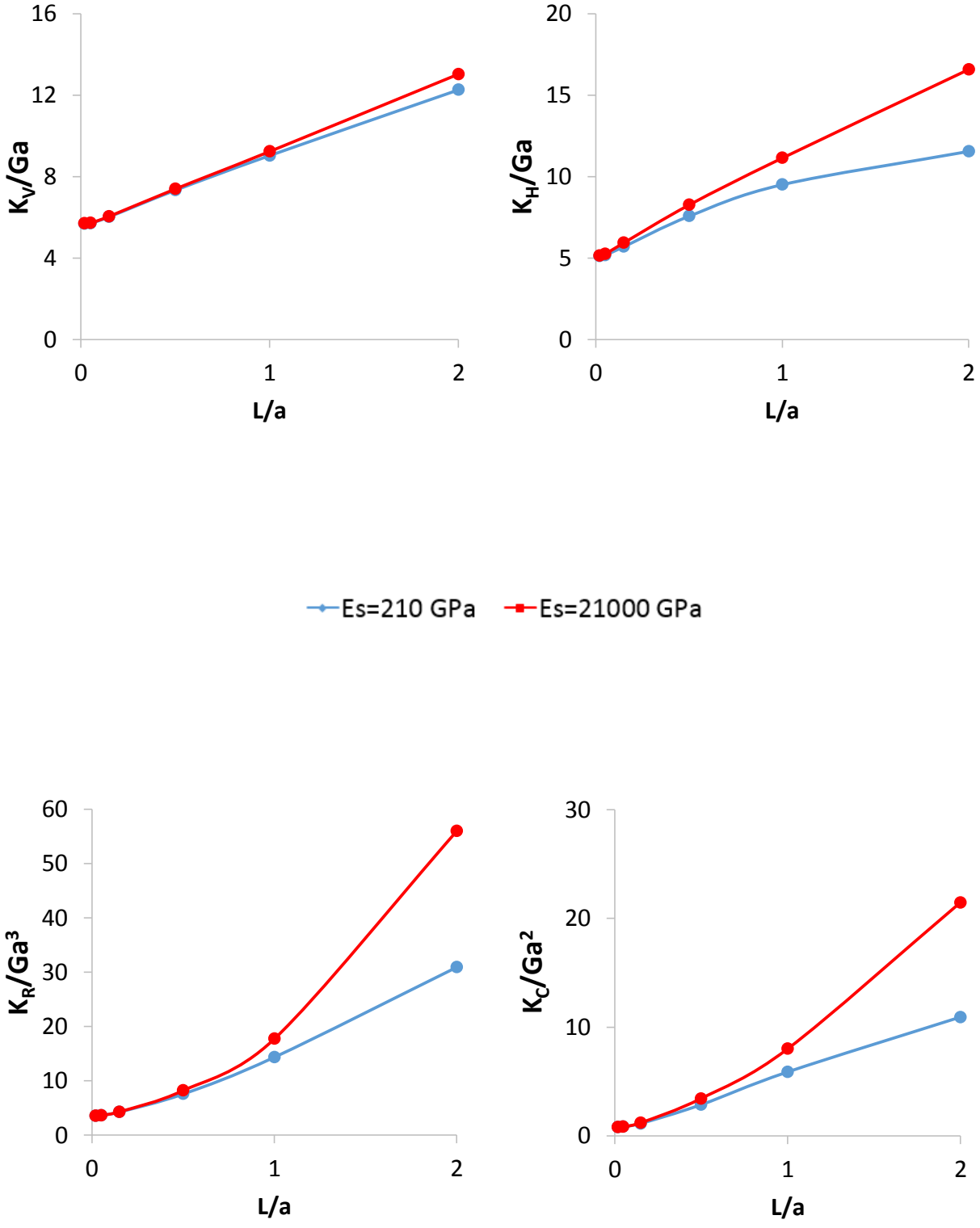

Fig.4.8. Dimensionless elastic stiffnesses of the suction caisson of radius a=5m embedded in the homogeneous soil stratum of H=30 m for Poisson's ratio v=0.1 and skirt thickness t=0.02 m

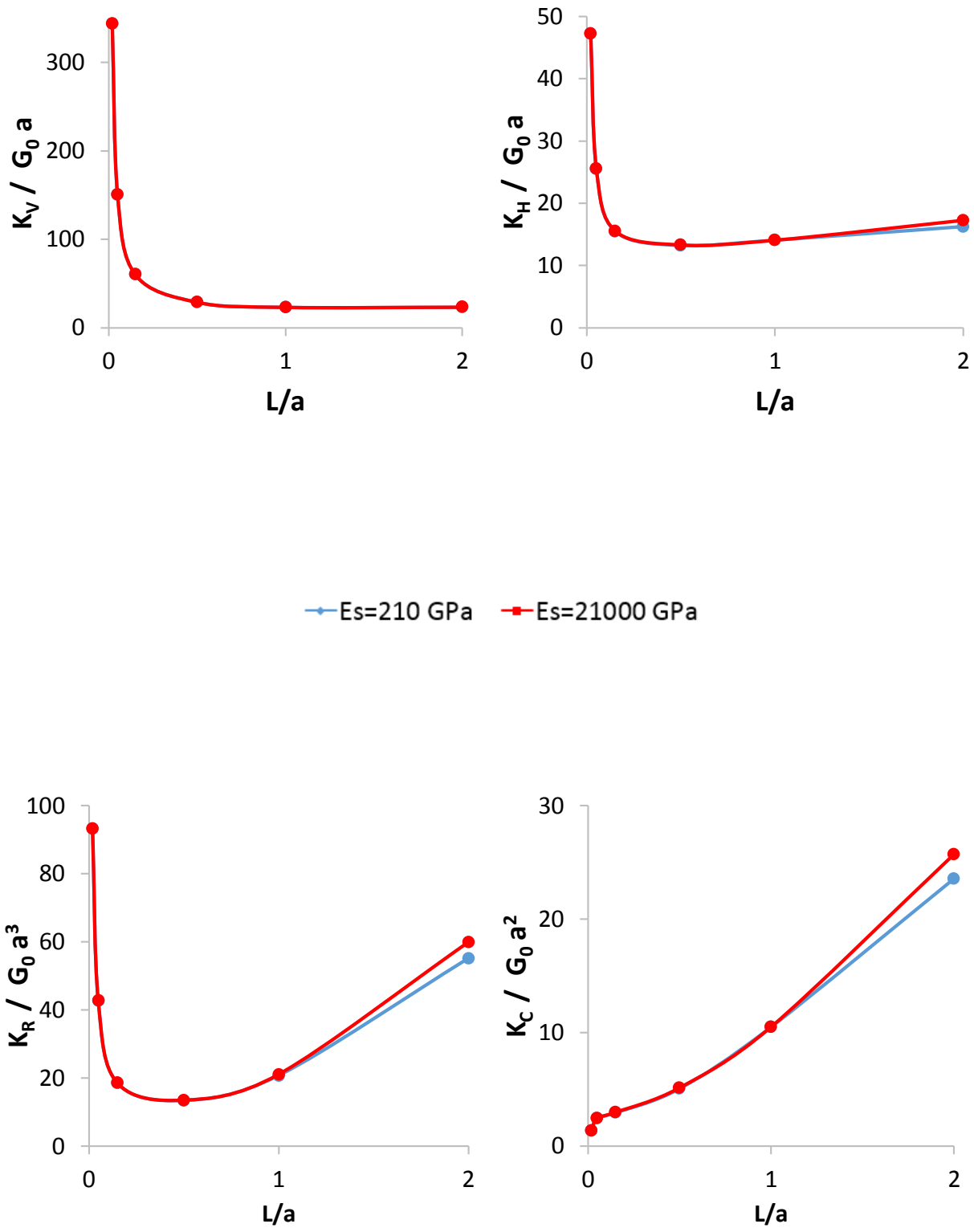

Fig.4.9. Dimensionless elastic stiffnesses of the suction caisson of radius a=5m embedded in the soil stratum of H=30 m, for soil Young Modulus E=*k*z, Poisson's ratio v=0.49 and skirt thickness t=0.02 m

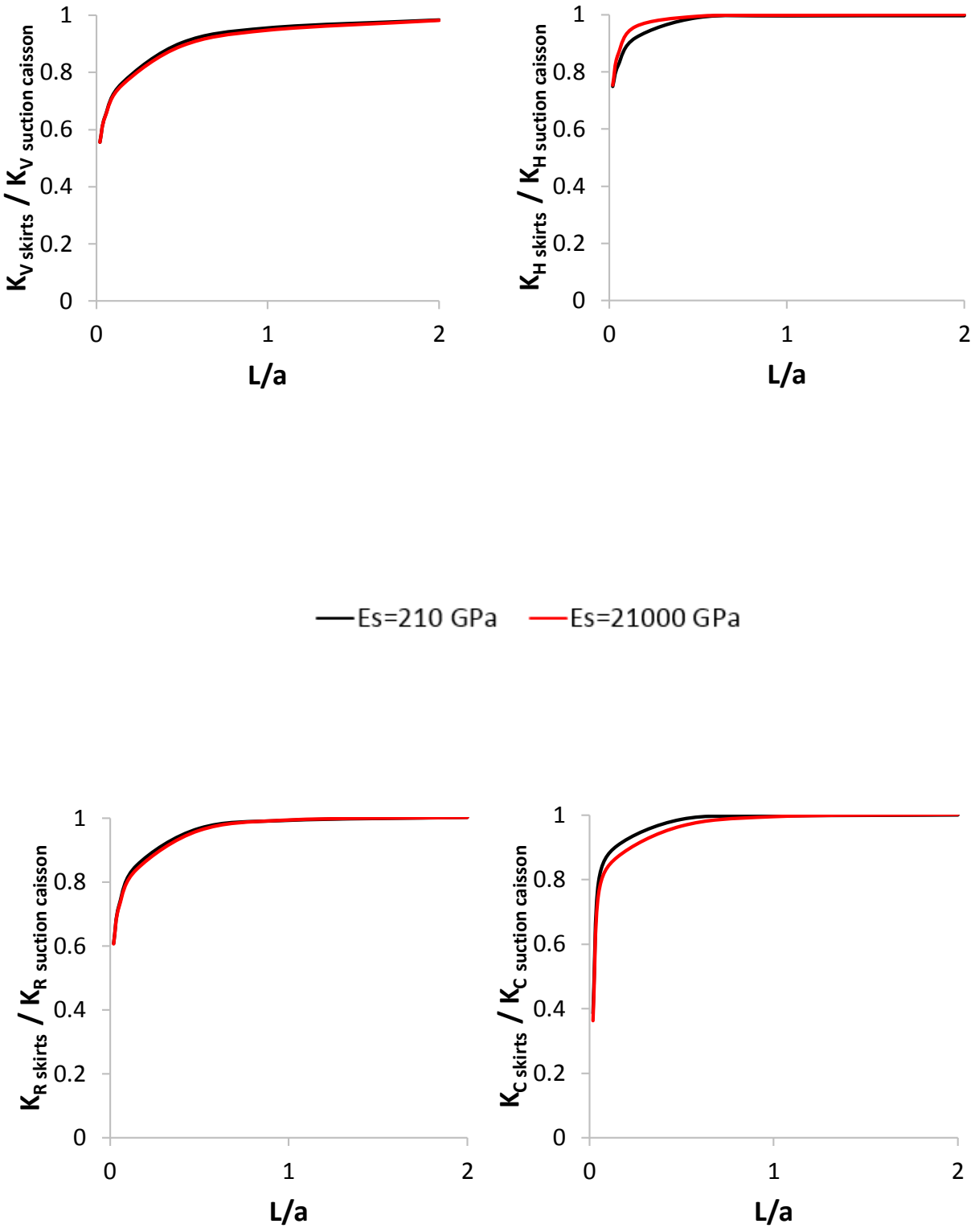

Fig.4.10. Ratio of the skirts alone to suction caisson stiffness as a function of embedment ratio in the homogeneous soil profile for v=0.49

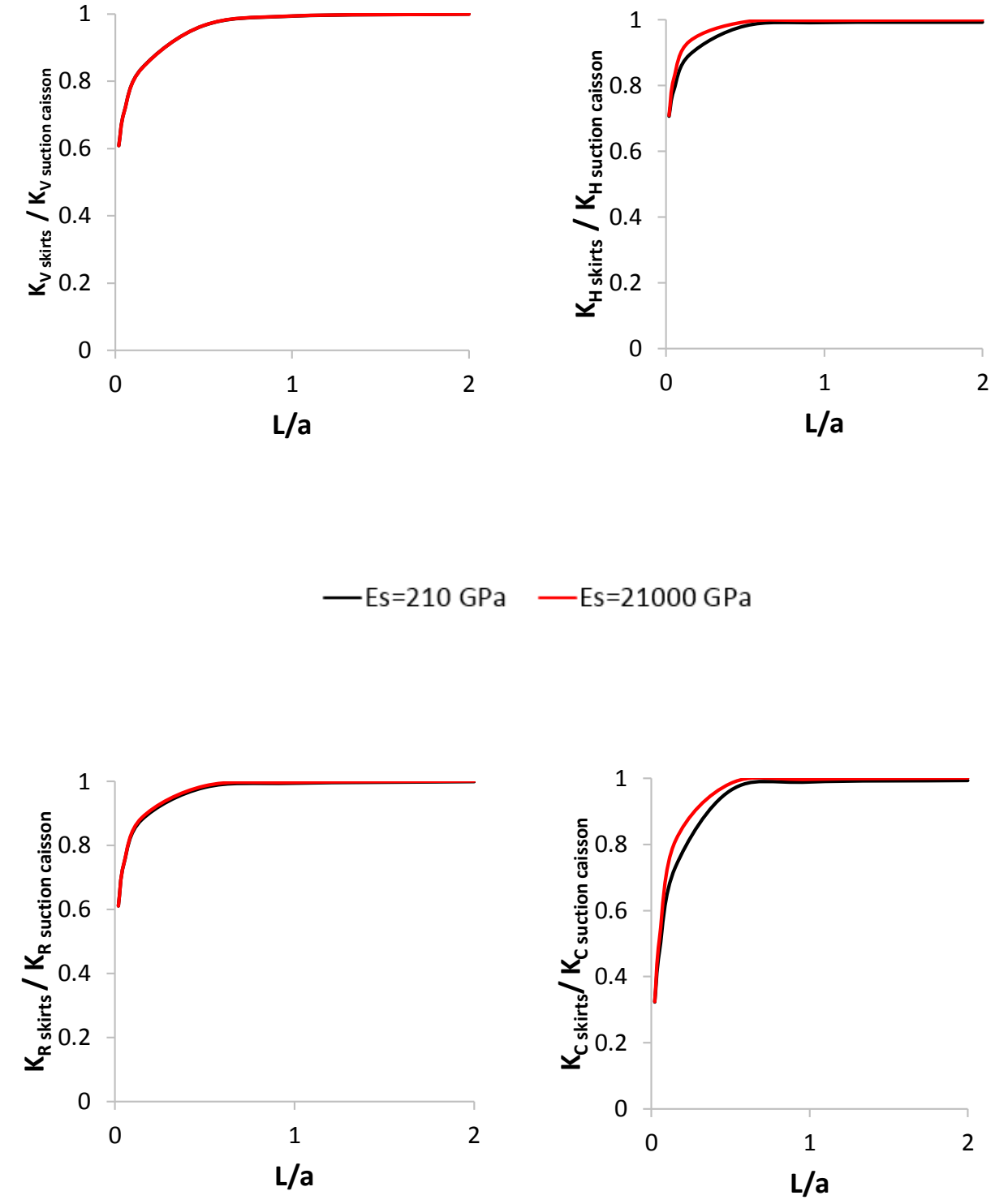

Fig.4.11. Ratio of the skirts alone to suction caisson stiffness as a function of embedment ratio in the homogeneous soil profile for ν=0.1

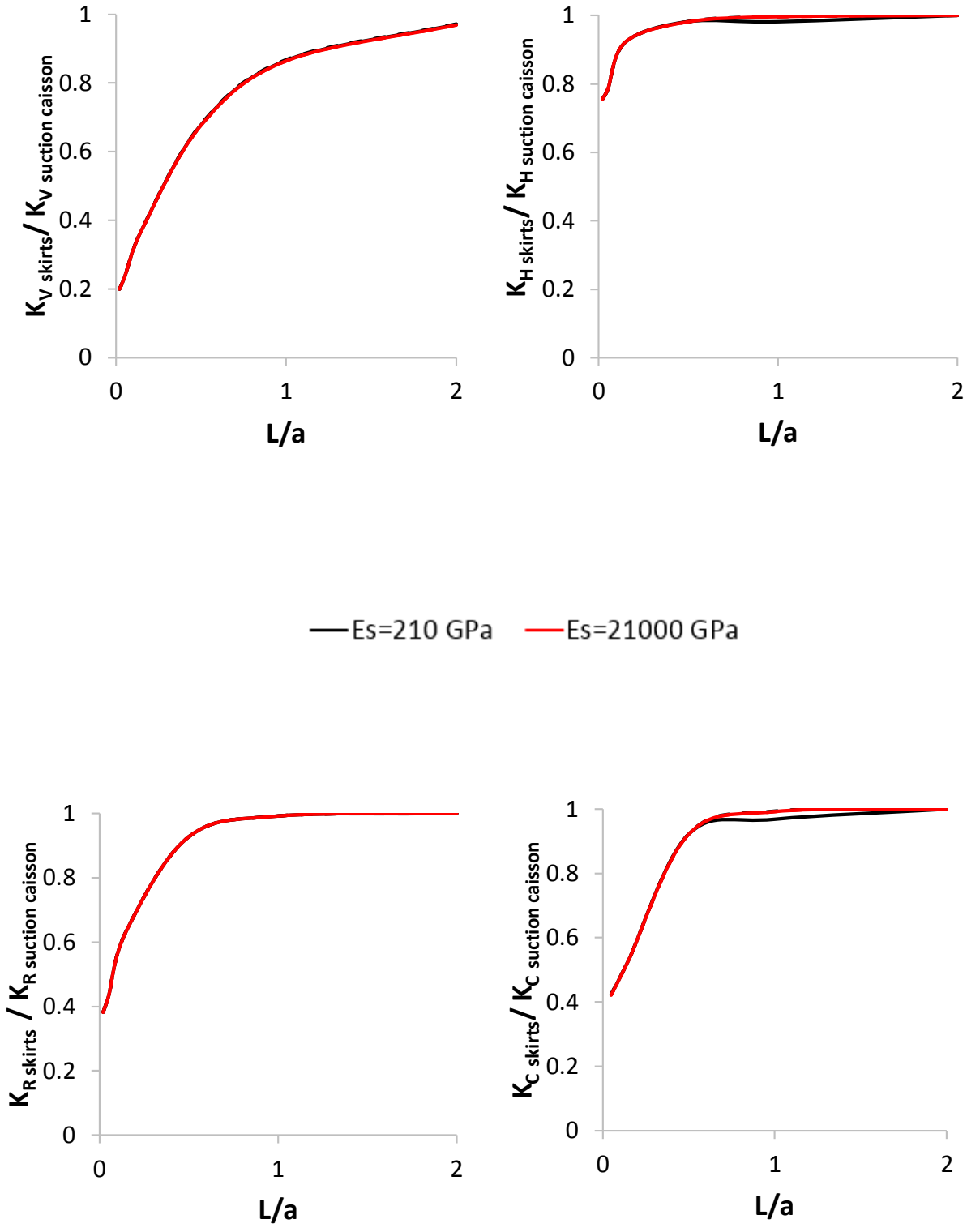

Fig.4.12. Ratio of the skirts alone to suction caisson stiffness as a function of embedment ratio in the inhomogeneous soil profile with linearly increasing strength for ν=0.49

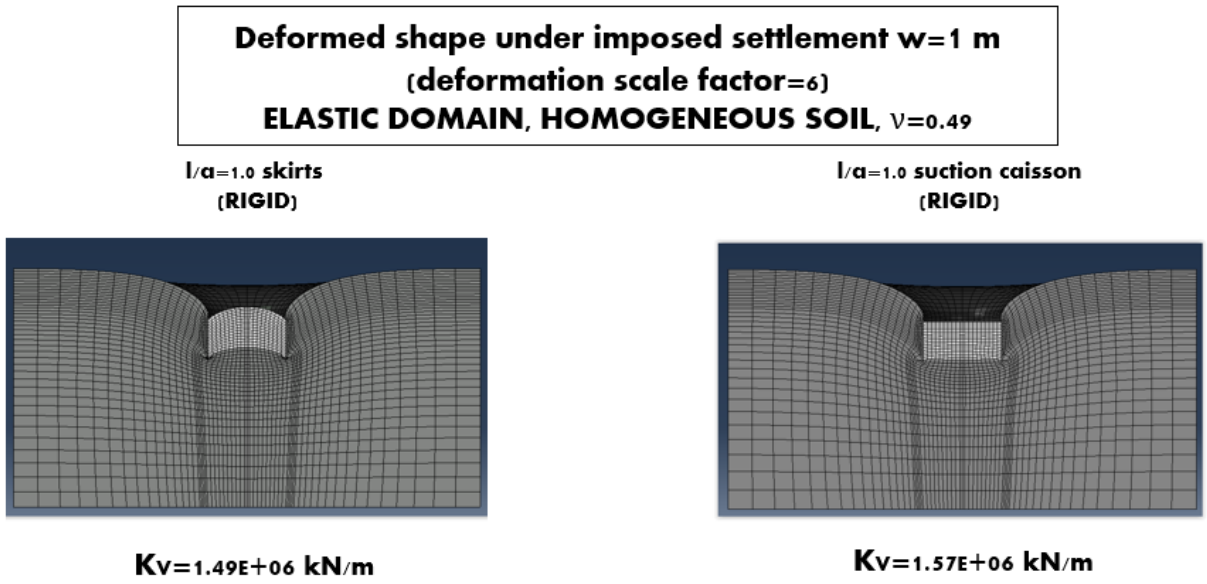

Fig.4.13. Comparison of deformed shapes between skirts alone (*left*) and suction caisson (*right*) under vertical loading in the elastic domain

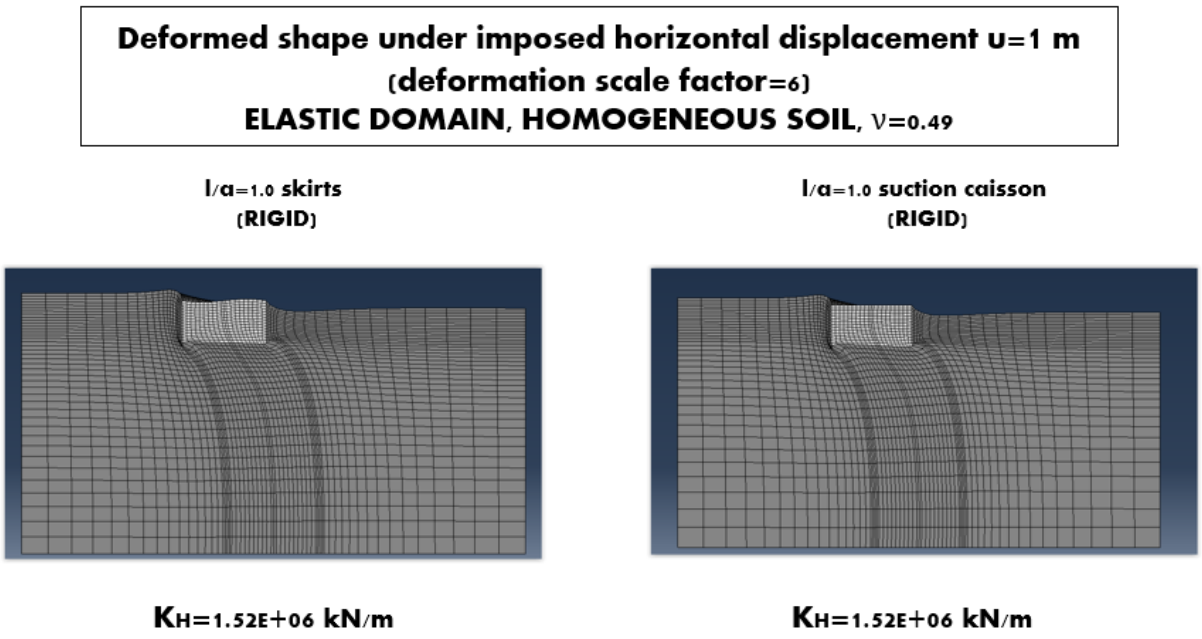

Fig.4.14. Comparison of deformed shapes between skirts alone (*left*) and suction caisson (*right*) under horizontal loading with the rotational degree of freedom constricted, in the elastic domain

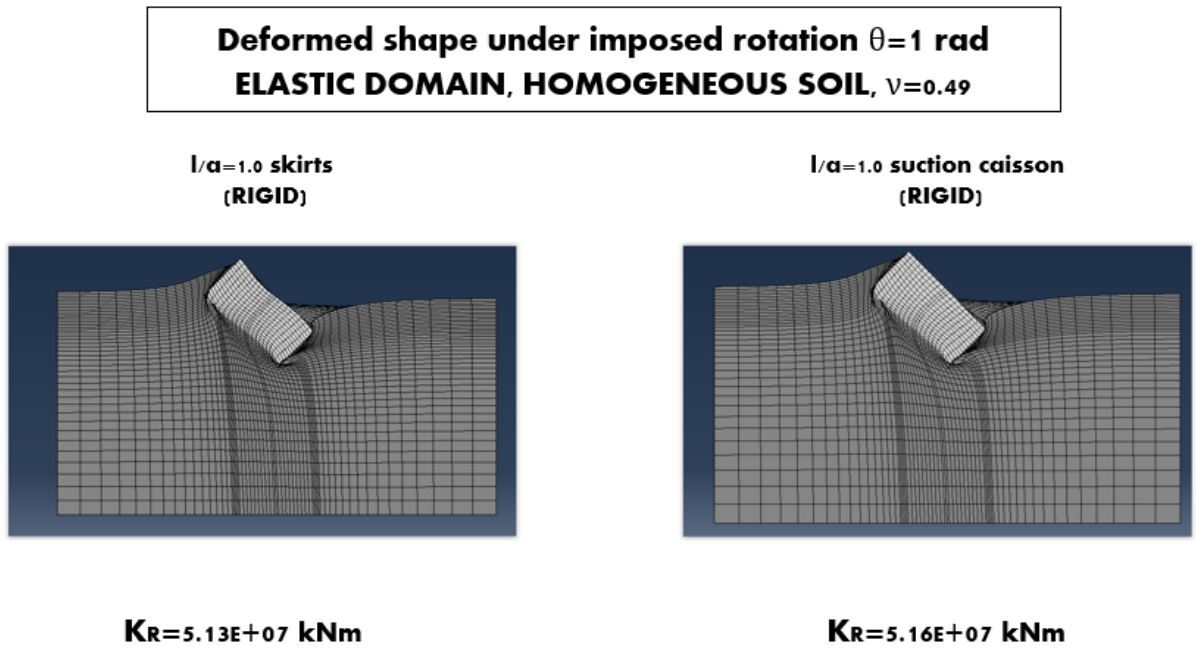

Fig.4.15. Comparison of deformed shapes between skirts alone (*left*) and suction caisson (*right*) under moment loading with the horizontal degree of freedom restricted, in the elastic domain

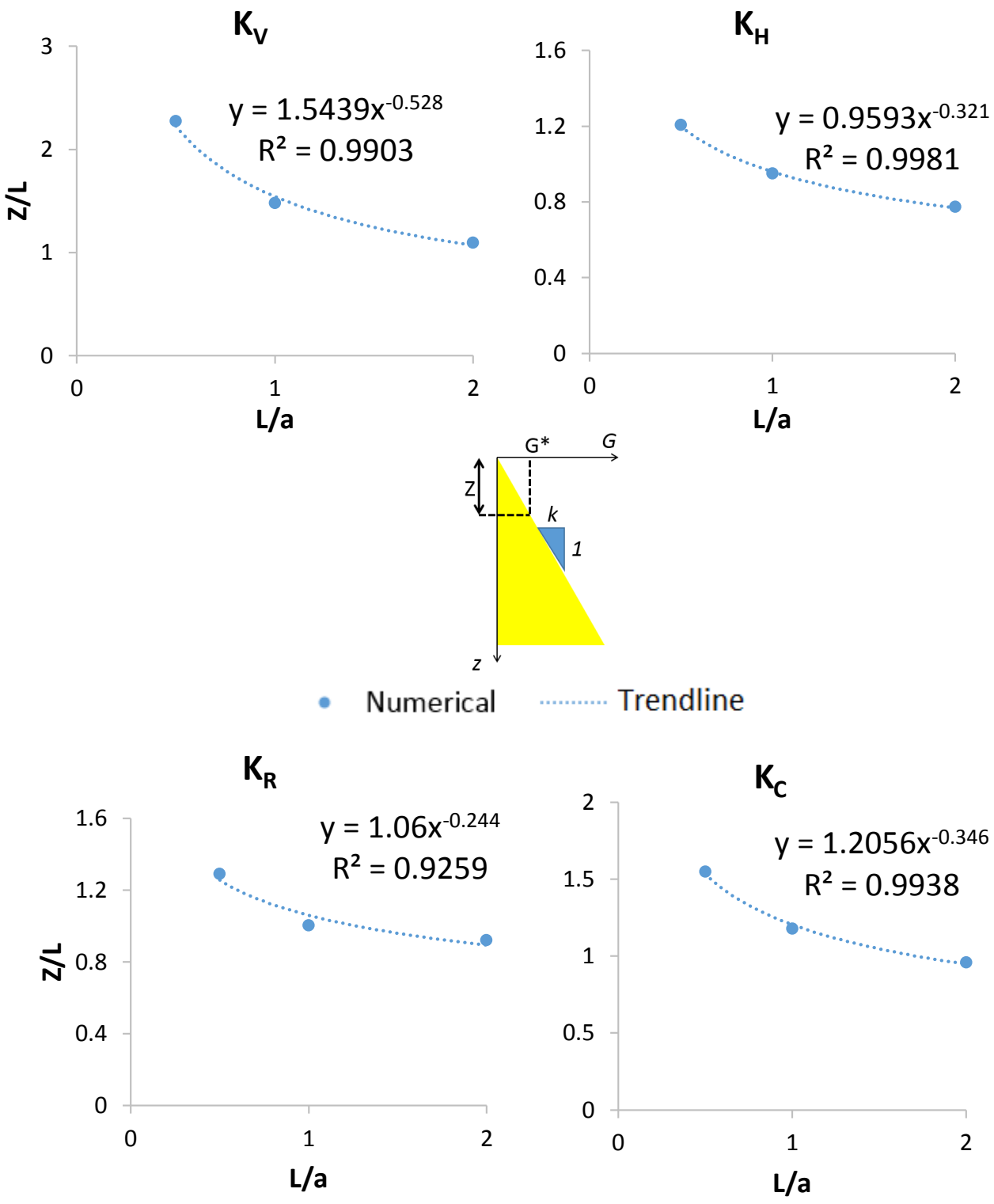

Fig.4.16. From the practical methodology proposed in this study for the determination of the elastic stiffness of a suction caisson in Gibson soil for ν=0.49: Normalized depth Z/L of the equivalent shear Modulus G* as a function of embedment ratio for each stiffness component

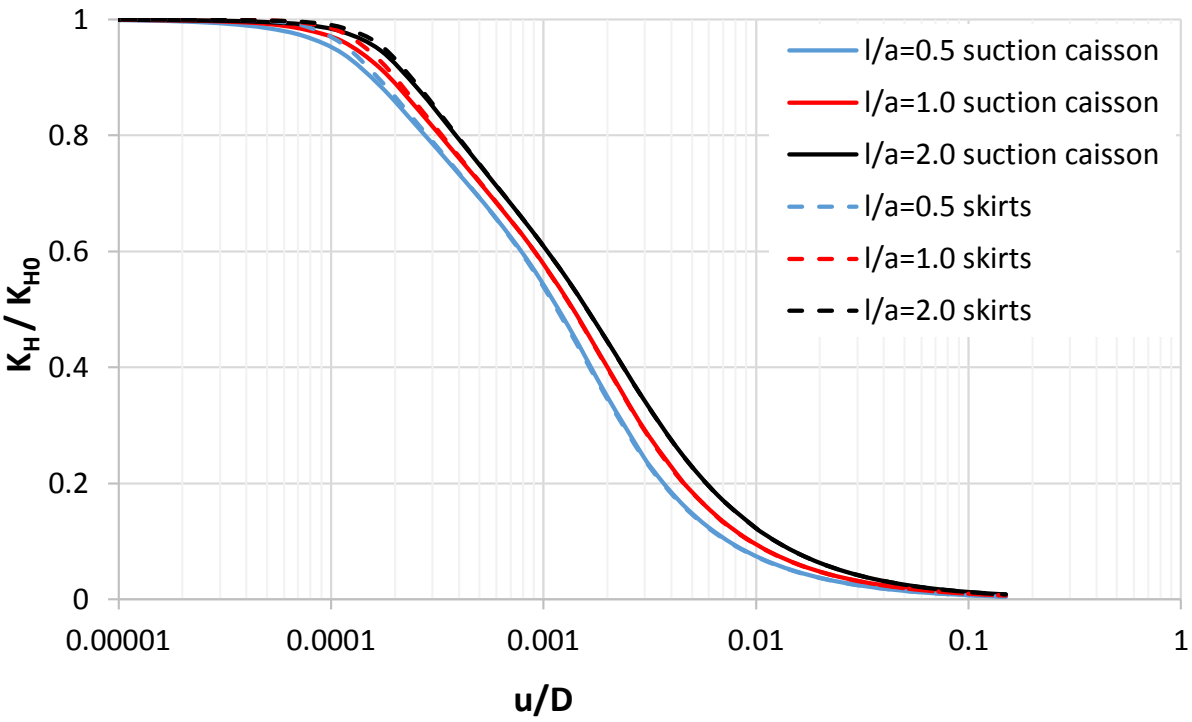

Fig.4.17. Dimensionless chart of the reduction in the horizontal stiffness with increasing horizontal displacement, under zero rotation [FBC]

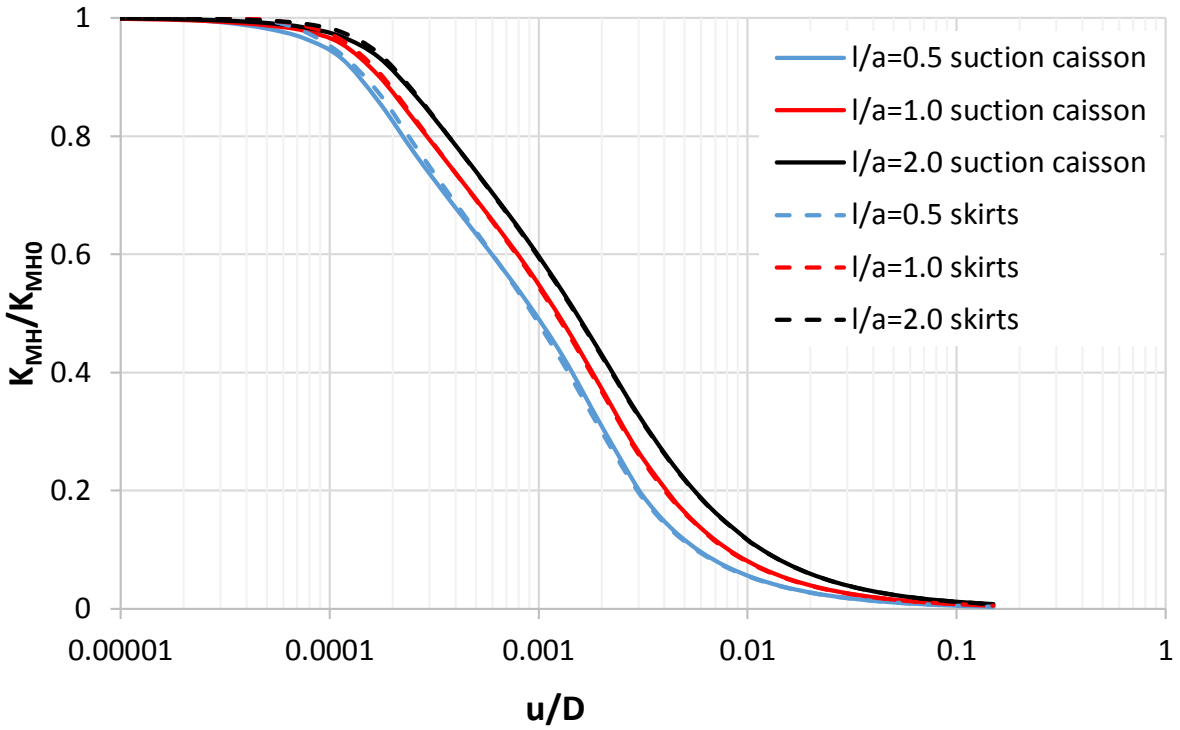

Fig.4.18. Dimensionless chart of the reduction in the coupled swaying-rocking stiffness with increasing horizontal displacement, under zero rotation [FBC]

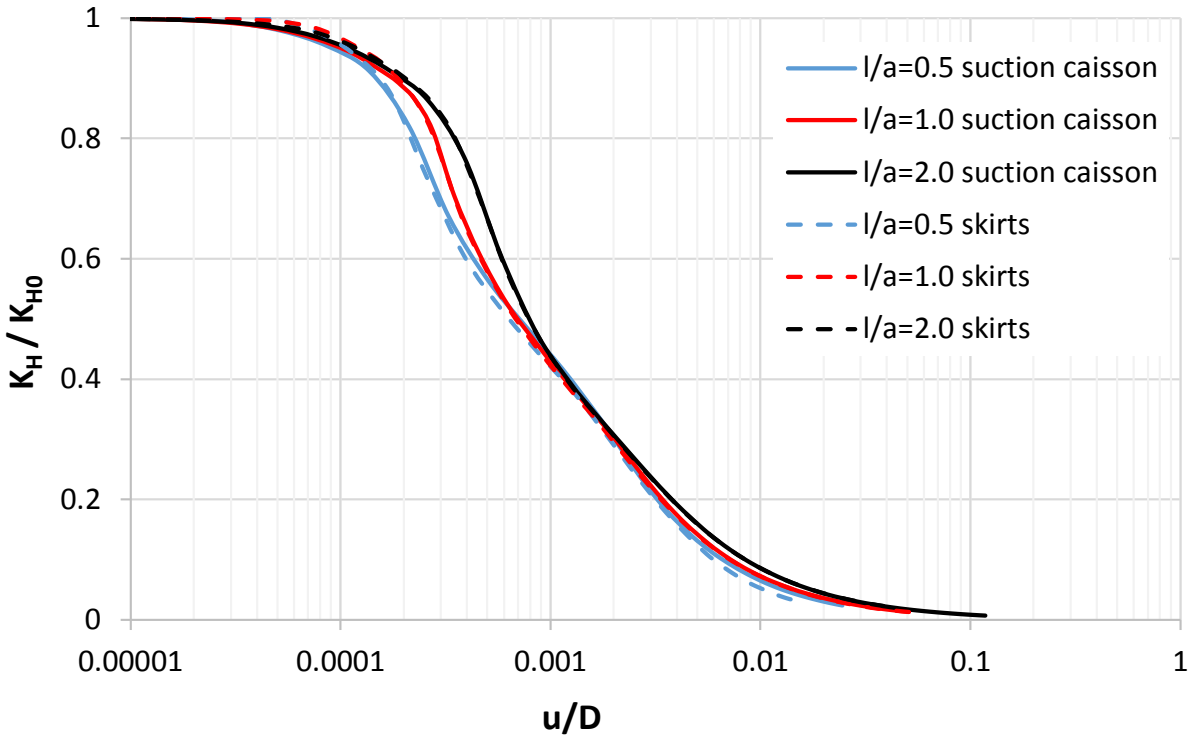

Fig.4.19. Dimensionless chart of the reduction in the horizontal stiffness with increasing horizontal displacement, under zero rotation [TSI]

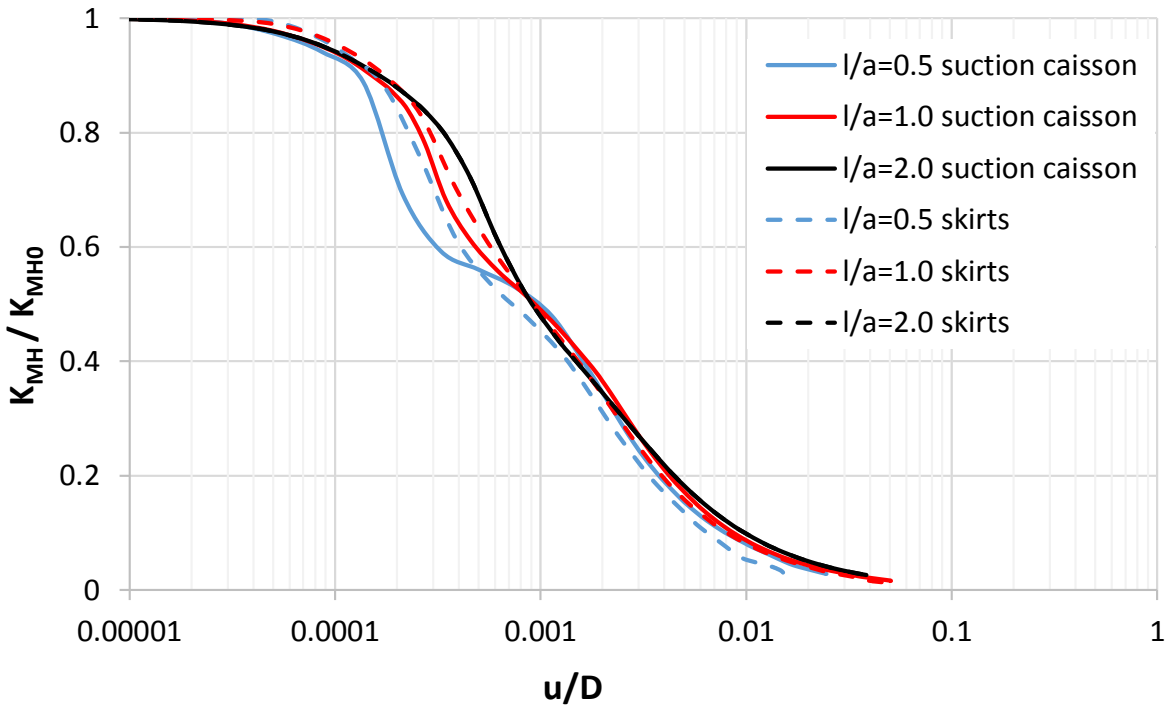

Fig.4.20. Dimensionless chart of the reduction in the coupled swaying-rocking stiffness with increasing horizontal displacement, under zero rotation [TSI]

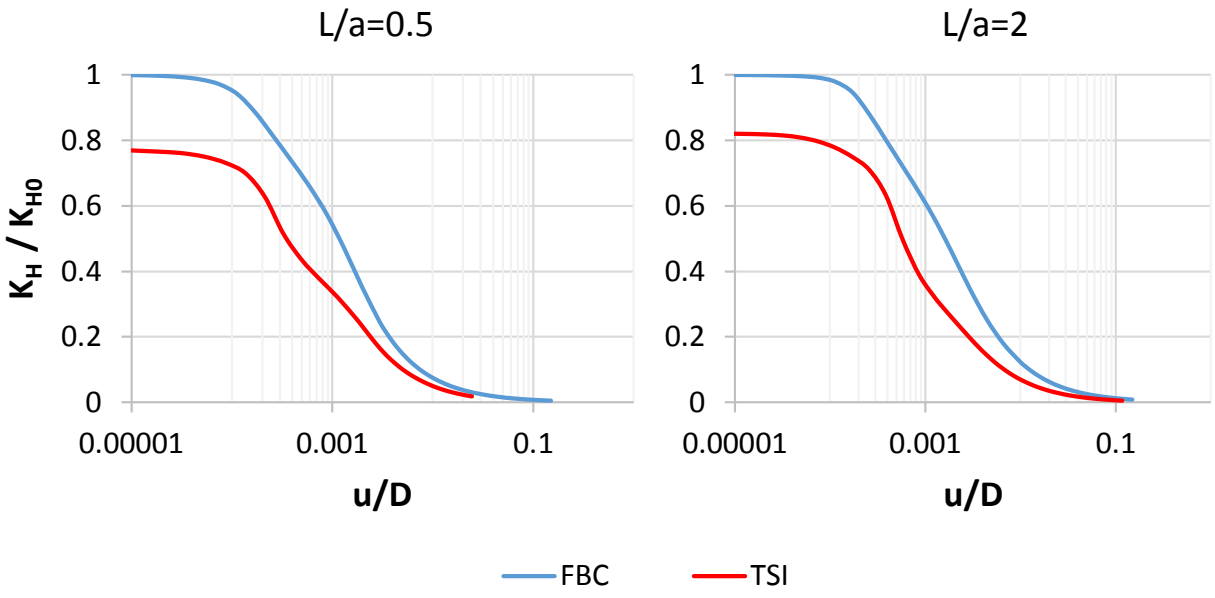

Fig.4.21. Reduction in horizontal stiffness of the suction caisson with increasing horizontal displacement, under zero rotation - FBC and TSI assumption for L/a=0.5 (*left*) and L/a=2 (*right*)

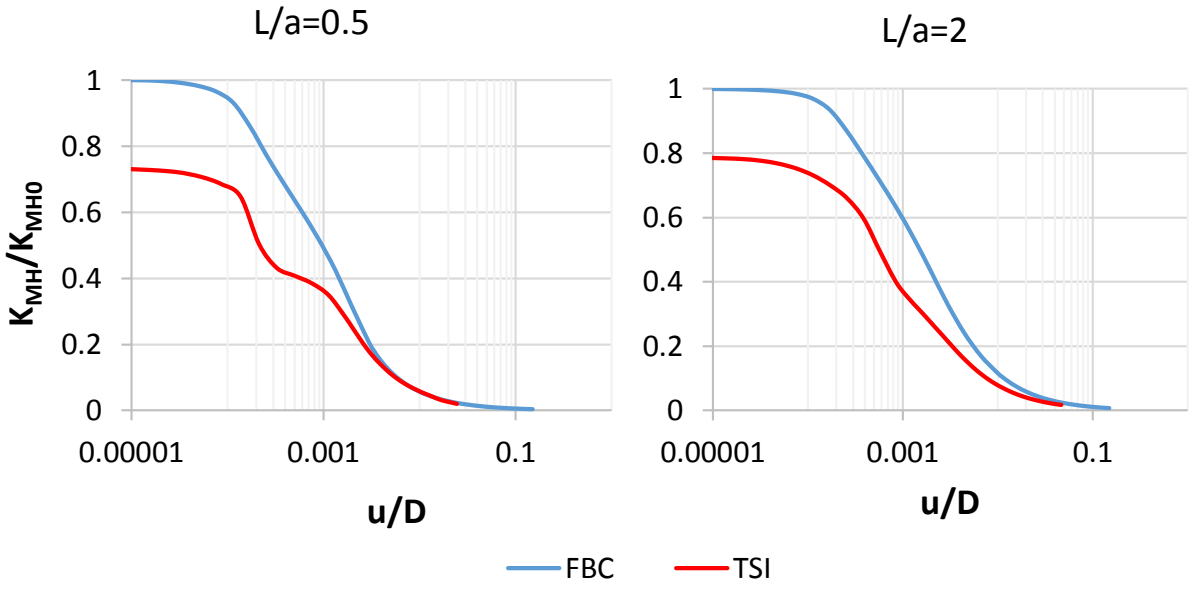

Fig.4.22. Reduction in cross-coupling stiffness of the suction caisson with increasing horizontal displacement, under zero rotation - FBC and TSI assumption for L/a=0.5 (*left*) and L/a=2 (*right*)

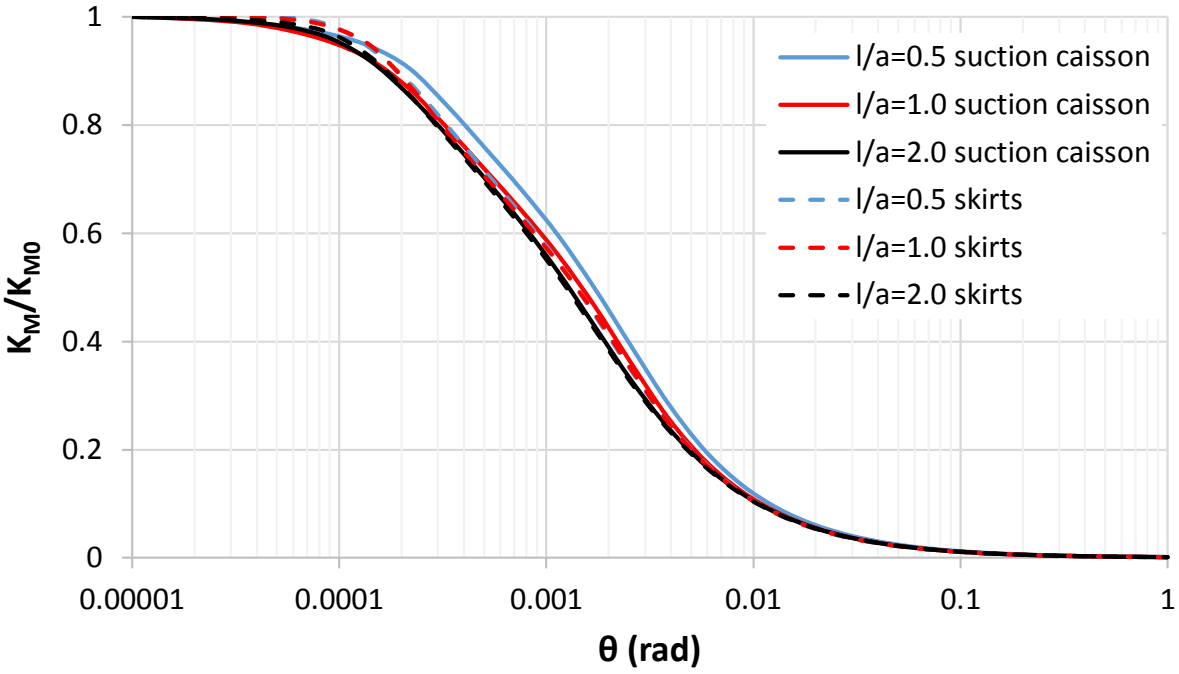

Fig.4.23. Dimensionless chart of the reduction in the rocking stiffness with increasing rotation, under zero horizontal displacement [FBC]

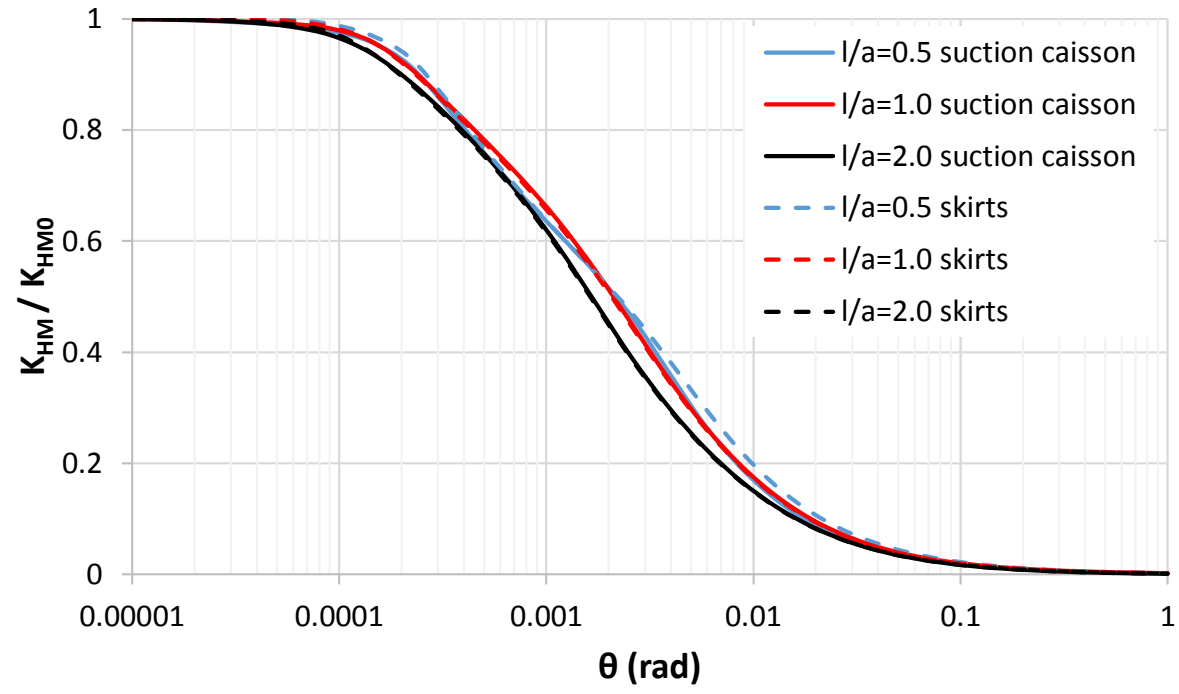

Fig.4.24. Dimensionless chart of the reduction in the cross-coupling stiffness with increasing rotation, under zero horizontal displacement [FBC]

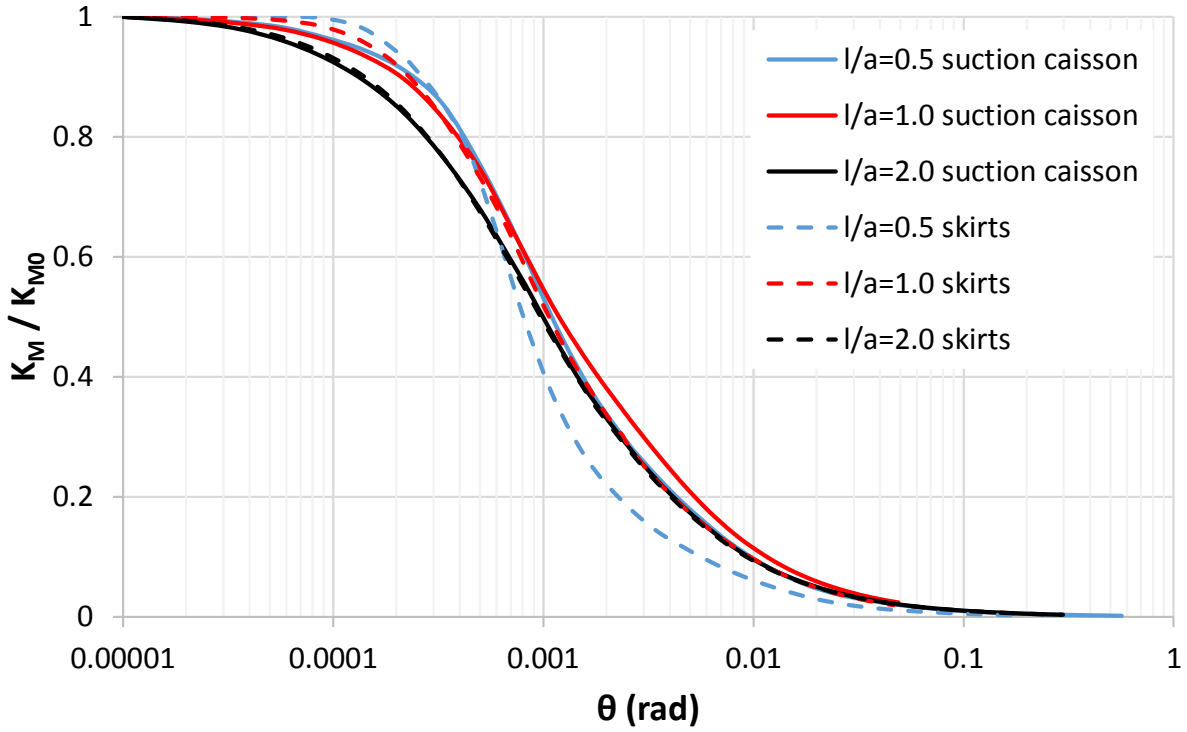

Fig.4.25. Dimensionless chart of the reduction in the rocking stiffness with increasing rotation, under zero horizontal displacement [TSI]

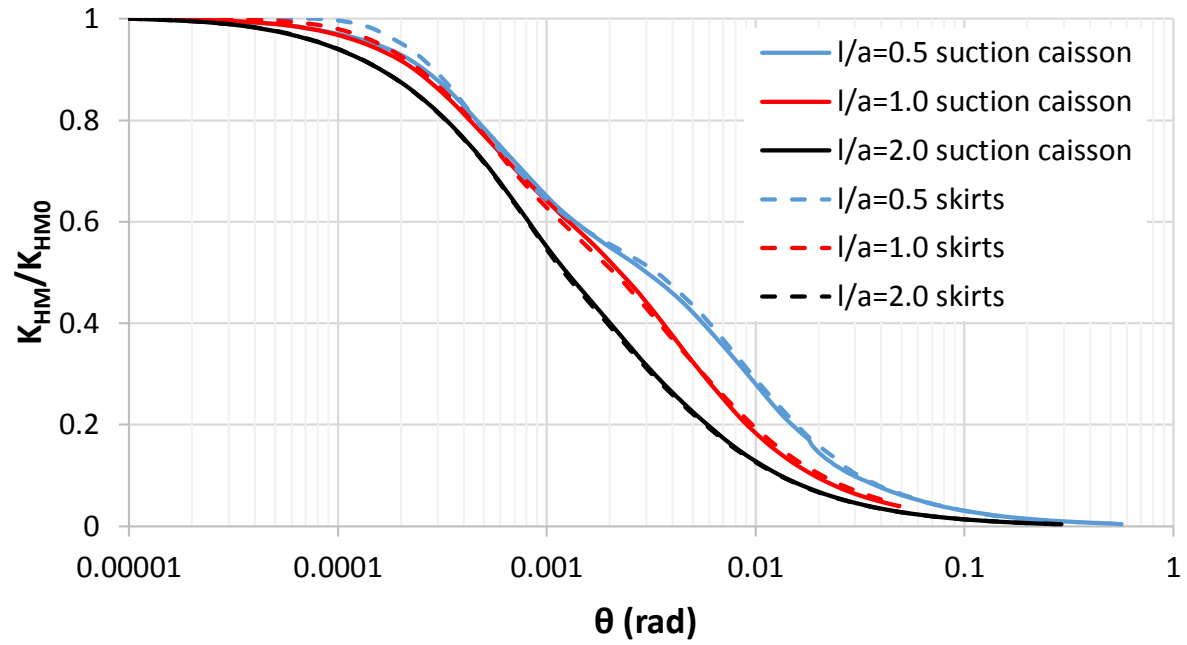

Fig.4.26. Dimensionless chart of the reduction in the cross-coupling stiffness with increasing rotation, under zero horizontal displacement [TSI]

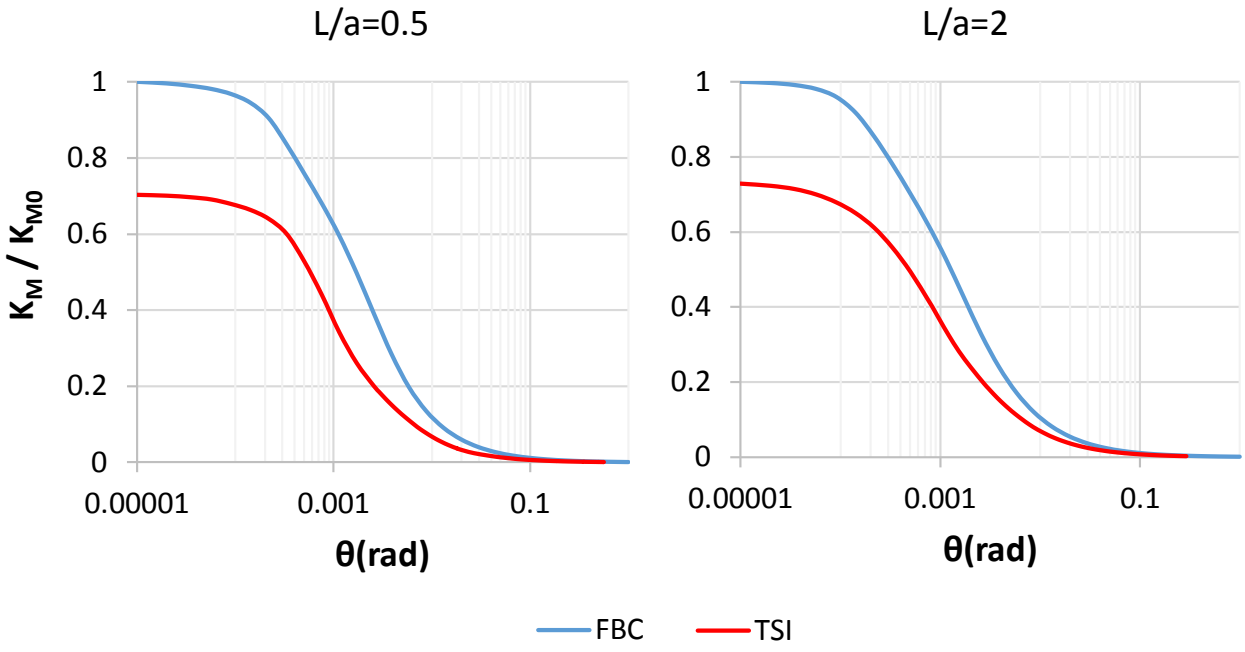

Fig.4.27. Reduction in rocking stiffness of the suction caisson with increasing rotation, under zero horizontal displacement - FBC and TSI assumption for L/a=0.5 (*left*) and L/a=2 (*right)*

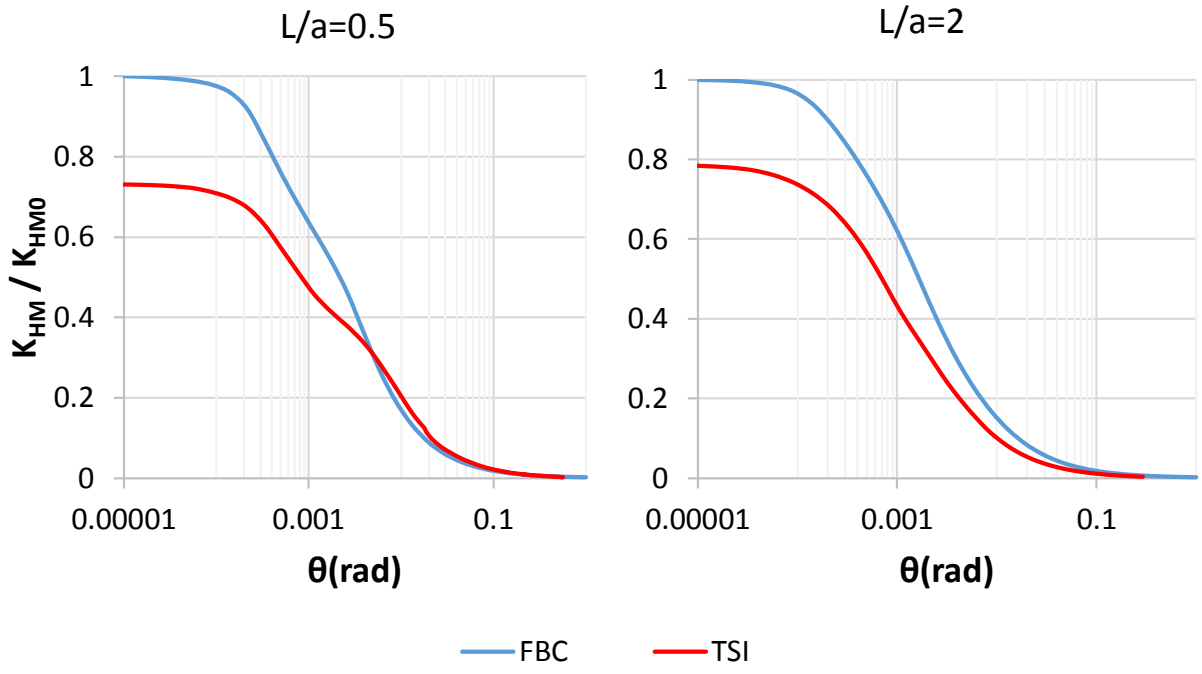

Fig.4.28. Reduction in cross-coupling stiffness of the suction caisson with increasing rotation, under zero horizontal displacement-FBC and TSI assumption for L/a=0.5 (*left*) and L/a=2 (*right)*

Chapter 5

Kinematic Interaction

5 Kinematic Interaction

5.1 Preface

During an earthquake, the generated seismic waves, lead the soil to deform and carry with it the foundation-superstructure system. Inertial forces are produced due to the induced motion of the superstructure, leading to the development of dynamic stresses at the foundation, which are then transmitted to the supporting soil, causing further deformations. The additional waves from the soil-foundation interface result in extra dynamic displacements of the foundation and the supported structure, generating thus further inertial forces and so on. Despite the fact that these phenomena act simultaneously, for the sake of conceptual and computational convenience, their separation into two successive phenomena, known as "kinematic interaction" and "inertial interaction", is applied for the determination of the response of the soil-foundation-structure system, deriving from the superposition of the two interaction effects, as depicted in **Figure 5.1**.

Kinematic interaction (KI) is the phenomenon that refers to the effects of seismic waves to the system consisting of the foundation and the supporting soil, considering the mass of the superstructure and the foundation equal to zero. As will be further discussed, embedment plays a significant role in the kinematic response. The major consequence of KI, which constitutes the object of this study, is that it results in a "foundation input motion" (FIM), which, in the majority of cases, is smaller than the motion of the free-field soil and contains both a translational and a rotational component. The first is caused by the overall translation of the subgrade, whereas the latter occurs due to the development of shear stresses along the interface between the sidewalls and the soil. As a matter of fact, the difference between the horizontal displacement of the soil on the surface and at the level of embedment leads to a "pseudo-rotation" of the soil, producing the aforementioned shear stresses, with the soil-foundation stiffness being the main resistance to this rotation. Consequently, the depth of embedment influences significantly the incompatibility between the motion of the foundation and that of the free-field. It is understandable that the increase of embedment leads to enhanced resistance of the foundation to follow the displacements of the free-field. Indeed, in the case of a surface foundation, which is subjected to vertically propagating shear waves, there is no KI, since the footing considered to be massless would follow in perfect agreement the motion of the surface.

The effects of KI are portrayed by the introduction of kinematic interaction factors, which are ratios that relate the amplitude of acceleration, displacement or rotation of the foundation to that of the free-field. Each one of these transfer function categories presents difference in the values and phases of the amplitudes between the free-field and the foundation, so the KI factors turn out to be complex functions of frequency. Herein, emphasis is placed on the absolute values of the KI factors, which is actually sufficient for applications of practical interest.

Inertial interaction (II) refers to the response of the complete soil-foundation-structure system under the excitation by D' Alembert forces, which derive from the acceleration of the superstructure due to KI. Inertial interaction is not the object of the present study.

In this chapter, the kinematic response of the suction caisson to modified Gabor pulses as excitation is examined and compared to that of the skirts alone. More specifically, appropriate transfer functions and dynamic soil pressures acting on the sidewalls are determined in order to gain insight into the problem of kinematic interaction.

5.2 Seismic Model Properties

Embedded foundations respond to dynamic excitation mainly by lateral displacements and rotation. Due to the kinematic and cyclic nature of the excitation, reaching the bearing capacity does not necessarily result in failure of the foundation or structure, since this occurs momentarily.

In order to properly simulate the problem under dynamic conditions, the implementation of certain changes in the model was essential. Firstly, the distance of the lateral boundaries is already adequate so that the unfavorably reflected waves do not significantly affect the calculated response in the area of interest. However, for the dynamic analyses the peripheral nodes at every height are tied together to form a shear beam, which is a situation similar to that in a laminar box. In that way, the free-field is modelled correctly and the excitation is well imposed at the base of the soil stratum.

The hysteretic damping ratio of the soil is selected as approximately ξ=5% by using the Rayleigh damping in ABAQUS. For this purpose, different coefficients alpha (a_R) and beta (β_R) are introduced, depending on the case of dynamic excitation. The a_R factor defines mass proportional damping and introduces damping forces due to the absolute velocities of the model. The β_R factor accounts for damping, which is proportional to the elastic material stiffness.

The dynamic analyses were performed for the L/a=2 rigid (Es=21000 GPa) foundation embedded in elastic, homogeneous soil of Young modulus E=240 MPa, Poisson's ratio v=0.49 and shear wave velocity V_S=200 m/s. Fully bonded contact (FBC) in the interface between the foundation and the surrounding soil was taken into account, allowing for no detachment or sliding.

Modified Gabor pulses of harmonic type were imposed as excitation at the base of the soil stratum, in one horizontal direction exclusively. The acceleration amplitude was the same for all the analyses, namely A_{max}=1 g. Since the influence of the excitation frequency f is the subject of this study, a variety of f =0.2 ÷ 10 Hz were examined.

Finally, the response of the foundation was investigated for the recorded earthquake motions of Monastiraki (1999) and Aegion (1995) with acceleration peak values at 0.54 g and 0.55 g,

respectively. The acceleration time histories and elastic response spectra are presented in the relative sections.

5.3 Eigenmode Analysis

Before proceeding to the investigation of the kinematic response of the foundation, the determination of the eigenmodes and eigenfrequencies of the system was achieved both theoretically and numerically.

Since the case examined herein is that of a homogeneous soil stratum lying on bedrock, according to the one-dimensional 'amplification' theory, for vertically propagating shear waves, the various eigenfrequencies of a system with zero internal (hysteretic) damping can be provided by the expression:

$$f_n = (2n-1)\frac{V_S}{4 \times H} \quad , \text{ n = 1 , 2 , 3 ....} \tag{5.1}$$

where V_S : shear wave velocity

H : depth of soil stratum

The idea is that a soil stratum resting on rocky substratum is able to oscillate, as long as two boundary conditions are satisfied: displacements at the base and stresses at the free field need to be constantly zero. Through the general harmonic solution of the wave equation derives the aforementioned expression for the eigenfrequencies (5.1), as well as the equation for the eigenmodes of the system, which is:

$$\frac{u_x}{u_0} = \cos\left[(2n-1)\frac{\pi}{2}\frac{x}{H}\right], n = 1 , 2 , 3.... \tag{5.2}$$

where u_x : displacement of the soil at distance x from surface

u_0 : displacement of the surface (free field)

It must be stressed out that the shear wave velocity refers to the medium, for which the eigenmodes are calculated, that is to say the soil layer of thickness H and not the bedrock, since their relative motion constitutes the object of examination. Certainly, in terms of absolute values, the final motion is the product of the characteristics of all the layers that may rest in general below the stratum of examination.

When the frequency of the excitation, which is imposed at the base of the soil stratum, coincides with one of its eigenfrequencies, soil resonance takes place. This means that

significant amounts of energy are released and displacements of the free-field exceed those of the base, with their ratio known as amplification, tending to infinity in the case of resonance. An expression for the amplification is given by the one-dimensional wave theory as can be observed in **Figure 5.2**.

In addition, the amplification amplitude is declining with frequency when internal damping is taken into account, as depicted in **Figure 5.3**. This can be attributed to the fact that less soil mass is accelerated in the same direction and reflections increase due to the nature of high eigenmodes. For this reason, emphasis is placed on the first three eigenfrequencies.

The numerical results for the eigenfrequencies of the soil-foundation system show negligible deviation from the theoretical ones, as can be seen in **Table 5.1**. The maximum difference between the theoretical and numerical results is at 1.3% for the case of the third eigenfrequency of the soil stratum with the skirts alone. Since the eigenmodes of the soil stratum with the suction caisson on the one hand and the skirts alone on the other are almost identical, the former ones are presented in **Figures 5.4-5.6**. The corresponding theoretical curves are available in **Figure 5.7**.

	***f* (Hz)**		
	THEORETICAL	**NUMERICAL w/ SUCTION CAISSON**	**NUMERICAL w/ SKIRTS**
1st eigenfrequency	1.67	1.67	1.68
2nd eigenfrequency	5	5.04	5.06
3rd eigenfrequency	8.33	8.39	8.44

Table 5.1. Eigenfrequencies results

5.4 Acceleration Time Histories

Of significant importance for the evaluation of the kinematic interaction is not only to compare the motion of the free-field with that of the foundation, but also to effectively assess the response of the suction caisson itself in terms of acceleration of its two edges as depicted in the cross-section in **Figure 5.8**; the surface and the embedded one, which will therefore be called top and bottom edge, respectively. For that purpose, the acceleration time histories of the free-field, the top and bottom edge of the suction caisson for certain excitation frequencies *f* of modified Gabor pulses are presented in **Figures 5.9-5.12.**

While for f=0.2 Hz and f=1.5 Hz, the top and bottom edge of the foundation accelerate in phase, with the acceleration amplitudes being almost identical, the picture is different for the other frequencies. When the frequency of the excitation coincides with the second eigenfrequency of the system, that is to say at 5 Hz, there is an approximately π/2 phase difference between the acceleration of the top and bottom edge. This can better be observed in **Figure 5.13**, where the isolation of a part of the acceleration time histories is shown. Indeed, the value of acceleration is approximately at the same time zero for the top and maximum for the bottom edge respectively. In addition, for the case of 5 Hz, the acceleration amplitude of the free-field and the top edge exceed more than twice that of the bottom edge. Practically, the foundation starts to respond mainly by rotation as higher eigenmodes than the first one are mobilized. The fact that the phase difference is not precisely π/2, as would be expected by the one-dimensional amplification theory for the activation of the second eigenfrequency, is attributed to the excitation with modified Gabor, and not pure harmonic pulses.

Finally, for the case of f=10 Hz, a π phase difference in general can be noticed, since the imposed excitation is close to the third eigenfrequency of the system, which is f_3=8.33 Hz. In **Figure 5.14** a clearer picture is provided due to the enlargement of a part of the acceleration time histories. Another striking point is that the value of acceleration of the bottom edge is greater in comparison with the top one. This could be attributed to the fact that the influence of embedment is stronger at a high value of frequency, deamplifying thus the response of the top edge.

All the aforementioned conclusions can be further comprehended with the displacement profiles of the soil stratum that correspond to every eigenfrequency, as illustrated in the theoretical eigenmode curves of **Figure 5.7**. The initial position of the skirts of the foundation is depicted in those figures too. However, as aforementioned, these theoretical curves are produced in the basis of an excitation with purely harmonic waves and not modified Gabor pulses, which are used herein. Thus, the comparison is rough and the small deviations occur due to the different type of excitation.

Obviously, for excitation frequencies equal and lower than the first one, the top and bottom edge follow the displacement of the soil profile. For the second eigenmode, the inflection point is shown to fall right to the skirt tip, so the approximately π/2 phase difference can be justified. Additionally, by observing the third eigenmode, the top and bottom edge are well expected to accelerate with almost π difference.

Lastly, a comparison between the acceleration of the top edge of the suction caisson and the skirts alone is provided in **Figures 5.15-5.18**. As deduced by the results of the Eigenmode Analysis in Section 5.3, the system of the soil stratum does not seem to be affected by the presence of either the suction caisson or the sidewalls alone; thus, the acceleration time history of the free-field is the same for the two cases and presented once again in the above charts for comparative purposes. The results show that the kinematic response of the suction caisson and the skirts alone is practically identical in terms of acceleration time history.

5.5 Kinematic Interaction Factors

The effects of kinematic interaction are quantified by appropriate kinematic interaction factors, which are transfer functions relating the motion of the embedded foundation to that of the free-field and are presented below:

- The translational kinematic interaction factors $I_{U\,top} = u_{top} / u_{FF}$, $I_{U\,bot} = u_{bot} / u_{FF}$

  where u_{top} : the maximum horizontal displacement of the top edge

  u_{bot} : the maximum horizontal displacement of the bottom edge

  u_{FF} : the maximum horizontal displacement of the free-field

- The rotational kinematic interaction factor $I_{\Phi} = \theta\, R / u_{FF}$

  where θ : the maximum rotation of the foundation calculated as $\max [u_{top} - u_{bot}] / L$

  u_{FF} : the maximum horizontal displacement of the free-field

- The acceleration kinematic interaction factors $I_{A\,top}=A_{top} / A_{FF}$, $I_{A\,bot}=A_{bot} / A_{FF}$

  where A_{top} : the maximum acceleration of the top edge

  A_{bot} : the maximum acceleration of the bottom edge

  A_{FF} : the maximum acceleration of the free-field

In the case where there is no kinematic interaction, the translation of the foundation is equal to the free-field ground surface motion. Consequently, the value of both I_U and I_A will be equal to unit, whereas I_{Φ} will be zero, since no rotation takes place.

The practical importance of such transfer functions is obvious: by multiplying a free-field design response spectrum with the suitable transfer function, one can obtain the design response spectrum which should be used as input at the base of the superstructure or at the base of the foundation.

In **Figures 5.19–5.21**, the transfer functions regarding the suction caisson for the various imposed excitation frequencies of the modified Gabor pulses are depicted. For low frequencies, the foundation follows the motion of the free-field and no signs of kinematic interaction exist. It is understandable that as frequencies get higher, I_U and I_A decrease, while the case is opposite for I_{Φ}. Increasing frequency certainly leads to incompatibility between the motion of the embedded structure and that of the free-field, with the first one including not only a translational, but also a rotational component too.

Furthermore, it is obvious that as the frequency of the excitation increases, the difference between the top and bottom edge relatively to the translation of the free-field tends to get greater, overall. The bottom edge presents more difficulty to follow the free-field, in contrast to the top edge of the foundation which lies on the surface.

The minimum translational kinematic interaction factor $I_{U\ top}$=0.73, as well as the maximum rotational transfer function I_{Φ}=0.47 appear at the frequency of f=8.7 Hz, which is close to the third eigenfrequency (f_3=8.33 Hz), whereas the minimum value of $I_{A\ top}$=0.51 is observed at f=10 Hz. It can be deduced from this, that as we proceed to higher eigenmodes the difficulty of the embedded foundation to follow the motion of the free-field increases dramatically.

A comparison between the suction caisson and the skirts alone is achieved in terms $I_{U\ top}$, $I_{A\ top}$ and I_{Φ} with the results showing small differences, as can be seen in **Figures 5.22-5.24**. Therefore, the skirts are expected to respond in a similar manner as the suction caisson under dynamic conditions.

Finally, the results for the kinematic interaction factors I_U and I_{Φ} are compared to the solutions by Kausel et al. (1978) and Gazetas (1984).

Kausel et al. (1978) studied the case of an embedded cylindrical foundation in an elastic, homogeneous soil stratum resting on bedrock, with internal hysteretic damping ξ=5 % and Poisson's ratio ν=0.3. Since the comparison is qualitative, the approximate solution by Kausel et al. (1978) is used.

In **Figures 5.25–5.26** the results for the suction caisson of this study, in terms of $I_{U\ bot}$ and I_{Φ} are compared to the approximate curve by Kausel et al. (1978), generally showing acceptable agreement.

A numerical study by Gazetas (1984) provided results for the kinematic response of end-bearing piles. The solution includes average I_U curves, which take into account a variety of Young moduli, as well as pile length to diameter ratios. Considering the suction caisson similar to a short pile, a comparison with the results by Gazetas (1984) is attempted.

The kinematic interaction factor I_U is introduced by Gazetas (1984) as a function of a dimensionless frequency parameter F_C, which is given by the following expression:

$$F_C = \frac{f}{f_1} \cdot \left(\frac{E_p}{E_s}\right)^{0.30} \cdot \left(\frac{L}{d}\right)^{-0.50} \tag{5.3}$$

where f_1: fundamental shear frequency (1st eigenfrequency) of the soil stratum

E_P: Young Modulus of the pile

E_S: Young Modulus of the soil

L: Length of the pile

d: Diameter of the pile

In the case examined herein, the above parameters were properly substituted by those of the suction caisson.

However, as can be observed in **Figure 5.27** there are significant deviations from the I_U curve by Gazetas (1984). This can be attributed to the fact that the average I_U curves were developed with length to diameter ratios appropriate for piles, that is to say $L/d > 10$. As a conclusion, the dynamic response of the suction caisson shows considerable difference from that of a single pile and the above solution is inappropriate for the cases examined in this study.

5.6 Seismic Earth Pressures

5.6.1 Kinematic Response to Modified Gabor Pulses

The seismic soil pressures, which are developed behind an embedded structure, are of uncertain nature, with a variety of parameters affecting the final result, such as the soil-structure stiffness, the special characteristics of the earthquake and topology etc.

In this section, an attempt is made to shed light on the influence of the excitation frequency on the dynamic soil pressures that develop behind the foundation. Since the foundation examined herein is cylindrical and the excitation is imposed in the horizontal direction, the seismic stresses chosen to be presented are those that are developed normally to the sidewalls; case, which is actually valid for a single column of finite elements on the right and left to the suction caisson, as depicted in **Figure 5.28**. The dynamic earth pressures are presented when the maximum acceleration of the top edge of the foundation takes place, which also coincides with the maximum rotation of the foundation. In the majority of the cases, the resultant seismic force on the sidewalls was maximum (or close to maximum) at the selected time.

As can be observed in **Figure 5.29,** which provides the dynamic earth pressures in the case of the suction caisson as a function of excitation frequency, it appears that their amplitude actually fluctuates with frequency. Stresses on the periphery of the foundation maximize with the activation of the first eigenmode of the system, which turns out to be the most critical for dynamic earth pressures. As a matter of fact, the soil stresses that result from the other excitation frequencies are clearly outperformed.

Another remarkable fact is that the situation for the seismic earth pressures is practically the same for the frequencies of 5 and 1 Hz, although the displacement profiles are totally different. The lowest amplitude of the seismic earth pressures can be noticed for the highest imposed frequency of 10 Hz.

Due to the nature of eigenmodes higher than the first one, in combination with the evident role of kinematic interaction, the suction caisson responds mostly by rotating and resists

following the free-field displacements; thus, dynamic stresses would tend to increase. However, the absolute displacement of the soil at such high frequencies is very small, and hence, the increase is negated.

Interestingly, the amplitude of seismic stresses on the sidewalls maximizes when the first eigenmode is mobilized, that is to say, when the frequency of the excitation imposed at the base of the soil stratum coincides with the first eigenfrequency of the system, leading to soil resonance. Although the shape of soil deflection is similar to the rigid body displacement, stresses on the sidewall are maximum, because the whole displacement profile is much larger.

As the frequency of the excitation approaches zero, which constitutes a manner of static imposition, dynamic stresses minimize. Specifically, if the extreme case where f=0 is considered, due to the resulting vertical free-field soil profile and the absence of kinematic interaction, seismic earth pressures would become zero.

More details concerning four excitation frequencies are presented, in order to shed light into the mechanisms of the kinematic interaction.

In **Figure 5.30** is presented the acceleration time history, as well as the elastic response spectrum of the f=0.2 Hz Gabor excitation. Additionally, the dynamic earth pressures on the left and right side of the suction caisson and the skirts alone are shown together for the time of maximum acceleration at the top edge that coincides with maximum rotation of the foundation. The symmetry between the left and right side stresses is due to the elasticity of the problem and the full contact between the foundation and the soil. The differences in the earth pressures on the two foundation types are overall negligible, with the exception of the edges, where some deviations appear. **Figure 5.31** shows the contours of the normal stresses on the suction caisson, while **Figure 5.32** the external soil with contours of the normal and shear stresses acting on the foundation. Finally, **Figure 5.33** provides the horizontal displacement and acceleration with depth of the free-field and the left side, from the edge that is common for the soil and the foundation. Corresponding results from excitation frequencies 1.5, 5 and 10 Hz are available in **Figures 5.34-5.45**. Overall, the response of the skirts alone under dynamic excitation is approximately the same to the suction caisson for practical purposes.

One point that needs to be stressed out is the sign of the dynamic earth pressures on the top and bottom edge, which is reverse in comparison with the stresses acting on the central part of the sidewalls, as was seen in the aforementioned figures. For this purpose, the right side of the external soil, for f=1.5 Hz excitation, is shown isolated in **Figure 5.46**. As it can been seen, the soil at the top and bottom edge translates locally towards the opposite direction from the central part, forced by the rotational component of the foundation's motion and the fully bonded contact considered between the foundation and the surrounding soil. The local buckling, which can be observed at the bottom edge, is a consequence of these increased stresses.

5.6.2 Comparison with Brandenberg et al. (2015)

Brandenberg et al. (2015) developed a kinematic interaction approach providing a framework for the estimation of seismic earth pressures on an embedded rigid strip foundation, with assumptions summarized as follows:

- Infinitely long U-shaped rigid structure embedded in a soil profile of uniform shear wave velocity
- Horizontally coherent vertically propagating shear waves
- Negligible base slab averaging effects
- Full contact between soil and structure
- Interaction between the soil and vertical walls characterized by stiffness intensity terms k^i_y and k^i_z and interaction between the soil and base slab by stiffness terms K_Y and K_{XX}

A definition of the problem can be found in **Figure 5.47.** The notation used by Brandenberg et al. (2015) is useful for the comprehension of the charts, thus it is presented below:

P_E : kinematic seismic force increment

For ground motion in the y-direction, P_E is calculated as a force per unit length

$$P_E = \int_0^H k_y^i [u_{g0} \cos kz - u_w(z)] dz$$

H : wall height

$u_w(z)$: wall displacement at depth z

u_{g0} : free field displacement on the surface

k_y^i : soil-wall reaction stiffness in y-direction (normal stresses) per unit of wall area (superscript i denotes stiffness intensity measured in units of F/L^3)

λ : wave length

k (= $2\pi/\lambda$) : wave number

Vs : shear wave velocity

Horizontal Wall–Soil Stiffness Intensity k_y^i

$$k_y^i = \chi_y \frac{\pi}{\sqrt{(1-\nu)(2-\nu)}} \frac{G}{H} \sqrt{1-\left(\frac{2\omega H}{\pi V_s}\right)^2}$$

Vertical Wall–Soil Stiffness Intensity k_z^i

$$k_z^i = \chi_{xx} \frac{\pi}{2} \sqrt{\frac{2-\nu}{1-\nu}} \frac{G}{H} \sqrt{1-\left(\frac{2\omega H}{\pi V_s}\right)^2}$$

Base Slab Stiffness Terms K_y and K_{xx}

$$K_y = \chi_y \frac{2.1G}{2-\nu}\left(1+2\frac{B}{D-H}\right)$$

$$K_{xx} = \chi_{xx} \frac{\pi G B^2}{2(1-\nu)}\left(1+\frac{1}{5}\frac{B}{D-H}\right)$$

Figure 5.48 provides charts for the calculation of the translational and rotational static interaction factors x_y and x_{xx}.

First of all, the comparison with the results by Brandenberg et al. (2015) is conducted in a qualitative manner, due to the different nature of the foundations and the specific characteristics chosen. P_E, the kinematic seismic force increment, is the integral of the horizontal stress increment over the wall height. In this study, P_E is calculated as the integral of the dynamic stresses acting on the left or right side (as defined in **Figure 5.28**) of the suction caisson.

As shown in **Figure 5.49**, Brandenberg et al. (2015) presented the dynamic force increment P_E normalized by the free-field displacement u_{g0}, the horizontal wall-soil stiffness intensity k^i_y and the wall height H, as a function of wave length to wall height ratio λ/H. The part of the diagram that falls to the right of the longest wavelength (lowest frequency, since $\lambda=V_S/f$) peak in normalized P_E and corresponds to λ/H≥2.3 is of great importance for typical structures and earthquake ground motions. The explanation for this is quite simple: the site resonant frequency is calculated as λ/D=4, which can be formatted as λ/H=4D/H. Taking into consideration the fact that the depth of the soil stratum in general exceeds to a considerable extent the wall height (i.e., generally D >> H), consequently λ/H will exceed the value of 4, which can be seen right to the lowest frequency peak at λ/H≥2.3. The appearance of the peaks and troughs in the normalized P_E, which can be seen for λ/H<2.3, is due to the alternation of the direction of the horizontal stress increment developing over the wall as frequency changes.

Using the same normalization with Brandenberg et al. (2015), **Figure 5.50** illustrates the results from the kinematic response of the suction caisson to modified Gabor pulses. The analyses of this study refer to λ/H>2. Apparently, the same trend with the solution by Brandenberg et al.

(2015) is observed. The peak of the normalized P_E can be noticed for λ/H=2.3, which corresponds to f=8.7 Hz in our case; a price which is close to the third eigenfrequency of the system at f_3=8.33 Hz.

However, since the displacement of the free-field (u_{g0}) is a parameter, which varies with the frequency of the imposed excitation (as will be explained below and shown in **Figure 5.53**), a different normalization that does not involve u_{g0} is implemented in order to display a more realistic picture of the dynamic earth pressures. Specifically, in **Figure 5.51** dynamic force P_E is normalized by $k^i_y H^2$ (which is a constant term since the dynamic component in the stiffness term is omitted) and is once again illustrated as a function of normalized wave length λ/H.

It is important to note that P_E in fact fluctuates with frequency and that seismic earth pressures appear maximum when the first eigenfrequency of the system (f_1=1.67 Hz) is activated, that is to say when λ/H=11.9. This diagram shows agreement with the results of the dynamic soil stresses on the sidewalls in **Figure 5.29**, where the amplitude of dynamic earth pressures appears to fluctuate with excitation frequency.

Another interesting fact is that the value, which corresponds to λ/H=6.67 (f=3Hz) is lower than that of λ/H=4 (f=5 Hz). In order to enlighten this, a chart of the amplification as a function of frequency is provided in **Figure 5.52**. It is reminded here that the ratio of the free-field displacement to that of the soil stratum base is known as amplification A. The equation of the one-dimensional amplification theory (**Figure 5.2**) is used for the theoretical curve, which is presented along with the ratios of the suction caisson results. The differences between the theoretical solution and the numerical results in the values of A at the eigenfrequencies are attributed to the fact that the imposed excitation includes modified Gabor pulses and not harmonic waves, which is the case of the one-dimensional amplification theory. Obviously, amplification for the excitation frequency of 3 Hz is lower than that of 5 Hz, which happens to be the second eigenfrequency of the system.

As a result, it is of great importance where each case of excitation falls in the amplification chart. Thus, the fluctuation of the dynamic force P_E with frequency is proven - it is not expected to follow an overall standard pattern. The conclusions of Brandenberg et al. (2015) that kinematic pressures are clearly high near the peak at 2.3 due to large relative deformations of the wall and soil, as well as that P_E rapidly decreases as λ/H increases beyond 2.3 are consequently proven false. In **Figure 5.53** the results of the free-field displacement as a function of frequency from this study are presented. It is apparent that u_{g0} fluctuates with frequency, thus the normalization of P_E by u_{g0} does not offer under any circumstances a realistic picture of the development of the seismic stresses as a function of the excitation frequency.

5.6.3 Kinematic Response to Aegion (1995) and Monastiraki (1999) Earthquake Motion

The kinematic response of the suction caisson and the skirts alone was investigated for the recorded earthquake motions of Aegion (1995) and Monastiraki (1999) with acceleration peak values at 0.55 g and 0.54 g, respectively. Emphasis is placed on the seismic earth pressures acting on the sidewalls.

Figure 5.54 illustrates the acceleration time history and the elastic response spectrum of the Aegion earthquake motion. The acceleration peak value is at 0.55 g. As can be clearly seen in the response spectrum, the dominant period is at 0.48 s, which in terms of frequency corresponds to 2.1 Hz. The first eigenfrequency of the soil-foundation system under examination herein is at 1.67 Hz or otherwise the first eigenperiod is equal to 0.6 s, falling to the right of the dominant period at the response spectrum.

The acceleration time histories of the top and bottom edge of the suction caisson, as well as of the free-field are provided in **Figure 5.55**. The differences of the foundation's edges in comparison with the free-field are small, due to the fact that the excitation's dominant frequency is quite close to the first eigenfrequency of the system, where the foundation follows overall the motion of the free-field, with limited resistance.

The seismic earth pressures on the sidewalls of the two foundation types are shown in **Figure 5.56** for the time of maximum acceleration of the top edge. Overall, the differences between the suction caisson and the skirts alone are once again negligible, with the exception of the bottom edge. A comparison with the modified Gabor pulses of f=0.7, 5 and 1.5 Hz is shown in **Figure 5.57**, for the case of the suction caisson. It seems that the agreement is good with the results from the excitations of frequencies 0.7 and 5 Hz. This can be further comprehended with **Figure 5.52**, which shows the amplification as a function of excitation frequency. According to the numerical results mainly, an excitation of 2.1 Hz leads to amplification, which is approximately the same to that from an excitation of 5 and 0.7 Hz. It is once again reminded that the theoretical curve is developed in the basis of harmonic waves as excitation. However a rough comparison with the case of the dominant frequency of a seismic record and the modified Gabor pulses is possible, since the general trend is not expected to differ dramatically. **Figures 5.58** and **5.59** show a snapshot of the model, as well as contours of normal and shear stresses acting on the suction caisson for the time of maximum acceleration of the top.

The acceleration time history and the elastic response spectrum of the Monastiraki earthquake motion are shown in **Figure 5.60.** The peak acceleration is at 0.54 g, which can be seen in the acceleration time history, as well as in the response spectrum corresponding to T=0. The dominant period of the excitation is at 0.16 s or alternatively, the dominant frequency is at 6.25 Hz. As can be observed in the response spectrum, the second eigenperiod T_2=0.2 s of the system examined herein, falls at right relatively to the dominant period. Consequently, the soil-foundation system is expected to respond to the excitation, with a motion that matches to the second eigenmode approximately.

The acceleration time histories of the top and bottom edge of the suction caisson, as well as of the free-field are available in **Figure 5.61,** where the difference of the bottom comparatively to the top edge and the free-field is quite significant. It seems thus, that the foundation has difficulty in following the motion of the free-field, which, as was discussed in previous sections, leads to increased rotation for high excitation frequencies.

In **Figure 5.62** can be found the seismic earth pressures on the sidewalls of both the suction caisson and the skirts alone for the time of maximum acceleration of the top (t=3.995 s), where it is seen that for practical purposes the response is almost the same. A comparison of the seismic earth pressures acting on the suction caisson with those resulting from excitation with modified Gabor pulses, is available in **Figure 5.63**. The development of the soil stresses over the height of the sidewalls in the case of the Monastiraki earthquake motion matches closely the case of f=8.7 Hz modified Gabor. This is once again explained by **Figure 5.52**, where amplification is shown as a function of excitation frequency. Obviously, the dominant frequency 6.25 Hz of the excitation results in similar amplification as the frequency of 8.7 Hz, which is quite close to the third eigenfrequency of the system. In conclusion, amplification is a parameter of detrimental importance in the amplitude of the seismic earth pressures.

Lastly, **Figures 5.64** and **5.65** depict a snapshot of the model at the time of the maximum acceleration of the top, as well as normal and shear stresses acting on the sidewalls of the suction caisson. Indeed, the motion resembles that with the activation of the second eigenmode of the system, where rotation is increased. Nevertheless, as it was stressed out previously, the amplitude of seismic earth pressures depends on the amplification, which varies with the frequency of the excitation.

5.7 Conclusions

The kinematic response of the rigid L/a=2 suction caisson and skirts alone in a homogeneous, elastic soil stratum was examined under excitation with modified Gabor pulses of maximum acceleration at 1g, as well as with the recorded earthquake motions of Aegion (1995) and Monastiraki (1999) with peak acceleration values of 0.55g and 0.54 g respectively. The following deductions have been made:

- Maximum seismic stresses acting on the sidewalls of the foundation appear when the 1st eigenmode of the soil-foundation system is mobilized
- The amplitude of seismic stresses fluctuates with excitation frequency
- Amplification which varies with excitation frequency determines the amplitude of seismic earth pressures
- Rotational kinematic interaction factor I_{Φ} tends to increase generally with excitation frequency in the area of interest
- Translational and acceleration kinematic interaction factors I_U and I_A, respectively, present overall a declining trend with excitation frequency in the area of interest
- Due to the effect of kinematic interaction and the nature of eigenmodes higher than the 1st one, the rotation of the foundation increases and at the same time the translation declines
- The kinematic response of the suction caisson and the skirts alone is approximately the same to seismic loading

Chapter 5: Figures

Kinematic Interaction

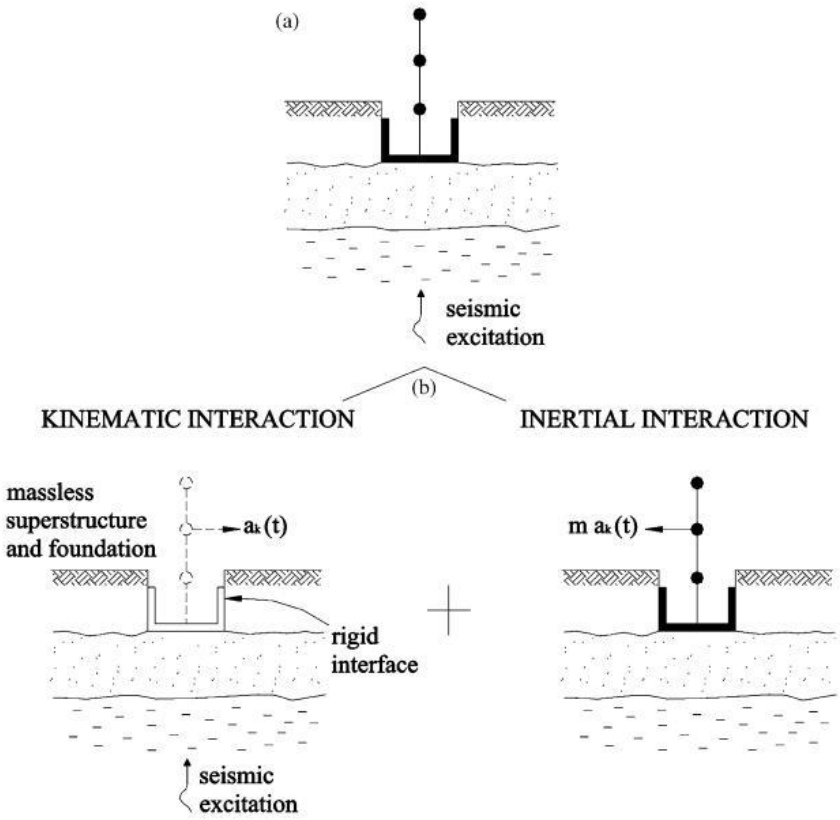

Fig.5.1. Geometry of soil-structure interaction problem and decomposition into kinematic and inertial interaction problems (Mylonakis et al. 2006)

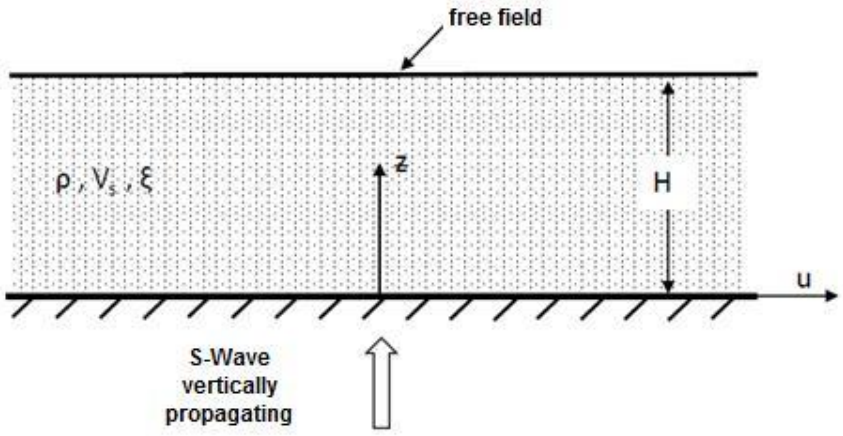

$$A = \frac{u_{z=H}}{u_{z=0}} = \frac{1}{\cos\left(\frac{\omega \times H}{V_s}\right)}$$

Fig.5.2. Amplification of motion for the case of a soil stratum on bedrock with vertically propagating shear waves (Soil Dynamics Notes, Gazetas)

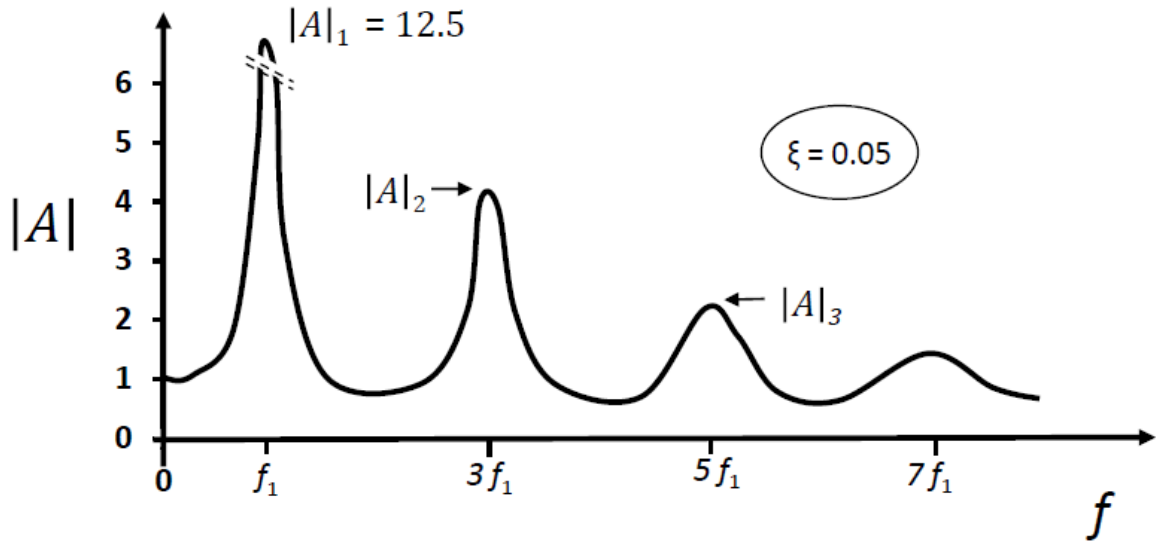

Fig.5.3. Decline of amplification amplitude with frequency, in the case of hysteretic damping (Soil Dynamics Notes, Gazetas)

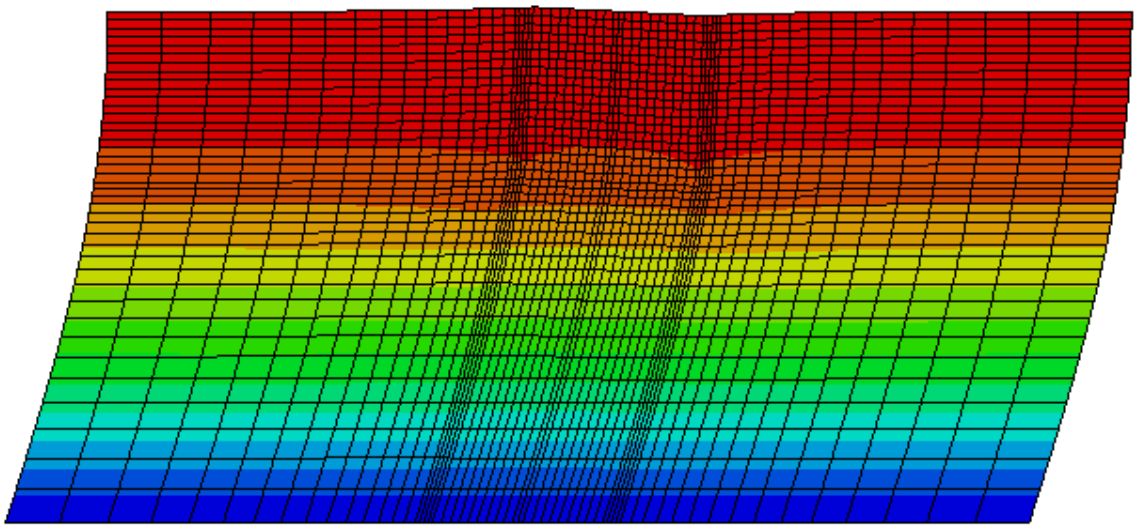

Fig.5.4. 1st eigenmode of the soil stratum with the suction caisson

f_1=1.67 Hz

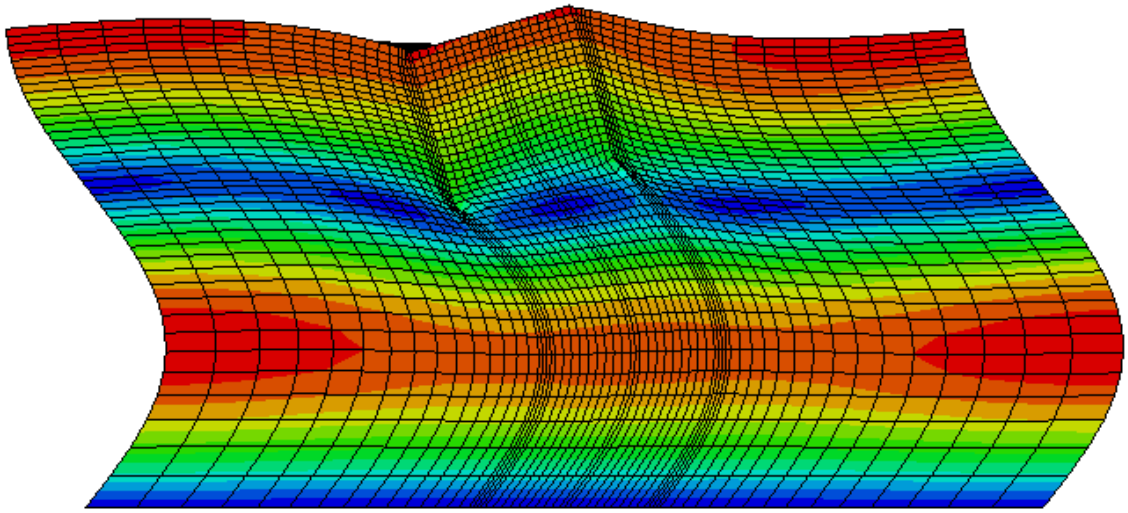

Fig.5.5. 2nd eigenmode of the soil stratum with the suction caisson

f_2=5.04 Hz

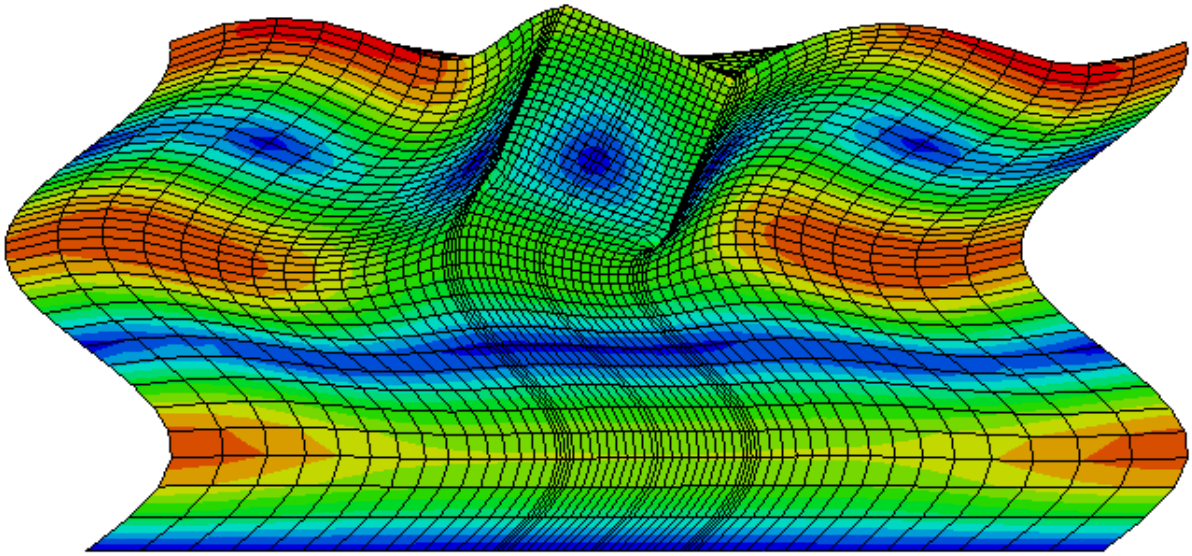

Fig.5.6. 3rd eigenmode of the soil stratum with the suction caisson

f_3=8.39 Hz

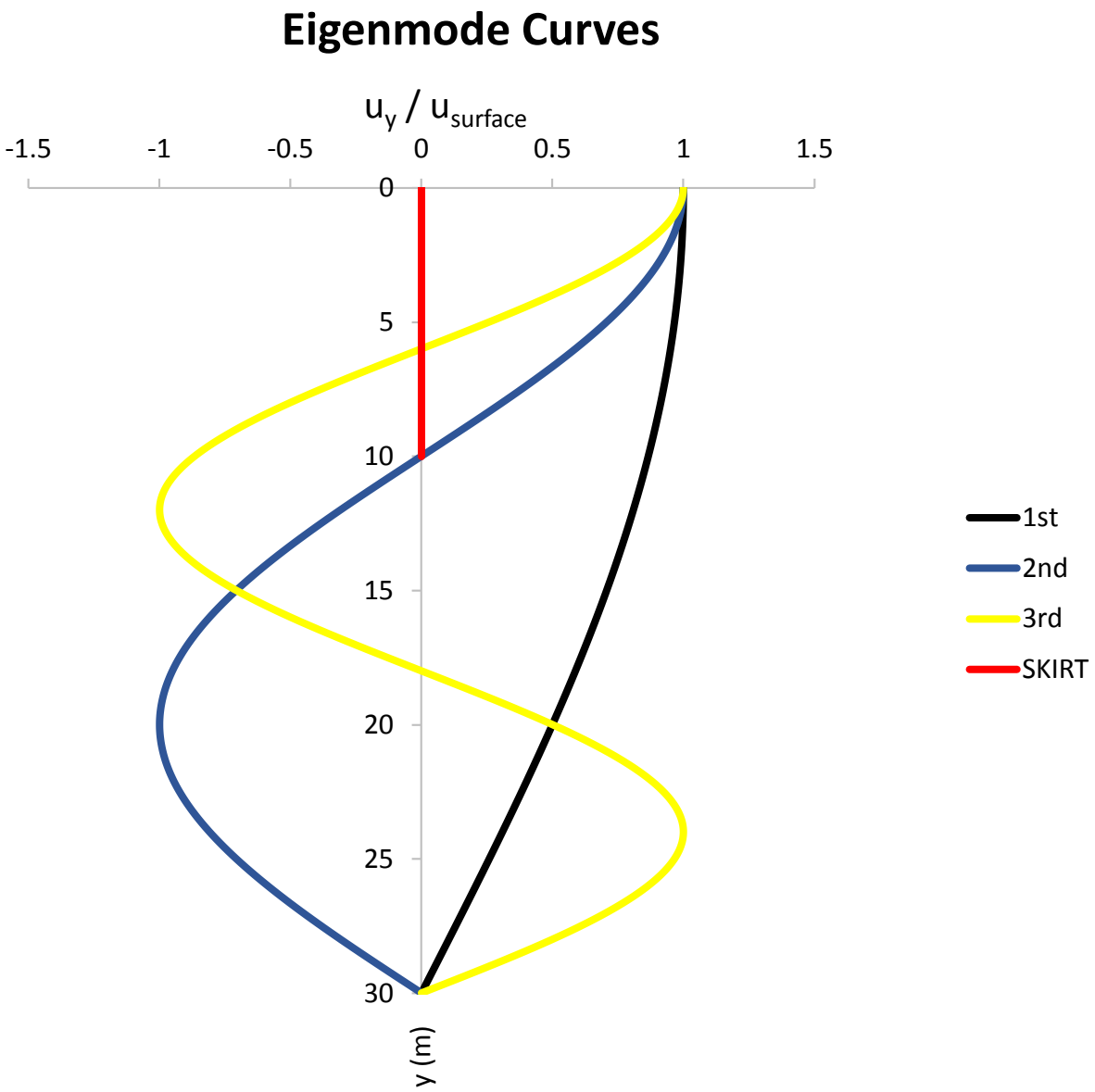

Fig.5.7. Theoretical curves of the first three eigenmodes of the system

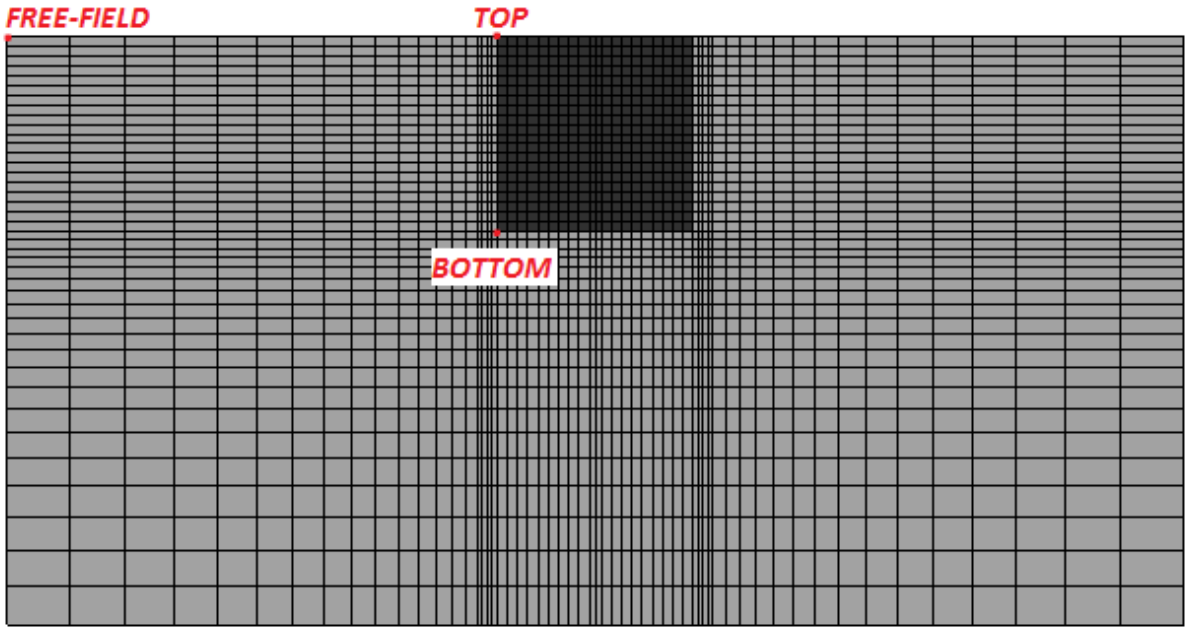

Fig.5.8. Definition of the top and bottom edge of the foundation

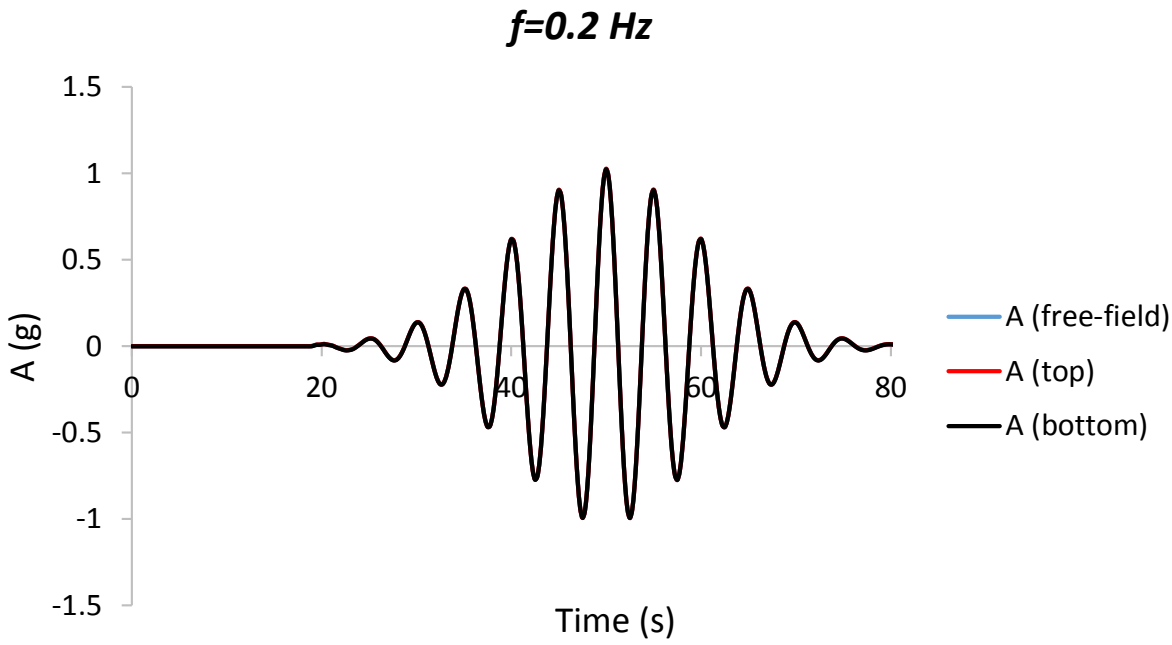

Fig.5.9. Acceleration time histories of the top and bottom edge of the suction caisson and of the free-field for excitation frequency *f*=0.2 Hz

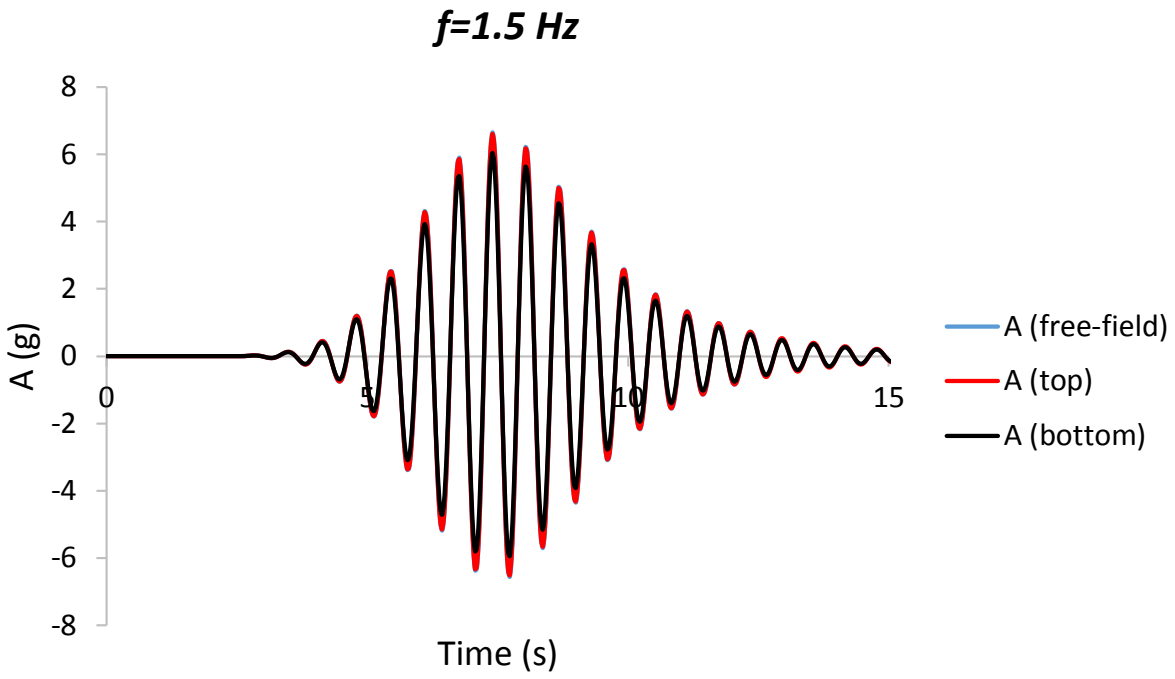

Fig.5.10. Acceleration time histories of the top and bottom edge of the suction caisson and of the free-field for excitation frequency *f*=1.5 Hz

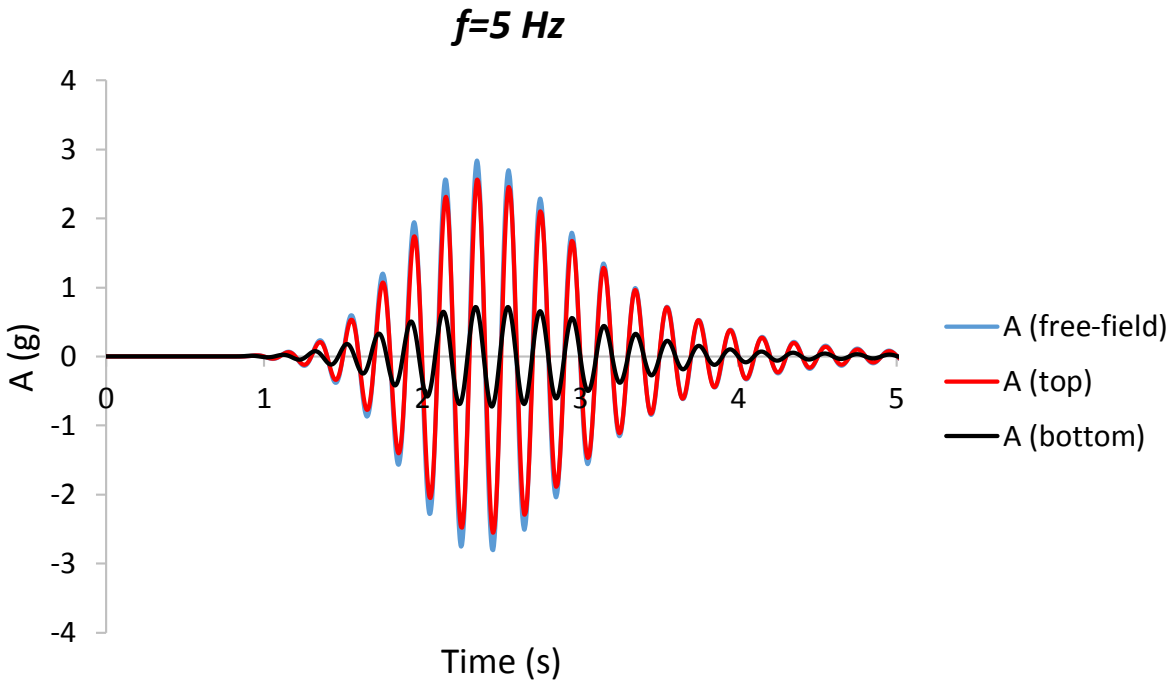

Fig.5.11. Acceleration time histories of the top and bottom edge of the suction caisson and of the free-field for excitation frequency *f*=5 Hz

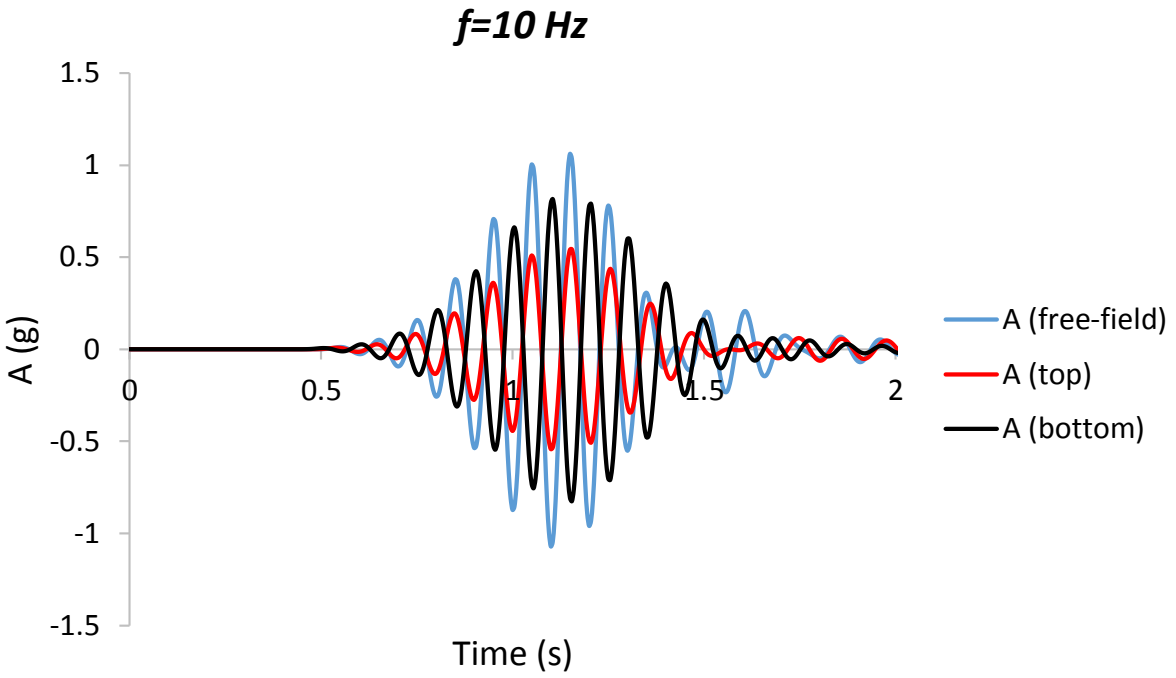

Fig.5.12. Acceleration time histories of the top and bottom edge of the suction caisson and of the free-field for excitation frequency *f*=10 Hz

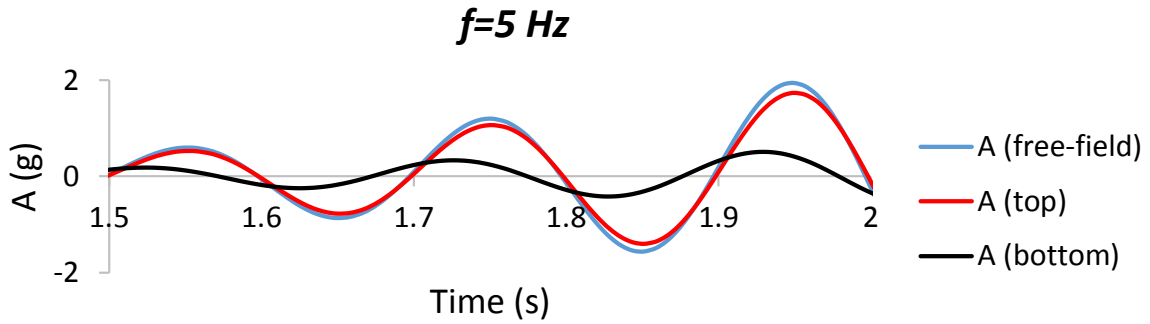

Fig.5.13. Part of the acceleration time histories of the top and bottom edge of the suction caisson and of the free-field for excitation frequency *f*=5 Hz

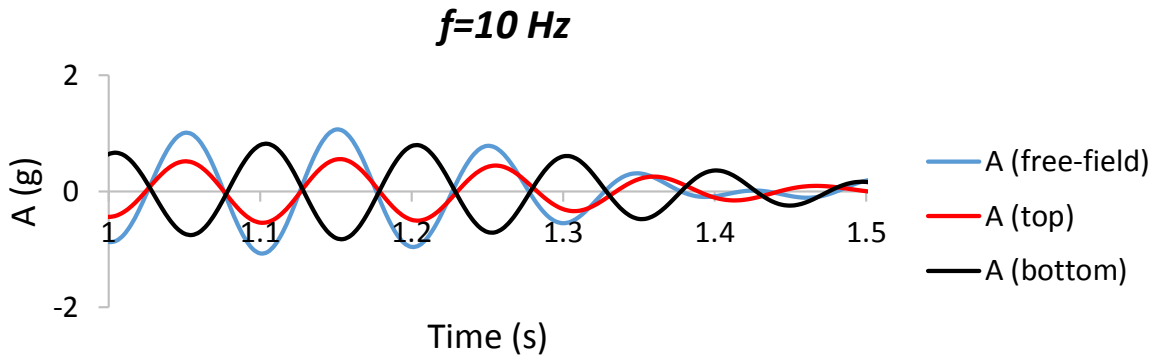

Fig.5.14. Part of the acceleration time histories of the top and bottom edge of the suction caisson and of the free-field for excitation frequency *f*=10 Hz

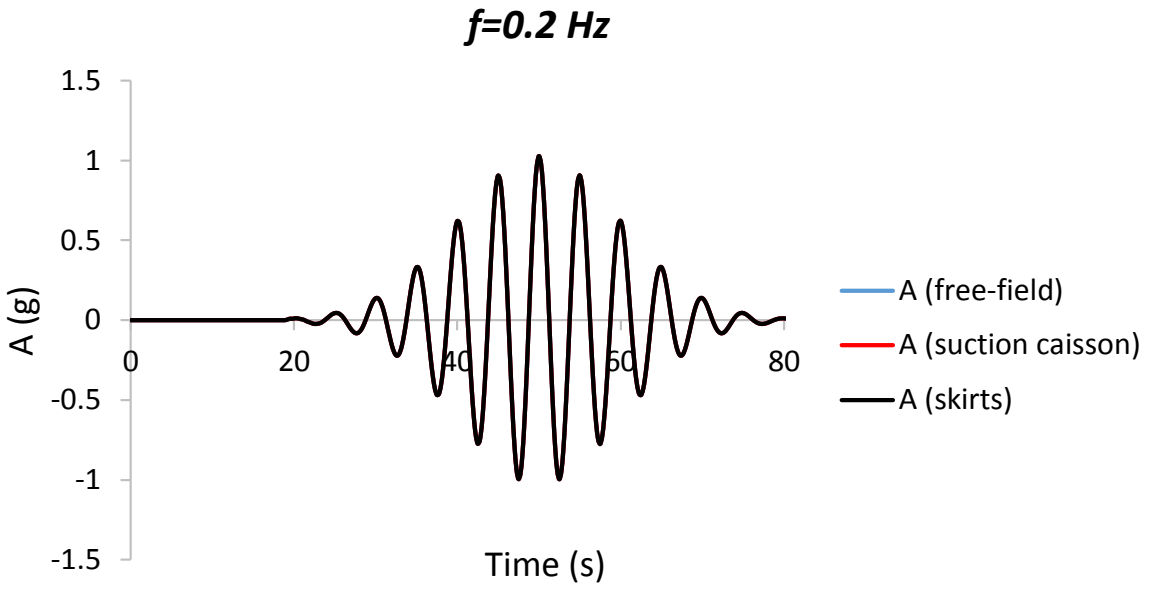

Fig.5.15. Acceleration time histories of the free-field and the top edge of the suction caisson and the skirts for excitation frequency *f*=0.2 Hz

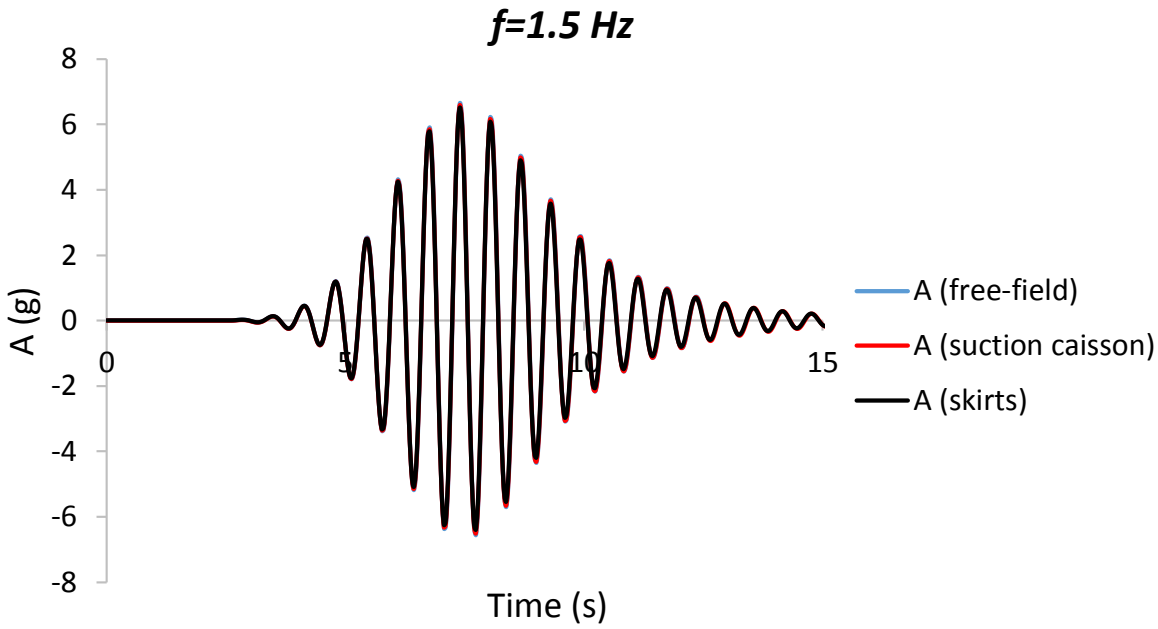

Fig.5.16. Acceleration time histories of the free-field and the top edge of the suction caisson and the skirts for excitation frequency *f*=1.5 Hz

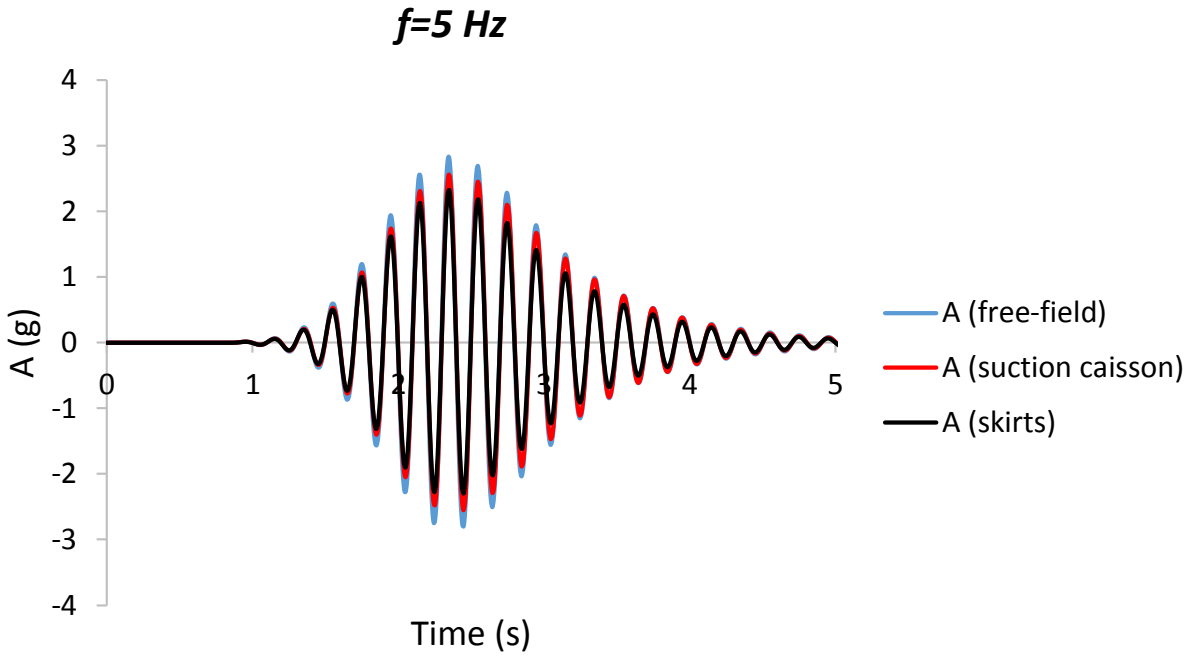

Fig.5.17. Acceleration time histories of the free-field and the top edge of the suction caisson and the skirts for excitation frequency *f*=5 Hz

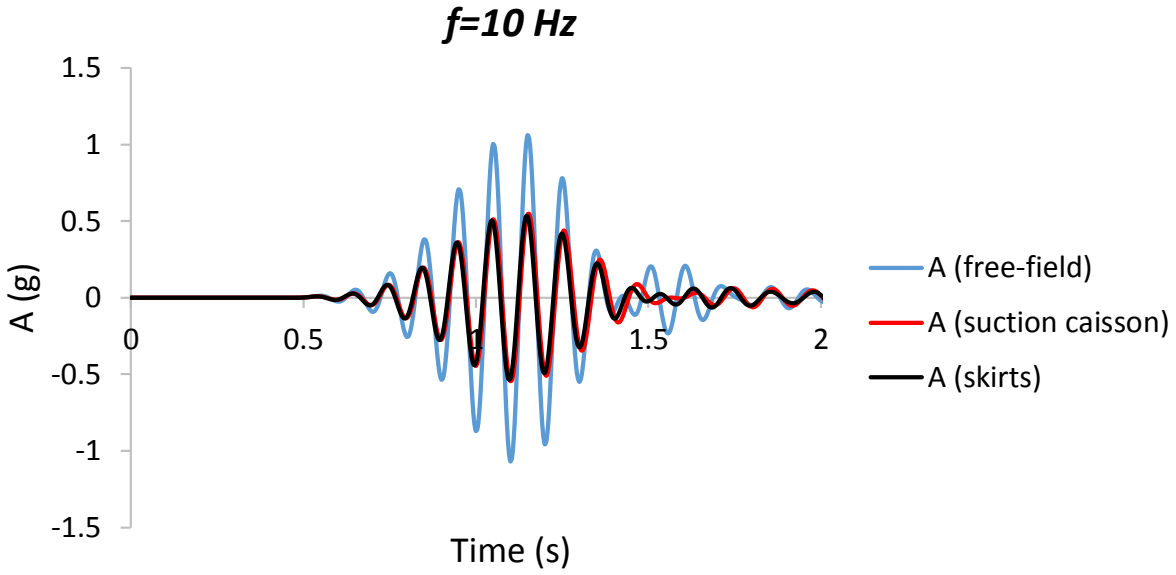

Fig.5.18. Acceleration time histories of the free-field and the top edge of the suction caisson and the skirts for excitation frequency *f*=10 Hz

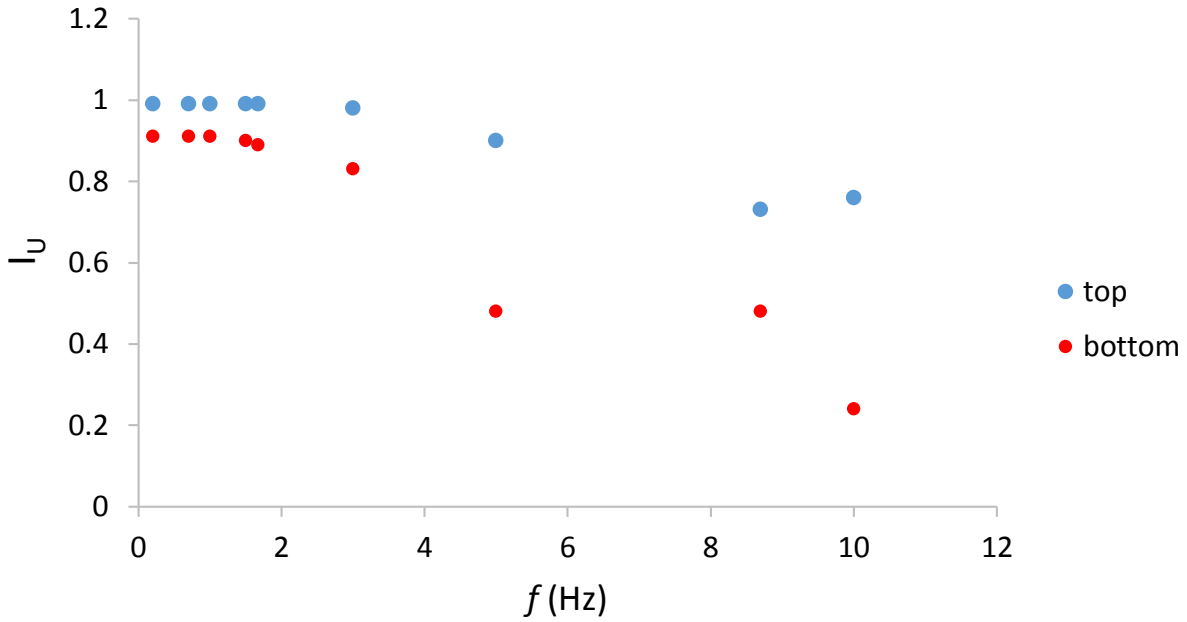

Fig.5.19. Kinematic Interaction factors $I_{U\ top}$ and $I_{U\ bot}$ in terms of frequency

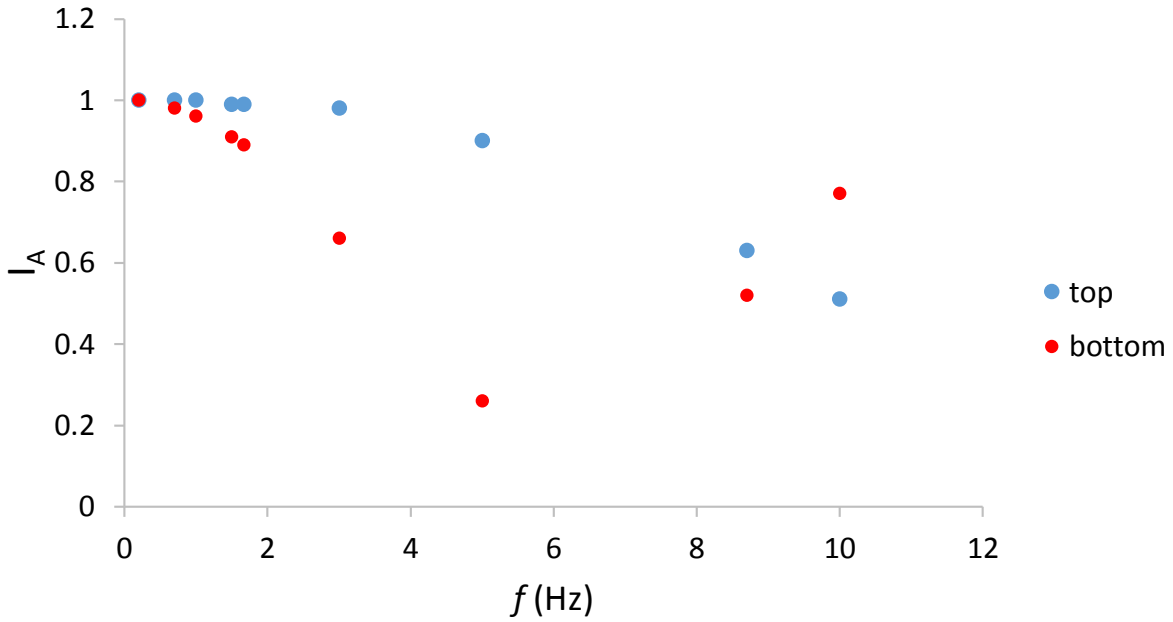

Fig.5.20. Kinematic Interaction factors $I_{A\ top}$ and $I_{A\ bot}$ in terms of frequency

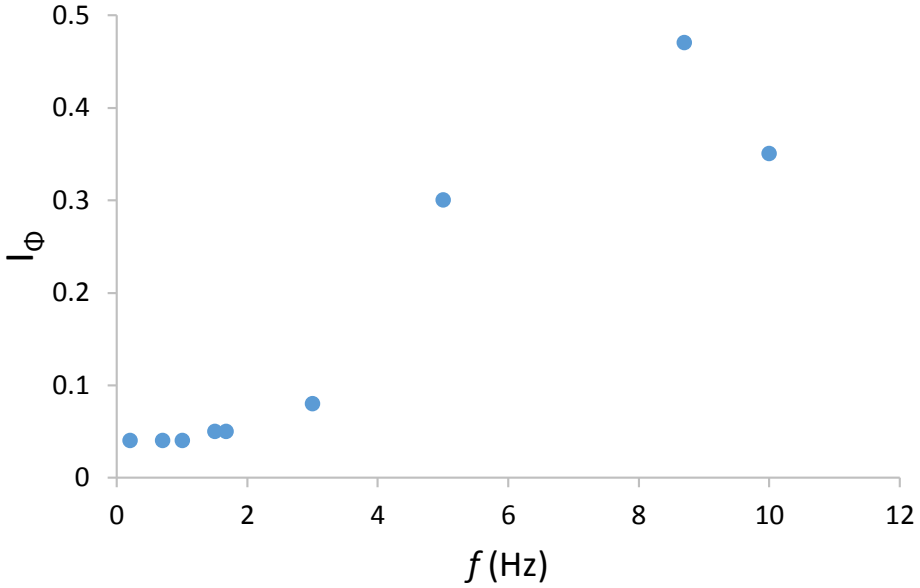

Fig.5.21. Kinematic Interaction factor I_Φ in terms of frequency

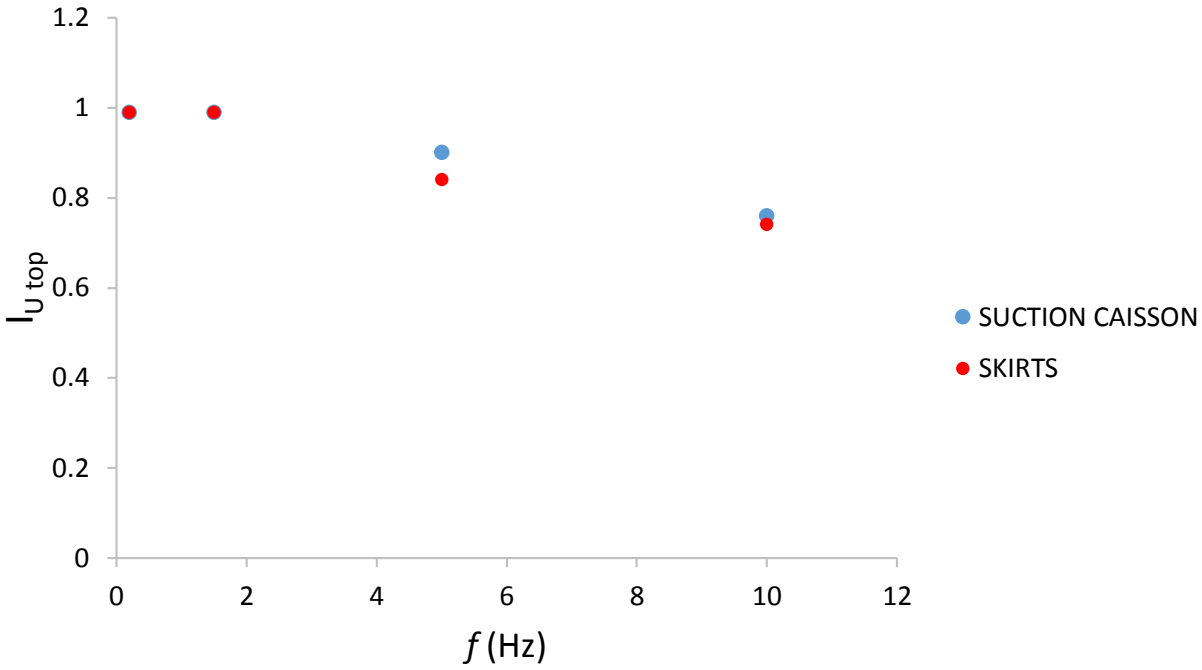

Fig.5.22. Comparison between the suction caisson and the skirts alone in terms of $I_{U\ top}$

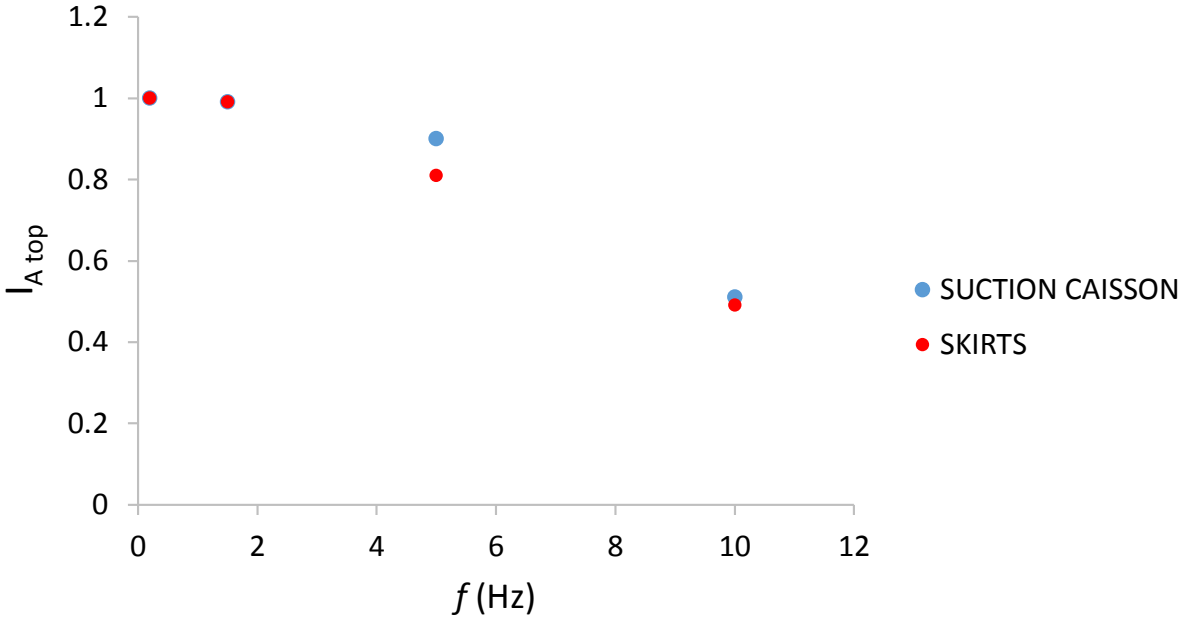

Fig.5.23. Comparison between the suction caisson and the skirts alone in terms of $I_{A\ top}$

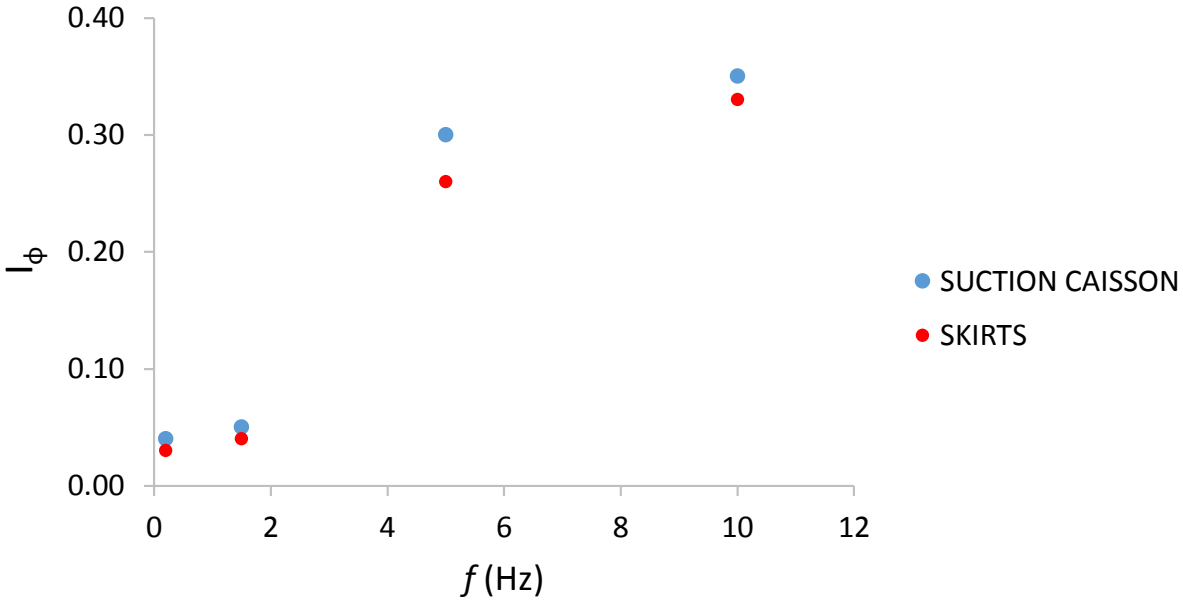

Fig.5.24. Comparison between the suction caisson and the skirts alone in terms of I_{Φ}

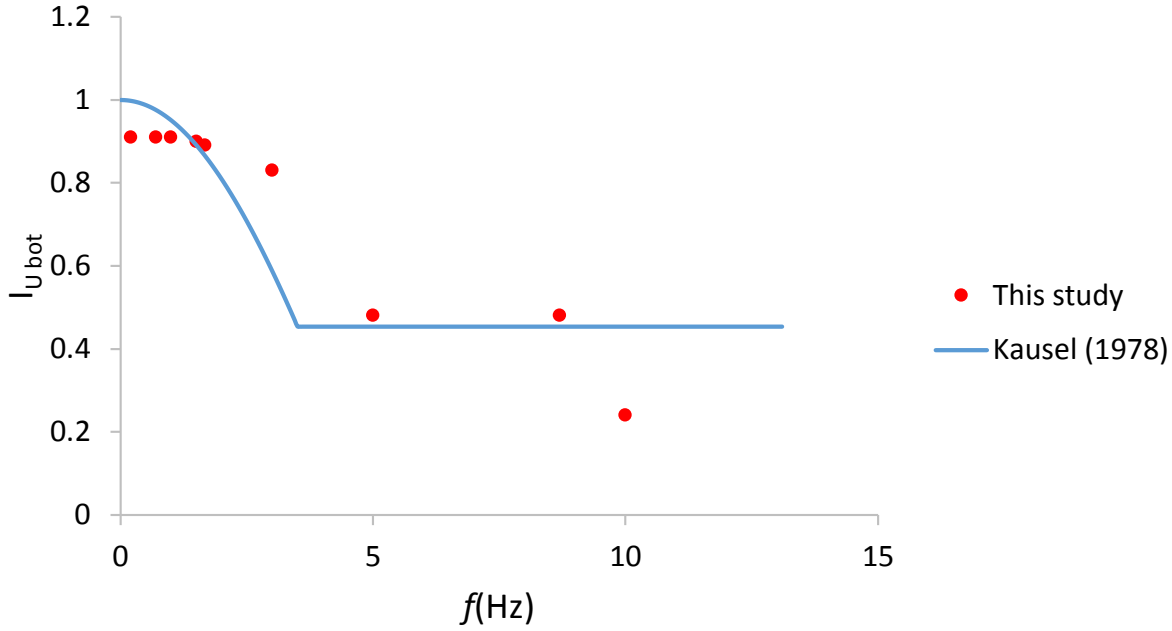

Fig.5.25. Comparison of $I_{U\,bot}$ with the approximate solution by Kausel et al. (1978)

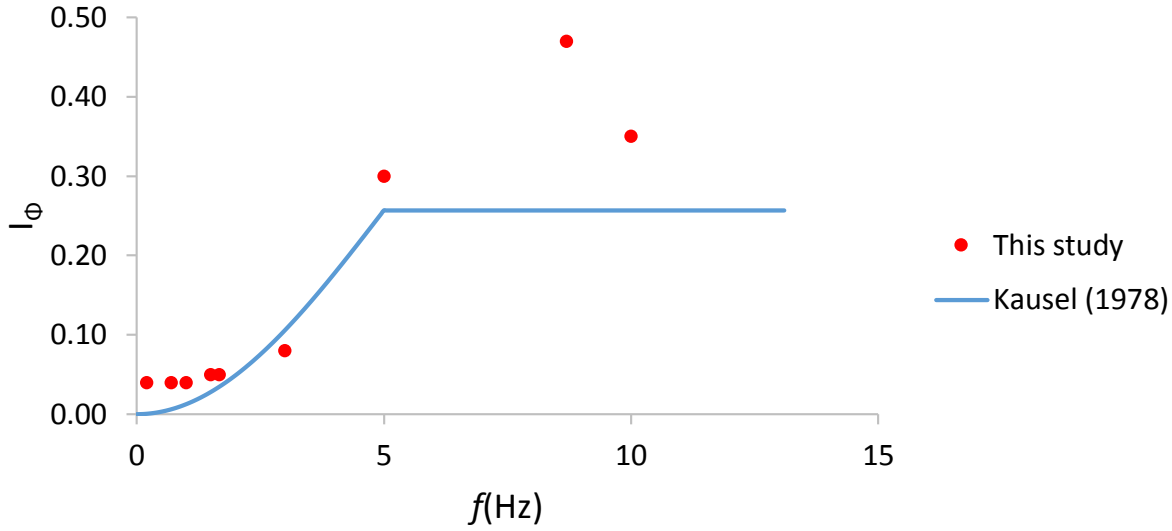

Fig.5.26. Comparison of I_{Φ} with the approximate solution by Kausel et al. (1978)

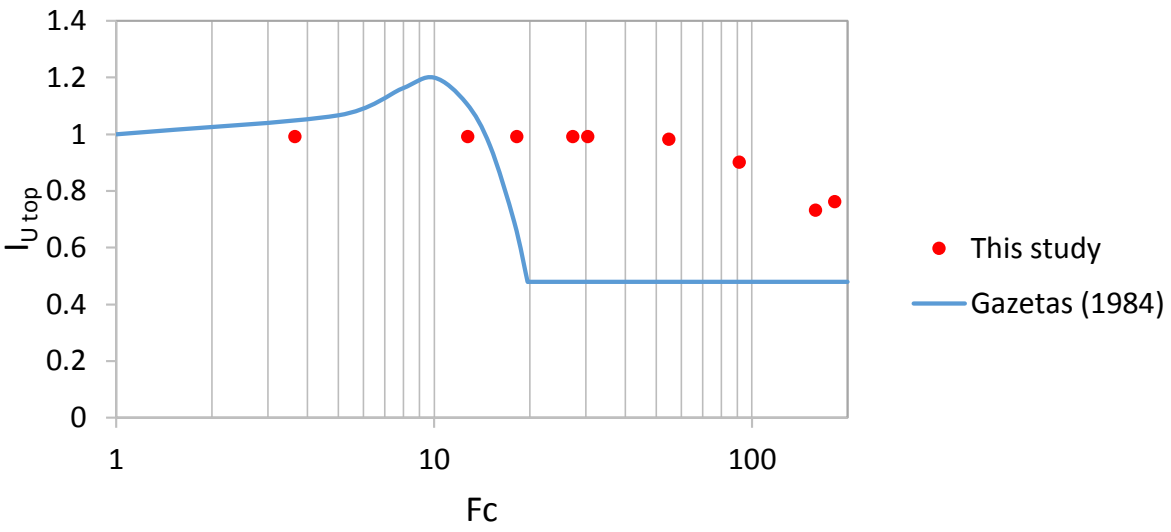

Fig.5.27. Comparison of $I_{U\,top}$ with the average curve by Gazetas (1984)

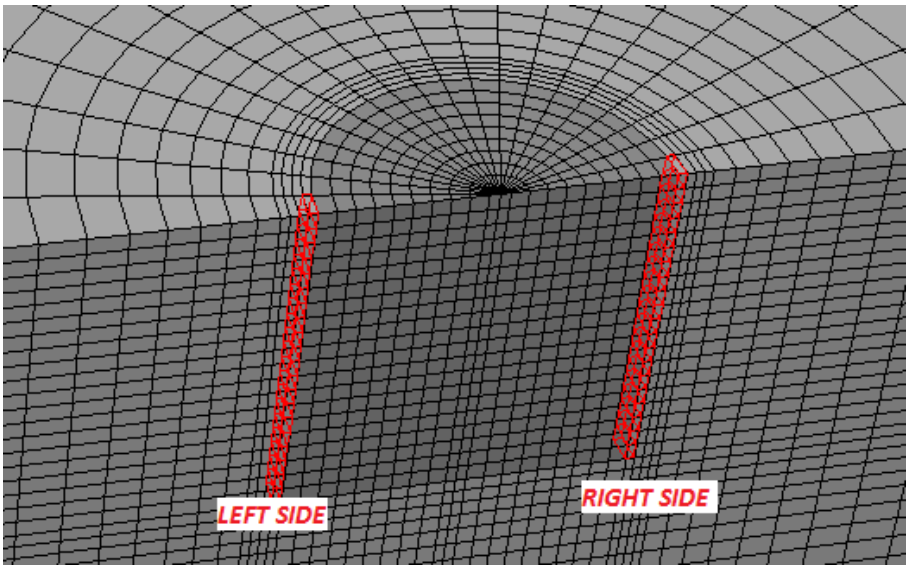

Fig.5.28. Definition of left and right side for the seismic earth pressures

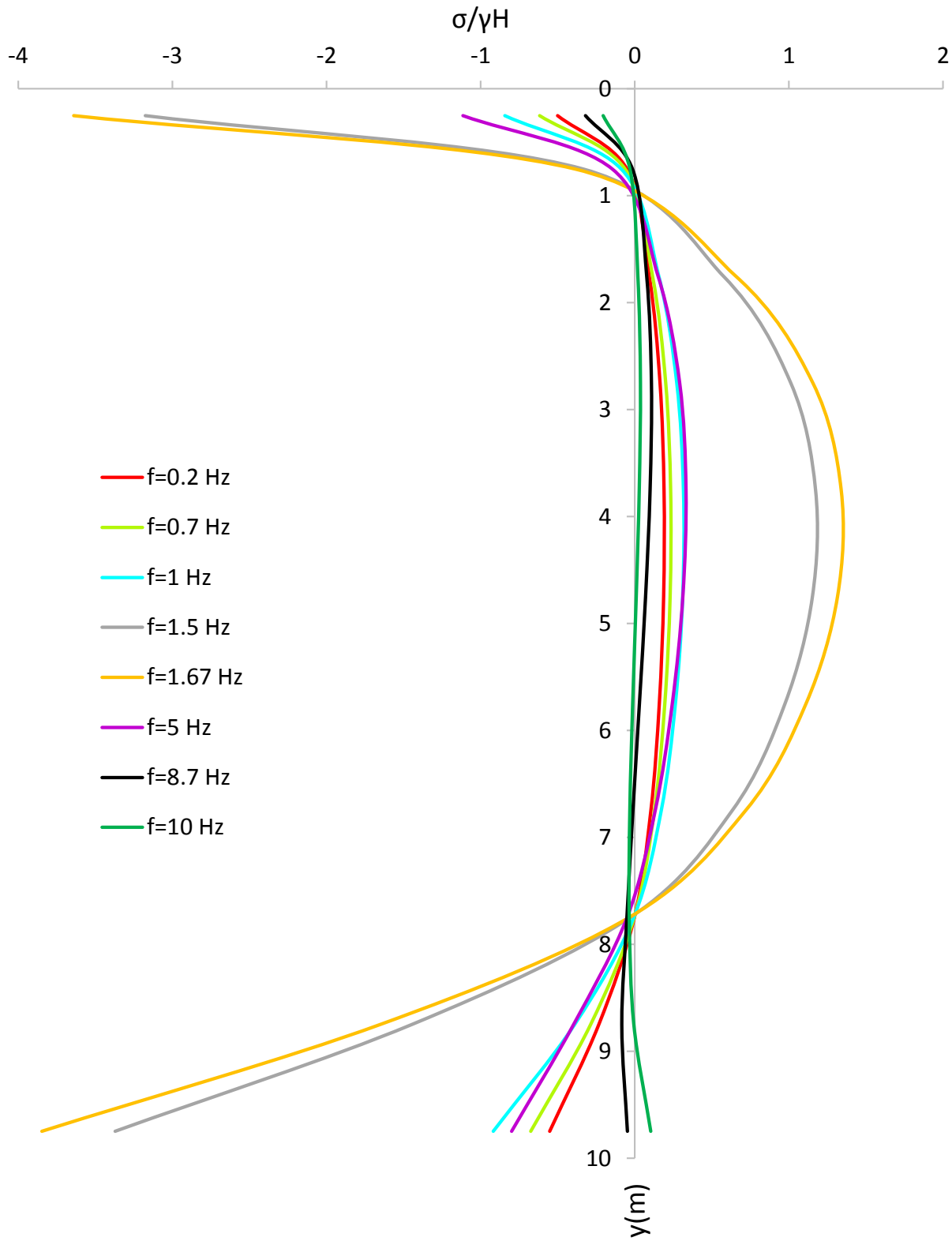

Fig.5.29. Seismic earth pressures for various excitation frequencies in the case of the suction caisson

a)

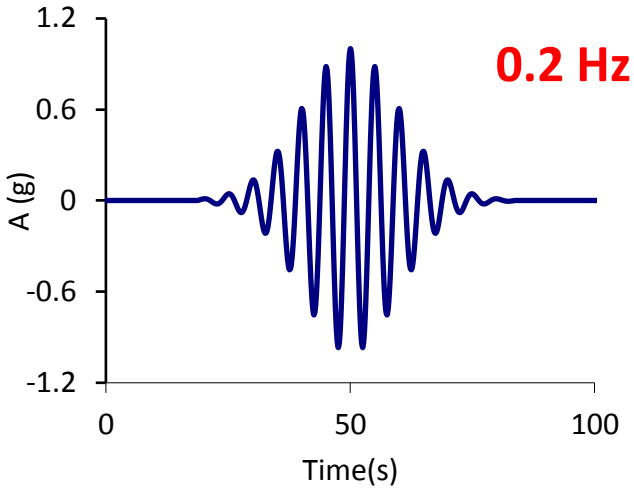

b)

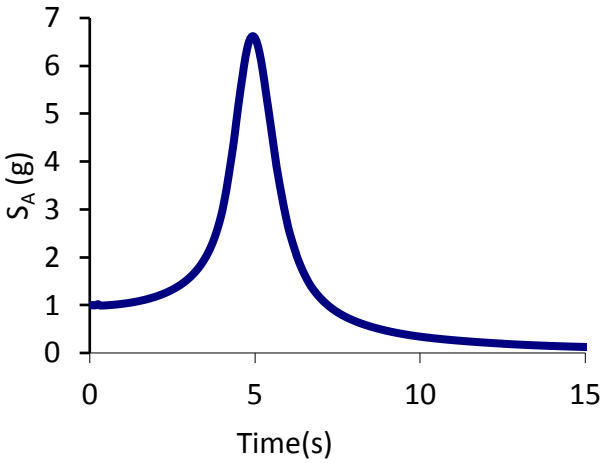

c)

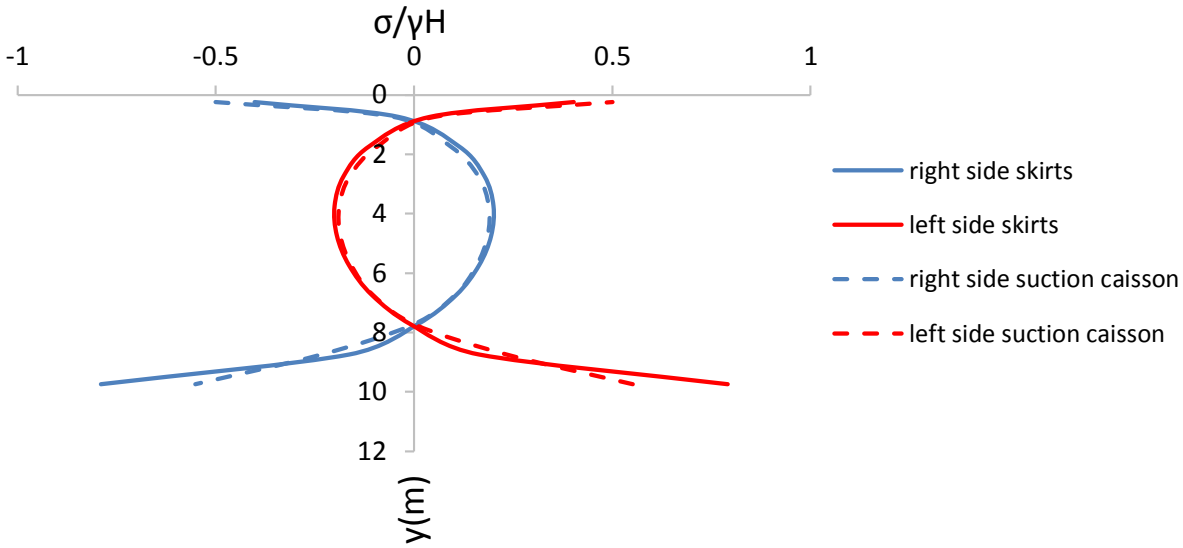

Fig.5.30. a) Acceleration time history of the excitation [*f*=0.2 Hz] b) Response spectrum of the excitation c) Seismic earth pressures (t=50 s)

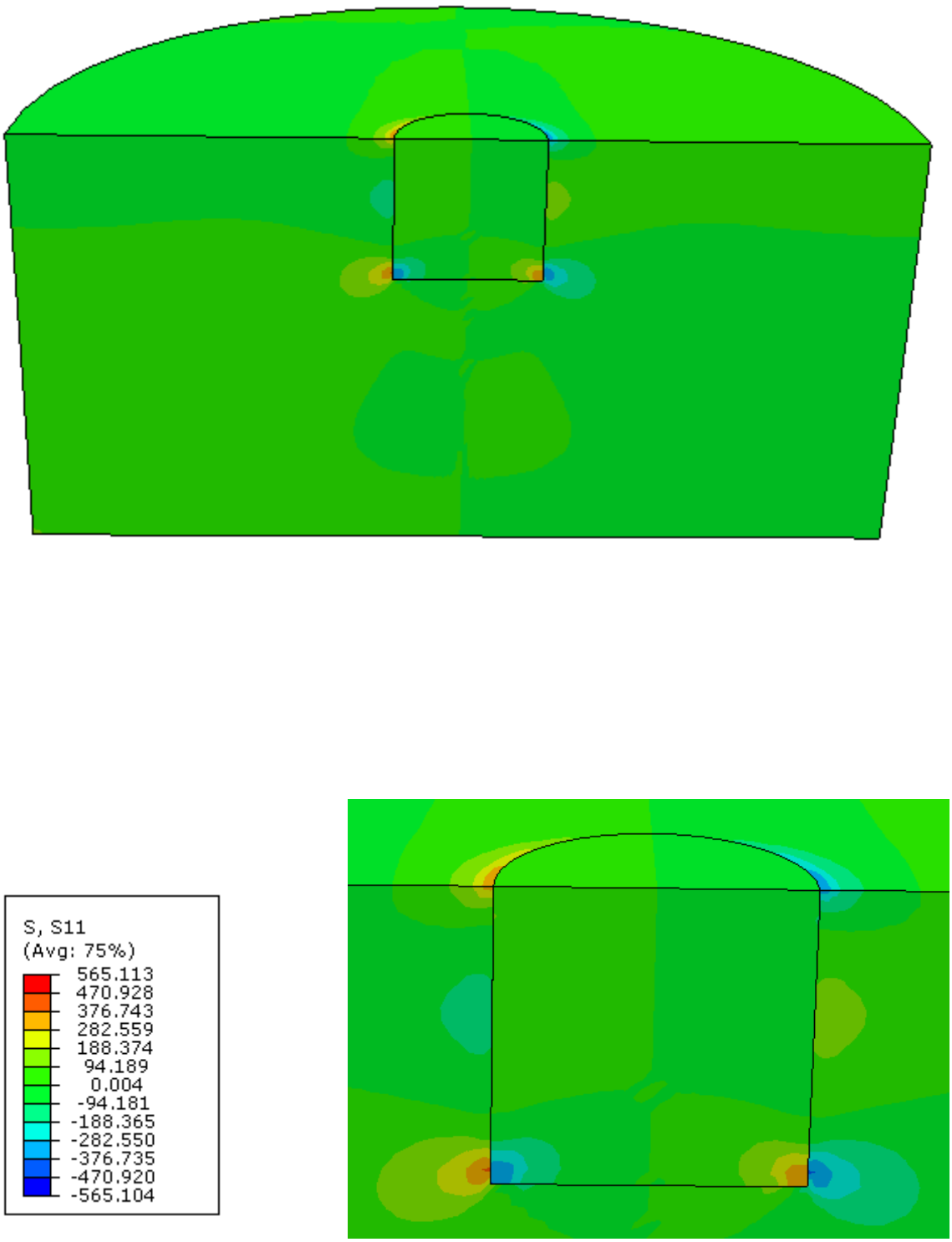

Fig.5.31. Snapshot of the model and contours of normal stresses on the suction caisson for excitation frequency *f*=0.2 Hz [t=50 s]; deformation scale factor: 1

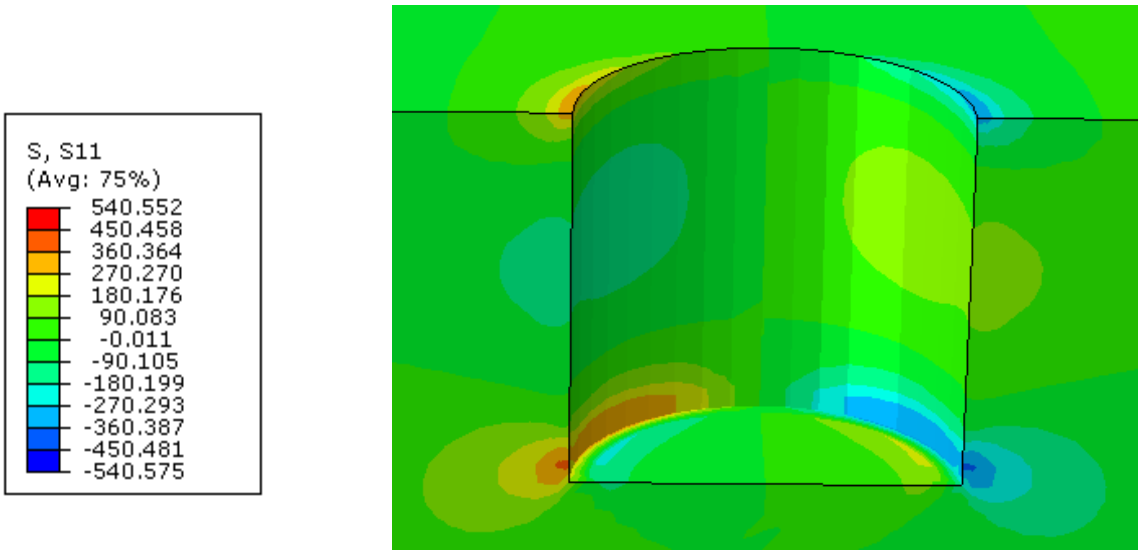

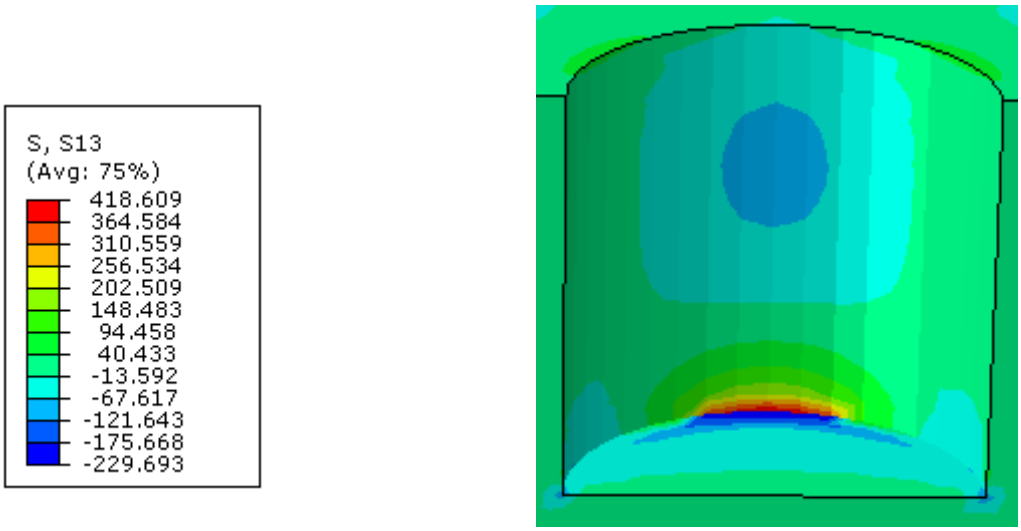

Fig.5.32. External soil alone: Contours of normal (*top*) and shear (*bottom*) stresses on the suction caisson for excitation frequency *f*=0.2 Hz [t=50 s]; deformation scale factor: 1

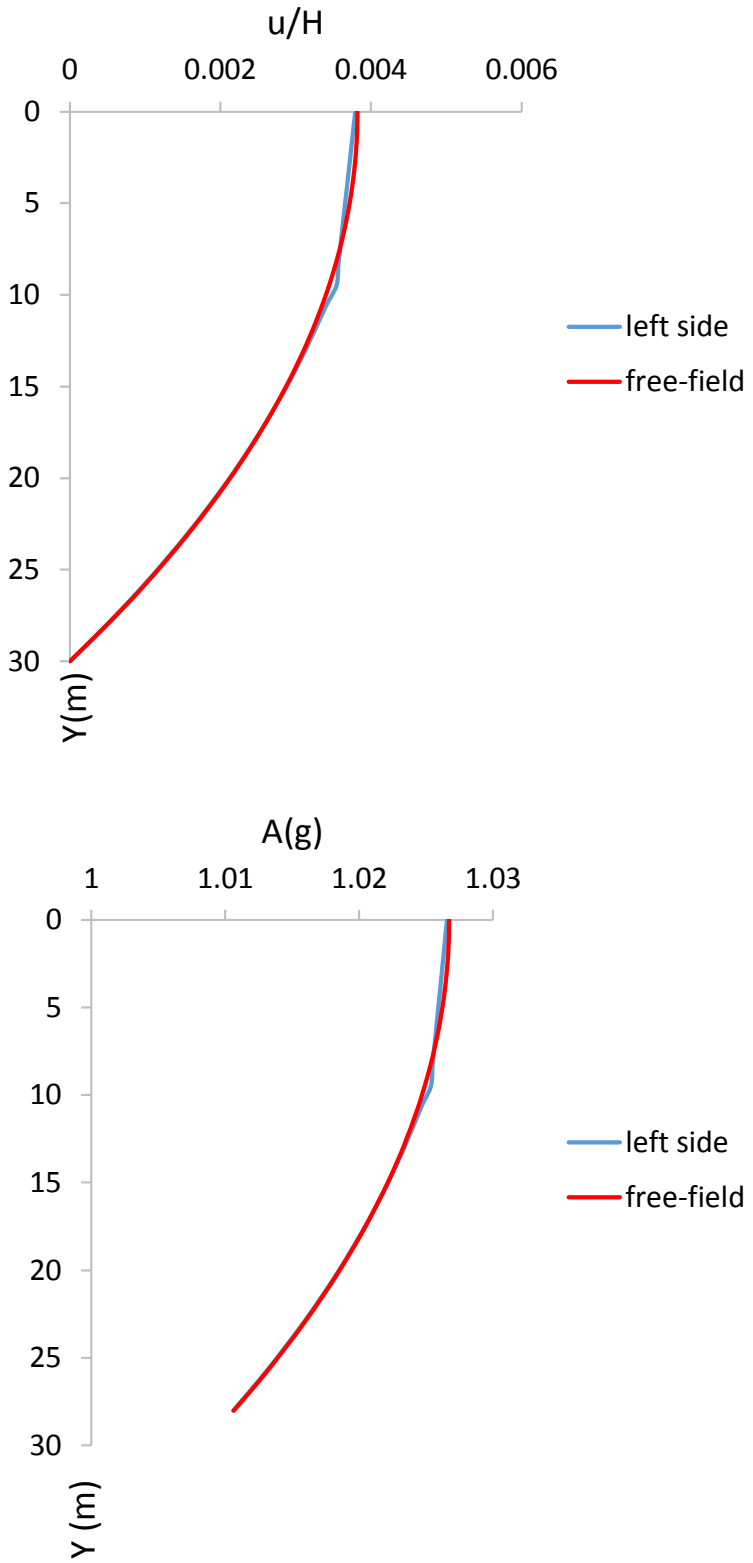

Fig.5.33. Horizontal displacement (*top*) and acceleration (*bottom*) profiles of the free-field and left side for excitation of the suction caisson with *f*=0.2 Hz [t=50s]

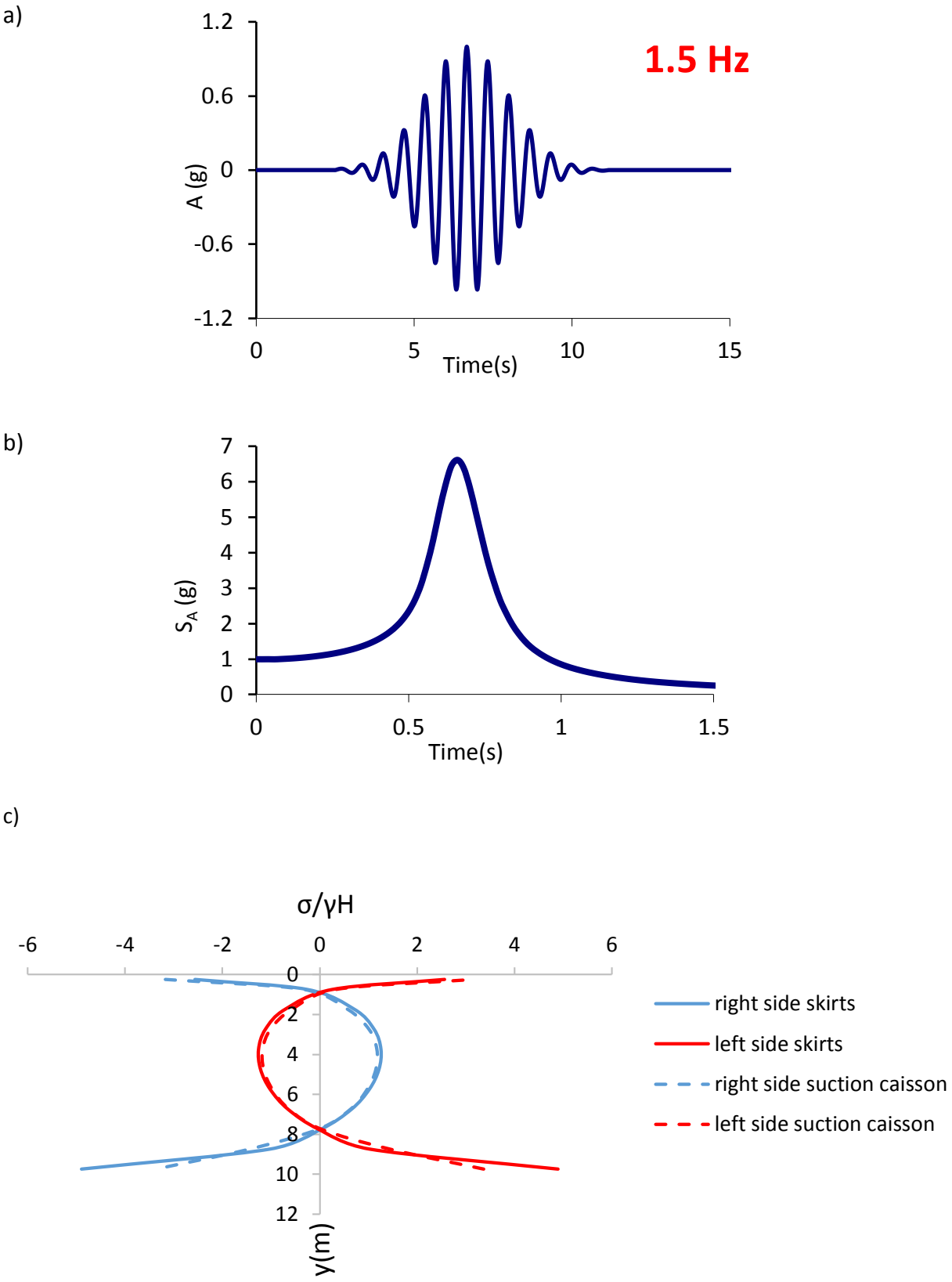

Fig.5.34. a) Acceleration time history of the excitation [*f*=1.5 Hz] b) Response spectrum of the excitation c) Seismic earth pressures (t=7.4 s)

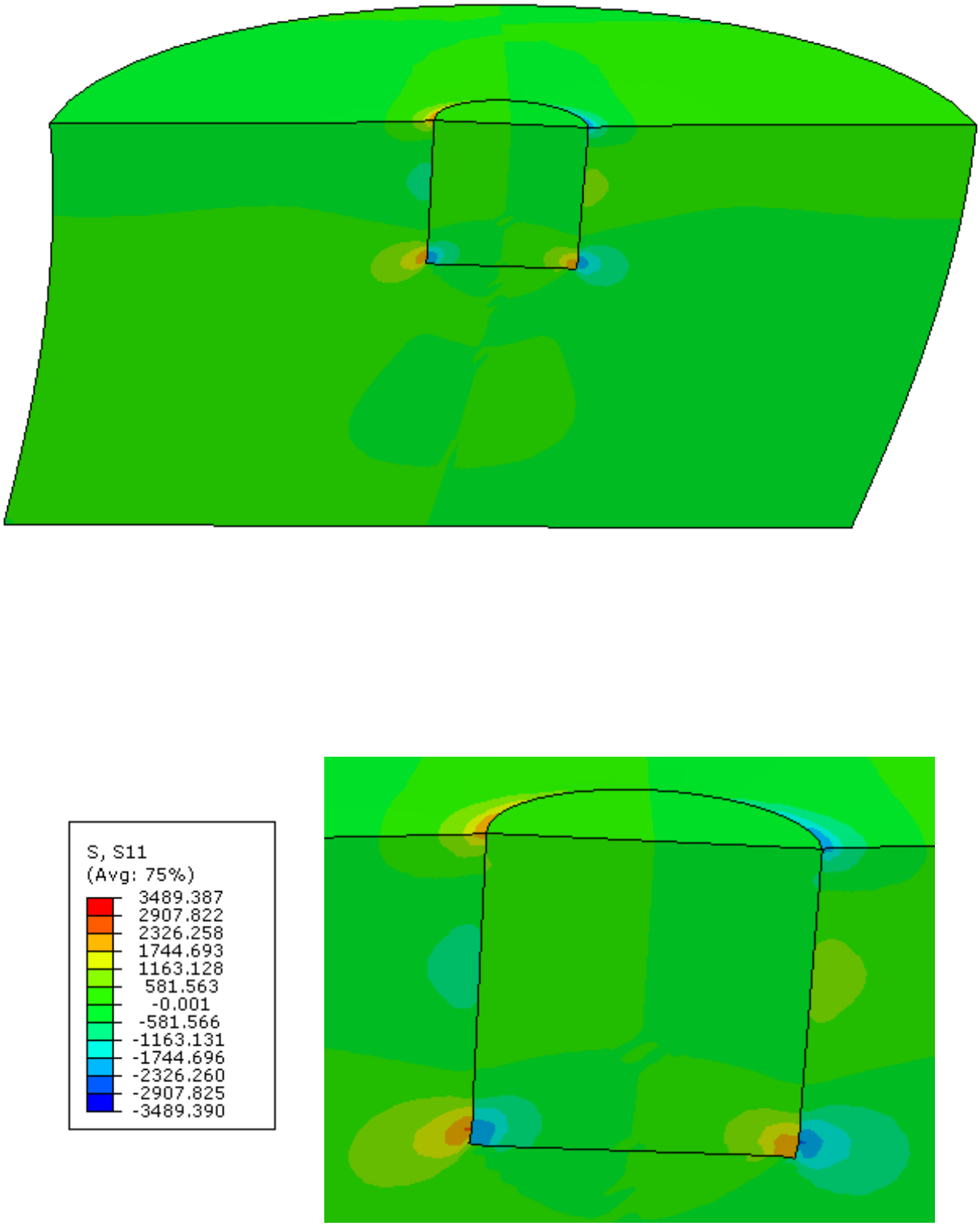

Fig.5.35. Snapshot of the model and contours of normal stresses on the suction caisson for excitation frequency *f*=1.5 Hz [t=7.4 s]; deformation scale factor: 9

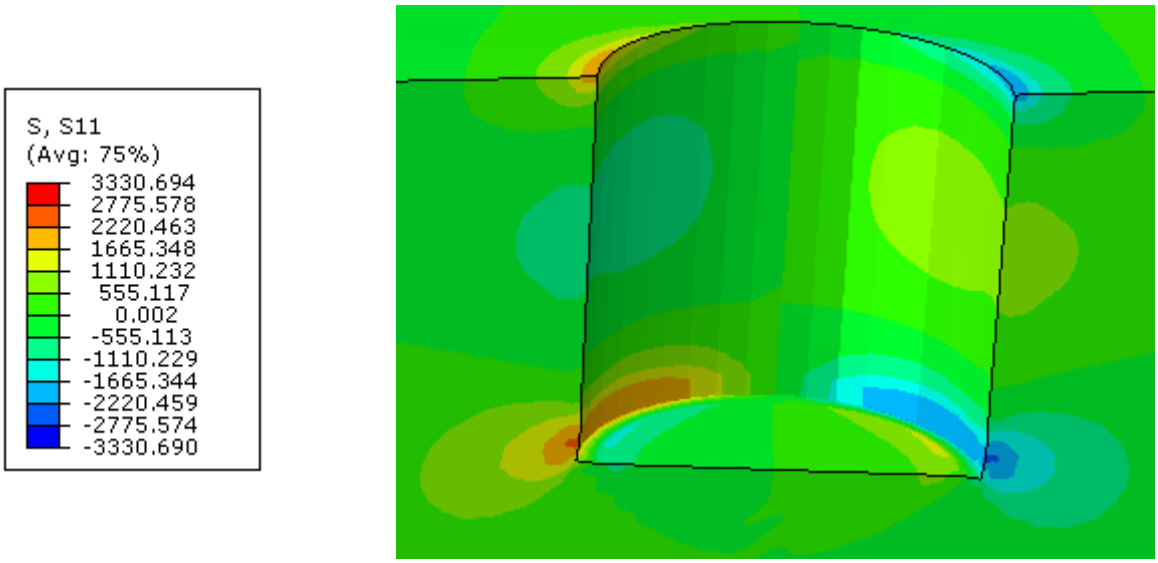

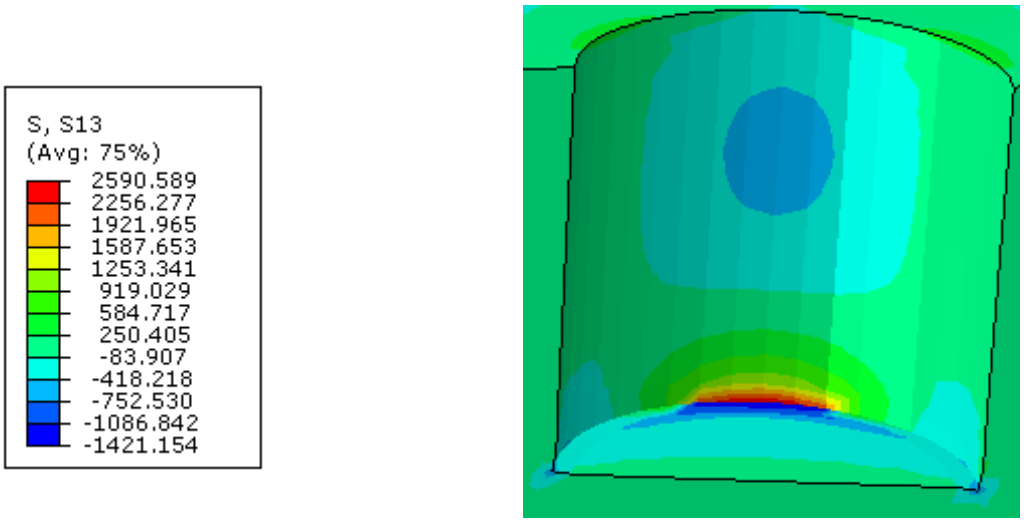

Fig.5.36. External soil alone: Contours of normal (*top*) and shear (*bottom*) stresses on the suction caisson for excitation frequency *f*=1.5 Hz [t=7.4 s]; deformation scale factor: 9

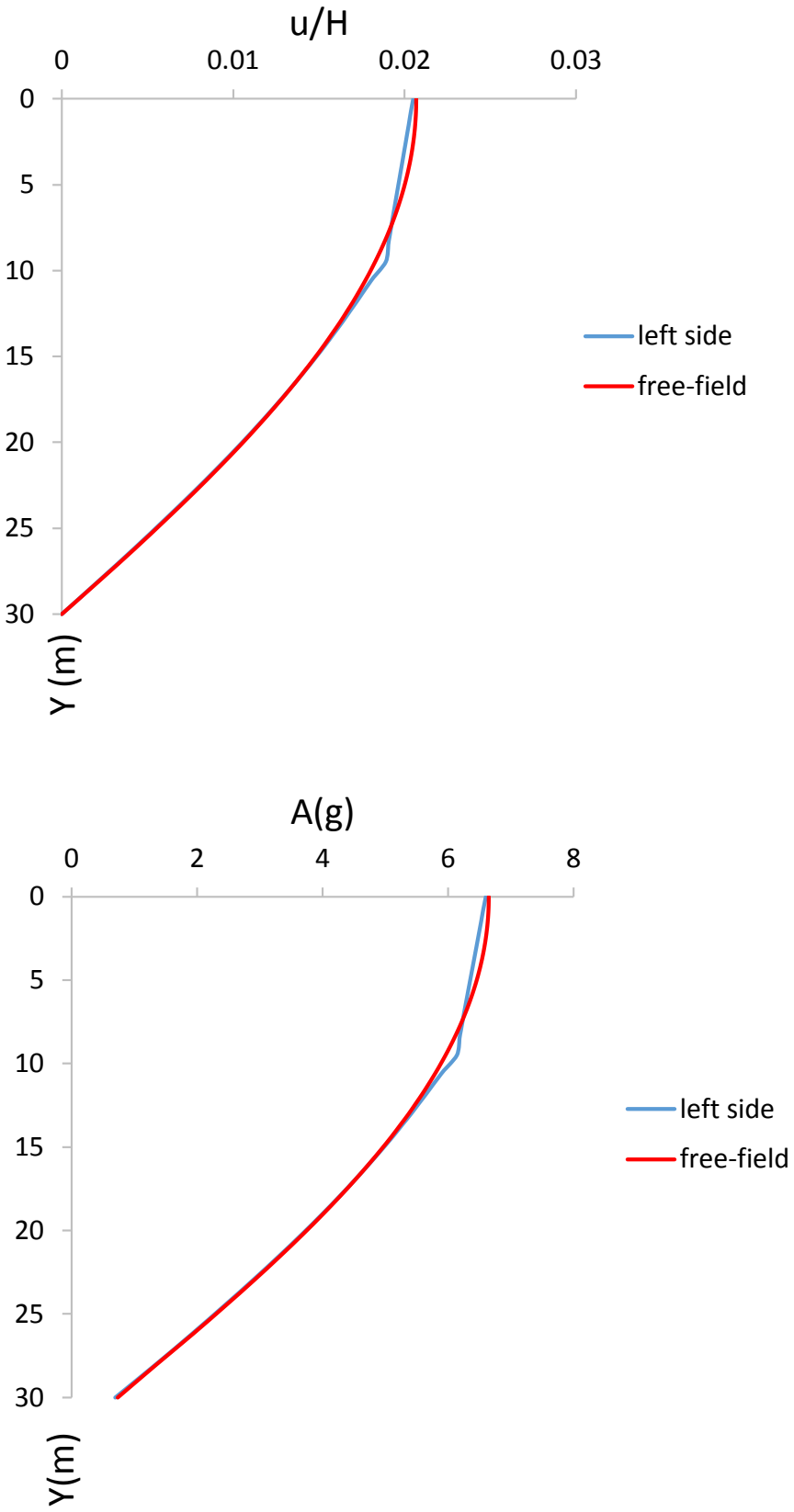

Fig.5.37. Horizontal displacement (*top*) and acceleration (*bottom*) profiles of the free-field and left side for excitation of the suction caisson with *f*=1.5 Hz [t=7.4s]

a)

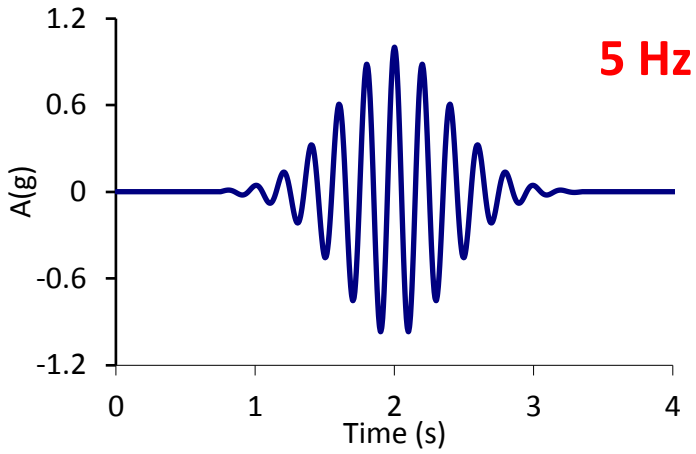

b)

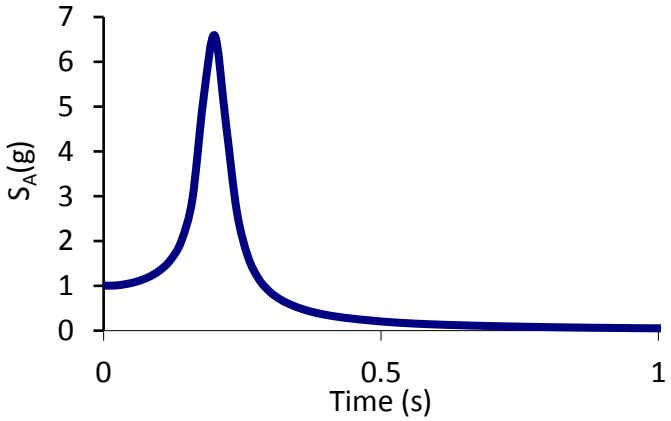

c)

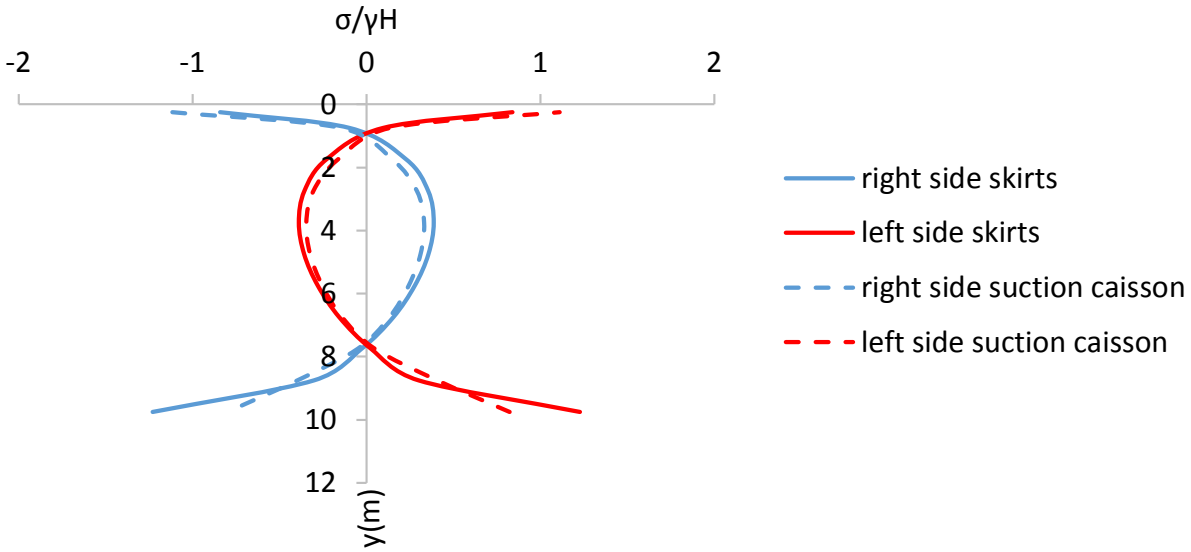

Fig.5.38. a) Acceleration time history of the excitation [*f*=5 Hz] b) Response spectrum of the excitation c) Seismic earth pressures (t=2.35 s)

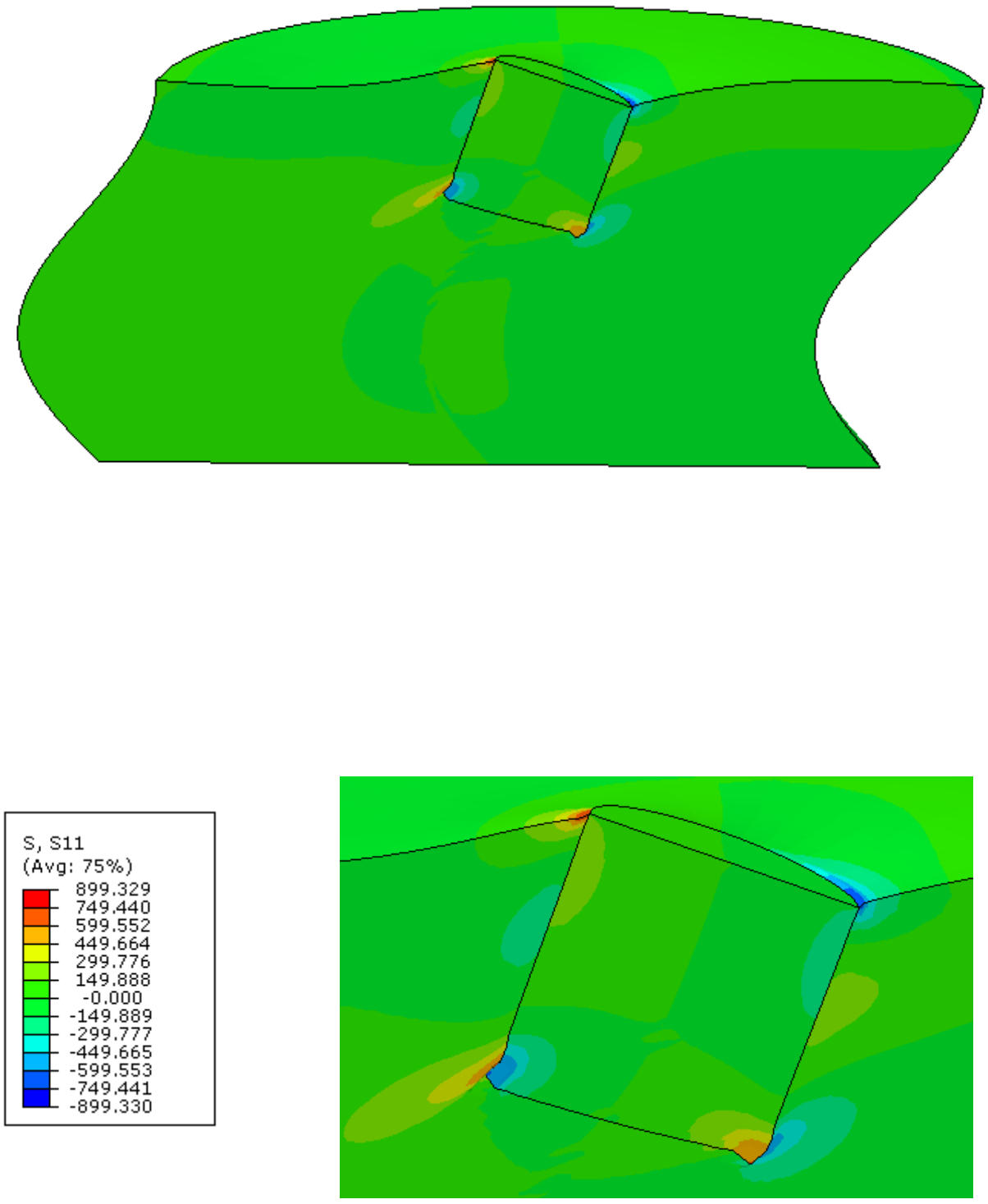

Fig.5.39. Snapshot of the model and contours of normal stresses on the suction caisson for excitation frequency f=5 Hz [t=2.35 s]; deformation scale factor: 200

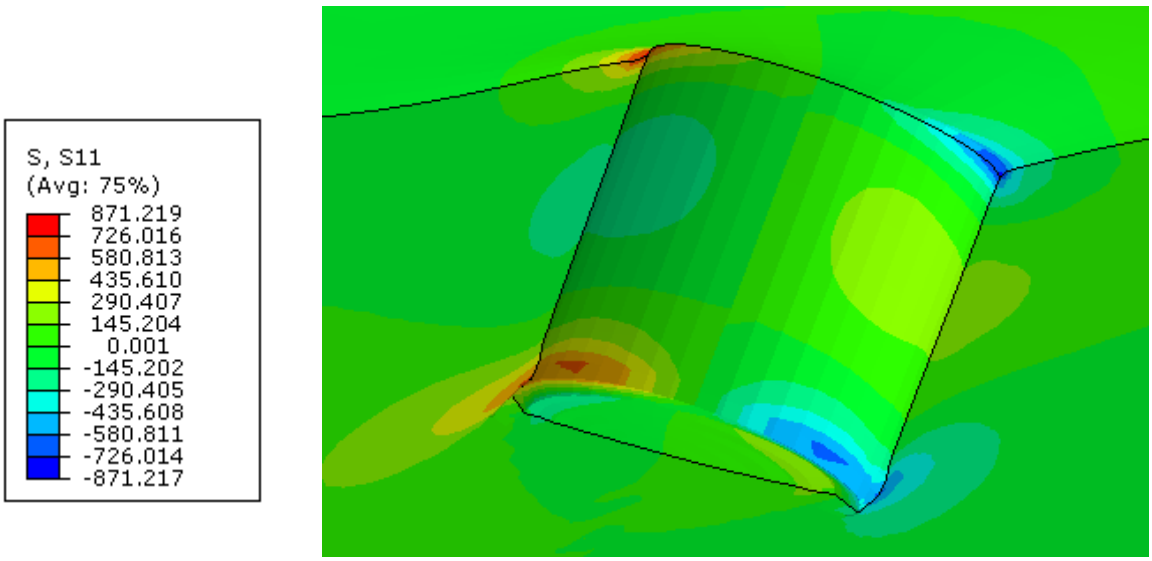

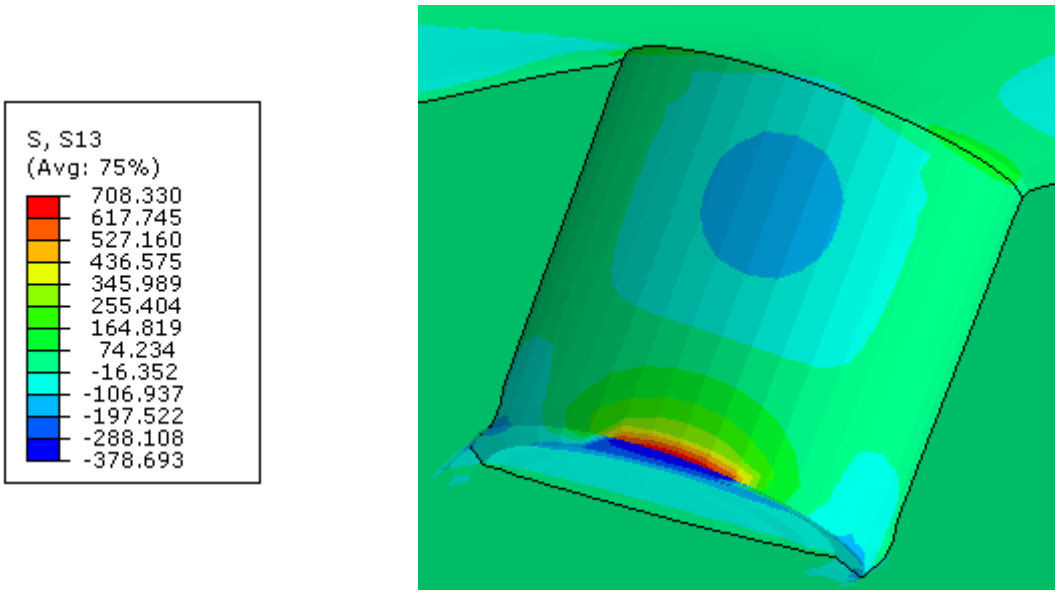

Fig.5.40. External soil alone: Contours of normal (*top*) and shear (*bottom*) stresses on the suction caisson for excitation frequency f=5 Hz [t=2.35s]; deformation scale factor: 200

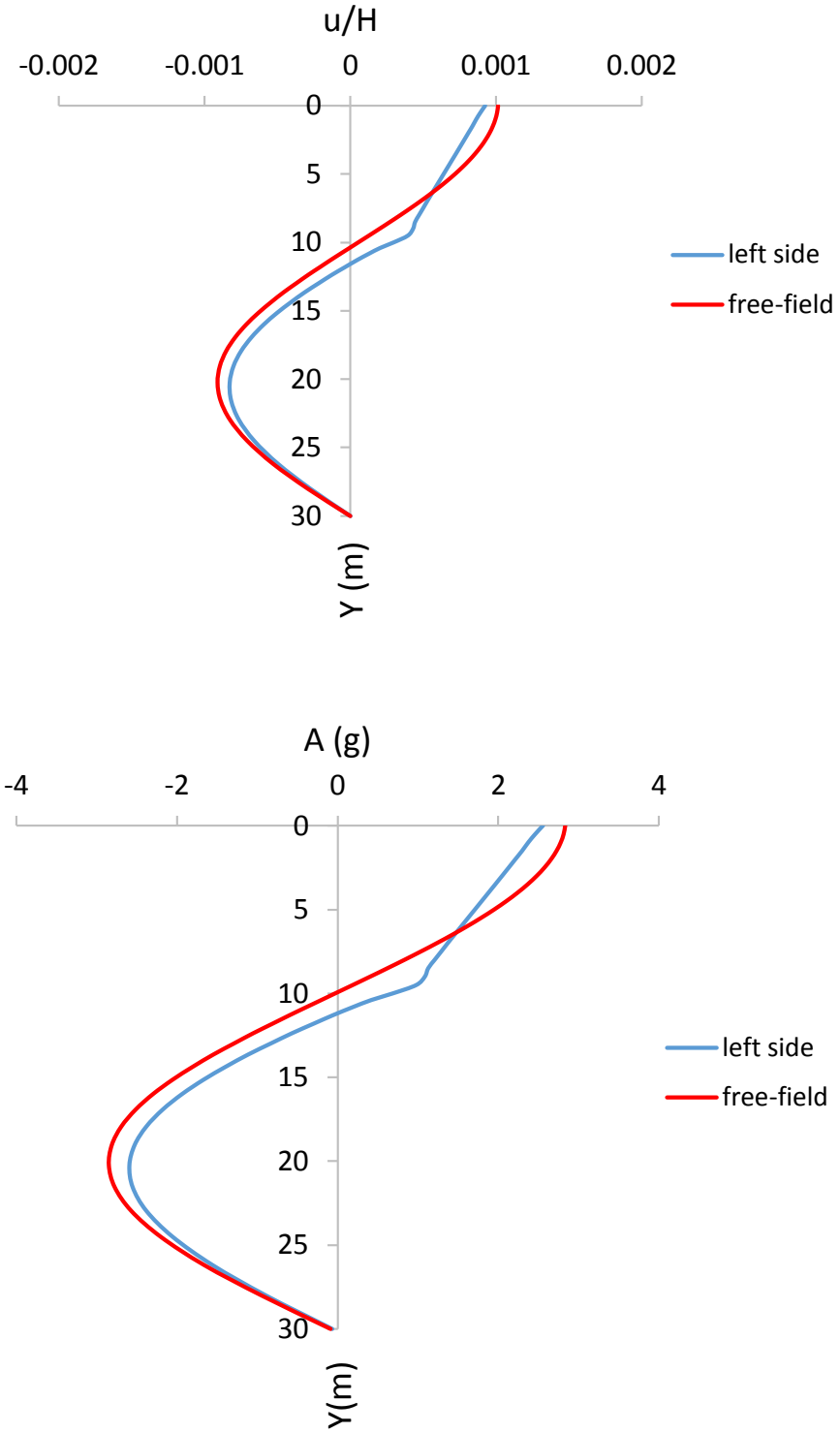

Fig.5.41. Horizontal displacement (*top*) and acceleration (*bottom*) profiles of the free-field and left side for excitation of the suction caisson with *f*=5 Hz [t=2.35 s]

a)

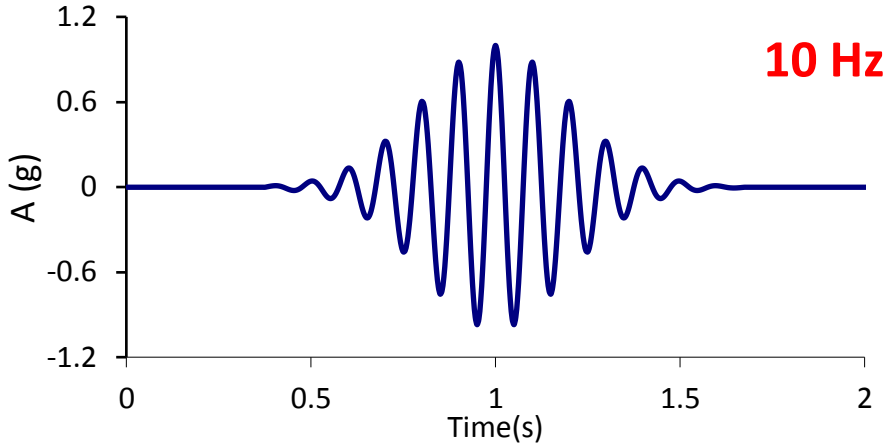

b)

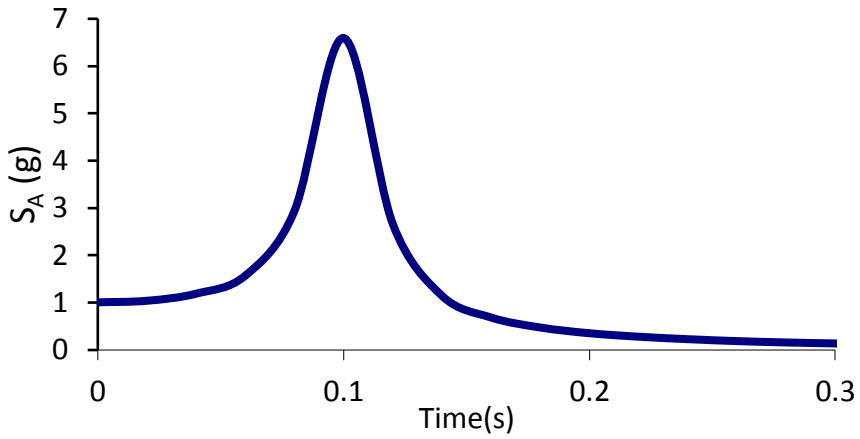

c)

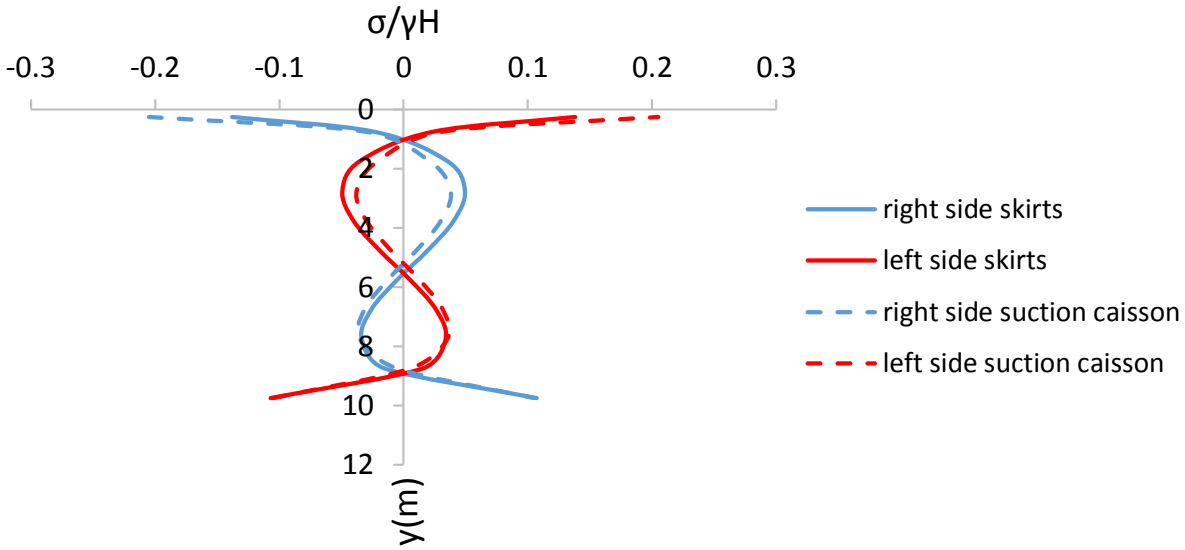

Fig.5.42. a) Acceleration time history of the excitation [*f*=10 Hz] b) Response spectrum of the excitation c) Seismic earth pressures (t=1.155 s)

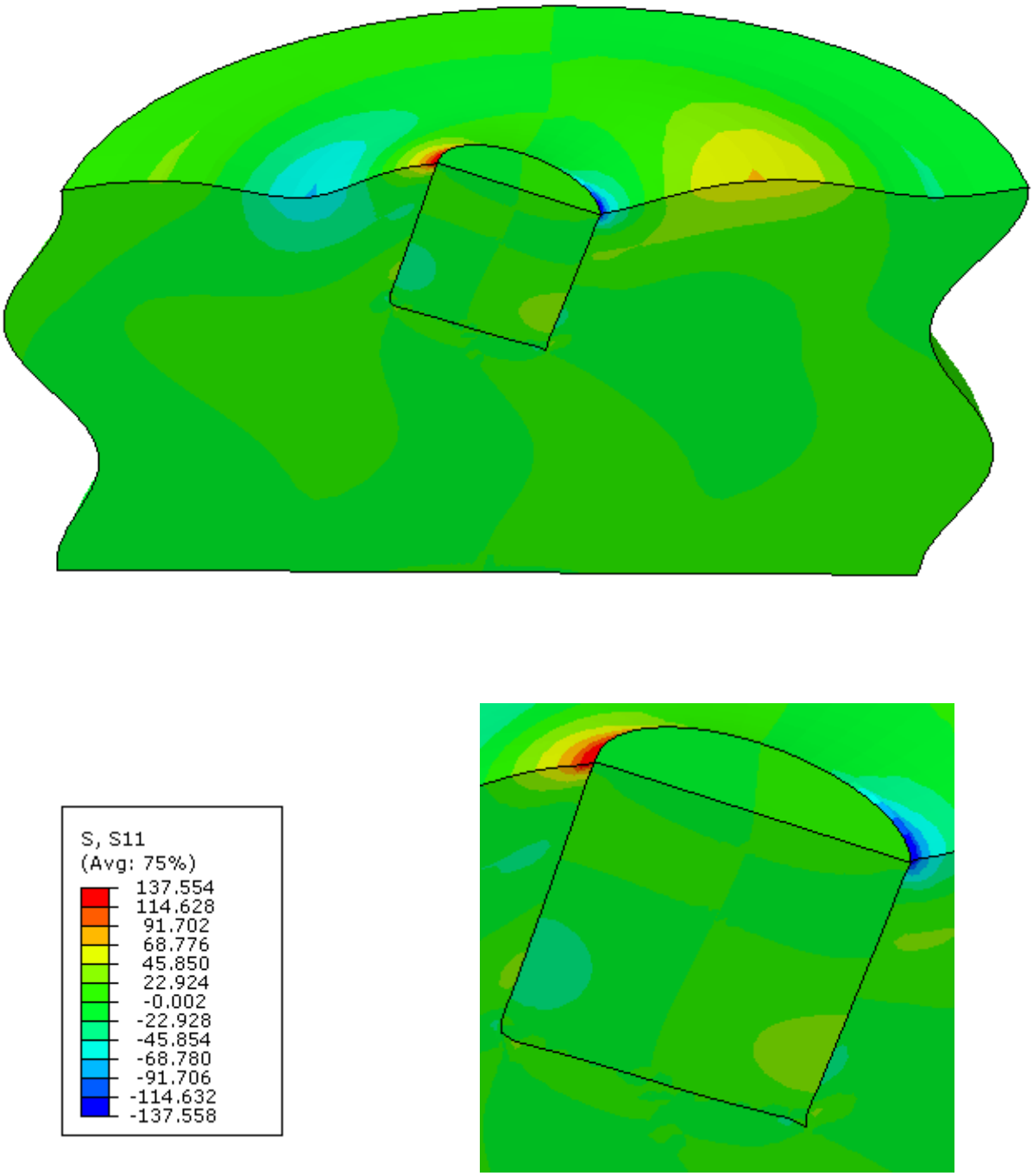

Fig.5.43. Snapshot of the model and contours of normal stresses on the suction caisson for excitation frequency *f*=10 Hz [t=1.155 s]; deformation scale factor: 1000

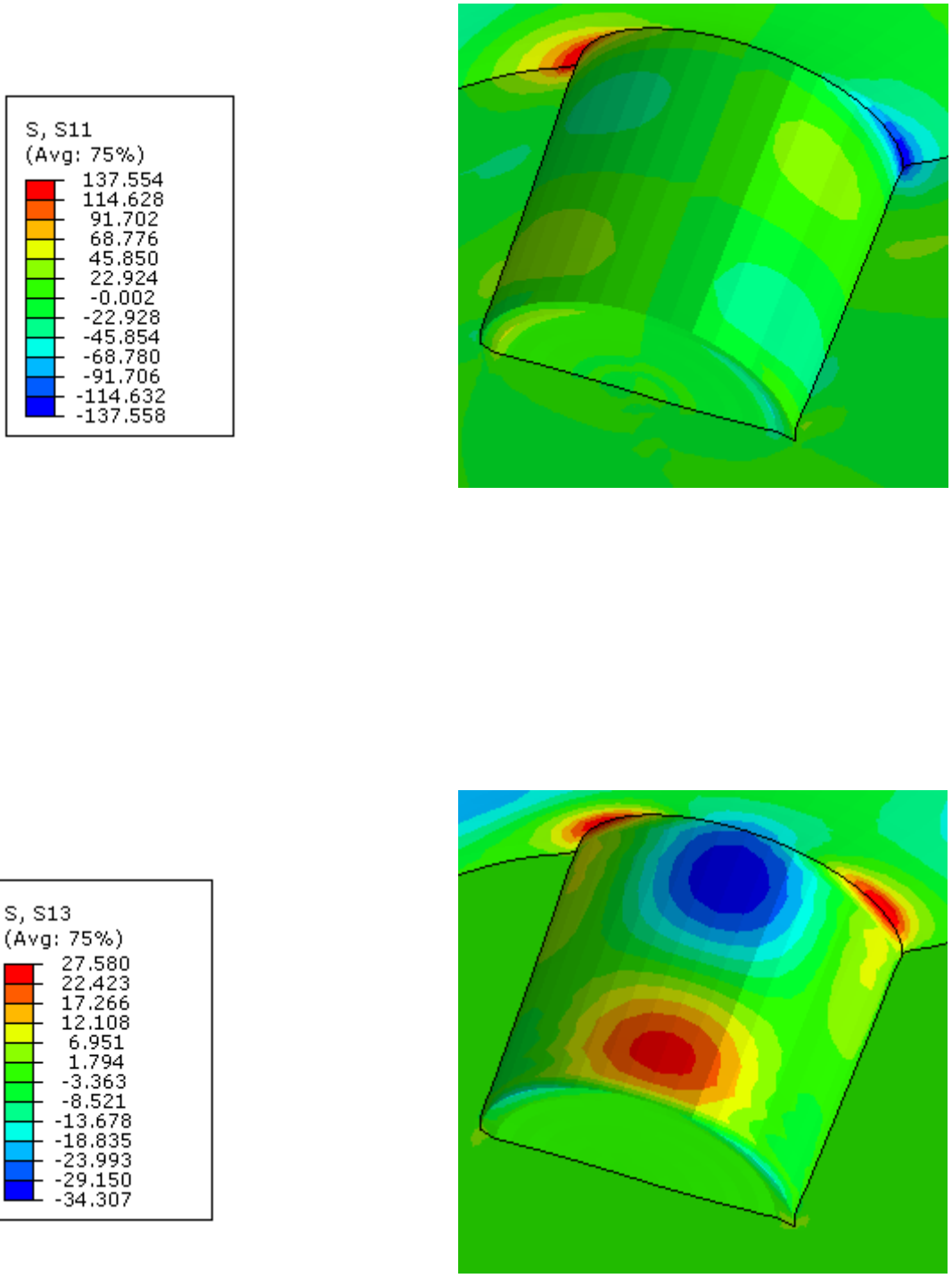

Fig.5.44. External soil alone: Contours of normal (*top*) and shear (*bottom*) stresses on the suction caisson for excitation frequency *f*=10 Hz [t=1.155s]; deformation scale factor: 1000

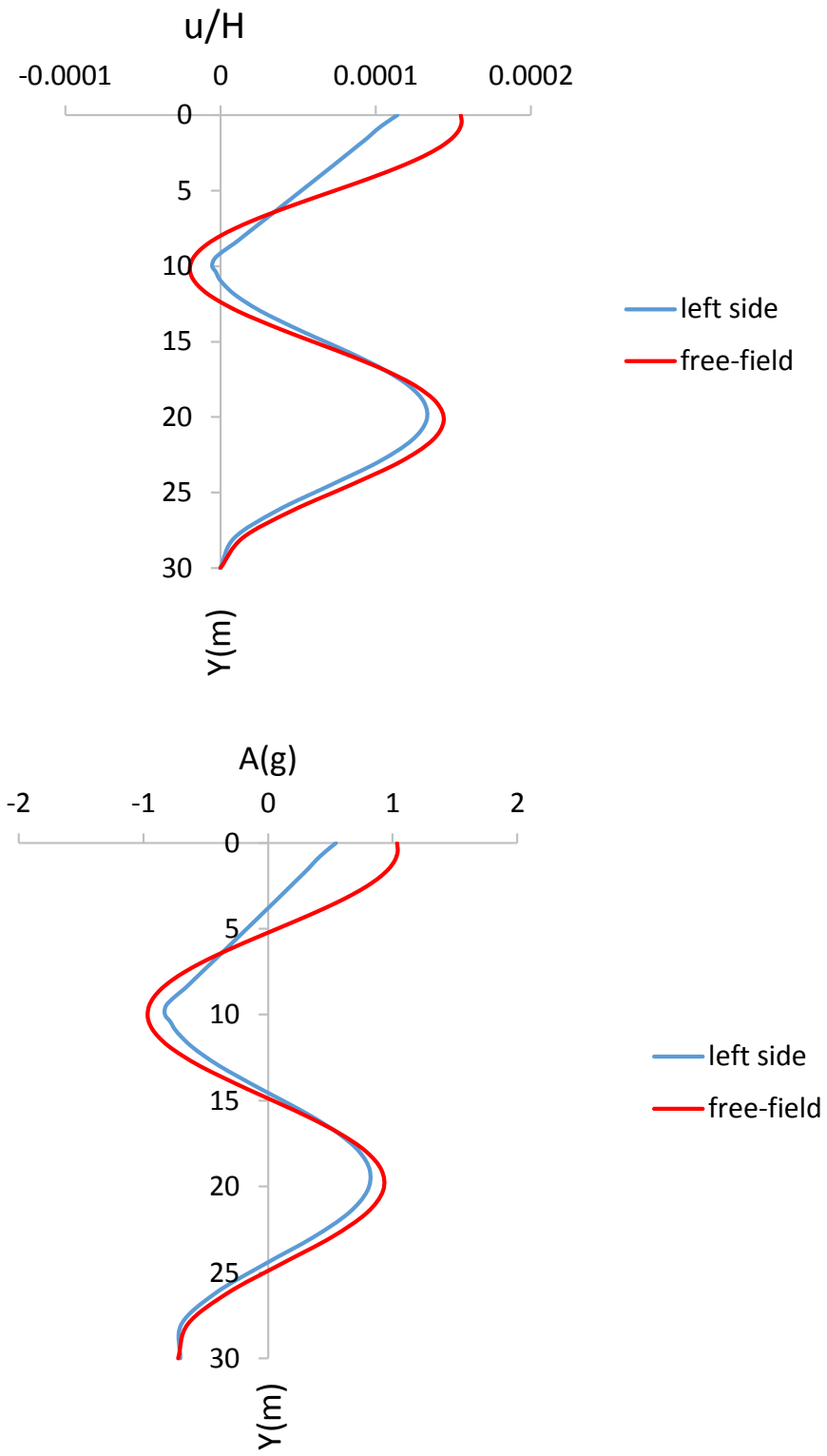

Fig.5.45. Horizontal displacement (*top*) and acceleration (*bottom*) profiles of the free-field and left side for excitation of the suction caisson with *f*=10 Hz [t=1.155 s]

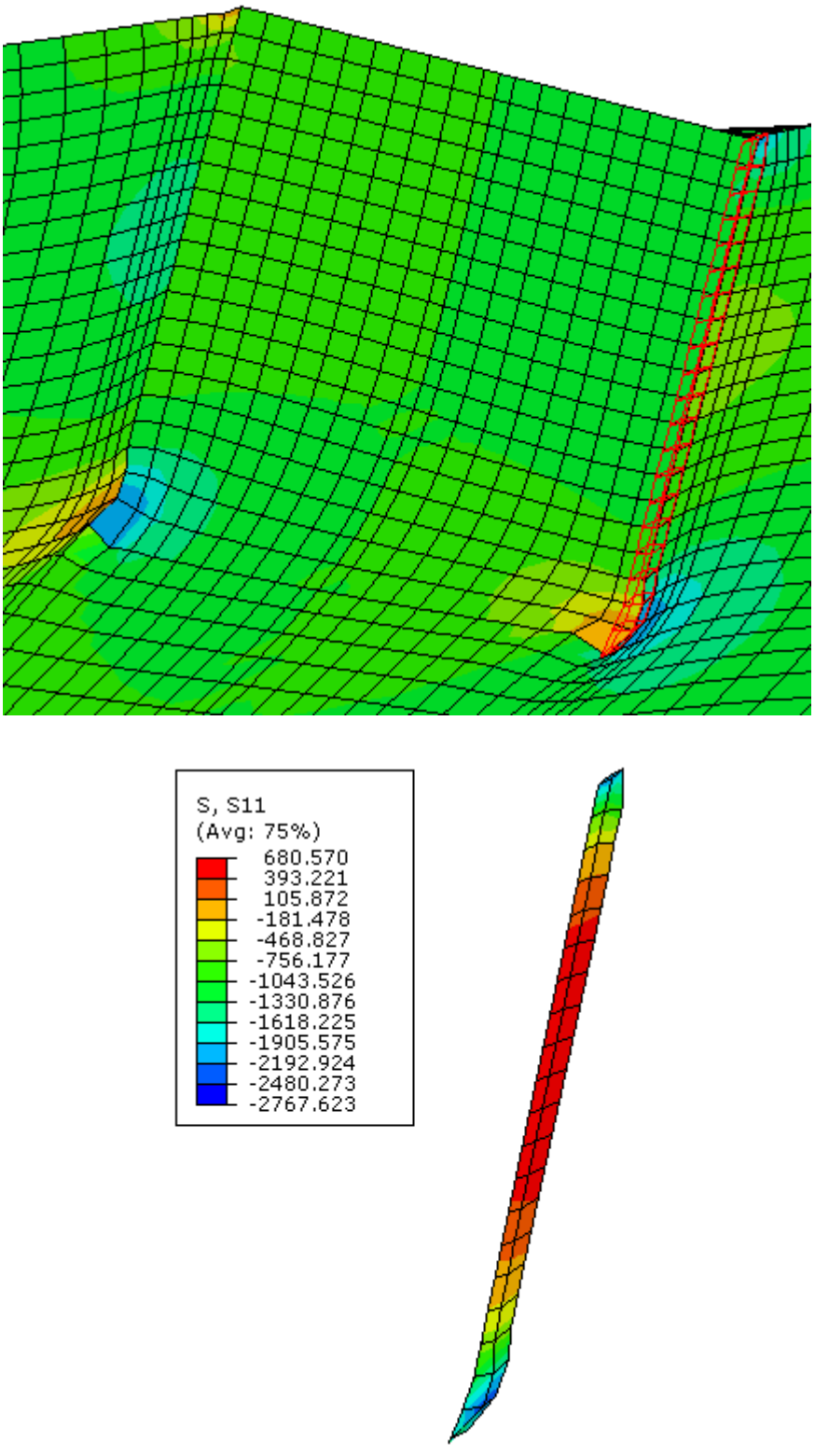

Fig.5.46. Isolation of the right side of external soil in the case of *f*=1.5 Hz excitation at the time of maximum rotation t=7.4 s

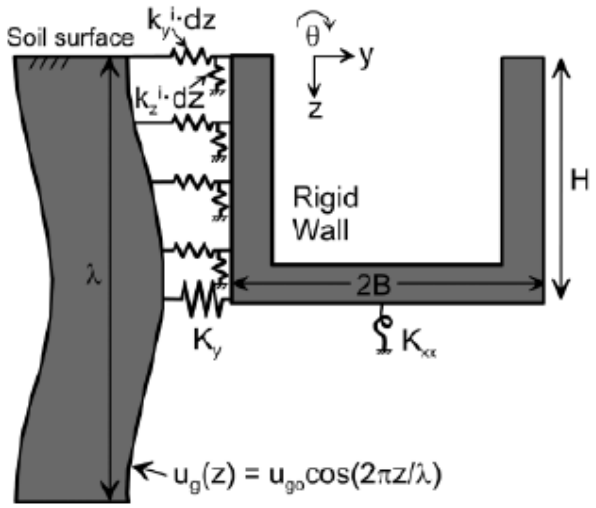

Fig.5.47. Schematic of embedded rigid strip foundation subjected to vertically propagating shear waves, in absence of base slab averaging effects (Brandenberg et al. 2015)

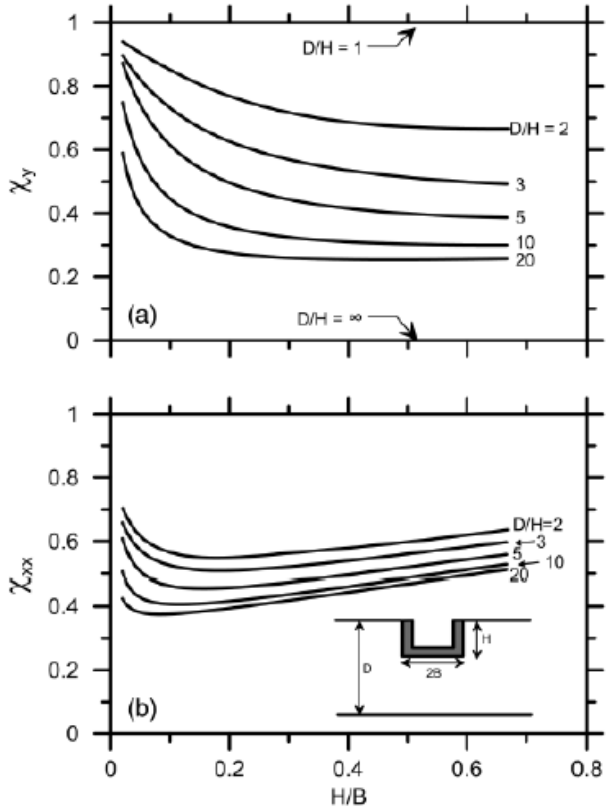

Fig.5.48. Translational and rotational static stiffness interaction factors (Brandenberg et al. 2015)

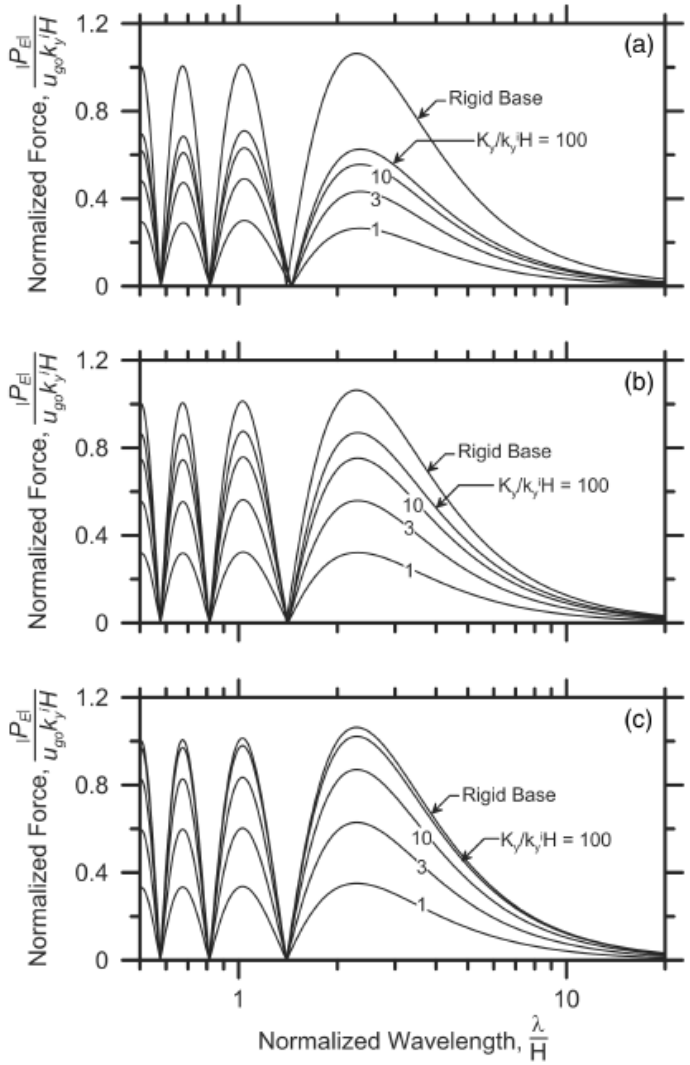

Fig.5.49. Normalized P_E versus normalized wavelength λ/H for various contributions of wall normal stress to translational and rotational stiffness represented as $(K_{xx}+2k^i_zHB^2)$ / $(k^i_y H^2/3)$ = (a) 3; (b) 10; (c) 100 (Brandenberg et al. 2015)

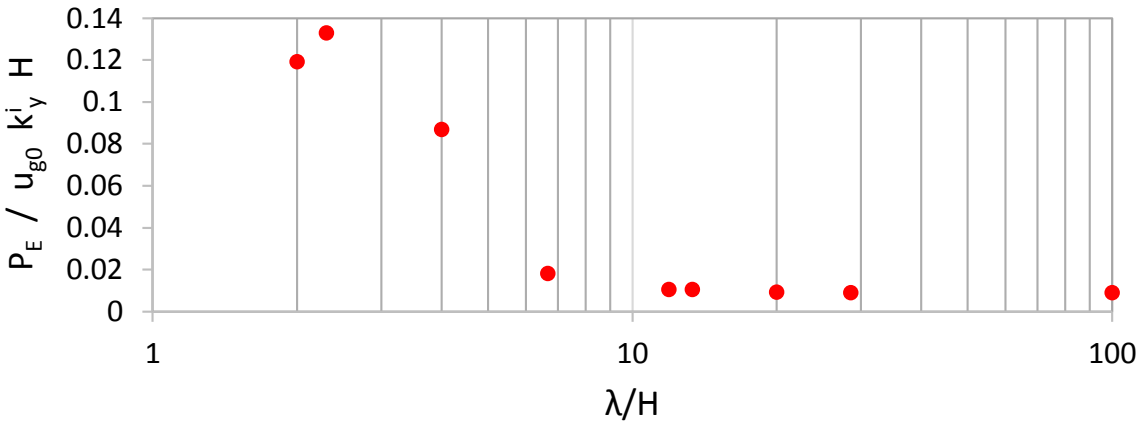

Fig.5.50. Normalized dynamic force P_E on suction caisson versus normalized wavelength λ/H

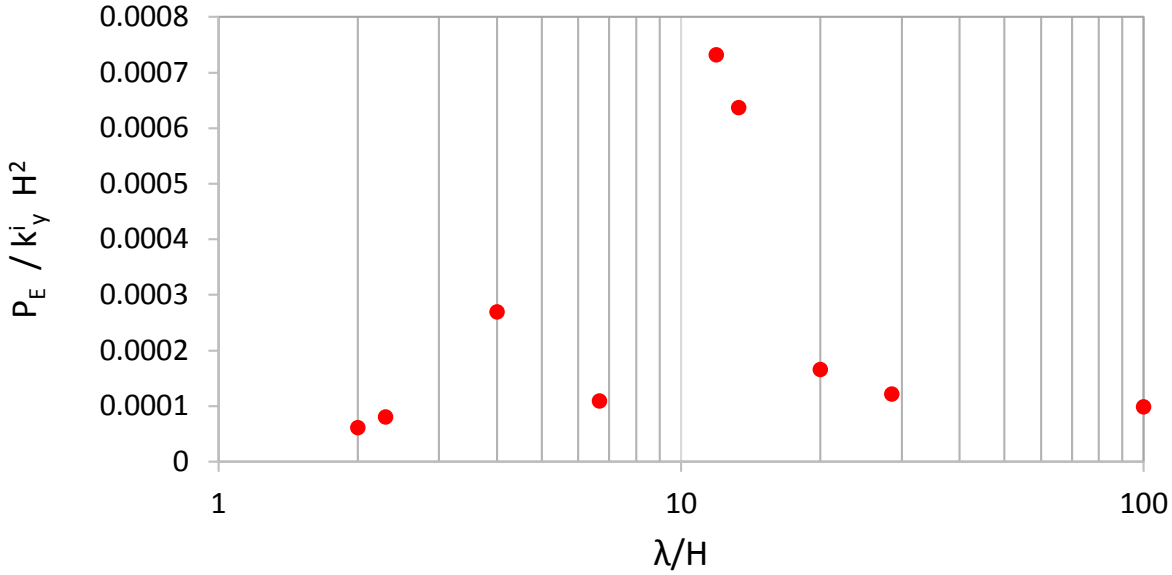

Fig.5.51. Normalized dynamic force P_E on suction caisson versus normalized wavelength λ/H

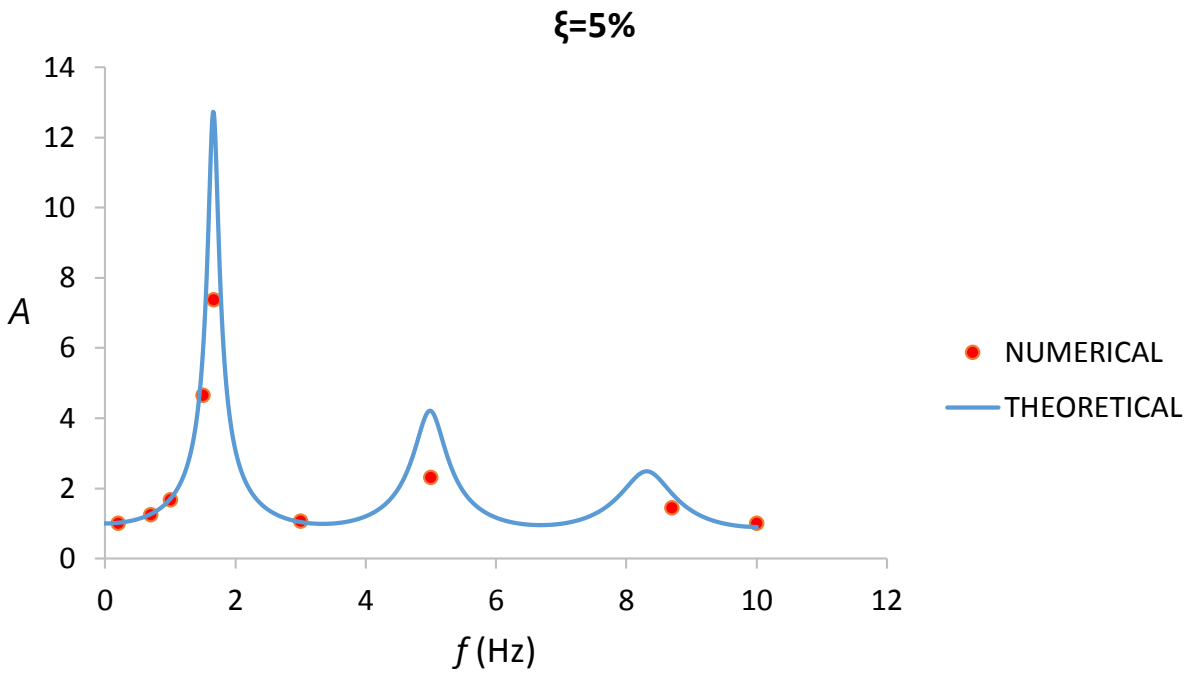

Fig.5.52. Amplification as a function of frequency derived numerically and theoretically

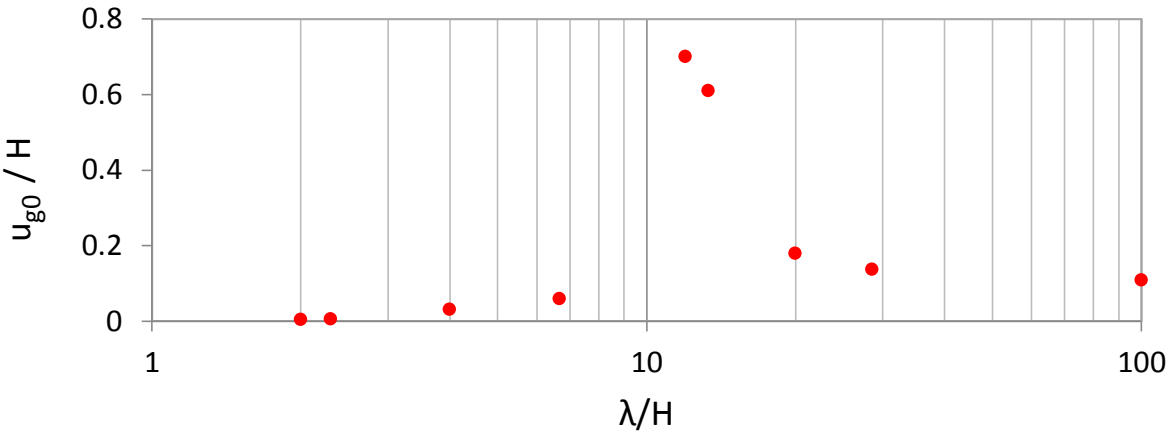

Fig.5.53. Normalized free-field displacement u_{g0} by sidewall height H as a function of λ/H

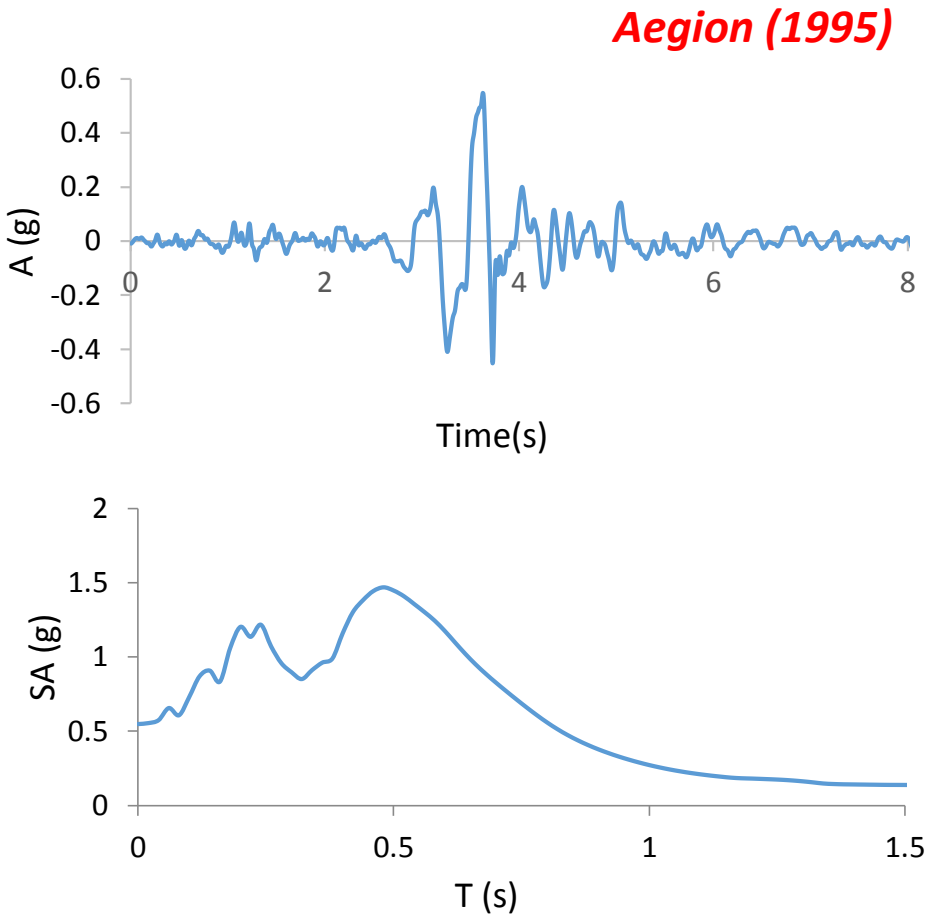

Fig.5.54. Acceleration time history (*top*) and elastic response spectrum (*bottom*) of the Aegion Earthquake Motion

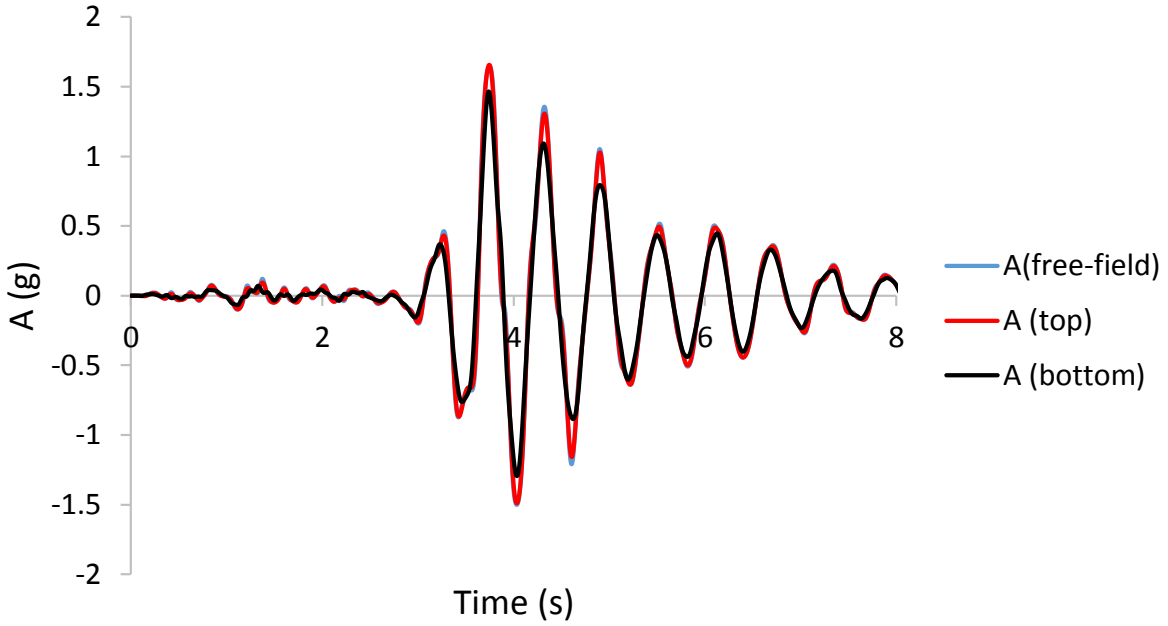

Fig.5.55. Acceleration time histories of the top and bottom edge of the suction caisson and of the free-field, for the Aegion Earthquake Motion as excitation

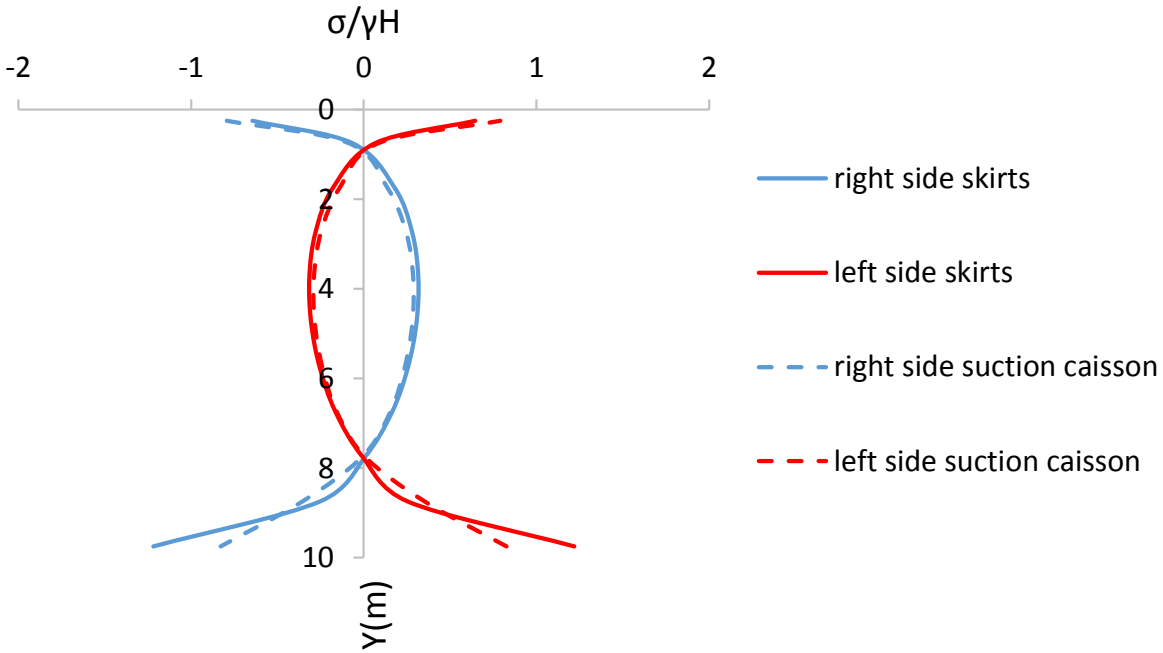

Fig.5.56. Seismic earth pressures for the Aegion earthquake motion as excitation at t=3.75 s, time of maximum acceleration of the top edge

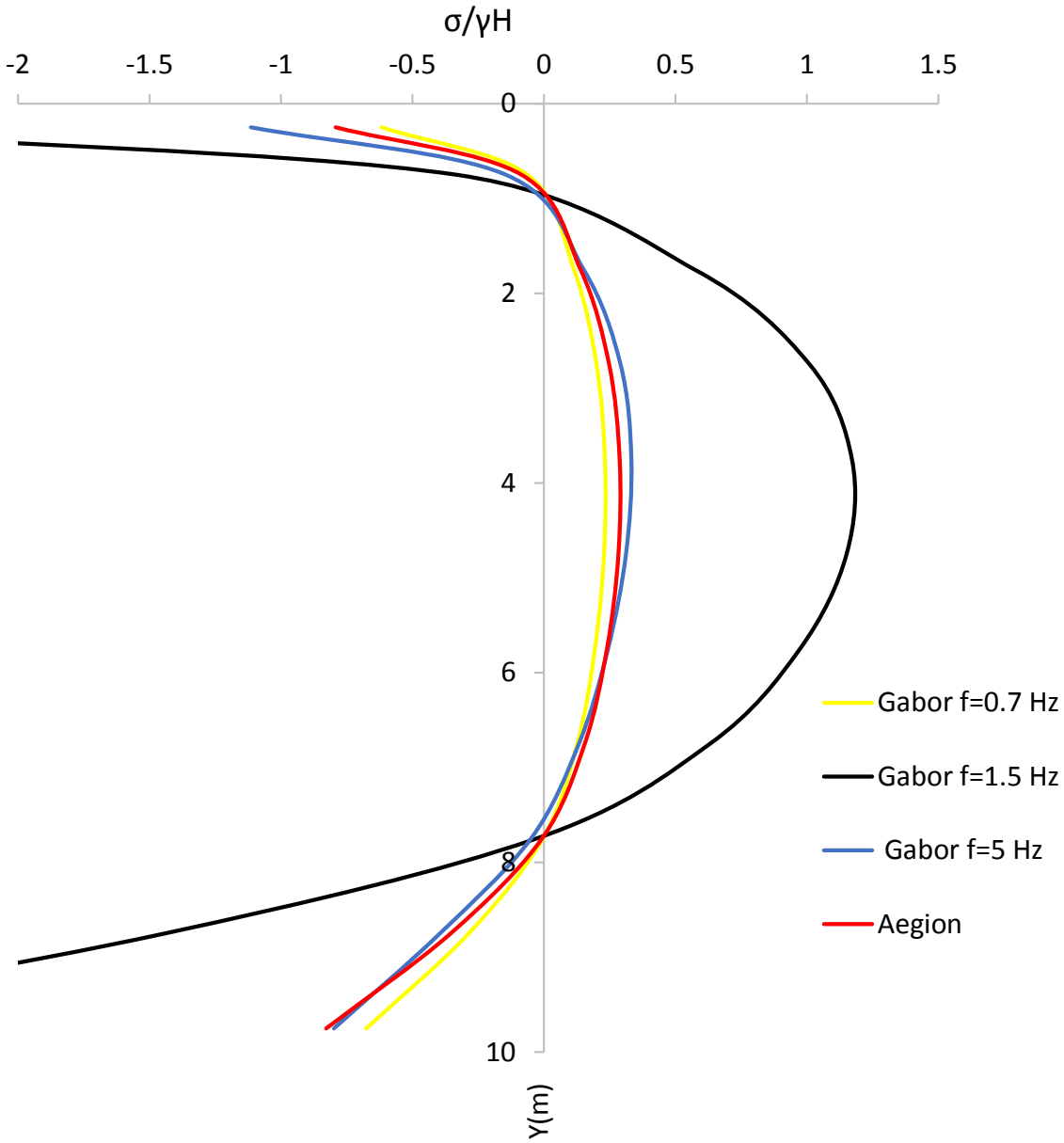

Fig.5.57. Comparison of seismic earth pressures for the Aegion earthquake motion with results from Gabor type pulses as excitation

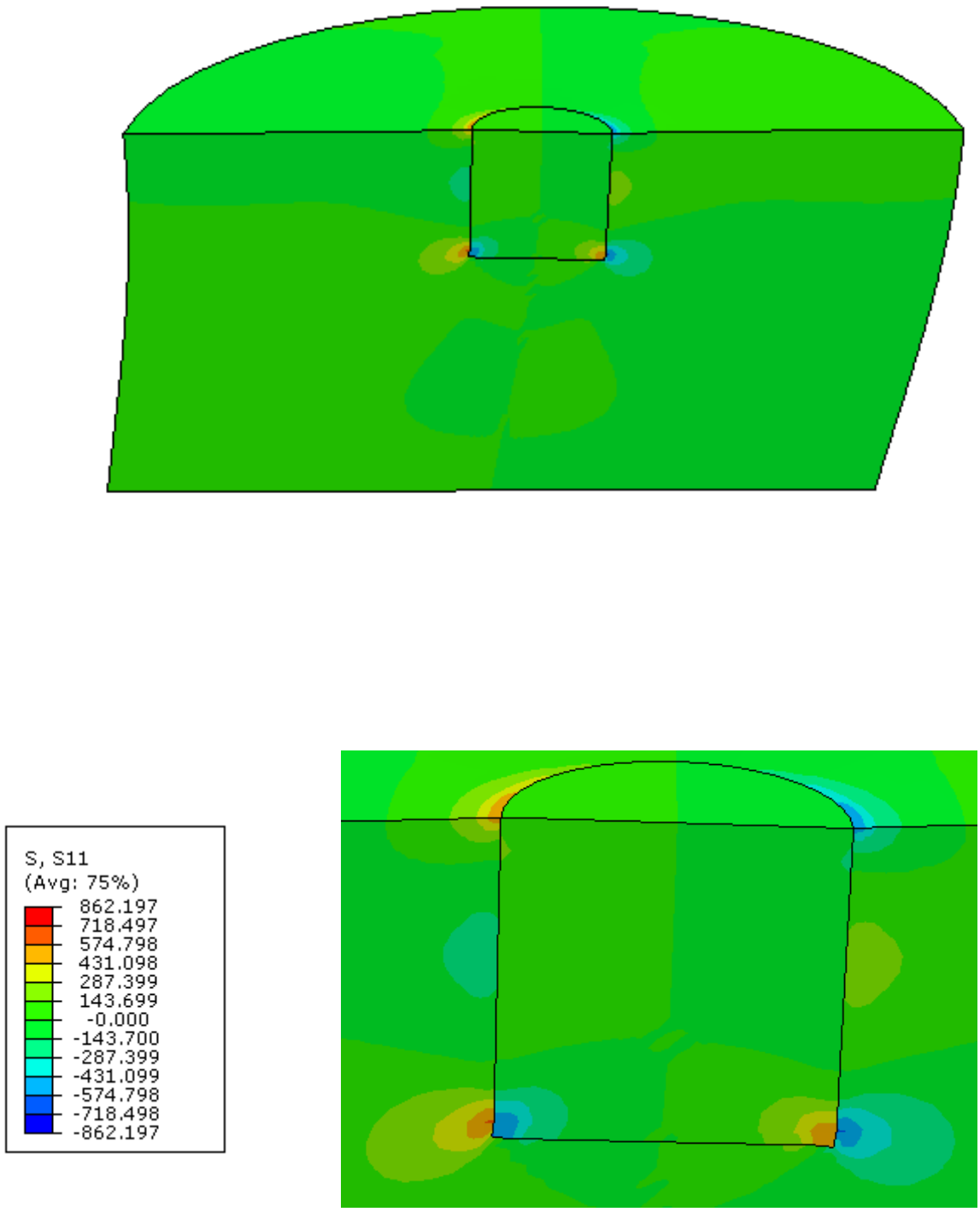

Fig.5.58. Snapshot of the model and contours of normal stresses on the suction caisson for Aegion earthquake motion as excitation [t=3.75 s]; deformation scale factor: 30

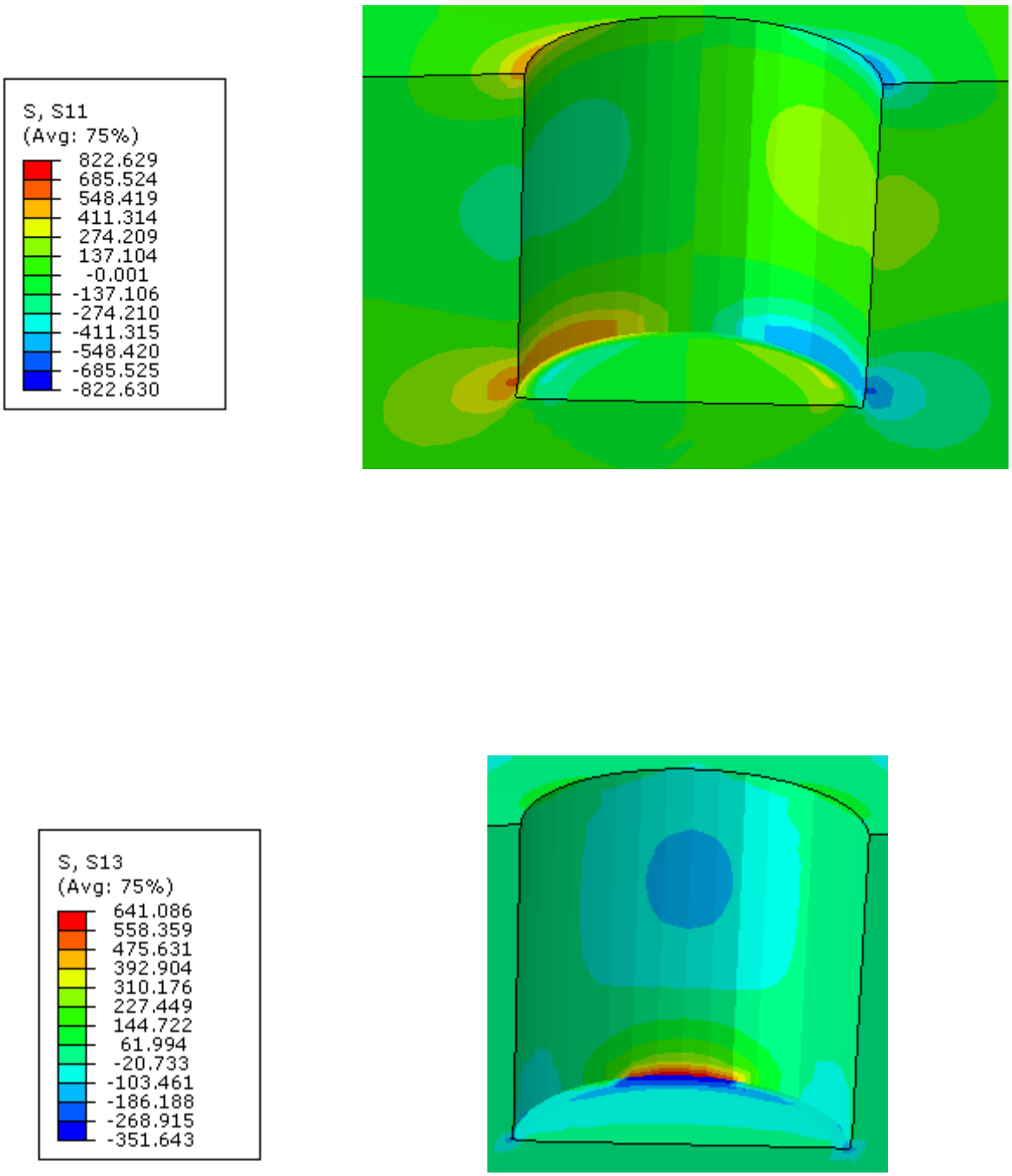

Fig.5.59. External soil alone: Contours of normal (*top*) and shear (*bottom*) stresses on the suction caisson for Aegion earthquake motion as excitation [t=3.75 s]; deformation scale factor: 30

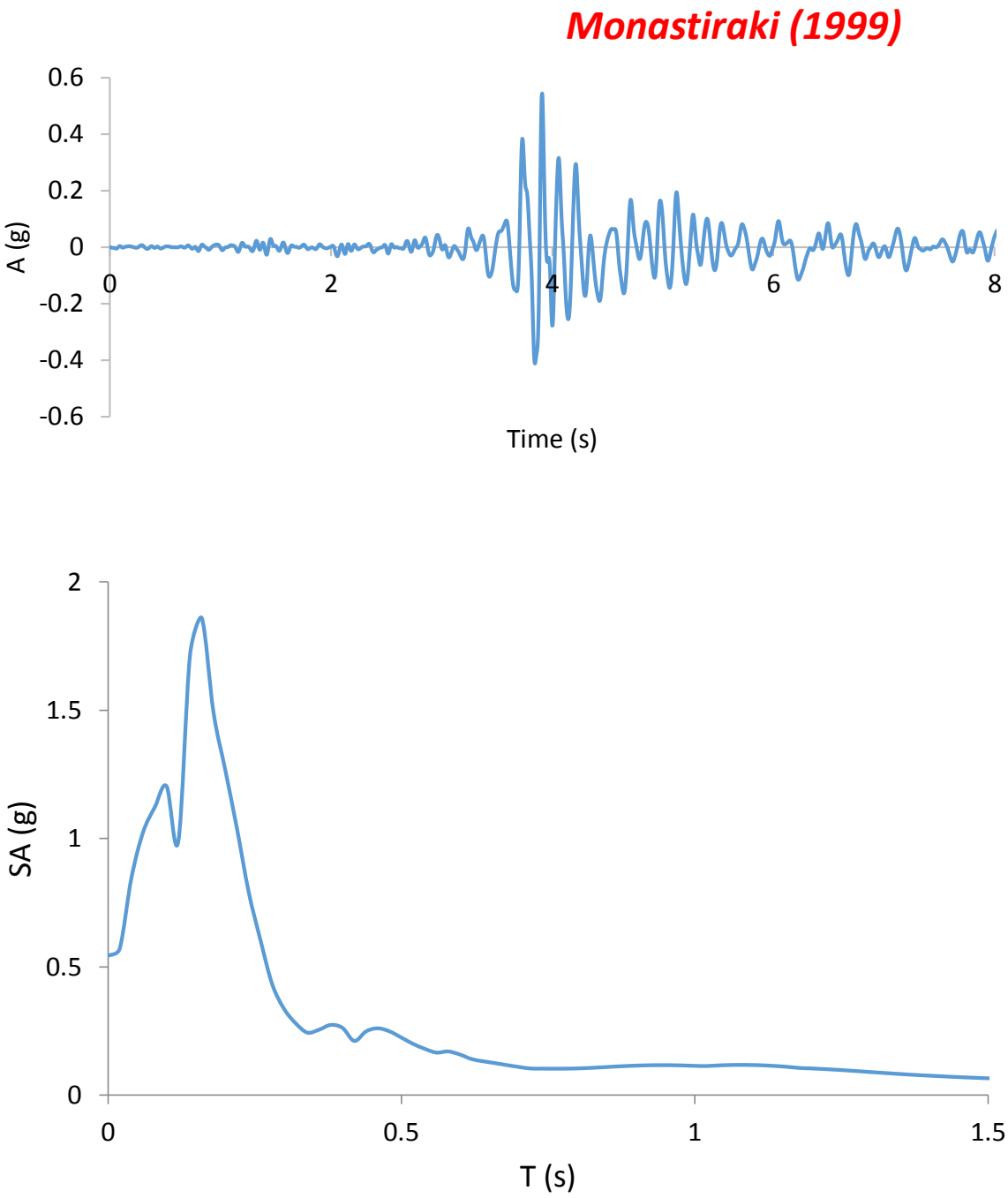

Fig.5.60. Acceleration time history (*top*) and response spectrum (*bottom*) of the Monastiraki Earthquake Motion

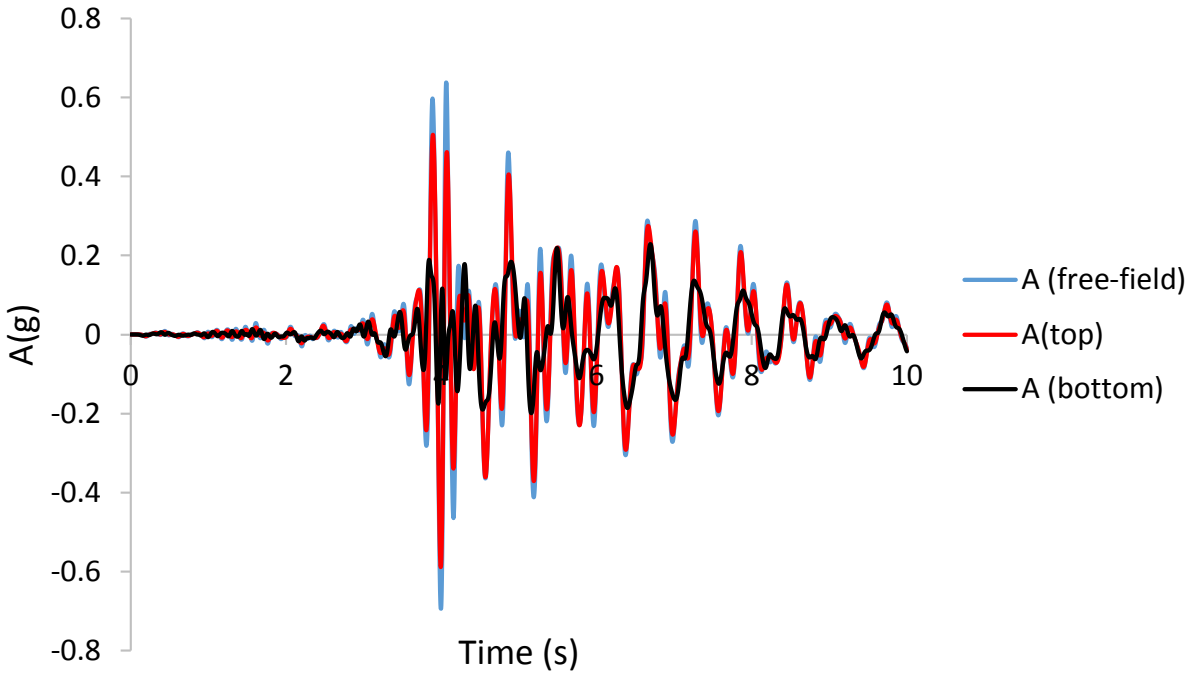

Fig.5.61. Acceleration time histories of the top and bottom edge of the suction caisson and of the free-field, for the Monastiraki earthquake motion as excitation

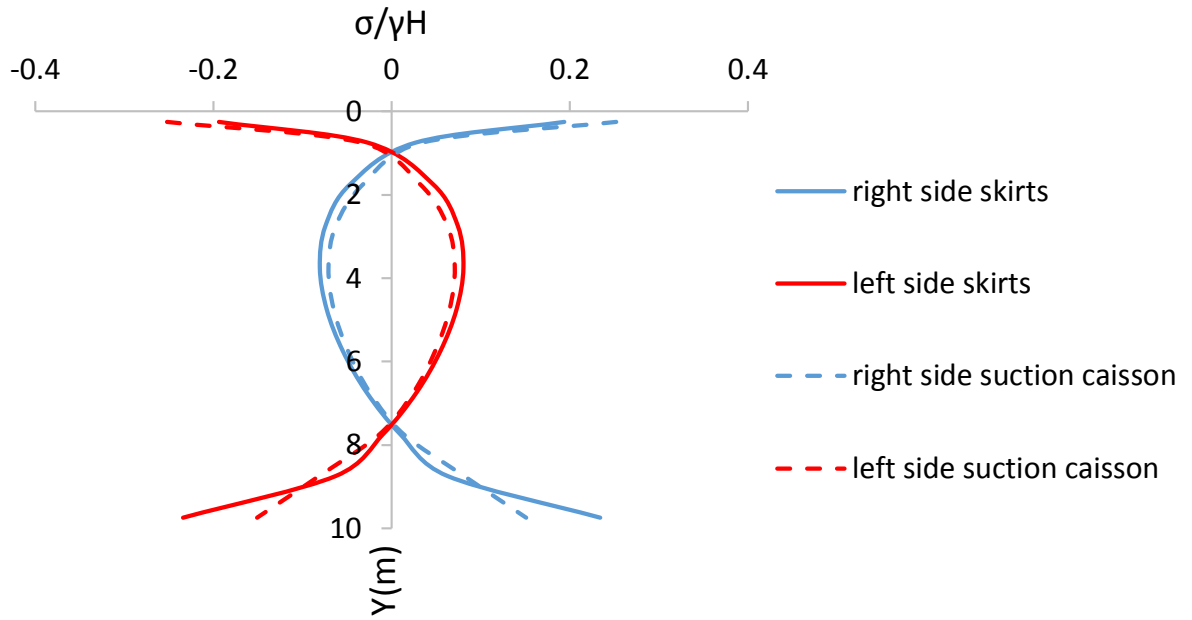

Fig.5.62. Seismic earth pressures for the Monastiraki earthquake motion as excitation at t=3.995 s, time of maximum acceleration of the top edge

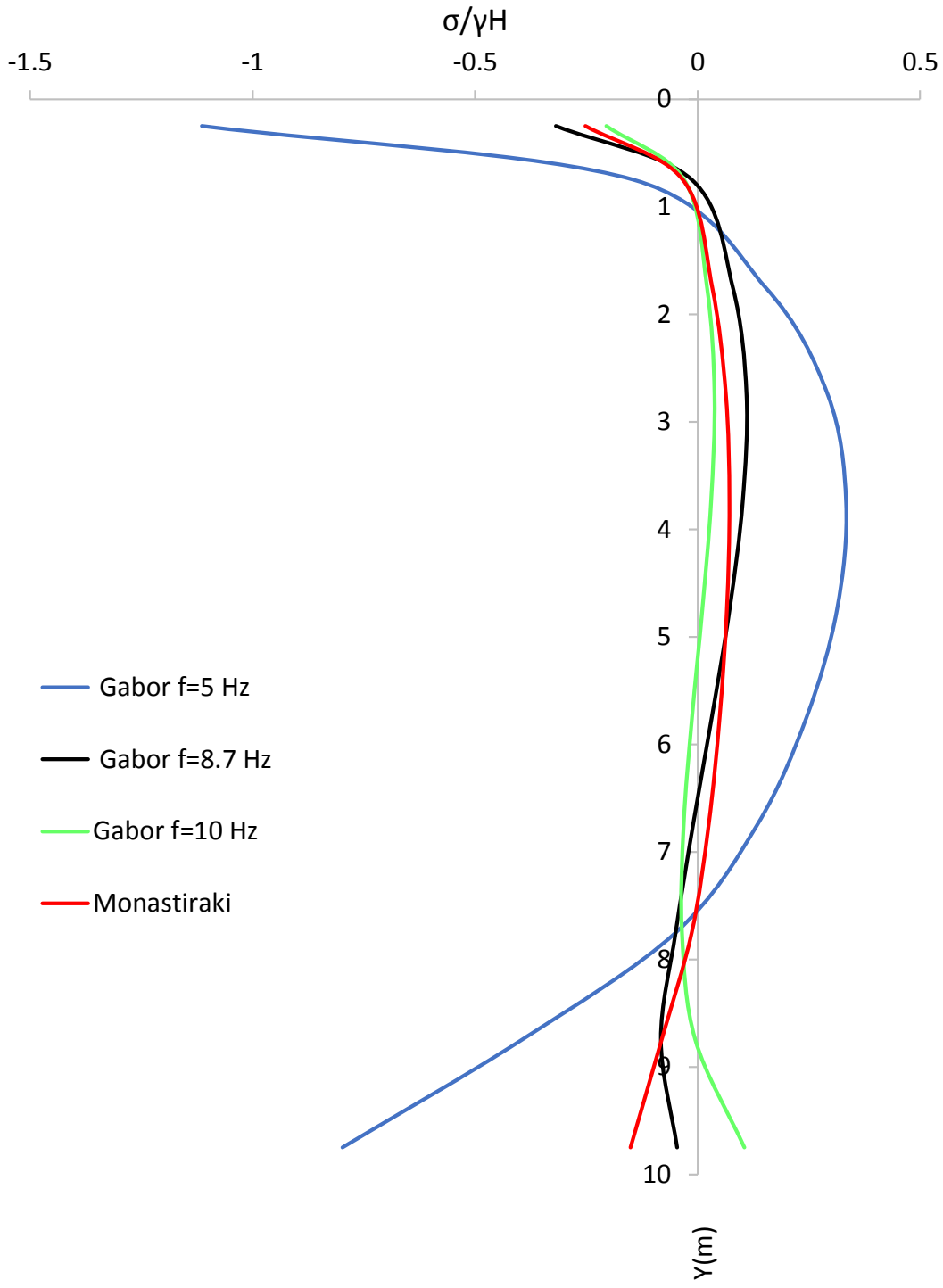

Fig.5.63. Comparison of seismic earth pressures from the Monastiraki earthquake motion with results from Gabor type pulses as excitation

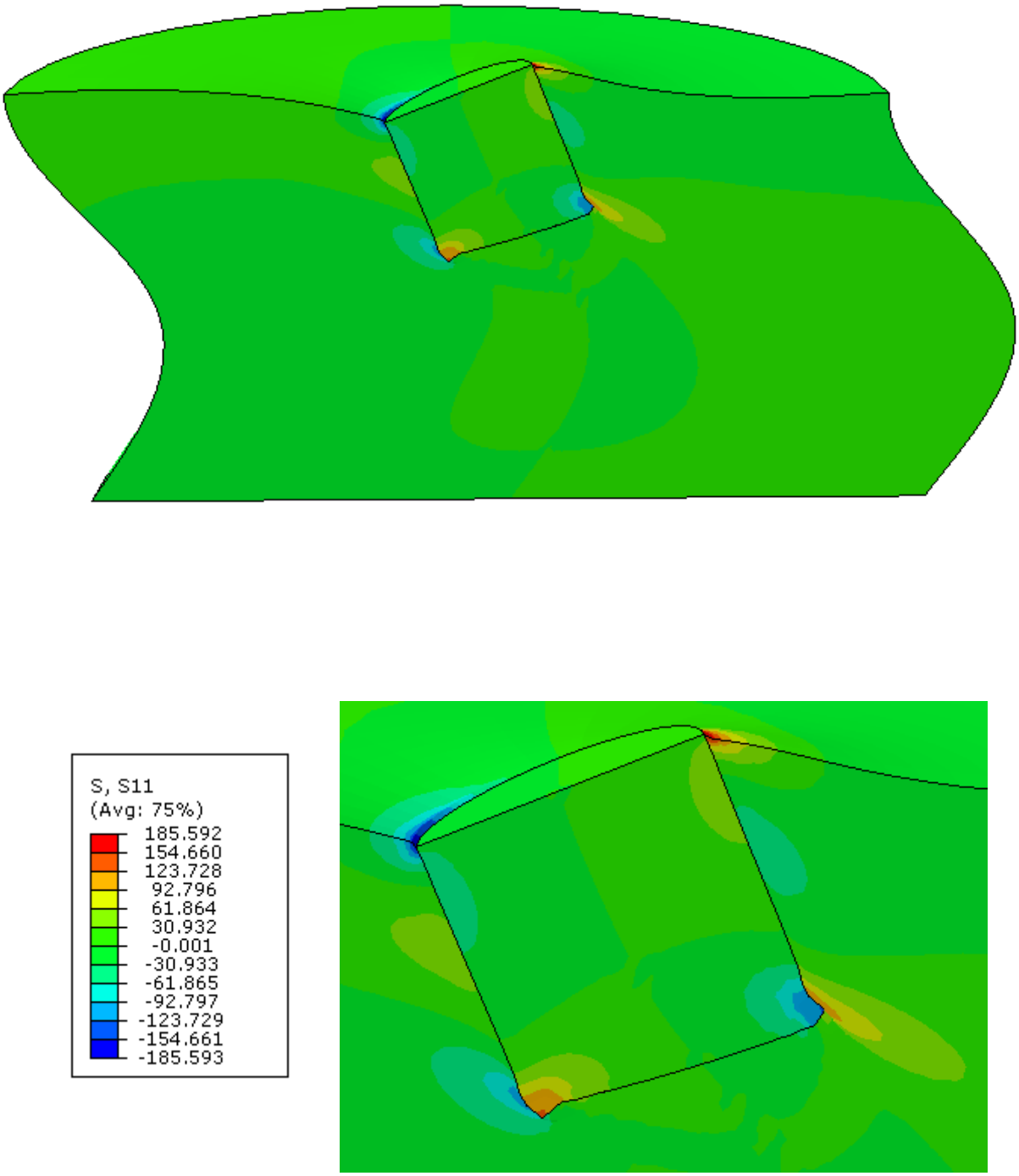

Fig.5.64. Snapshot of the model and contours of normal stresses on the suction caisson for Monastiraki earthquake motion as excitation [t=3.995 s]; deformation scale factor: 960

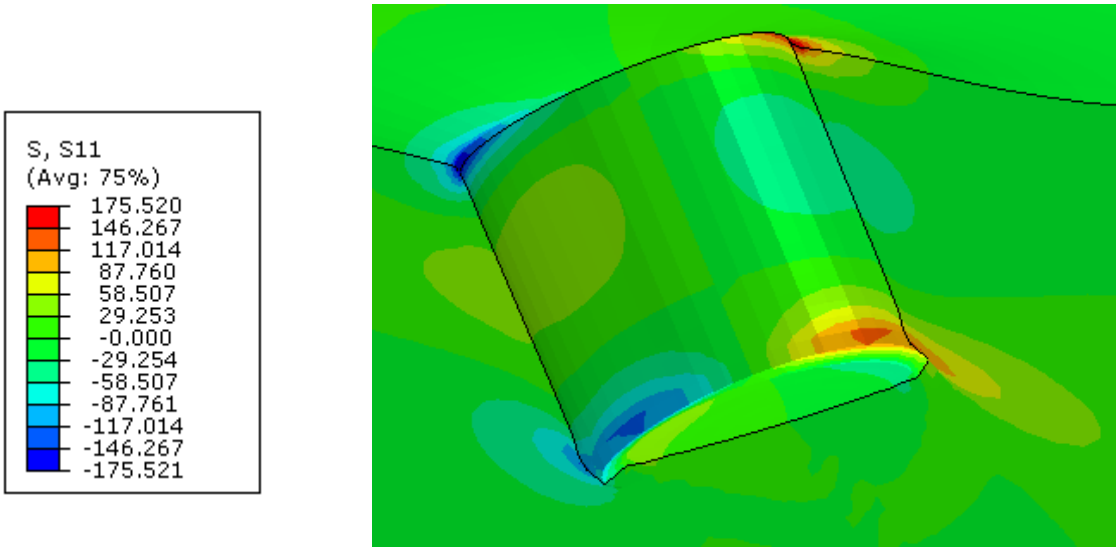

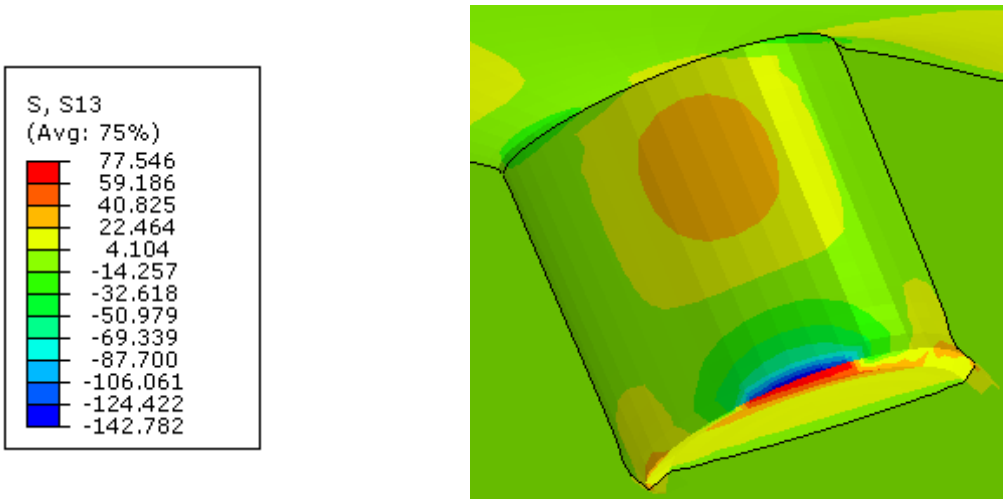

Fig.5.65. External soil alone: Contours of normal (*top*) and shear (*bottom*) stresses on the suction caisson for Aegion earthquake motion as excitation [t=3.995 s]; deformation scale factor: 960

Chapter 6

Concluding Remarks

6 Concluding Remarks

This study investigates the static and dynamic response of the suction caisson foundation, which is an alternative to the monopile that currently dominates the offshore wind turbine industry. Apart from the suction caisson, its sidewalls, also known as skirts, are examined alone and compared to the full foundation for all cases addressed herein. By identifying the role of the skirts alone, further insight is gained into the mechanics of the problem and the possibility of a hybrid foundation on this basis. Emphasis is placed on three areas of interest:

- The bearing capacity of skirted foundations
- The elastic and nonlinear stiffness of the soil-foundation system
- The kinematic interaction of the soil-foundation system

The key conclusions from the above analyses are summarized below:

Bearing Capacity

The suction caisson and the skirts alone were examined in a soil stratum of uniform soil shear strength for three embedment ratios L/a=0.5, 1 and 2.

The most striking point is that for both the assumptions of Fully Bonded Contact (FBC) and Tensionless Sliding Interface (TSI) between the foundation and the soil, under horizontal and moment loading, especially as embedment ratio increases over 0.5, the loads acting on the suction caisson and the skirts alone, are transferred to the base, and the foundation along with the constrained soil plug move as a rigid body, with the bearing capacity of the two foundation types being practically the same. The lid does not play any role in these loading types. However, under vertical loading, the failure mechanisms of the suction caisson and the skirts are different. More specifically, for the first, the main contribution to the resistance under vertical loading lies to the mobilization of the soil below the skirt tip level, while for the latter, the major mechanism involves development of shear stresses along the sidewalls, both internally and externally. As a result, the suction caisson outperforms the skirts alone in terms of bearing capacity, especially when the assumption of TSI is taken into account, where serious sliding takes place.

Finally, the suction caisson can be replaced by the skirts alone under specific circumstances, where a satisfying capacity under vertical loading is achieved.

Stiffness

The elastic, static stiffness components of the suction caisson and the skirts alone are calculated for a homogeneous and a Gibson soil, where the soil Young Modulus E increases linearly with depth from the surface z, in a manner of $E=kz$. It needs to be stressed out that the stiffness is produced by imposing displacements and rotations on the lid of the suction caisson and on the top periphery of the skirts alone, in order to properly take into account the influence of the flexibility of the sidewalls, after Doherty et al. (2005). The basic results are the following:

- The determination of the stiffness of the skirts alone can be achieved through curves developed in this study that present it as a proportion of the suction caisson stiffness, for embedment ratios L/a ranging from 0.02 to 0.2.
- Interestingly, the differences between the two foundation types in terms of elastic stiffness are inexistent for L/a=2 for all the cases investigated, while they become more evident as embedment ratio decreases.
- A methodology of practical nature is suggested for the estimation of the elastic stiffness of a rigid suction caisson, and as an extension of a solid cylindrical foundation, embedded in Gibson soil of ν=0.49.

Additionally, the degradation of the soil-foundation stiffness for an infinite FS_V is assessed in the large-strain domain, both under FBC and TSI assumption. The suction caisson and the skirts alone are examined in a soil stratum of uniform undrained shear strength, for three embedment ratios L/a=0.5, 1 and 2. Charts were developed that show the degradation in the stiffness components as imposed displacements and rotations increase. Interestingly, the degradation in stiffness is the same for the L/a=2 suction caisson and skirts alone, while differences tend to manifest themselves as embedment ratio decreases.

Kinematic Interaction

The kinematic response of the rigid L/a=2 suction caisson and skirts alone in a homogeneous, elastic soil stratum under FBC assumption was examined to excitation with modified Gabor pulses of maximum acceleration at 1g, as well as to the recorded earthquake motions of Aegion (1995) and Monastiraki (1999) with peak acceleration values of 0.55g and 0.54 g respectively. The following inferences have been made:

- Maximum dynamic earth pressures acting on the sidewalls of the foundation appear when the 1st eigenmode of the soil-foundation system is mobilized.
- The amplitude of seismic stresses fluctuates with excitation frequency.
- Amplification of motion, which varies with excitation frequency, determines the amplitude of seismic earth pressures.
- Rotational kinematic interaction factor I_Φ tends to increase generally with excitation frequency in the area of interest, while translational and acceleration kinematic interaction factors I_U and I_A, respectively, present overall a declining trend with excitation frequency.
- Due to the effect of kinematic interaction and the nature of eigenmodes higher than the 1st one, the rotation of the foundation increases and at the same time the translation declines.
- The kinematic response of the suction caisson and the skirts alone is approximately the same to seismic loading.

General conclusion

From extensive comparisons between the suction caisson and the skirts alone, it can be deduced that the latter are in position to replace the full foundation in conditions where adequate capacity in vertical loading is achieved.

In this study is proposed the concept of a hybrid foundation consisting of the skirts alone, which could be used for onshore applications too. The connection between the offshore wind turbine tower with this hollow cylindrical hybrid foundation could be achieved with steel radial stiffeners, as presented in **Figure 6.1**. The choice of the radial stiffeners instead of a lid could lead to substantial cost and material savings.

Suggestions for further research

Skirted foundations constitute a promising alternative to the monopile, which is the conventional solution for the foundation of offshore wind turbines. Therefore, further research needs to be carried out on this subject. The following topics may be addressed in future studies:

- Analysis of a group of skirted foundations for an offshore wind turbine
- Examination of base uplift
- Introduction of additional skirts and investigation of the confined soil response
- Full modelling of the superstructure and fatigue analysis in the cyclic response of the system
- Comparison between a skirted foundation and a monopile for a typical wind turbine, including financial analysis

Chapter 6: Figures

Concluding Remarks

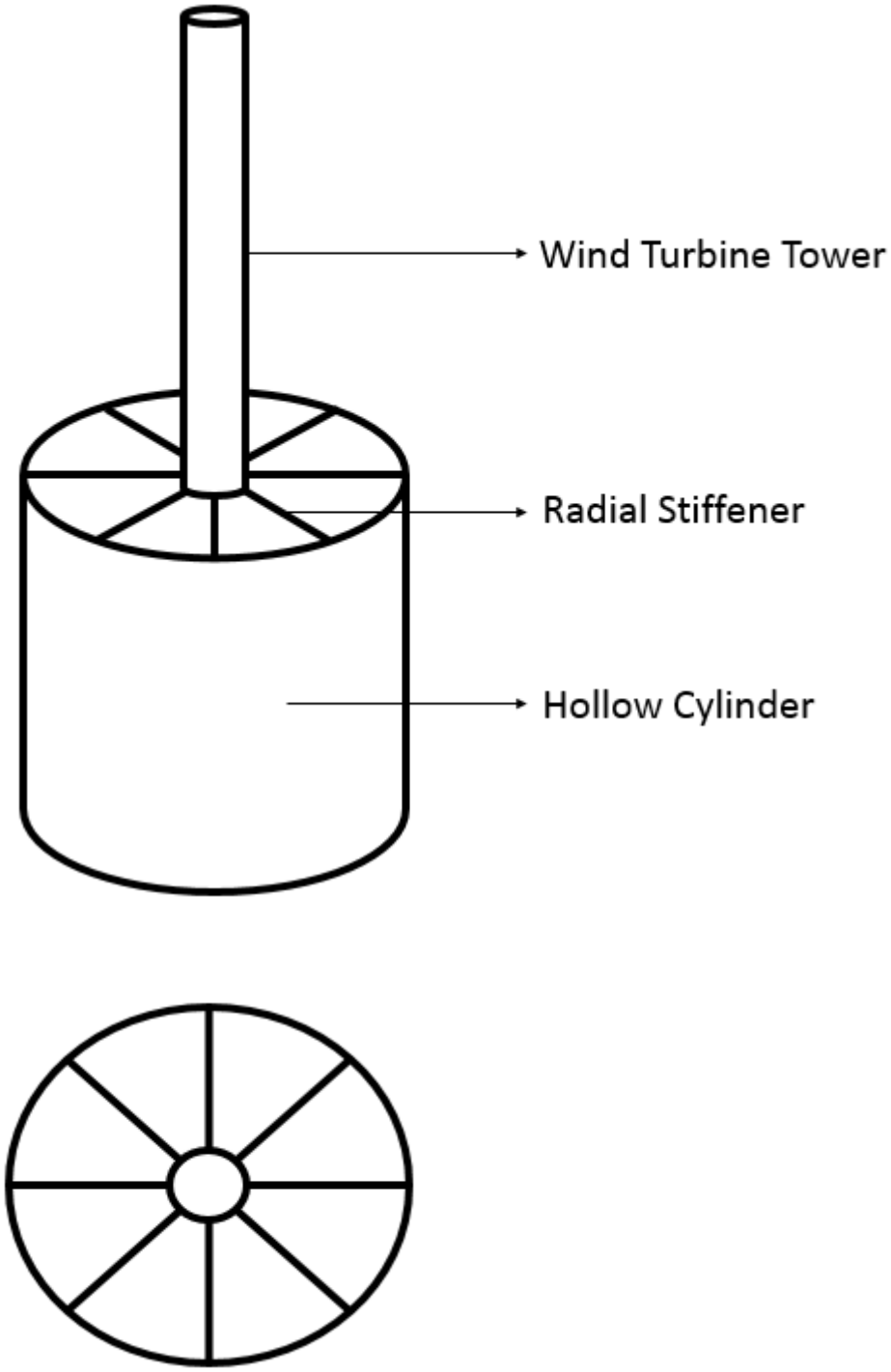

Fig.6.1. Sketch of the hybrid foundation proposed in this study. *Top*: Perspective of the foundation *Bottom*: Top view

References

ABAQUS 6.10. [2010]. Standard user's manual. Dassault Systèmes Simulia Corp., Providence, RI, USA.

Allotey, N., Naggar, MHE. [2003]. “Analytical moment–rotation curves for rigid foundations based on a winkler model”, Soil Dynamics and Earthquake Engineering, 23 (5): 367–381

Allotey N., Naggar, MHE. [2008]. “An investigation into the Winkler modeling of the cyclic response of rigid footings”, Soil Dynamics and Earthquake Engineering, 28 (1): 44–57

Anastasopoulos, I., Gazetas, G., Loli, M., Apostolou, M. and Gerolymos, N. [2010]. "Soil Failure can be used for Seismic Protection of Structures", Bulletin of Earthquake Engng, 8 (2): 309-326

Anastasopoulos, I., Georgarakos, T., Georgiannou, V., Drosos, V. and Kourkoulis R. [2010]. “Seismic performance of bar-mat reinforced-soil retaining wall: shaking table testing versus numerical analysis with modified kinematic hardening constitutive model”, Soil Dyn Earthq Eng, 30 (10)

Anastasopoulos, I., Gelagoti, F., Kourkoulis, R. and Gazetas, G. [2012]. "Simplified Constitutive Model for Simulation of Cyclic Response of Shallow Foundations: Validation against Laboratory Tests", Journal of Geotechnical and Geoenv. Eng., ASCE, 137 (12): 1154-1168

Anastasopoulos, I. and Theofilou, M. [2015]. “Hybrid foundation for offshore wind turbines: Environmental and seismic loading”, Soil Dynamics and Earthquake Engineering, 80: 192-209

Andersen, K. H. and Jostad, H. P. [1999]. "Foundation design of skirted foundations and anchors in clay", Proc. 31st Offshore Tech. Conf., Houston, Paper OTC 10824

Bienen, B., Gaudin, C., Cassidy, M.J., Rausch, L., Purwana, O.A. and Krisdani, H. [2012]. “Numerical modelling of a hybrid skirted foundation under combined loading”, Computers and Geotechnics, 45: 127-139

Bienen, B., Dührkop, J., Grabe, J., Randolph, M.F. and White D.J. [2012]. “Response of piles with wings to monotonic and cyclic lateral loading in sand”, Journal of Geotechnical and Geoenvironmental Engineering, 138 (3): 364-375

Bozorgnia, Y. and Bertero, V.V. [2004]. "Earthquake Engineering: From Engineering Seismology to Performance-Based Engineering", CRC Press

Bransby, M. F. and Randolph, M. F. [1997]. "Shallow foundations subject to combined loadings" Proc. 9th Int. Conf. on Comp. Methods and Advances in Geomechcs, Wuhan 3, 1947–1952

Bransby, M.F. and Randolph, M.F. [1998]. “Combined loading of skirted foundations”, Geotechnique, 48 (5): 637-655

Bransby, M.F. and Randolph, M.F. [1999]. “The effect of embedment depth on the undrained response of skirted foundations to combined loading”, Soils and Foundations, 39 (4): 19-33

Bransby, M.F. and Yun, G.J. [2009]. “The undrained capacity of skirted strip foundations under combined loading”, Geotechnique, 59 (2): 115-125

Brinch Hansen, J. [1970]. “A revised and extended formula for bearing capacity”, Danish Geotechnical Institute, Copenhagen, Bulletin No. 28: 5-11

Butterfield, R. & Gottardi, G. [1994]. “A Complete Three Dimensional Failure Envelope for Shallow Footings on Sand”, Geotechnique, 44: 181−184

Byrne, B. W. [2000]. “Investigations of suction caissons on dense sand”, DPhil thesis, University of Oxford, UK

Byrne, B. W. and Houlsby, G. T. [2002]. “Experimental investigations of the response of suction caissons to transient vertical loading”, *J. Geotech. Geoenviron. Engng* 128: 926–939

Byrne, B.W. and Houlsby, G.T. [2003]. “Foundations for offshore wind turbines”, Phil. Trans. R. Soc. Lond. A, 361: 2909–2930

Byrne, B. W., Villalobos, F., Houlsby, G. T. & Martin, C. M. [2003]. “Laboratory testing of shallow-skirted foundations in sand”, Proc. British Geotechnical Association Int. Conf. On Foundations, Dundee, 2–5 September 2003, London: Thomas Telford, 161–173

Byrne, B. W. and Houlsby, G. T. [2006]. “Assessing novel foundation options for offshore wind turbines”, World maritime technology conference, London

Chang, C.-Y., Power, M.S., Idriss, I.M., Sommerville, P.G., Silva, W. and Chen, P.C. [1985]. “Engineering characterization of ground motion. Task II: Observational data on spatial variations of earthquake ground motion” Rpt. No. NUREG/CR-3805, U.S. Nuclear Regulatory Commission, Washington DC

Clukey, E. C. and Morrison, J. [1993]. "A centrifuge and analytical study to evaluate suction caissons for TLP applications in the Gulf of Mexico", In Design and Performance of Deep Foundations: Piles and Piers in Soil and Soft Rock, ASCE Geotechnical Special Publication 38: 141-156

Colliat, J-L., Boisard, P., Andersen, K. and Schroder, K. [1995]. "Caisson foundations as alternative anchors for permanent mooring of a Process Barge Offshore Congo", Proc. 27th Offshore Tech. Conf., Houston, Paper OTC 7797, 919-929

Davis, E. H. and Booker, J. R. [1973]. “The effect of increasing strength with depth on the bearing capacity of clays”, Geotechnique, 23 (4): 551-563

Davis, R. O. and Selvadurai, A. P. S. [2002]. “Plasticity and Geomechanics”, Cambridge University Press

Day, S.M. [1978]. “Seismic response of embedded foundations,” Proc. ASCE Convention, Preprint No. 3450, Chicago, IL

Dimmock, P., Clukey, E., F.ASCE, Randolph, M.F., Murff, D., Dist.M.ASCE and Gaudin, C. [2013]. “Hybdrid subsea foundations for subsea equipment”, Journal of Geotechnical and Geoenvironmental Engineering, ASCE, 139: 2182-2192

Doherty, J. P. and Deeks, A. J. [2003]. “Elastic response of circular footings embedded in a non-homogeneous half-space”, Geotechnique, 53(8): 703-714

Doherty, J.P. and Deeks, A.J. [2005]. “Adaptive coupling of the finite-element and scaled boundary finite-element methods for non-linear analysis of unbounded media”, Computers and Geotechnics, 32 (6): 436-444

Doherty, J. P., Houlsby, G. T. and Deeks, A. J. [2005]. “Stiffness of flexible caisson foundations embedded in nonhomogeneous elastic soil”, Journal of Geotechnical and Geoenvironmental Engineering, ASCE, 131 (12): 1498-1508

Elsabee, F. and Morray, J.P. [1977]. “Dynamic behavior of embedded foundations,” Publication No. R77-33, MIT, Cambridge, MA

Faccioli, E., Paolucci, R. and Vivero, G. [2001]. “Investigation of seismic soil – footing interaction by large scale cyclic tests and analytical models”, Proceedings of 4th International Conference on Recent Advances in Geotechnical Earthquake Engineering and Soil Dynamics, S. Prakash (Ed.), Paper no. SPL-5, San Diego, CA

FEMA 356, [2000]. “Prestandard and Commentary for the Seismic Rehabilitation of Buildings”, Federal Emergency Management Agency, Washington DC

Fuglsang, L. D. and Steensen-Bach, J. O. [1991]. "Breakout resistance of suction piles in clay", Proc. Int. Conf. On Centrifuge Modeling: Centrifuge 91, Boulder, Colorado, 163-159

Gajan, S. & Kutter, B. L. [2008]. “Capacity, settlement, and energy dissipation of shallow footings subjected to rocking”, J. Geotechnical & Geoenv. Engng, ASCE, 134 (8): 1129-1141.

Gajan, S., Kutter, B.L., Phalen, J.D., Hutchinson, T.C. and Martin, G.R. [2005]. “Centrifuge modeling of load-deformation behavior of rocking shallow foundations”, Soil Dynamics and Earthquake Engineering, 25 (7-10): 773–783

Gazetas, G. [1983]. “Analysis of machine foundation vibrations: state of the art”, Soil Dynamics and Earthquake Engineering, 2 (1): 2-42

Gazetas, G. [1984]. “Seismic response of end-bearing piles”, Soil Dynamics and Earthquake Engineering, 3 (2): 82-93

Gazetas, G. [1987]. “Simple physical methods for foundation impedances”, Dynamics of Foundations and Buried Structures, Benerjee PK and Butterfield R., editors, Elsevier Applied Science, Chapter 2, 44-90

Gazetas, G. [1991]. “Formulas and charts for impedances of surface and embedded foundations”, Journal of Geotechnical Engineering, ASCE, 117 (9): 1129–1141

Gazetas, G., Anastasopoulos, I. and Apostolou, M. [2007]. “Shallow and Deep Foundations under Fault Rupture or Strong Seismic Shaking”, Earthquake Geotechnical Engineering, Pitilakis K., Editor, Springer: Berlin, 185–210.

Gazetas G., Anastasopoulos I., Adamidis O. and Kontoroupi Th. [2013]. "Nonlinear Rocking Stiffness of Foundations", Soil Dynamics & Earthquake Engineering, 47: 83-91.

Gazetas, G., Apostolou, M. and Anastasopoulos, I. [2003]. "Seismic Uplifting of Foundations on Soft Soil with Examples from Adapazari (Izmit 1999, Earthquake)", BGA International Conference on Foundation Innovations, Observations, Design & Practice, Univ. of Dundee, Scotland, September 25, 37–50

Gazetas, G. and Apostolou, M. [2004]. "Nonlinear soil-structure interaction : foundation uplifting and soil yielding", Proceedings of the 3rd US–Japan Workshop on Soil-Structure Interaction, Menlo Park, California

Gazetas G. and Hatziconstantinou, C., [1988]. "Elastic Formulae for Lateral Deflection and Rotation of Arbitrarily Shaped Embedded Foundations," *Geotechnique,* 38 (3): 439-444

Gazetas G. and Tassoulas J. L. [1987]. "Horizontal Stiffness of Arbitrarily-Shaped Embedded Foundations ", Journal of Geotechnical Engineering, ASCE, 113 (5): 440-457

Gazetas G. and Tassoulas, J.L. [1987]. "Horizontal Damping of Arbitrarily-Shaped Embedded Foundations," Journal of Geotechnical Engineering, ASCE, 113 (5): 458-475

Gelagoti F. (2012). "Rocking Isolation of Frames on Shallow Footings : Design Limitations", Proceedings of the First Bulletin of the Second International Conference on Performance –Based Design in Earthquake Geotechnical Engineering, 28-30 May, Taormina (Italy)

Gerolymos, N. and Gazetas, G. [2006]. "Static and dynamic response of massive caisson foundations with soil and interface nonlinearites – validation and results", Soil Dynamics and Earthquake Engineering, 26 (5): 377-394

Giannakos, S., Gerolymos, N. and Gazetas, G. [2012]. "Cyclic lateral response of piles in dry sand: finite element modeling and validation", Comput Geotech, 44

Gottardi, G., Houlsby, G. T. & Butterfield, R. [1999]. "The plastic response of circular footings on sand under general planar loading", Geotechnique, 49 (4): 453–470

Gourvenec, S. [2007]. "Failure envelopes for offshore shallow foundations under general loading", Geotechnique, 57 (9): 715-728

Gourvenec, S. [2008]. "Effect of embedment on the undrained capacity of shallow foundations under general loading", Geotechnique, 58 (3): 177-185

Gourvenec, S., Acosta-Martinez, H. E. and Randolph, M. F. [2009]. "Experimental study of uplift resistance of shallow skirted foundations in clay under transient and sustained concentric loading", Geotechnique, 59 (6): 525-537

Gourvenec, S. and Randolph, M. F. [2003]. "Effect of strength non-homogeneity on the shape of failure envelopes for combined loading of strip and circular foundations on clay", Geotechnique, 53 (6): 575-586

Gourvenec, S. and Randolph, M.F. [2007]. “Failure envelopes for offshore shallow foundations under general loading”, Geotechnique, 57 (9): 715-728

Green, A. P. [1954]. “The plastic yielding of metal junctions due to combined shear and pressure”, J. Mech. Phys. Solids, 2 (3): 197-211

Houlsby, G. T., Kelly, R. B. and Byrne, B. W. [2005]. “The tensile capacity of suction caissons in sand under rapid loading”, Frontiers in Offshore Geotechnics, Taylor & Francis Group, London

Houlsby, G. T., Kelly, R. B., Huxtable, J. and Byrne, B. W. [2006]. “Field trials of suction caissons in clay for offshore wind turbine foundations”, Geotechnique, 55 (4): 287-296

Houlsby, G. T. and Martin, C. M. [2003]. “Undrained bearing capacity factors for conical footings on clay", Geotechnique, 53 (5): 513-520

Houlsby, G. T. and Wroth, C. P. [1983]. “Calculation of stresses on shallow penetrometers and footings”, Proc. IUTAM/IUGG Seabed Mechanics, Newcastle, 107-112

House, A. R. and Randolph, M. F. [2001]. "Installation and pull-out capacity of stiffened suction caissons in cohesive sediments", Proc. Eleventh (2001) Intl. Offshore and Polar Engng Conf., Vol. 2, ISBN 1-880653-2

Ishii, K., Itoh, T. and Suhara, J. [1984]. “Kinematic interaction of soil-structure system based on observed data”, Proc. 8th World Conference in Earthquake Engineering, 3:1017-1024

Johnson, J.J. [1981]. “Soil-structure interaction: the status of current analysis methods and research”, Lawrence Livermore National Library (LLNL), UCRL-53011, NUREG/CR-1780

Kausel, E. and Ushijima, R. [1979]. “Vertical and torsional stiffness of cylinder footings”, Research Rep. R76-6, MIT

Kausel, E., Whitman R.V., Morray J.P. and Elsabee F. [1978]. “The spring method for embedded foundations”, Nuclear Engineering and Design, 48: 377-392

Kelly, R. B., Houlsby, G. T. and Byrne, B. W. [2006]. "Transient vertical loading of model suction caissons in a pressure chamber", Geotechnique, 56 (10): 665-675

Kim, S. and Stewart, J.P. [2003]. “Kinematic Soil-Structure Interaction from strong motion records”, Journal of Geotechnical and Geoenvironmental Engineering, 129(4): 323-335

Kourkoulis, R.S., Gelagoti, F.M., Kaynia, A.M. [2012]. “Seismic response of offshore wind turbine foundations”, 15th WCEE, Lisbon

Kourkoulis, R.S., Lekkakis, P.C., Gelagoti, F.M., Kaynia, A.M. [2014]. “Suction caisson foundations for offshore wind turbines subjected to wave and earthquake loading: Effect of soil-foundation interface”, Geotechnique, 64 (3)

Kutter, B. L., Martin, G., Hutchinson, T. C., Harden, C., Gajan, S., Phalen, J. D. [2003]. "Workshop on modeling of nonlinear cyclic load-deformation behavior of shallow foundations", Report of the PEER Workshop, University of California, Davis

Lekkakis, P. [2012]. “Analysis of skirted foundations for offshore wind turbines”, Diploma Thesis, NTUA

Liingaard, M., Andersen, L. and Ibsen, L. B. [2007]. “Impedance of flexible suction caissons”, Earthquake Engng Struct. Dyn. 2007; 36: 2249-2271

Luke, A. M., Rauch, A. F., Olson, R. E. and Mecham, E. C. [2005]. "Components of suction caisson capacity measured in axial pull-out tests", Ocean Engng, 32: 878-891

Luco, J.A. and Mita, A. [1987]. “Response of a circular foundation on a uniform half-space to elastic waves”, Earthquake Engineering and Structural Dynamics, 15: 105-118

Makris, N. and Roussos, Y. [2000]. “Rocking Response of rigid blocks under near source ground motions”, Geotechnique, 50 (3): 243-262

Martin, C. M. [1994]. “Physical and numerical modeling of offshore foundations under combined loads”, PhD thesis, University of Oxford, UK

Martin, C.M. [2001]. “Vertical bearing capacity of skirted circular foundations on Tresca soil” Proc. Int. Conf. Soils Mech. and Geotech. Engineering (ICSMGE), Istanbul

Martin, G. R. and Lam, I. P. [2000]. “Earthquake Resistant Design of Foundations: Retrofit of Existing Foundations”, Proc. GeoEng 2000 Conference, Melbourne

Mello, J. R. C., Moretti, M. J., Sparrevik, P., Schroder, K. and Hansen, S. B. [1998]. "PI9 and P26 moorings at the Marlim field. The first permanent taut leg mooring with fibre rope and suction anchors", Proc. FPS '98 Conf., London.

Meyerhof, G.G. [1951]. “The ultimate bearing capacity of foundations”, Geotechnique, 2 (4): 301-332

Meyerhof, G.G. [1953]. "The bearing capacity of foundations under eccentric and inclined loads" Proc. 3rd Int. Conf. Soil Mech. Fndn Engng, Zurich,1: 440-445

Mita, A. and Luco, J.E. [1989]. “Dynamic response of a square foundation embedded in an elastic halfspace”, Soil Dynamics and Earthquake Engineering, 8(2): 54-67

Murff, J. D. [1994]. “Limit analysis of multi-footing foundation systems”, Proc. 8th Int. Conf. Comput. Methods, Adv. Geomech., Morgantown 1, 440-445

Nova, R., Montrasio, L. [1991]. “Settlement of shallow foundations on sand”, Geotechnique, 41 (2): 243-256

Ntritsos, N., Anastasopoulos, I., & Gazetas G. [2015]. “Static and Cyclic Undrained Response of Square Embedded Foundations”, *Géotechnique*, 65(10): 805-823

Paolucci, R., Shirato, M. and Yilmaz, M.T. [2008]. “Seismic behaviour of shallow foundations: Shaking table experiments vs numerical modelling”, Earthq Eng Struct Dyn, 37(4): 577–595

Pecker, A. [1998]. “Capacity Design Principles For Shallow Foundations in Seismic Areas”, Proc. 11th European Conference on Earthquake Engineering, A.A. Balkema Publishing

Pecker, A. [2003]. “A seismic foundation design process, lessons learned from two major projects: the Vasco de Gama and the Rion Antirion bridges”, ACI International Conference on Seismic Bridge Design and Retrofit, La Jolla

Pender, M. [2007] “Seismic design and performance of surface foundations”, 4th International Conference on Earthquake Geotechnical Engineering, Thessaloniki, Greece

Poulos, H. G. and Davis, E. H. [1974]. “Elastic solutions for soil and rock mechanics”, John Wiley & Sons, Inc., New York, London, Sydney, Toronto

Puech, A., Iorio, J-P., Garnier, J. and Foray, P. [1993]. "Experimental study of suction effects under mudmat type foundations", Proceedings of Canadian Conference on Marine Geotechnical Engineering, St. John's, Newfoundland, 3: 1062-1080

Prandtl, L. [1921]. “Über die Eindringungsfestigkeit (Harte) plastischer Baustoffe und die Festigkeit von Schneiden”, Zeitschrift für angewandte Mathematik und Mechanik, 1 (1): 15-20

Randolph, M. F. and Gourvenec, S. [2011]. “Offshore geotechnical engineering”, Spon Press

Randolph, M. F. and House, A. R. [2002]. “Analysis of suction caisson capacity on clay”, Proc. Annual Offshore Tech. Conf., Houston, Paper OTC 14236

Randolph, M. F. and Puzrin, A. M. [2003]. “Upper bound limit analysis of circular foundations on clay under general loading”, Geotechnique, 53 (9): 785-796

Rao, S. N., Ravi, R. and Ganapathy, C. [1997]. "Pullout behaviour of model suction anchors in soft marine clays", Proc. Int. Offshore and Polar Engng Conf., ISOPE '97, Honolulu 1, 740-744

Roesset, J. M. [1980]. “Stiffness and damping coefficients of foundations”, Dynamic Response of Foundations: Analytical Aspects, M.W. O' Neil and R. Dobry (eds), ASCE, 1-30

Roesset J. M. [1980]. “The use of simple models in soil-structure interaction”, Civil Engineering and Nuclear Power, ASCE, 1: 1-25

Rowe, R.K. (Ed.) [2001]. “Geotechnical and Geoenvironmental Engineering Handbook”, Springer Science & Bussiness Mafia, New York

Salgado, R., Lyamin, A. V., Sloan, S. W. and Yu, H. S. [2004]. “Two and three-dimensional bearing capacity of foundations in clay”, Geotechnique, 54 (5): 297–306

Seed, H.B. and Lysmer, J. [1980]. “The seismic soil-structure interaction problem for nuclear facilities”, Lawrence Livermore Lab., UCRL-15254, Livermore, CA

Skempton, A.W. [1951]. “The bearing capacity of clays”, Building Research Congress, London, 1: 180-189

Steensen-Bach, J. O. [1992]. "Recent model tests with suction piles in clay and sand", Proc. Annual Offshore Tech. Conf., Houston, Paper OTC 1882

Stone, K., Newson, T. and El Marassi, M. [2010]. “An investigation of a monopile-footing foundation”, Proc of the international conference on physical modelling in geotechnics (ICPMG2010), Rotterdam, 829-833

Taiebat, H. A. and Carter, J. P. [2000]. “Numerical studies of the bearing capacity of shallow foundations on cohesive soil subjected to combined loading”, Geotechnique, 50 (4): 409–418

Taiebat, H. A. and Carter, J. P. [2002]. “Bearing Capacity of Strip and Circular Foundations on Undrained Clay Subjected to Eccentric Loads”, Geotechnique, 52 (1): 61-64

Taylor, P.W., Bartlett, P.E. and Wiessing, P.R. [1981]. “Foundation rocking under earthquake loading”, Proceedings of 10th International Conference on Soil Mechanics and Foundation Engineering, AA Balkema, Stockholm, Sweden, Rotterdam, Netherlands, 3: 313–322

Terzaghi, K. [1943]. “Theoretical soil mechanics”, John Wiley & Sons Inc., London and New York

Ukritchon, B., Whittle, A. J. and Sloan, S. W. [1998]. “Undrained limit analyses for combined loading of strip footings on clay", Journal of Geotechnical and Geoenvironmental Engineering, 124 (3): 265-276

Van der Tempel, J. [2006]. "Design of support structures for offshore wind turbines", PhD thesis

Veletsos, A.S., and Prasad, A.M., (1989). “Seismic interaction of structures and soils: stochastic approach,” J. Struct. Engrg., ASCE, 115(1.4): 935-956

Veletsos, S.A. and Tang Y. [1987]. “Vertical vibration of ring foundations”, Earthquake Engineering and Structural Dynamics, 15: 1-21

Veletsos, S.A. and Tang Y. [1987]. “Rocking vibration of rigid ring foundations”, Journal of Geotechnical Engineering, 113: 1019-1032

Vesic, A.S. [1975]. “Bearing capacity of shallow foundations”, Foundation Engineering Handbook, Eds Winterkorn & Fang, Van Nostrand Reinhold, New York, 121-147

Vulpe, C., Bienen, B. and Gaudin, C. [2013]. “Predicting the undrained capacity of skirted spudcans under combined loading”, Ocean Engineering, 74: 178-188

Watson, P. G. and Randolph, M. F. [1997a]. “Vertical capacity of suction caisson foundations in calcareous sediments”, Proc. 7th Int. Offshore Polar Engng Conf. Honolulu 1, 784-790

Watson, P. G., Randolph, M. F. and Bransby, M. F. [2000]. “Combined lateral and vertical loading of caisson foundations”, Proc. Annual Offshore Tech. Conf., Houston, Paper OTC 12195

Yun, G. and Bransby, M. F. [2007]. “The horizontal-moment capacity of embedded foundations in undrained soil”, Can. Geotech. J., 44 (4): 409-424